CHARACTERIZATION OF DIFFUSION BEHAVIOR OF A NOVEL EXTRA-CELLULAR SPHINGOLIPID ASSOCIATED PEPTIDE PROBE BY FLUORESCENCE CORRELATION SPECTROSCOPY AND IMAGING TOTAL INTERNAL REFLECTION FLUORESCENCE CORRELATION SPECTROSCOPY

MANOJ KUMAR MANNA

(*M. Sc., Chemistry, University of Delhi*)

A THESIS SUBMITTED

FOR THE DEGREE OF DOCTOR OF PHILOSOPHY

DEPARTMENT OF CHEMISTRY

NATIONAL UNIVERSITY OF SINGAPORE

2010

Characterization of Diffusion Behavior of a Novel Extra-cellular Sphingolipid Associated Peptide Probe by Fluorescence Correlation Spectroscopy and Imaging Total Internal Reflection Fluorescence Correlation Spectroscopy

MANOJ KUMAR MANNA

(*M. Sc., Chemistry, University of Delhi*)

A Thesis Submitted

for the Degree of Doctor of Philosophy

Department of Chemistry

National University of Singapore

2010

Acknowledgements

Working aboard, in a multi-disciplinary field is never easy without a friendly atmosphere and sincere support from others. Therefore, at the beginning I would like to thank those people without whom this work would not have been successful and those, whose presence made my graduation days so joyous that I never felt away from home.

First of all I would like to express my gratitude for my supervisor Prof. Thorsten Wohland for his kind support in every aspect during my PhD. His continuous valuable tips, confident guidance for data analysis and his sincere never ending care not only makes my graduation project successful but also helped me to develop more methodical and organized research skills.

I am really lucky to have Prof. Rachel Susan Kraut as my co-supervisor. Her continuous guidance, help in work plan and literature, motivation and care make this work much easier.

I would like to thank all of my lab members in NUS. Especially, Guo Lin for training me on the instrumentations and the valuable scientific discussions I shared with him; Jagadish Sankaran for his sincere help in writing the software for the ITIR-FCS and ITIR-FCCS techniques and help in data analysis; Dr. Pan Xiaotao, who guided me in learning the confocal FCS instrumentation during the initial days of my research; Dr. Balakrishnan Kannan for his valuable tips and guidance for laser alignment and construction of the ITIR-FCS instrumentation; Teo Lin Shin and Foo Yong Hwee to stand by me with their sincere help, whenever I needed them, either by helping me doing experiments over at Biopolis or by sharing any valuable thoughts. Its giving me immense pleasure to thank Dr. Shi Xianke, Dr. Liu Ping, Dr. Huang Ling Ching, Dr. Yu Lanlan, Dr. Sebastian Leptin, Dr. Celic Turgay, Liu Jun, Ma Xiaoxiao, Tapan Mistri, Rafi Rashid to be there always as good friends and charming lab mates to make the lab atmosphere more homely and friendly.

I love to grab the opportunity to thank the lab members in Dr. Kraut's lab. Especially, I would like to thank Steffen Steinert for teaching me how to culture cells and Dr. Zhang Dawei for showing me how to perform protein transfections. It's my pleasure to thank Esther Lee, Yunshi Wong, Angelin Lim, Ralf Hortsch, Rico Muller, Dr. Guileumme Tresset and Dr. Sarita Hebbar for sharing some wonderful time during my attachment with Dr. Kraut's lab.

I am really grateful to my whole family, specially my parents for their continuous support, motivation and unconditional care throughout my career and in every aspect of my life.

The thanks giving can't be complete without expressing my appreciation for my graceful wife, Kriti, without whose love, care, support and understanding, I would not have able to enjoy my work and complete it successfully. She became the inspiration and motivation of my every work since she came into my life.

And last but not the least I would like to express my deepest Love and care to my sweet little son Aayush.

Table of Content

Acknowledgements i
Table of Contents ii
Summary vi
List of Figures viii
List of Tables xi
List of Abbreviations and Symbols xii
List of Publications xv

Chapter 1: Introduction 1-25
1.1 Motivation 1
1.2 Microdomains 5
1.2.1 Introduction to lipid microdomains/rafts 5
1.2.2 History of development as an emerging field 6
1.2.3 Formation of lipid rafts in live cells. 8
1.2.4 Properties of lipid microdomains/rafts 10
1.2.4.1 Structural properties 10
1.2.4.2 Biochemical properties 12
1.2.4.3 Biophysical properties 13
1.2.5 Functions of lipid rafts 15
1.2.5.1 Role of lipid rafts in signal transduction pathways 16
1.2.5.2 Role of lipid rafts as platforms for entry of pathogens 18
1.3 The Sphingolipid Binding Domain (SBD) peptide 20
1.3.1 Importance of SBD as a lipid raft marker 23
1.3.2 Properties of SBD as a lipid raft marker 24

Chapter 2: Methodology 26-50
2.1 Introduction 26
2.2 Fluorescence Correlation Spectroscopy (FCS) 27
2.2.1 Principle and theory of fluorescence correlation spectroscopy 27
2.2.1.1 The autocorrelation function and autocorrelation curve 28
2.2.1.2 General information obtained from autocorrelation curve 29
2.2.1.3 Mathematical expressions for different fitting models 31

2.2.2 Advantages of fluorescence correlation spectroscopy 33
2.2.2.1 Determination of diffusion coefficients from diffusion times 34
2.2.2.2 Determination of concentrations from the autocorrelation function 35
2.2.3 Instrumental set up for fluorescence correlation spectroscopy 36
2.3 Imaging Total Internal Reflection Fluorescence Correlation Spectroscopy (ITIR-FCS) 38
2.3.1 Principles of ITIR-FCS 41
2.3.2 Instrumental set up for imaging total internal reflection fluorescence correlation and cross-correlation spectroscopy 43
2.3.2.1 Measurement technique for ITIRFCS and ITIRFCCS 45
2.3.3 Comparison between ITIR-FCS and confocal FCS 46
2.3.4 Total Internal Reflection-Fluorescence Cross Correlation Spectroscopy (ITIR FCCS) 47
2.3.4.1 Principles of ΔCCF 48
2.3.4.2 Methodology of ΔCCF 49

Chapter 3: Study of diffusion properties of SBD as a novel lipid raft marker 51-69
3.1 Introduction 51
3.2 Materials and Methods 52
3.2.1 Cell culture and plating 53
3.2.2 Incubation procedure of different markers 53
3.2.2.1 DiI 53
3.2.2.2 Bodipy FL Sphingomyelin 54
3.2.2.3 Cholera toxin 54
3.2.2.4 SBD-TMR and SBD-OG 54
3.2.3 Drug treatment 55
3.2.3.1 MβCD treatment 55
3.2.4 Instrumentation 55
3.2.4.1 Confocal FCS 55
3.2.4.2 ITIR FCS 55
3.3 Results 56
3.3.1 Comparison between different raft and non-raft markers 56
3.3.2 Comparison between raft and nonraft markers after cholesterol depletion 61
3.3.3 Effects of different laser powers on SBD and CTxB data due to varing extent of photobleaching 62
3.3.4 Effects of titrated cholesterol depletion by MβCD on the mobility of SBD 63

3.3.4.1 Confocal FCS results 63
3.3.4.2 ITIR-FCS results 65
3.4 Discussion 67
3.5 Summary 69

Chapter 4: SBD uptake pathway 70-89
4.1 Introduction 70
4.2 Materials and Methods 72
4.2.1 Cell Culture 73
4.2.2 si-RNA-Flotillin knockdown 73
4.2.3 Clostridium treatment 73
4.2.4 Combined drug treatment 74
4.3 Results 74
4.3.1 Kinetics of SBD internalization in SH-SY5Y neuroblastoma 74
4.3.2 Differentiation of intra- & extra- cellular SBD from the membrane bound fraction 75
4.3.3 Differentiation between intracellular and extracellular SBD 78
4.3.4 Inhibition Rho GTPase or flotillin affects interaction of SBD with the cell surface 80
4.3.5 Comparison of the effects of drug treatments with control experiments 84
4.4 Discussion 85
4.5 Summary 89

Chapter 5: Investigation of dynamic cell membrane organization 90-110
5.1 Introduction 90
5.2 Materials and methods 91
5.2.1 Cell culture and staining with markers 92
5.2.2 MβCD treatment 92
5.2.2.1 End point measurements 92
5.2.2.2 Time chase measurements 92
5.2.3 Latrunculin-A treatment 93
5.2.4 Instrumentation 93
5.3 Results 93
5.3.1 System compatibility 93
5.3.2 Autofluorescence of SHSY5Y Neuroblastoma cells 94
5.3.3 Independency of diffusion parameter with concentration 95

5.3.4 Autocorrelation based small scale organizational analysis 99
5.3.5 Cross-correlation based large scale organizational analysis 102
5.3.6 Confirmation of saturation of drug effect 108
5.4 Discussion 109
5.5 Summary 109

Chapter 6: Importance of sphingolipids and glycosphingolipids for microdomain organization 111-132

6.1 Introduction 111
6.2 Materials and Methods 113
6.2.1 Cell culture and staining with the markers 114
6.2.2 Alteration of sphingolipids content of the cell surfacet 114
6.2.2.1 Fumonisin B1 treatment 114
6.2.2.2 Recovery from Fumonisin B1 treatment 115
6.2.3 Alteration of glycosphingolipids content of the cell surfacet 115
6.2.3.1 NB-DNJ treatment 115
6.2.3.2 Adding back GM1 to the NB-DNJ treated cells 115
6.2.4 Alteration of sphingomyelin content of the cell surface 116
6.2.4.1 Sphingomyelinase treatment 116
6.2.4.2 Adding back Sphingomyelin to Smase treated cells 116
6.3 Results 117
6.3.1 Identification of raft like diffusion behavior of J116S 117
6.3.2 Effect of disruption of sphingolipid metabolism and recovery 118
6.3.3 Effect of inhibition of glycosphingolipid biosynthesis and recovery 123
6.3.4 Effect of sphingomyelin disintegration and recovery 127
6.4 Discussion 130
6.5 Summary 132

Chapter 7: Conclusion and Outlook 133-138

7.1 Conclusion 133
7.2 Outlook 136

References: 139-160

Summary

Cell membrane is a very interesting and widely studied research area due to its physiological importance. Membrane heterogeneity also gained interest over the last few decades due to their relevance with different diseases. The heterogeneity arises due to some membrane proteins surrounded by some selective classes of lipids. The lipids of interest to this work belong to the sphingolipid family. Faulty intracellular trafficking or storage of sphingolipids and cholesterol can lead to an array of lipid storage diseases. Therefore studies of sub-cellular movements of sphingolipids and domains consist of sphingolipids have high level of importance. The major limitation associated with the field of sphingolipid trafficking is lack of commercially available reliable markers that can be used to trace lipid microdomains or sphingolipids in living cells. The easily synthesizable molecular fluorophore conjugated, 25 amino acid sequence of Amyloid *beta* peptide has been characterized in this study, to test the hypothesis that this peptide, the Sphingolipid Binding Domain (SBD), could mediate tagging of the sphingolipid rich domains found in the plasma membrane that constitute rafts. For the characterization of SBD's diffusion behaviour on live cell surface, Fluorescence Correlation Spectroscopy, a widely used biophysical technique has been used in this study. Furthermore to visualize dynamic heterogeneous cell membrane organization traced by SBD, two new biophysical tool Imaging Total Internal Reflection-Fluorescence Correlation Spectroscopy (ITIR-FCS) and Imaging Total Internal Reflection-Fluorescence Cross Correlation Spectroscopy (ITIR-FCCS) has been introduced in this study. The thesis has been organized in the following manner:

Chapter one includes the motivation of the study and brief description about lipid rafts and organization of membrane lipids. The till now best known structural and biochemical properties of the peptide probe, SBD, have also been described in this chapter.

Chapter two is based on the descriptions of the experimental techniques used in this study, namely they are FCS, ITIR-FCS and ITIR-FCCS. The principle of the techniques, instrumental set ups and sequential measurement steps are illustrated there.

Chapter three compares the diffusion behaviour of SBD with other known raft- and non-raft associated markers on live SHSY5Y cell membranes using confocal FCS to check SBD's raft like slow movement on the cell surface. The histogram analysis of all the diffusion time values of SBD shows a bimodal distribution, consistent with some other reported studies. Further diffusion times of all the raft- and nonraft- associated probes have been compared on methyl beta cyclodextrin (MβCD) treated cells, to validate SBD's association with the plasma membrane on a cholesterol dependent manner. The outcome of this chapter suggests that, SBD can be used as a fluorescent tracer for the cholesterol-dependent, glycosphingolipid-containing slowly diffusing (raftlike) microdomains in living cells.

Chapter four focus on the cellular uptake path way of SBD, and propose the possible mechanism for SBD's bimodal diffusion distribution. Unlike other so far characterized microdomain-associated cargoes, SBD thought to be endocytosed approximately equally by two different pathways, one is cdc42-mediated, and the other is lipid-raft-associated adaptor protein, flotillin mediated. The experimental results show that, blocking of either flotillin or cdc42 dependent pathways results only in partial suppression of the uptake of SBD into cells, whereas knocking out both pathways simultaneously nearly eliminates uptake. This work suggests that these two pathways probably not separate, but that they are synergistic, or operate together. This part of the study summarizes that cdc42- and flotillin-associated uptake sites both correspond to domains of intermediate mobility, but they can cooperate to form low-mobility, and efficiently internalize domains.

Chapter five focus on the membrane heterogeneity and to visualize the dynamic organizations of cell membrane. In order to do so, this part of the study introduces a new suitable biophysical tool, ITIR-FCCS, that can incorporate spatial as well as temporal measurements of diffusing bodies. The organization of the liquid ordered phase, tracked by SBD, and the liquid disordered phase, represented by DiI, has been described in this part of the study. Further the cells were perturbed by the removal of cholesterol and by the disruption of the cytoskeleton to observe the relative difference in the dynamic organizations of these two phases. The results of this part narrates that the cytoskeleton is the main barrier to the diffusion of SBD and the coupling of SBD to the cytoskeleton is mediated by cholesterol.

Chapter six describes the importance of sphingolipids and glycosphingolipids for membrane microdomain organization. The dynamic properties of several raft- and non-raft associated probes including SBD have been looked under sphingolipid and glycosphingolipid disrupted conditions to describe the importance of these lipids in the dynamic cell membrane organization. Additionally, this chapter strengthens the application of ITIR-FCS and ITIR-FCCS as very promising biophysical tools to resolve membrane dynamics and membrane heterogeneity.

Chapter seven concludes the findings of the entire work of the thesis and envisions the possible future steps for further characterization of SBD to make it a more reliable sphingolipid tracer. The outlook of the story also discuss about the possible way to broadening the application of ITIR-FCS and ITIR-FCCS.

List of Figures

Figure 1.1: The Fluid Mosaic Model. 7

Figure 1.2: **S**chematic diagram for formation of lipid rafts in physiological condition. 9

Figure 1.3: Lipid organization in raft microdomains, a simplified model based on the theoretical shape of membrane lipids. 11

Figure 1.4: A common sphingolipid-binding domain in HIV-1, Alzheimer and prion proteins. 21

Figure 1.5: The representation of the conjugated spacer $[AEEAc]_2$ in SBD. 23

Figure 2.1: Explanation of autocorrelation function in the light of overlapping signals. 29

Figure 2.2: Changes in autocorrelation curve duo to the change in residence time of the fluorescent particles in the confocal volume. 30

Figure 2.3: Changes in autocorrelation curve duo to the change in concentration of the fluorescent particles. 31

Figure 2.4: Schematic representation of confocal FCS instrumental setup. 37

Figure 2.5: Schematic diagram of the imaging total internal reflection-fluorescence cross-correlation spectroscopy (ITIR-FCCS) setup. 44

Figure 2.6: Experimental steps for ITIRFCS and ITIRFCCS measurements. 46

Figure 2.7: Graphical representation explaining CCF and ΔCCF for homogenous and heterogeneous systems. 49

Figure 3.1: Correlation curves of SBD-TMR versus other raft and nonraft markers. 57

Figure 3.2: The G(τ) graph of auto-fluorescence of SHSY5Y and autocorrelation curve of SBD-TMR in solution. 58

Figure 3.3: The distributions of diffusion times and average diffusion times for SBD along with raft- and nonraft markers before and after cholesterol depletion. 60

Figure 3.4: Correlation curves of SBD-TMR versus other raft and nonraft markers under cholesterol depleted condition. 61

Figure 3.5: Average τ_D for SBD-TMR, CTxB and DiI different laser powers. 63

Figure 3.6: The distribution of diffusion times for SBD-TMR under different extent of cholesterol depletion. 64

Figure 3.7: Average diffusion times for SBD-TMR, measured on the upper and lower membrane with confocal FCS and ITIR-FCS instrument respectively with varying concentrations of MβCD. 65

Figure 3.8: Pictorial representation for the diffusion times of SBD-TMR at each pixel of the whole ROI after treatment with varying concentrations of MβCD. 66

Figure 4.1: Uptake rate of SBD into human neuroblastoma SH-SY5Y cells. 75

Figure 4.2: Proper focusing condition for the membrane measurements. 76

Figure 4.3: Autocorrelation curves obtained for extracellular membrane bound intracellular signals. 77

Figure 4.4: Extracellular vs. cytosolic τ_D values for SBD. 79

Figure 4.5: Flotillin-2 and a Rho family GTPase dependency of SBD uptake. 81

Figure 4.6: Both flotillin and Rho family GTPase are required for the slow raft-like diffusion component of SBD. 83

Figure 4.7: Unaffected diffusion of non-raft marker, DiI under SiRNA flotillin-2 and clostridium treatment. 85

Figure 4.8: Model showing proposed origin of the slow-, medium- and fast-diffusing SBD components. 87

Figure 5.1: Representative ACFs of single pixels obtained from background measurements, the autofluorescence of human Neuroblastoma (SHSY5Y) cells, and SBD-TMR labeled cells. 94

Figure 5.2: 1x1 binned number of particle and diffusion time images for the autofluorescence of SHSY5Y cells. 95

Figure 5.3: Quantitative pictorial representations of number of particles and diffusion times of no drug treated control cell membranes during the time chase experiments. 97

Figure 5.4: ACF images of same position of SBD-TMR labeled single cell after various times of incubation with MβCD. 98

Figure 5.5: Effects of MβCD and latrunculin-A treatments on the diffusion coefficients of SBD- and DiI-labeled cells. 100

Figure 5.6: ΔCCF histograms at different incubation times for cells labeled with SBD after Latrunculin-A and MβCD treatments. 103

Figure 5.7: Development of the kurtosis of the ΔCCF distributions for cells labeled with DiI and SBD with different drug treatments. 104

Figure 5.8: ΔCCF histograms at different incubation times for cells labeled with DiI after Latrunculin-A and MβCD treatments. 105

Figure 5.9: ΔCCF images of cells labeled with SBD-TMR at different time points of incubation with Latrunculin-A and MβCD. 107

Figure 5.10: ΔCCF distributions of SBD-TMR on SHSY5Y cell membranes, untreated and MβCD treated cells for longer incubation times. 108

Figure 6.1: The comparison of distribution of diffusion times for J116S with other raft associated markers SBD and CTxB. 118

Figure 6.2: Gradual effects of Fumonisin B1 treatment at different time points of the incubation. 119

Figure 6.3: Effects of disruption of the sphingolipid metabolism on different markers at different phases of the experiments. 121

Figure 6.4: Gradual effects of Fumonisin B1 treatment over the entire incubation period on the distributions of the ΔCCF histograms of different markers. 122

Figure 6.5: Effects of inhibition of glycosphingolipid biosynthesis at different phases of the experiments. 124

Figure 6.6: Effects of inhibition of glycosphingolipid biosynthesis on different markers at different phases of the experiments. 126

Figure 6.7: Gradual effects of disintegration of sphingomyelin into ceramide and phosphocholine on different markers at different time points of the incubation period. 127

Figure 6.8: Effects of disintegration of sphingomyelin on different markers at different phases of the experiments. 128

List of Tables

Table 5.1: Average diffusion coefficients of raft and non-raft markers before and after Latrunculin-A and MβCD treatments. 101

Table 6.1: Average diffusion coefficients of raft and non-raft markers before any drug treatment, FB1, NB-DNJ, Smase treatments and recoveries from respective treatments. 130

Abbreviations Actual phrase

ΔCCF	Difference in cross-correlation functions
2D-1P-1T	Two dimentional one particle one triplet
2D-2P-1T	Two dimentional two particle one triplet
3D-1P-1T	Three dimentional one particle one triplet
3D-2P1T	Three dimentional two particle one triplet
AC	Apochromat
ACF	Autocorrelation function
AD	Alzheimer's disease
AEEAc	Amino ethoxy ethoxy acetyle
APD	Avalanche photodiode
App	Amyloid precursor protein
ATCC	American Type Culture Collection
Aβ	Amyloid beta peptide
CCD	Charge Coupled Device
CCF	Cross-correlation function
CLIC	Clathrin-independent endocytic pathway
CTxB	Cholera toxin subunit B
DC	Dichroic mirror
DiI	1,1'-dioctadecyl-3,3,3',3'-tetramethylindocarbocyanine perchlorate
DMEM	Dulbecco's Modified Eagle's Medium
DMSO	Dimethyl sulfoxide
DRM	Detergent Resistant Membrane fractions
EMCCD	Electron Multiplying Charge Coupled Device
ER	Endoplasmic reticulum
ERC	Endocytic recycling compartment
FB1	Fumonisin B1
FBS	Fetal bovine serum
FCS	Fluorescence Correlation Spectroscopy
FGFR	Fibroblast growth factor receptors
FGR	Fibroblast growth factors
Fig	Figure
GEEC	GPI-AP-enriched early endosomal compartments
GFP	Green fluorescent protein
Glu	Glutamic acid
GPI	Glycosylphosphatidylinositol
GPI-AP	Glycosylphosphatidylinositol anchored protein
GPL	Glycerophospholipid
GPMV	Giant Plasma Membrane Vesicle
GSL	Glycosphingolipid

HBSS	Hank's Buffered Salt Solution
HEPES	4-(2-hydroxyethyl)-1-piperazineethanesulfonic acid
HIV	Human immunodeficiency virus
ICS	Image Correlation Spectroscopy
ICCS	Image Cross-correlation Spectroscopy
ITIRFCS	Imaging Total Internal Reflection Fluorescence Correlation Spectroscopy
ITIRFCCS	Imaging Total Internal Reflection Fluorescence Cross Correlation Spectroscopy
Lat-A	Latrunculin-A
L_d	Liquid disordered phase
L_o	Liquid ordered phase
LO	Lipoxygenase
Lyn	Lysine
MCL	Mantle cell lymphoma
Min	Minute
MV	Measles virus
MβCD	Methyl beta-cyclodextrin
NBDNJ	N-Butyldeoxynojirimycin
NF	Neutral density filter
OG	OregonGreen
OL	Oligodendrocyte
PBS	Phosphate saline buffer
PM	Plasma membrane
PMT	Photomultiplier tube
PSF	Point spread function
RICS	Raster Image Correlation Spectroscopy
ROI	Region of interest
SBD	Sphingolipid binding Domain
SM	Sphingomyelin
Smase	Sphingomyelinase
SPR	Surface Plasmon resonance
STICS	Spatio-temporal Image Correlation Spectroscopy
TGN	Trans-Golgi network
TIR	Total Internal Reflection
TIRFM	Total internal reflection fluorescence microscopy
TMR	Tetramethylrhodamine
UV	Ultra violet

Symbols Actual name

ρ	Mass density of molecule
µg	microgram
µl	micro liter
µM	micro molar
µm	micrometer
µW	micro Watt
η	viscosity of solution
τ_D	Diffusion time
ω	radial distances of the confocal volume
D	Diffusion coefficient
$G(\tau)$	Autocorrelation Function
g	gram
k	Boltzmann's constant
k	kurtosis
K	Structure factor
M	mass of a single molecule
mg	milligram
MHz	mega Hertz
ml	milliliter
mM	milli molar
mm	millimeter
ms	millisecond
N	Number of particle
nM	nano molar
R	hydrodynamic radius
s	second
T	Absolute temperature
V	volume
V_{eff}	effective detection volume
z	distances of the confocal volume

List of Publications

1. Sarita Hebbar, Esther Lee, **Manoj Manna,** Steffen Steinert, Goparaju Sravan Kumar, Markus Wenk, Thorsten Wohland and Rachel Kraut.
   A fluorescent sphingolipid binding domain peptide probe interacts with sphingolipids and cholesterol-dependent raft domains; **Journal of Lipid Research 2008, 49(5), 1077-1089.**

2. Zhang Dawei, **Manoj Manna,** Thorsten Wohland, and Rachel Kraut
   Alternate raft pathways cooperate to mediate slow diffusion and efficient uptake of a sphingolipid tracer to degradative vs. recycling pathways.
   Journal of Cell Science 2009, 122, 3715-3728.

3. Jagadish Sankaran[†], **Manoj Manna[†],** Guo Lin, Rachel Kraut, Thorsten Wohland
   Diffusion, transport, and cell membrane organization investigated by imaging fluorescence cross-correlation spectroscopy.
   Biophysical Journal, 2009, 97(9), 2630-2639
   [†] **These two authors contributed equally to this work.**

4. **Manoj Manna,** Guillaume Tresset, Tobias Braxmeier, Gary Jennings, Thorsten Wohland, Rachel Kraut
   TIRF-based spectroscopic analysis of plasma membrane diffusion behavior reveals coexisting lipid- and cytoskeleton-controlled heterogeneities of distinct length-scales.
   [***Manuscript ready to communicate***].

Chapter 1:
Introduction

1.1 Motivation of the work

The main goal of this study is to observe the characteristic diffusion behavior of lipid raft- or sphingolipid-interacting probes on live cell membrane, and how that behavior depends on raft components and cytoskeleton.

Plasma membrane lipids consist of phospholipids, also sphingolipids, glycolipids and sterols. The lipids of interest to this work belong to the sphingolipid family, namely, glycosphingolipids [GSLs], sphingomyelin, and ceramide all of which contain a ceramide backbone. Sphingolipids, associate preferentially on the plasma membrane into cholesterol-rich nano-domains, referred to as lipid rafts **[1]**, which are mainly found on the extracellular leaflet of the lipid bilayer and are involved in signaling the endocytic vesicular trafficking **[1, 2]**. These domains and the lipid species found within them have also been implicated in neurodegenerative diseases such as Alzheimer's, Parkinson's, Niemann-Pick disease **[3-8]** and are trafficked through the degradative (endolysosomal) and secretory (Golgi) pathways of the cell **[9, 10]**. Complex sphingolipid derivatives, like glycosphingolipids (GSLs) and sphingomyelin, get broken down to their component parts, including lipids and sugars, via the degradative pathway in lysosomes **[11]**.

Simpler sphingolipids, e.g. ceramide, get modified by the addition of a head group (ethanolamine, choline, or polysaccharide) in the Golgi, and thereafter are transported back to the plasma membrane **[12-14]**. Faulty intracellular trafficking and storage of sphingolipids and cholesterol due to either deficit in enzymes that break down sphingolipids, or defects in lipid transport failure can lead to an array of lipid storage diseases **[15-18]**. These diseases cause

accumulation of sphingolipids and cholesterol in the endolysosomal compartment, and lead to neurodegeneration and mental retardation. Trafficking of cholesterol is believed to occur through a related pathway to that of sphingolipid transport, though cholesterol and sphingolipid storage and trafficking appear to be interdependent **[19]**.

The levels of cholesterol and sphingolipids in Alzheimer's afflicted neurons may affect the processing of the amyloid precursor protein (App) which gets cleaved possibly within the raft domains, to the amyloidogenic form (Aβ), **[20, 21]**. This is released from cells and aggregates to form "senile plaques", which are the pathogenic hallmark of the disease. Since the lipid raft-borne sphingolipids and cholesterol are thought to be involved in the pathogenesis of different disease including Alzheimer's, it is interesting to characterize their sub-cellular behavior (mainly on the membrane for this study), which will help to identify the processes that lead to aberrant lipid accumulations that are associated with those diseases.

The major limitation associated with this field is, that currently there are no well known reliable markers that can be used to trace lipid microdomain or sphingolipid trafficking in living neurons or other cells. Several groups including Pagano's group have characterized these lipid analogs and have used fluorescently labeled sphingolipid analogs (BODIPY-ceramide, BODIPY-GSLs, and BODIPY-sphingomyelin) in artificial membranes and cultured neuroblastoma, fibroblast and other cell types. They assayed the trafficking behavior of these lipids in normal vs. diseased cells or under perturbed conditions that simulate the disease state **[22-24]**. Although these fluorescent lipid analogs are useful, serious questions have been raised regarding their biophysical behavior in the membrane. According to Pagano and colleagues, these sphingolipid analogs are properly metabolized, but other studies show that they do not behave like endogenous sphingolipids in the membrane, as aberrant orientation of the lipid chains has been observed, as well as abnormal trafficking behavior **[25, 26]**. Several studies with artificial membranes suggest strongly that these lipids do not show the same type of

behavior as would be expected if they occupied the lipid microdomains. Pagano's group have shown that BODIPY labeled sphingolipids do get metabolized in their experiments on several cell lines including HeLa, rat fibroblasts, implying that these lipids at least partially traffic through the expected intracellular pathways **[27]**. In this context it has to be kept in mind that there may be differences in the behavior of artificial membranes vs. real cells, and that statements can be made only by comparing different types of lipids in relation to each other as well as their behavior in perturbed systems, even though they don't strictly reflect the *in vivo* situation.

The group of Kobayashi has developed a toxin known as lysenin from the earthworm as a lipid raft and intracellular trafficking tracing molecule **[28]**. Lysenin binds strongly and specifically to sphingomyelin, which is found in lipid rafts. The problem associated with this molecule is that, it is very large (~300 amino acids, and ~240 amino acids in its minimal non-toxic truncated form), and has been expressed by Kobayashi only as a GFP fusion protein, whose synthesis is not easy to manipulate.

Although various people use lysenin-GFP [**29**], perfringolysin-O-GFP [**30**], non-invasive small-molecule tracers that can be used to visualize the binding and trafficking of sphingolipid containing microdomains are currently not commercially available. Therefore, it would be advantageous to design modified smaller versions of lysenin or other toxin peptides, which would be easily synthesizable and conjugable with small fluorophore molecules. It is possible that peptides can be derived from various naturally occurring toxins and GSL-binding proteins that can be used as lipid-specific tracers or diagnostic tools. Along these lines, the establishment of a potential marker as a tool to distinguish the different pathways of various types of sphingolipids and their behavior in perturbed conditions (e.g. cholesterol modification, mutation) has been chosen as the ultimate goal of this project.

The motivation of the study was to carry out a biophysical characterization of the sphingolipid-containing plasma membrane domains. The link of sphingolipids and sphingolipid-rich membrane domains to degenerative diseases, particularly the sphingolipid storage diseases, has been well-established **[31]**. These sphingolipid storage diseases have much in common with neurodegenerative diseases such as Alzheimer's, and they seem to affect similar intracellular trafficking processes (e.g. lysosomal function, amyloid peptide generation, and sphingolipid accumulation) **[32-34].** The molecular fluorophore conjugated, 1st 25 amino acid sequence of Aβ, derived from the Amyloid precursor protein (App), and termed sphingolipid-binding domain (SBD), has been analyzed in this study, to test the hypothesis that this peptide will mediate tagging of the sphingolipid rich domains found in the plasma membrane that constitute rafts. By structural analysis, the sphingolipid-binding domains found in several proteins, have similar conformation to the V3-like domain of gp120 of HIV-1 and Prion Protein (*Fig. 1.4*), suggesting a common mechanism that is used by HIV- 1, prion and Alzheimer proteins to interact with lipid rafts **[3]**. An important consideration in this context is that the raft-borne sphingolipids of interest are located to the outer leaflet of the plasma membrane, presenting a topological problem for GFP-based probes that are produced intra-cellular. Therefore, a sphingolipid-targeted exogenous probe for live imaging studies would be a useful tool in studying diseases whose pathogenesis is glycosphingolipid-dependent. Moreover, a sphingolipid-binding-fluorophore probe (like SBD) more faithfully mimics the actual situation encountered by a neuron when attacked by an extracellular virus or the Alzheimer amyloid peptide. That is why it may be a more effective tracking tool among the others.

After successful completion of this project, the established fluorescent-sphingolipid-binding peptide would be a powerful tool to examine the distribution and trafficking routes of sphingolipids in cell. Further development of this method could lead to diagnostic tools and/or drug screening methods involving imaging of the peptide in affected cells/neurons.

1.2 Microdomains

1.2.1 Introduction to lipid microdomains/rafts

According to the definition by Kai Simons, "Lipid rafts are fluctuating nanoscale assemblies of sphingolipids, cholesterol and proteins that can be stabilized to coalesce, forming platforms that function in membrane signaling and trafficking" **[35].** The raftophilic membrane proteins localize to these compartments probably because of protein-protein interaction and/or their affinity for the raft associated lipids [**36-38**]. These raft associated proteins are normally linked to the actin cytoskeleton and play important roles in holding these clusters together [**36**]. According to Kusumi *et al.*, the plasma membrane naturally contains dynamic structures, e.g. molecular complexes and domains that exist in various sizes and are forming and dispersing continually at different time scales within the cell membrane [**39**]. These microdomains can be considered as small (probably on the order of 5-10 nm diameter) rafts floating on the more-liquid glycerolipid-rich bulk of the plasma membrane. Compared to this glycerolipid-rich surrounding lipid bilayer, the rafts are more ordered, where cholesterol might function as a dynamic glue [**40**]. These specialized microdomains compartmentalize cellular processes by serving as organizing platforms for the assembly of signaling molecules and form a less fluid, more ordered phase. Moreover they play important roles in membrane protein trafficking, receptor trafficking, regulating neurotransmission as well as activation of the immunological synapse, and numerous other signaling events **[41, 42]**. In addition, lipid rafts serve as portals for the entry of various pathogens, including viruses, bacteria and toxins, including Aβ and prion protein **[3]**. Some interesting evidence indicates that lipid rafts are involved in the formation of amyloid plaques in Alzheimer's diseases through the interaction of Aβ with certain raft lipids, in particular the highly sialylated gangliosides **[35]**. Therefore, the study of lipid rafts and their role in cell biology and medicine gained interest over the last couple of decades.

1.2.2 Development of membrane heterogeneity as an emerging field

The existence of membrane microdomains was postulated in the 1970s based on experiments using biophysical approaches by Stier & Sackmann **[44]** and Klausner & Karnovsky **[45]**; however, until 1982, it was widely accepted that the phospholipids and membrane proteins were randomly distributed on a homogeneous phase of cell membranes, proposed in Singer-Nicolson's fluid mosaic model **[46]**. According to that model, membrane lipids are a two-dimensional solvent phase for membrane proteins (*Fig. 1.1*).

The above postulated microdomains were attributed to the physical properties and organization of lipid mixtures by Stier & Sackmann and Israelachvili *et al.* **[44, 47]**. The description of biological membranes as a 'mosaic of lipid domain' rather than a homogeneous fluid mosaic, and the proposal of "clusters of lipids" first emerged in 1974, due to the effects of temperature on membrane behavior [**49**]. In 1978, X-Ray diffraction studies led further to the development of the "cluster" concept defining the microdomains as "lipids in a more ordered state". Karnovsky and co-workers formalized the concept of lipid domains in membranes in 1982, which again indicated that there were multiple phases of the lipid environment on the membrane **[45]**. The existence of these cholesterol and sphingolipid rich microdomains, formed due to the segregation of these lipids into a separate phase, was shown to exist on the artificial membranes in 1979 **[49]** and cell membrane in 1982 **[50]**. Later, Kai Simons and Gerrit van Meer refocused interest on these glycolipids, sphingolipids and cholesterol enriched membrane microdomains, and subsequently, called these postulated microdomains "lipid rafts" **[51]**. From then onwards lipid rafts gained attention for studies of cell membranes, trafficking, receptor-mediated signal transduction, and lipid- associated diseases **[3-8, 15-18]**.

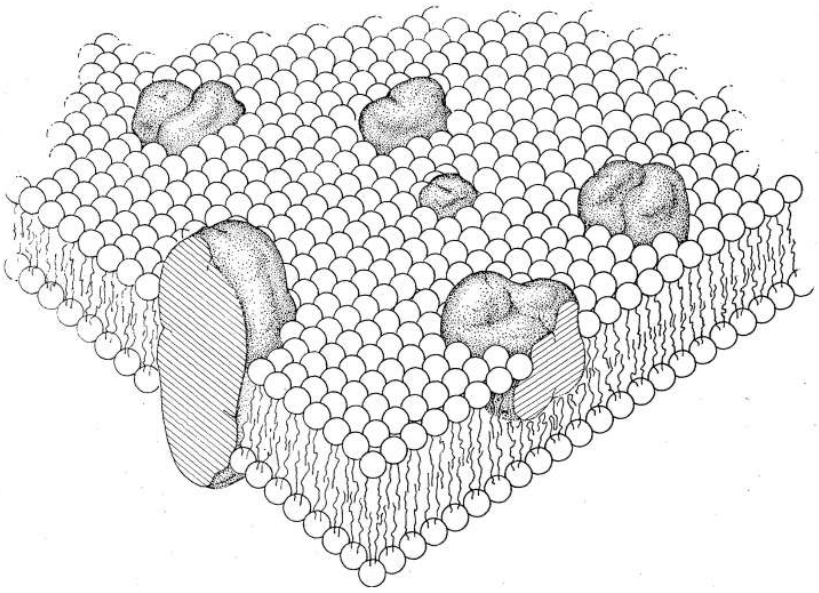

[*Picture from: S.J. Singer et al. 1972, Science, 175, 720–731.*]

***Figure 1.1*:** *The Fluid Mosaic Model.*

The original concept of rafts was used for explaining the transport of mainly sphingolipids and cholesterol from the trans-Golgi network to the plasma membrane, and was more formally developed in 1997 by Simons and Ikonen **[1]**. But still controversies persisted regarding the size and lifetime of these rafts and their biological / physiological relevance to *in vivo* systems. In recent years, lipid raft related studies are trying to address many of these key issues that caused those controversies **[42, 52, 53]**. At the 2006 Keystone Symposium of Lipid Rafts and Cell Function, lipid rafts were defined as "small (10-200nm), heterogeneous, highly dynamic, sterol- and sphingolipid-enriched domains that compartmentalize cellular processes. It was also stated there that the “small rafts can sometimes be stabilized to form larger platforms through protein-protein interactions”. Baumgart [**54**], Veatch & Keller [**55**], and others have studied the miscibility behaviour of lipid phases in giant plasma membrane vesicles (GPMVs) that are isolated directly from living cells. According to their demonstration, GPMVs contain two liquid phases at low temperatures and one liquid phase at high temperatures. Their study suggests that the compositions of mammalian plasma

membranes reside near a miscibility critical point and the heterogeneity in present in the GPMVs at physiological temperatures may be related to functional lipid raft domains in live cells [**54**]. Still there are several other questions yet to be answered in the field of lipid raft, for example, the dynamic partitioning of membrane lipids and lipid rafts [**17**], quantitative comparison of the different lipid compositions of rafts, miscibility of raft associated lipid components, proper life time/existence time of raft clusters [**39**], proper description of physiological functions of these lipid rafts. The effects of different lipid-perturbing and cytoskeleton disrupting drugs on the mobility of rafts and raft associated lipids have been described in this study.

1.2.3 Formation of lipid rafts in live cells

It has been documented several times that the lipid rafts are composed of membrane proteins surrounded by sphingolipids and cholesterols, but it is also important to note their formation at physiological conditions, which has been described schematically in *Fig. 1.2*.

Cholesterol and sphingolipids are synthesized in the endoplasmic reticulum (ER) **[56]**. Most of this synthesized cholesterol is transported directly from ER to the plasma membrane (PM) through a non-vesicular process. Non-vesicular transport from ER to PM proceeds via cytosolic FK506 binding protein 4 (FKBP4) and Caveolin-1 containing complex **[57, 58]**.

Relatively small amounts of cholesterol and *de novo* synthesized sphingolipids (mainly sphingomyelin) are transported from the ER to Golgi. Excess cholesterol in the ER is normally esterified by acyl-Coenzyme A: cholesterol acyl transferase 1 (ACAT1) and the esters are then stored in the form of cytoplasmic lipid droplets **[59]**, where the cholesteryl ester transfer protein (CETP) transports these cholesteryl esters into those storage droplets **[60]**. ACAT1 in ER is compartmentalized close to the endocytic recycling compartment (ERC) and very close to trans-Golgi network (TGN), but far from cis, medial Golgi **[61, 62]**.

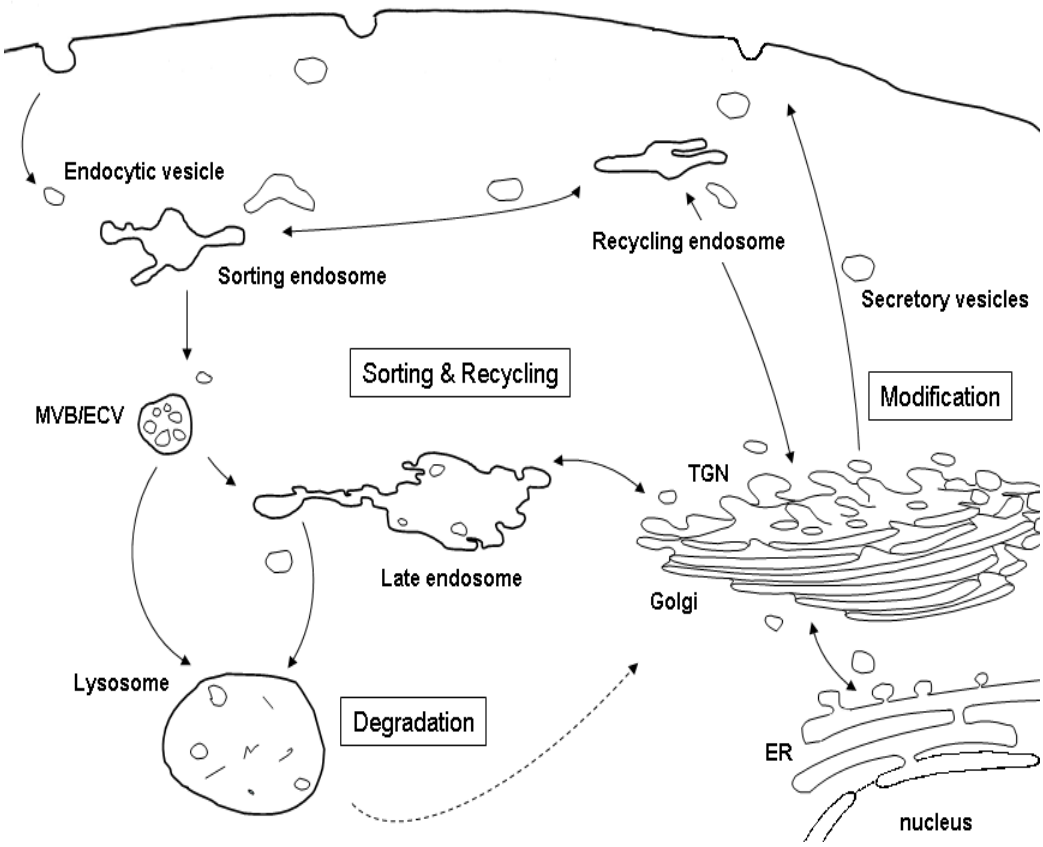

[*Picture by Steffen Steinert*]

***Figure 1.2*:** *The schematic diagram for formation of lipid rafts in physiological conditions. Production and transportation pathway of cholesterol and sphingolipids from ER to the plasma membrane via Golgi and recycling of the components via Endocytic vesicles are shown here.*

Since both TGN and ERC are engaged in extensive membrane traffic, these compartments might also play a role in esterification of cholesterol in membranes **[63]**. Gradually the concentration of cholesterol and sphingolipids increases in trans-Golgi network leading to the formation of rafts **[64]**. These caveolae or transport vesicles that contain cholesterol/sphingolipid-rich membrane patches are then assembled in the Golgi first and transported towards the plasma membrane to form rigid, less mobile clusters **[64]**. Lectin, mannose-binding protein (VIP 36) is one of the proteins which coordinate the polar traffic of caveolae to the plasma membrane **[65-67]**. These proteins receive these cargos (sphingolipids and cholesterol) from carriers, endosomes, lipid droplets or even directly from ER. The pool

of sphingolipids is enriched with sphingomyelin that is newly synthesized by sphingomyelin synthase 1 (SMS1) in ER as mentioned earlier. Sphingolipids move to the apical plasma membrane **[64, 66, 68]**, but unlike cholesterol, sphingomyelin is transported to the apical membrane preferentially in the vesicles **[69]**. These accumulated ordered structures form the so called rafts and the lipid components are recycled via the endocytic pathway.

1.2.4 Properties of lipid microdomains/rafts

1.2.4.1 Structural properties

The most important factor behind the cluster packing of membrane lipids is their amphipathic character, which contain a polar, hydrophilic head group region and a non-polar, hydrophobic part. In aqueous condition, these amphipathic lipid molecules normally orient themselves in such a way, so that the polar head groups associate with water molecules, whereas the hydrophobic chains interact with each other to exclude a maximal number of water molecules from the hydrophobic phase. The basic compositional difference between rafts and the surrounding plasma membranes is the difference in lipid composition and cholesterol content. Cholesterol preferentially interacts with the sphingolipids through hydrogen bonding with the amide groups containing backbone. Glycerophospholipids don't have this amide groups to interact with cholesterol.

According to another model, the function called "umbrella-ing" has also some role to play, as the spaces left between the bulky GSL headgroups, are thought to be filled by cholesterol molecules. The saturated chains of sphingolipids allow them to pack tightly together through van der Waals interactions, forming a more ordered phase (Liquid ordered phase L_o) at physiological temperature from which GPLs are excluded **[3]**. In addition, sphingolipids may associate among themselves through hydrogen bonds between the hydroxyl (OH) group of the sphingosine base and the amide group on the backbone. Simultaneously this self

association of sphingolipids results in a decrease in the phosphatidylcholine levels in the raft regions compared to that of the surrounding plasma membrane. Thus, the ratio of the lipids with saturated hydrophobic chains to the lipids with unsaturated hydrophobic chains is higher in the rafts, compared to that of the surrounding bilayer, usually referred to as the liquid disordered (L_d) phase **[42]**.

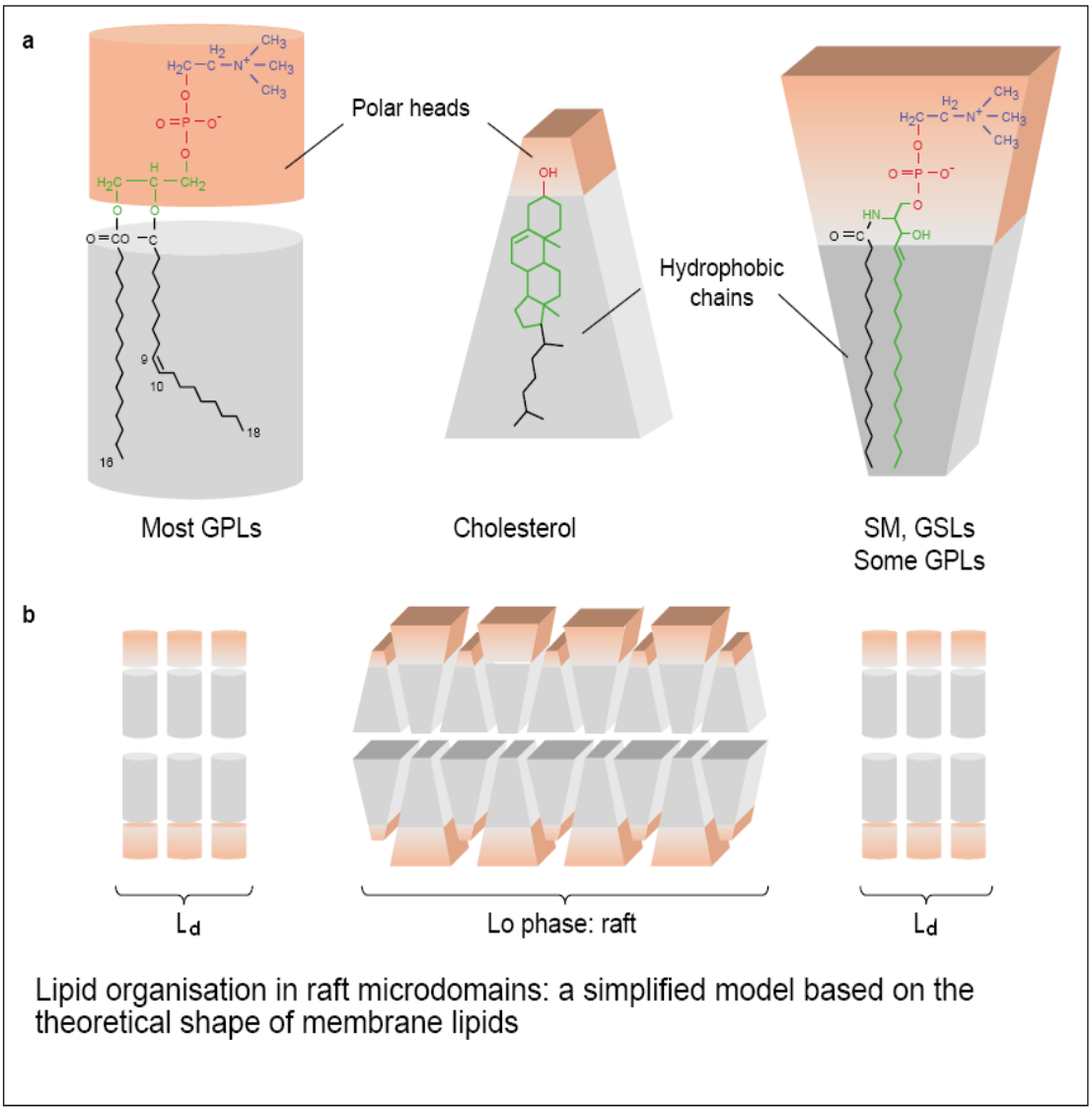

[Picture from J. Fantini, *et al*. 2002, E*xp. Rev. Mol. Med.*, 4 (27), 1-22.]

Figure 1.3: *(a) Glycerophospholipids (GPLs), which form the L_d phase of the plasma membrane, are normally cylindrical in shape; however, cholesterol and sphingolipids [especially glycosphingolipids (GSLs)] have a pyramidal or cone-like shape. In glycosylated sphingolipids the polar head group occupies a larger area than the hydrophobic region, whereas the scenario is reverse for cholesterol and ceramide. (b) The remarkable fit between the global shape of cholesterol and sphingolipids; cholesterol functioning as a molecular spacer. The enrichment of cholesterol in L_o phase domains is consistent with this model.*

Although not all of the sphingolipids within the rafts are fully saturated, still they are much more tightly packed compared to the liquid disordered phase; where the GPLs are in a loosely packed disordered state. Due to the rigidity of the sterol, cholesterol preferentially partitions into the raft phase **[42]**. Cholesterol has the ability to pack in between the lipid tails in rafts, serving as a molecular spacer and filling any voids between associated sphingolipids, making the cluster more rigid **[3]**. A simplified model of lipid organization in raft microdomains based on the theoretical shape of membrane lipids is shown in *Fig. 1.3*.

1.2.4.2 Biochemical properties

Because of the high degree of hydrogen bonding between lipid molecules, lipid rafts are relatively insoluble in certain detergents such as Triton X-100 **[70, 71]**, and are sometimes referred to as Detergent Resistant Membrane fractions (DRMs). On sucrose density gradients, the rafts can be readily purified as DRMs by ultracentrifugation in the form of molecular complexes from the buoyant fractions. The migration of DRMs with these low-density layers is consistent with the relatively high lipid content of these fractions. The morphological analysis of these DRMs by transmission electron microscopy revealed the presence of small membrane vesicles, though without any confirmation whether these are isolated endosomes, or microsomes resulting from the harsh purification procedure **[70]**. Biochemical analysis demonstrated a specific enrichment of GSLs, sphingomyelin and cholesterol in these DRMs. However, with the exception of phosphatidylinositol, these fractions are relatively poor in GPLs. In agreement with the concept that acyl chain saturation favors raft association, the GPLs present in the DRMs consist of mainly saturated and monounsaturated lipids, rather than polyunsaturated acyl chains **[72]** found in the disordered fluid phase of the membrane. However, the validity of the detergent resistance methodology, which requires isolation of membranes at 4°C, has recently been questioned due to the ambiguities in lipids and proteins

recovered. Moreover, it has been observed that the method itself can cause formation of phase separated clusters **[73]**. This emphasized the necessity to improve the solubilisation procedures that will certainly help to clarify the structure and dynamics of lipid rafts in the plasma membrane. Drevot *et al*. came up with a solution in the form of Brij 98 which can be used to prepare detergent-insoluble, raft-like microdomains at 37°C **[74]**. But irrespective of the detergent or the experimental condition, this method depends on the partition of lipids and proteins into detergent micelles, and produces a picture that does not directly report on the organization of native membranes. Hence, it is clear that biochemical studies alone are not sufficient to visualize rafts, and a reliable alternative method is needed.

1.2.4.3 Biophysical properties

In order to understand the membrane organization retaining the raft morphologies, biophysical approaches with intact artificial or real cell membranes gained interest over the biochemical methods **[75, 76]**. For example, the co-localization of several raft proteins with the ganglioside GM1 has been demonstrated in various cell types by confocal microscopy. Lateral segregation of specific molecules in the construction of signaling units and sorting platforms is the structural basis of rafts **[1]**. Quantitative spectroscopic microscopy techniques such as fluorescence resonance energy transfer, fluorescence correlation spectroscopy, fluorescence anisotropy measurements, provided the evidence for the existence of rafts *in vivo*, and allowed the researchers to carry on studies to evaluate the size and other biophysical characterization of these membrane heterogeneities referred as rafts **[52, 53, 77-81]**.

Rietveld & Simons first said that the physical properties of the liquid ordered (L_o) and liquid disordered (L_d) phase are not the same and showed the immiscibility of these two phases in model membranes **[82]**. Although the cause of this immiscibility is uncertain, it is thought that the immiscibility minimizes the free energy between the two phases [**83**]. Further studies

have confirmed that there is a difference in thickness of the lipid rafts and the surrounding membrane **[84, 85]** which results in hydrophobic mismatch at the boundary between the two phases. But the more interesting and obvious question was the size and spatial distributions of these domains on live cell surfaces.

Previously, there were lots of debates on the size of rafts, not suggesting a particular dimension but a distribution ranging from 10 to 200 nm **[86-88]** depending on the type of cell lines investigated and circumstances, like whether they've been induced to coalesce by cytokines or ligand binding **[36]**. A recent study by Goswami *et al*. suggests that these heterogeneities of the cell surface are organized on at least two length scales; one at the nano scale (~10 nm) and the other in optically resolvable scale (~450 nm) **[52]**. The large scale domains have properties similar to that of so called rafts. These clusters or rafts are cholesterol dependent and the organization on the cell surface is regulated by the actin cytoskeleton **[52, 89]**. Pinaud *et al.* have shown by single particle tracking (SPT) that GPI anchored proteins can pass GM1-clustered rafts unhindered. These clusters are laterally immobile but can form and dissolve at physiological temperature **[53]**. Smaller clusters sometimes stabilize by forming larger platforms through protein-protein or protein-lipid interaction **[90]**. Lectins, the multivalent glycoprotein-binding proteins are able to cluster rafts at the plasma membrane [**91**]. Apart from classic ligands and cytoskeletal scaffolds, this lectin-mediated clustering is an important phenomenon that could tell us more about raft dynamics **[92]**.

Together the diffusion parameters of different markers associated with the rafts and non-raft phase of the plasma membrane can indicate about the existence of membrane heterogeneity **[89]**. The raft associated markers have been documented in this work, and by others, to show bimodal distributions for their diffusion on live cell surface **[53, 89]**. Kusumi *et al.* proposed a model on cell surface dynamics where individual protein and lipid molecules at the plasma

membrane undergo short-term confined diffusion within a confined compartment and hop diffusion between the compartments, with an average hop frequency of once every 1–20 ms **[39]**. According to their model the restricted/hop diffusion is confined within membrane compartments boundaries consist of actin anchored proteins. These actin anchored-proteins can temporarily confine phospholipids, and the phospholipids themselves can also undergo hop diffusion [**94**]. In a recent review, Kusumi describes the plasma membrane as a heterogeneous entity, which contains diverse structures and compartments with a variety of lifetimes, where certain membrane molecules stay together for limited durations [**95**]. Within each membrane compartment several small rafts may exist, where the raft-associable molecules may enter and/or exit continuously. According to the model, these rafts form and disperse rapidly and capriciously, and can also coalesce and disintegrate [**95**]. Consistent with the model, this dynamic partitioning of diffusive behavior of raft associated markers is due to the random entry and exit of the raft associated proteins from these heterogeneous clusters **[53]**. Cholesterol depletion or cytoskeleton disruption resulted in faster movements of the raft associated markers indicating the reorganization of the membrane with faster diffusion coefficients, which has been supported by the results of this work as well **[77, 85, 96-98]**.

1.2.5 Functions of lipid rafts

It is well accepted that rafts phases are involved in signal transduction **[99]** and intracellular trafficking of lipids and proteins **[100]**, and they serve as the preferential sites for host–pathogen/toxin interactions as well **[101]**. Rafts also appear to be involved in the generation of pathological forms of proteins associated with Alzheimer's and prion diseases **[102, 103]**.

1.2.5.1 Role of lipid rafts in signal transduction pathways

Due to their ability to diffuse laterally on the plasma membrane, rafts can act as floating shuttles that transport and bring together activated receptors and transducer molecules **[104]**. In addition, certain raft-associated scaffolding proteins are associated with these lipids in a specific manner. Caveolin is one such protein, which binds to cholesterol. Presence of this protein within a lipid scaffold results in a structure on the plasma membrane called a caveola **[105].** Caveolae were originally identified ultrastructurally as local invaginations (50–100 nm diameters) of the plasma membrane in endothelial and epithelial cells **[105]**.

Following are some examples that show the proteins enriched in raft fractions, can play crucial roles in signal transduction:

(*i*) External proteins can bind to the outer leaflet of the plasma membrane by a GPI anchor (e.g. the GPI-linked form of prion protein PrP-c). GPI associated proteins are anchored on the external leaflet of the plasma membrane by two saturated chains (1- alkyl-2-acyl-glycerol) that make their association with the raft lipids [**106, 107**].

(*ii*) Transmembrane proteins (e.g. the IgE receptor FcεRI) **[104]**. IgE receptors (FcεRI) are normally localized outside membrane rafts. Upon binding to the multivalent antigen (Ag)–IgE complex to FcεRI and the coalescence of the rafts allows a physical interaction between FcεRI and Lyn, which triggers the signal transduction pathway.

(*iii*) Acylated protein tyrosine kinases of the Src family (e.g. Lyn) bound to the inner leaflet of the membrane **[108, 109]**. Acylated proteins are anchored in the internal leaflet with two or more saturated acyl chains (generally myristate and palmitate) that interact preferentially with raft lipids. Although sphingolipids are usually not found in the cytoplasmic leaflet of the plasma membrane, specific GPLs such as phosphatidylserine and phosphatidylethanolamine with saturated chains might form L_o domains through interaction with long sphingolipid acyl chains of the outer monolayer (***Fig. 1.1***).

In CD4 T cells, the main components of the T-cell receptor signal initiation machinery constitutively partition into a subset of membrane rafts **[74]**. Thus, some signal transduction units can be preassembled in lipid rafts of quiescent cells, allowing rapid and efficient signal initiation upon activation.

Cholesterol depletion experiments led to a clear decrease in these signaling steps, indicating the involvement of rafts in the initiation of this signaling cascade **[104]**.

In a separate study, Boyd *et al*. identified and purified plasma membrane and lipid raft associated proteins from B cells obtained from mantle cell lymphoma (MCL) patients in leukemic phase, based on shotgun proteomics and found that 5-lipoxygenase (5-LO), a lipid raft associated protein, which is a key enzyme in leukotriene biosynthesis, was up-regulated 7-fold in MCL compared with normal B cells **[110]**. Significantly, inhibitors of 5-LO activity and 5-LO-activating protein (FLAP) induced apoptosis in MCL cell lines and primary chronic lymphocytic leukemia cells, indicating an important role of the lipid rafts for the leukotriene biosynthetic pathway in MCL and other B cell malignancies. These proteins may play an important role in the pathology of the disease and are potential therapeutic targets in MCL **[110]**.

Bryant *et al.* have produced the first evidence for the association of FGFR with the cholesterol-glycosphingolipid-enriched ‘‘lipid raft’’ microdomains **[111]**. Fibroblast growth factors (FGFs) and their receptors (FGFRs) initiate diverse cellular responses that contribute to the regulation of oligodendrocyte (OL) function. FGFR2 phosphorylates the key downstream target, FRS2 in OLs. Investigation of the phosphorylation of signal transduction proteins and the role of lipid rafts, to understand the mechanisms by which FGFRs elicit these cellular responses, showed that the most abundant tyrosine-phosphorylated protein in OLs is the lipid raft microdomain associated FGFR2 and that it phosphorylates even in the absence of FGF2, suggesting a potential ligand independent function for this receptor. Raft disruption

resulted in loss of phosphorylated FRS2 from lipid rafts, emphasizing the importance of microenvironments within the cell membrane **[112]**.

Many more examples of the importance of rafts can be found in literature and many excellent reviews have been written. However, the above mentioned examples were selected to demonstrate that rafts are molecular sorting machines capable of coordinating the spatiotemporal organization of signal transduction pathways within selected areas of the plasma membrane **[3]**.

1.2.5.2 Role of lipid rafts as platforms for entry of pathogens

A broad range of pathogens, including viruses, bacteria, parasites and their toxins, use lipid rafts to enter host cells, utilizing both cell-surface GPI-anchored proteins, transmembrane receptors, and raft lipids (GSL, sphingomyelin and cholesterol) as primary or accessory receptors. For example, cholera toxin binds to ganglioside GM1, Shiga toxin binds to the neutral glycolipid Gb3, mycobacteria bind to cholesterol, *E. coli* strains expressing FimH bind to the GPI-anchored protein CD48.

The interaction of cholera toxin (the most widely used raft marker) with target cells can be taken as an example to start a brief illustration of the various roles of membrane rafts in the pathogenesis of bacterial toxins. Cholera toxin consists of five identical B polypeptides that bind to ganglioside GM1 and a single A1 peptide containing subunit and enters the cell and activates adenylyl cyclase **[113]**. The pentameric B subunit specifically binds to five GM1 molecules with high affinity. The main role of the raft in this case is to concentrate the toxin receptor, to ensure maximal binding capacity of the toxin to the cell surface **[101]**.

The interaction of tetanus and botulinum toxins with neural cells illustrates another aspect of raft–toxin interactions. These neurotoxins bind to several di- and trisialogangliosides (e.g. GD1a, GD1b and GT1b) on the surface of the presynaptic membrane **[113]**. This finding was

further strongly supported by the identification of a 58 kDa protein from rat brain synaptosomes that binds to botulinum and tetanus neurotoxins only in the presence of GT1b or GD1a **[113]**. This model is quite interesting because it illustrates the various properties of lipid rafts that are particularly useful to pathogens and their toxins:

(*i*) The raft environment provides multiple low affinity receptors that stabilize the invader on the cell surface;

(*ii*) The raft can deliver the invader to adequate high-affinity receptors; and

(*iii*) Specific lipids in the raft environment might act as chaperones, inducing conformational changes in the invader structure in the vicinity of the high affinity receptors.

This model helps to mechanistically explain the fusion reaction that occurs during infection by human immunodeficiency virus 1 (HIV-1) and that is dependent on glycolipids **[115]**.

The pore forming toxin aerolysin from *Aeromonas hydrophila* also target lipid rafts through multiple interactions with GPI-anchored proteins **[116]**. In fact, for most of the pore-forming toxins (e.g. *Vibrio cholera* cytolysin), rafts help by concentrating receptors and thereby provide either increasing binding affinity or promote toxin oligomerization. **[101]**. For some cases like Shiga toxin, the glycolipid receptor (Gb3) of the raft is important not only for providing cell-surface binding sites, but also for retrograde transporting of the toxin into the endoplasmic reticulum **[117, 118]**. After attachment with the receptor sites or to some major raft components such as cholesterol or sphingomyelin, the pathogens and their toxins sometimes exploit the normal cellular functions of lipid rafts (e.g. intracellular trafficking) to enter into host cells **[101]**. Some bacterial toxins may prevent the functions of any protein within the raft-domains by altering their localization; for example, the exotoxins produced by *Clostridium difficile*, causes defects in the epithelial barrier function, which under normal conditions prevents the passage of dissolved molecules from one cell to another **[119]**.

Leishmania donovani is an obligate intracellular parasite that infects macrophages of the vertebrate host, resulting in visceral leishmaniasis in humans, which is usually fatal if untreated. Cholesterol is a major constituent involved in this host–parasite interaction leading to attachment on the cell surface and subsequent internalization of the parasite. Cholesterol depletion from macrophage plasma membranes using MβCD results in a significant reduction in the extent of leishmanial infection **[120]**.

The human rhinovirus also uses the ceramide-enriched and large glycosphingolipid-enriched membrane domains as platforms to enter into the host cells. Destruction of glycosphingolipid-enriched membrane domains blocked infection of human cells with rhinovirus **[121]**. Measles virus (MV), which interacts with the surface of T cells and thereby efficiently interferes with stimulated dynamic re-organization of their actin cytoskeleton, causes ceramide accumulation in human T cells in a neutral and acid sphingomyelinase dependent manner. Moreover membrane ceramide accumulation causes down-modulation of chemokine-induced T cell motility on fibronectin. Altogether, these findings highlight a yet unrecognized concept of pathogens able to cause membrane ceramide accumulation to target essential processes in T cell activation and function by preventing stimulated actin cytoskeletal dynamics **[122]**.

1.3 The Sphingolipid Binding Domain (SBD) peptide

The name sphingolipid binding domain was given by Fantini and coworkers to a common V3 loop like structure/peptide sequence present in different proteins including Human Prion protein, Alzheimer's β amyloid peptide and glycoprotein gp120 of Human Immunodeficiency Virus HIV-1. This peptide sequence was proposed by Fantini and colleagues to bind to the membrane microdomains on the cell surface through attachment with some selected sphingolipids such as galactosylceramide and sphingomyelin. Fantini proposed that aromatic

and basic residue(s) in the SBD interact with galactose-terminals of glycolipids and sphingomyelin, and they tested the SBD sequence of Prion protein, HIV peptides and $A\beta_{1-40}$ fragment using Langmuir lipid film binding method at the lipid-air interface **[43]**.

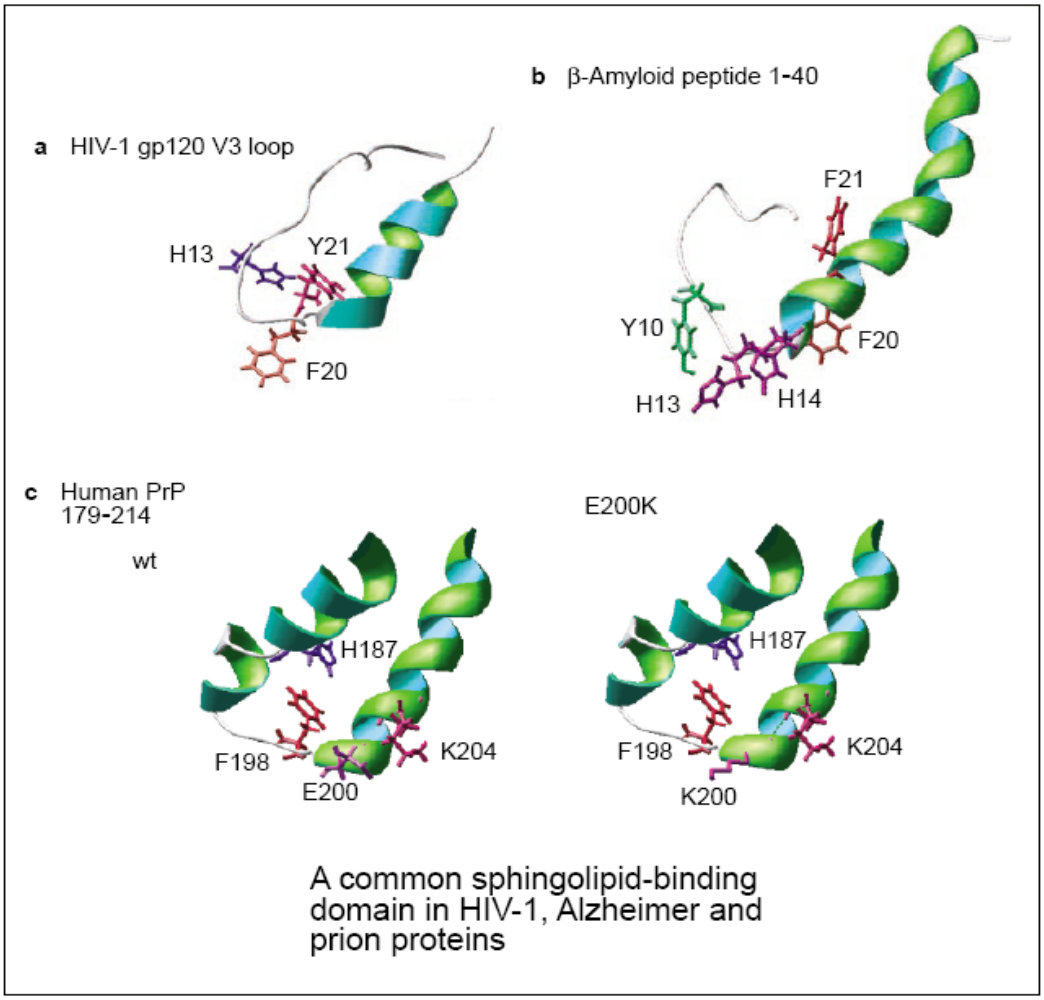

[Fig from J. Fantini, *et al*. 2002, E*xp. Rev. Mol. Med.*, 4 (27), 1-22.]

Figure 1.4: *A common sphingolipid-binding domain in HIV-1, Alzheimer and prion proteins. The lateral chains of the residues of pathologically important proteins known to be involved in binding to glycosphingolipids and sphingomyelin in plasma membranes are shown.*

The active conformation of Aβ contains two phenylalanine residues at 19th and 20th position, which interact in an anti-parallel way with the central region of Aβ. It was hypothesized by Fantini that the sugar rings of the GSLs could also serve as the binding site to this region of the peptide and modulate the conformational changes of Aβ [**3**]. The non-toxic shorter version of the Aβ (1-25) might also follow a similar mechanism, but any kind of

experimental study or characterization of this shorter sequence was not performed by any group before.

In addition to Fantini's proposal, biochemical studies done on the shorter sequence of Alzheimer's version of SBD (1-25 amino acid of Aβ), have shown evidence that it has potential applications as a sphingolipid trafficking tracer for cellular and animal models [**123**]. The diffusion based biophysical characterization of this exogenous, non-toxic probe has been carried out in this study on live cell membrane.

The sphingolipid binding domain (SBD) peptide consists of the first 25 amino acids of the amyloid Aβ peptide. After modification, at the N-terminus by two copies of an inert spacer ($[AEEAc]_2$) and conjugation to Oregon Green (OG) via a thiol linkage to an N-terminal Cysteine, or Tetraaminomethylrhodamine (TAMRA) via an amide linkage directly to the spacer, in order to trace it through fluorescence techniques, the final sequences becomes:

OG-Cys-$[AEEAc]_2$- DAEFRHDSGYEVHHQELVFFAEDVG and

TAMRA-$[AEEAc]_2$- DAEFRHDSGYEVHHQELVFFAEDVG respectively.

Since the most common form of wild type amyloid beta contains K at 16th position instead of E, the E at 16 has been highlighted here. The original sequence of SBD in Aβ reported by Fantini *et al*. contained E16. The E16 mutation does not affect the structure of 1-28 peptides **[124]**. The replacement of an acidic residue (Glu) by a basic one (Lys) in the sphingolipid binding site is likely to affect the binding of the peptide to positively charged lipids. In case of the prion protein, the main effects of the E200K (i.e. the reverse) mutation are (***i***) major changes in the distribution of charges on the protein surface and (***ii***) the loss of a salt-bridge interaction between the side chains of Glu^{200} and Lys^{204} **[43]**. Moreover the E200K mutation specifically increases the recognition of sphingomyelin; though it doesn't affect the conformation of Aβ [**43**]. Since lysine (K) has a free amine, it is also difficult to conjugate the fluorophore molecule in solution phase, with the peptide sequence containing lysine.

Addition of the inert spacer in the above mentioned peptide facilitates the conjugation of fluorophores to the amino-terminus by minimizing possible steric interference of the fluorophores with the amino acid sequence. The molecular structure of the spacer is given in *Fig. 1.5*.

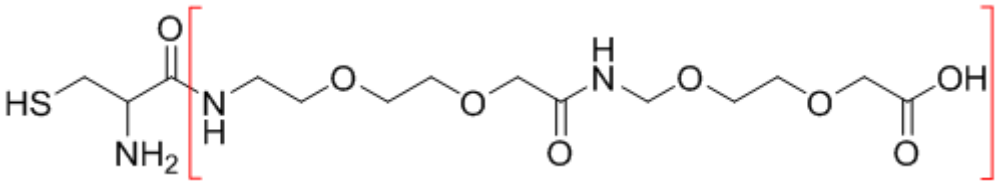

Figure 1.5: *The Representation of the Cysteine conjugated spacer $[AEEAc]_2$.*

1.3.1 Effectiveness of SBD as a lipid raft marker

The uptake and intracellular trafficking of sphingolipids, which self-associate into plasma membrane microdomains, is associated with many pathological conditions, including viral and toxin infection, lipid storage disease, and neurodegenerative disease. However, the means available to label the trafficking pathways of sphingolipids in live cells are extremely limited **[123]**. Until today, Cholera toxin B (CTxB) is the most commonly used sphingolipid-binding probe, which binds specifically and very tightly to a single target glycolipid, GM1 **[125]**. It is also important to note in this context that CTxB induces clustering of sphingolipids **[126–128]** and is internalized by both non-clathrin and clathrin-dependent uptake mechanisms **[129–131]**. CTxB and another commonly used microdomain tracer, the glycosyl-phosphatidylinositol (GPI)-anchor fused to any fluorescent protein, both traffic primarily to the Golgi **[132]** (although this has been contested **[133]**), and may occupy primarily non-raft domains **[134, 135]**. The markers that are normally used to trace non-clathrin mediate uptake pathways are green fluorescent protein (GFP) fusions of the endocytic adaptors Flotillin and caveolin **[136–138]**. Fluorescent protein fusions have the disadvantage that they have to be expressed from transgenes, and therefore may fluoresce in the biosynthetic pathway.

Moreover, these endocytic adaptor proteins are not found universally in all cell types, and thus they mainly correspond to a specific subtype of membrane microdomains **[139]**. Also, flotillin and caveolin are structural parts of the adaptor complex that mediates endocytic uptake by raft domains that use those complexes. This means that they might themselves influence the mobility or size of raft domains.

1.3.2 Properties of SBD as a lipid raft marker

The most important advantage about SBD is that, though this has been derived from Aβ, it is non-toxic **[123]** and can efficiently bind to liposomes with raft like compositions as well as different live systems including insect (Drosophila) and mammalian cells and neurons and Drosophila embryos **[89, 123, 140]**, hence it has the potential to become a powerful tool to trace the sphingolipid trafficking pathways over a wide range of cellular and full organism models.

According to previous reports based on SPR studies, Aβ binds more strongly to gangliosides with increased sialylation **[141]**, but the affinity of SBD towards these sialylated gangliosides is pH dependent. At neutral pH, SBD binds better to the triply sialylated GT1b in comparison to the less sialylated forms, GD3 (disialylated) and GM1 (monosialylated). On the other hand, at lower pH (~ pH 5), binding of SBD to all glycosphingolipids strikingly improves, and interestingly, interactions with less sialylated gangliosides GM1 and GD1a become even stronger **[123]**.

The above discussion provides evidence that SBD binds to the membrane through a cholesterol, sphingomyelin and glycolipid dependent manner. In this work the biophysical properties, mainly diffusion and anisotropic translocations of the probe have been studied on live cell membranes. Overall, the present study will help to complete the establishment of this motif as a powerful sphingolipid trafficking tracer for live biological model systems. In order

to study the biophysical properties of SBD, Fluorescence Correlation Spectroscopy, a widely used single molecule sensitive biophysical technique and one of its recently developed modalities, Imaging Total Internal Reflection Fluorescence Correlation (and Cross Correlation) Spectroscopy (ITIR-FCS and ITIR-FCCS) have been used in this work. Details about the techniques are discussed in the following chapter.

Chapter 2:

Methodology

2.1 Introduction

In order to determine the biophysical characteristics of fluorescently-tagged SBD on the plasma membrane of live cells, the techniques used in this study are conventional confocal fluorescence correlation spectroscopy (FCS), a technique which measures the diffusion time of the fluorophore through a stationary detection volume and a home built new method, imaging total internal reflection fluorescence correlation spectroscopy (ITIR FCS), which gives the advantage of multiplexing measurements **[142, 143]**. The fluidity of the membrane environment is reflected in the diffusion rate at which the fluorescently labeled markers travel through the confocal volume or the specified pixel area in cases of FCS and ITIRFCS respectively. Since the main interest of this study was to trace the relative changes in diffusion of different markers under varying perturbed conditions, only diffusion times have been reported for the confocal FCS measurements. These diffusion times can be easily converted to diffusion coefficients as explained later in the chapter. On the other hand, directly diffusion coefficient (D) values have been extracted using the newly developed technique, ITIRFCS. Furthermore, the heterogeneity and the anisotropic translocations on the cell surface have been investigated using imaging total internal reflection fluorescence cross-correlation spectroscopy (ITIR-FCCS), the extended format of ITIRFCS **[89]**, which has been described in details in later part of the chapter.

2.2 Fluorescence Correlation Spectroscopy (FCS)

2.2.1 Principle and theory of fluorescence correlation spectroscopy

FCS was first introduced by Douglas Madge, Elliot Elson and Watt Webb in 1972 and applied to measure the diffusion and chemical dynamics of DNA-drug interaction **[144]**. At present FCS is an efficient biophysical technique with single molecule detection sensitivity for *in vitro* as well as *in vivo* applications. With improved ultra-sensitive detectors and stable lasers, FCS delivers high signal to noise ratio and detection efficiency. A number of FCS applications have already been reported for the study of binding and diffusion behavior of subcellular membrane compartments in live cells **[145-156]**.

Unlike normal fluorescence spectroscopy, FCS is not based on the fluorescence intensity of the sample. Statistical analyses are carried out in FCS based on the ***fluctuations*** in fluorescence signals to investigate the dynamic molecular processes in a specified open probe observation volume. Cellular processes including translational diffusion, directed diffusion (flow), active transport, restricted movements of the fluorescently tagged probes cause fluctuations in fluorescence intensity. To extract the information of the underlying molecular processes, the fluctuations in the fluorescence signals are normally quantified by temporally autocorrelating the recorded photon count rates. Assuming constant excitation power, the fluctuations in the fluorescence signal can be defined as the deviations from the temporal average of the signal **[145]**, and can be expressed as:

$$\delta F(t) = F(t) - \langle F(t) \rangle \tag{2.1}$$

$$\langle F(t) \rangle = \frac{1}{T} \int_0^T F(t) dt \tag{2.2}$$

where, $F(t)$ is the detected fluorescence intensity as a function of time t $\langle F(t) \rangle$ denotes the mean fluorescence intensity and δF (t) is the fluorescence fluctuation around the mean value.

Then the autocorrelation function (ACF) can be defined as:

$$G(\tau) = \frac{\langle F(t)F(t+\tau)\rangle}{\langle F(t)\rangle^2}$$
$$= \frac{\langle [\langle F(t)\rangle + \delta F(t)][\langle F(t) + \delta F(t+\tau)\rangle]\rangle}{\langle \langle F(t)\rangle^2 \rangle} \quad (2.3)$$
$$= 1 + \frac{\langle \delta F(t)\delta F(t+\tau)\rangle}{\langle F(t)\rangle^2}$$

where, τ is the correlation time or lag time.

2.2.1.1 The autocorrelation function and autocorrelation curve

Correlation is a mathematical tool used frequently in signal processing for analyzing functions or series of values, such as time domain signals. Autocorrelation is simply the correlation of a signal with itself over successive time intervals, which is useful for finding repeating patterns in a signal, such as determining the presence of a periodic signal which has been buried under noise.

The principle of autocorrelation function is illustrated in *Fig. 2.1*, which indicates that a higher extent of overlap between signals results in a higher amplitude of the autocorrelation curve. Situation *A* in *Fig. 2.1*, shows the highest extent of overlap between two signals and the corresponding value of the ACF at that short time delay is reflected in the higher amplitude of the autocorrelation curve shown in *Fig. 2.1 D*. Similarly the moderate and weak overlap between two signals shown in situation *B* and *C* respectively, are represented in the middle and later part of the autocorrelation curve of *Fig. 2.1 D*. The corresponding ACF values are reflected by the respective amplitudes of the autocorrelation curve at moderate and longer time delay. So in FCS, the autocorrelation determines the extent to which a signal persists in time, and thus it determines the length of the molecular / dynamic process which causes the fluctuations in the fluorescence signal. Experimentally obtained autocorrelation curves for FCS

are actually representations of the average of many molecules over a certain period of time (measurement time).

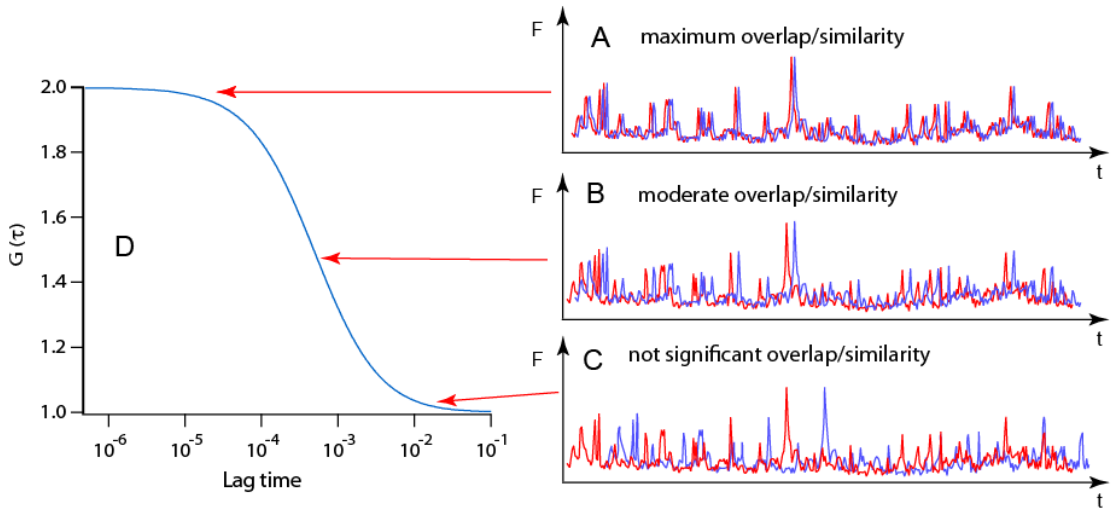

Figure 2.1: *Explanation of autocorrelation function in the light of overlapping signals. Different situations emphasize the extent of overlaps between the signals of a same particle separated by different amount of time; and their corresponding impact on the overall ACF.*

2.2.1.2 General information obtained from autocorrelation curve in FCS

In case of fluorescence correlation spectroscopy, the autocorrelation function represents the correlation between a signal from a particular fluorescent particle at a particular time instance and the signal from that same particle after a specified time difference τ. As an immediate outcome of the technique, the shape of the autocorrelation function (ACF) provides some information about the diffusive property of the particles of interest. The x-axis time value corresponding to the half maxima of the autocorrelation curve gives an estimation of the mean diffusion time τ_D, which indicates the average residence time of the particle of interest in the confocal volume. The gradual broadening of the autocorrelation curve indicates an increase in τ_D, and decrease in diffusion coefficient (*Fig. 2.2*); i.e. it gives direct information about the residence time of the particle of interest in the confocal volume.

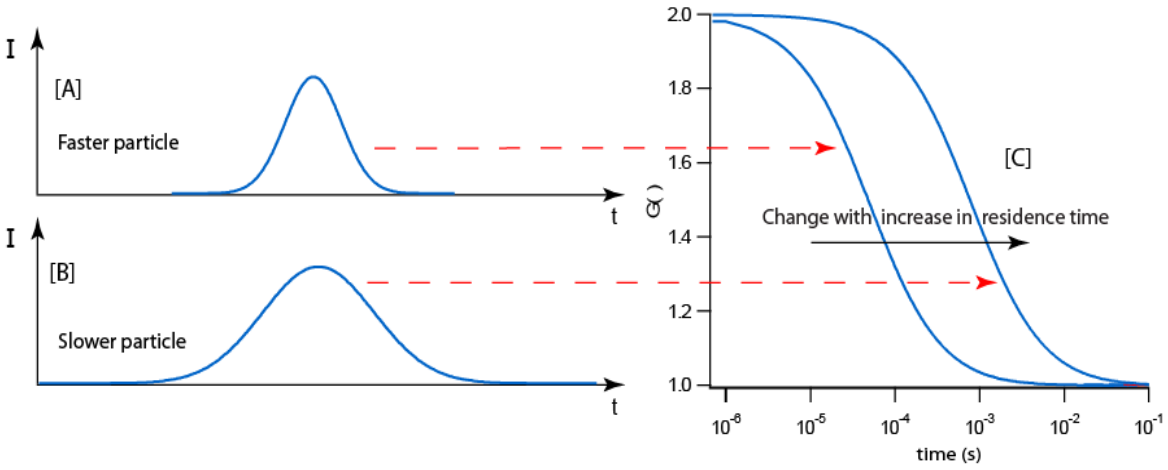

Figure 2.2: *Changes in autocorrelation curve due to the change in residence time of the fluorescent particles in the confocal volume.*

Similarly the autocorrelation curve gives information about the number of particles present in the confocal volume and thus about the concentration of the fluorophore in the solution. The fluctuation in the overall fluorescence intensity due to the entry or exit of a single fluorescent particle in the confocal volume is relatively greater when fewer numbers of particles are present there. For gradually higher fluorophore concentrations, (i.e. confocal volume being more populated) the average signal intensity gradually goes up.

As a result, the fluctuation caused due to one particle tends to have less and less effect on the overall intensity. Therefore, an increase in the number of particles (*N*), i.e. an increase in concentration of the fluorescent particles, is indicated by a decrease in the amplitude of the autocorrelation curve (*Fig. 2.3*). By this way, ACF gives direct information about the concentration and diffusion time of particles of interest.

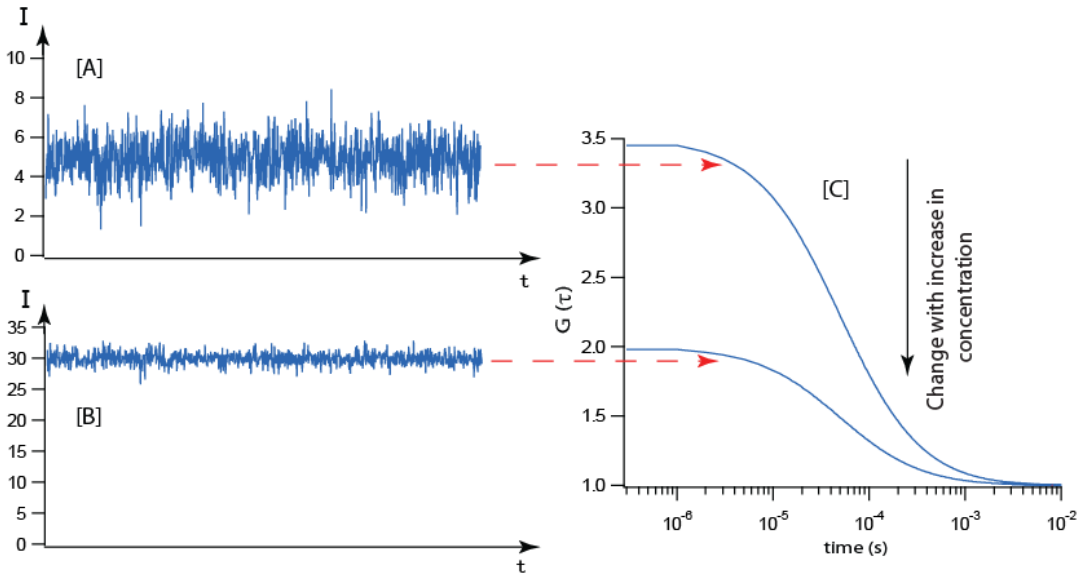

Figure 2.3: *Changes in autocorrelation curve duo to the change in concentration of the fluorescent particles.*

2.2.1.3 Mathematical expressions for different fitting models

The generalized autocorrelation function $G(\tau)$ for a sample containing n different fluorescent particles with only translational diffusion, can be expressed as:

$$G(\tau) = \frac{1}{N} \frac{\sum_{i=1}^{n} \alpha_i^2 F_i g_i(\tau)}{\left[\sum_{i=1}^{n} \alpha_i F_i\right]^2} + G_\infty \qquad (2.4)$$

Where the coefficient α_i is the ratio of the fluorescence yield of particle i (given in photon counts per particle and second); F_i are the mole fraction for the species i with N the average number of particles in the confocal volume and G_∞ is the convergence value for the ACF at long lag times. Normally after long time intervals, the signals lose their self similarity and behave like independent variables. Therefore the second term of equation 2.3 tends to zero, resulting the overall G_∞ close to 1 with increasing time lags.

Though the value of G_∞ usually converges to 1, but it is often advantageous to keep it as a fit parameter.

Depending on the molecular processes that cause the fluorescence fluctuations, *G(τ)* will have specific characteristic forms reflecting the time course of the process **[157-160]**. For example, in the case of a free three-dimensional (3D) translational diffusion of a single species, $G(\tau)$ is given by **[157, 161]**:

$$G(\tau) = \frac{1}{N}\left(1+\frac{\tau}{\tau_D}\right)^{-1}\left(1+\frac{\tau}{K^2\tau_D}\right)^{-1/2} + G_\infty \qquad (2.5)$$

where the diffusion time $\tau_D = \frac{\omega^2}{4D}$ (2.6)

and the structure factor $K = \frac{z}{\omega}$ (2.7)

Here τ_D is the lateral diffusion time of the fluorescent particle staying in the confocal volume, D is the diffusion coefficient, and ω and z are the radial and axial distances of the confocal volume at which the intensity has dropped by $1/e^2$ of the maximum intensity.

Fluorescent dye molecules often have a non-negligible triplet state population with a characteristic triplet state relaxation time at a sub-microsecond time-range. Since the intersystem crossing between singlet and triplet states also causes characteristic fluctuations in the fluorescence signal [**162**], it leads to additional contributions to the ACF at short times. Incorporating a triplet state term in equation 2.5, the overall expression for $G(\tau)$ becomes:

$$G(\tau) = \frac{1}{N}\cdot\left(1+\frac{F_{trip}}{1-F_{trip}}\cdot e^{-\frac{\tau}{\tau_{trip}}}\right)\cdot\left(1+\frac{\tau}{\tau_{diff}}\right)^{-1}\cdot\left(1+\frac{\tau}{K^2\tau_{diff}}\right)^{-1/2} + G_\infty \qquad (2.8)$$

where τ_{trip} is the triplet state relaxation time of fluorophores; F_{trip} is the fraction of fluorescent particles that stay in the triplet state and K is defined as the structure factor. Equation 2.8 is the fitting model for a single particle moving freely in 3 dimensional space that is normally used to calibrate the system before each experiment using a standard chemical dye.

Following are the expressions of $G(\tau)$ for different fitting models used in this study:

Two dimensional one particle one triplet fitting model (2D-1P-1T):

$$G(\tau) = \frac{1}{N} \times \left[\left\{ \frac{1}{(1+\tau/\tau_D)} \right\} \left\{ 1 + \frac{F_{trip}}{(1-F_{trip})} \times e^{-(\tau/\tau_{trip})} \right\} \right] + G_\infty$$

Two dimensional two particle one triplet fitting model (2D-2P-1T):

$$G(\tau) = \frac{1}{N} \left[\left\{ \frac{(1-F_2)}{(1+\tau/\tau_D)} \right\} + \left\{ \frac{F_2}{(1+\tau/\tau_{D_2})} \right\} \right] \left\{ 1 + \frac{F_{trip}}{(1-F_{trip})} \times e^{-(\tau/\tau_{trip})} \right\} + G_\infty$$

Three dimensional one particle one triplet fitting model (3D-1P-1T):

$$G(\tau) = \frac{1}{N} \left[\left\{ \frac{(1+\tau/\tau_D)^{-1}}{\sqrt{1+(\tau/\tau_D)K^{-2}}} \right\} \left\{ 1 + \frac{F_{trip}}{(1-F_{trip})} \times e^{-(\tau/\tau_{trip})} \right\} \right] + G_\infty$$

Three dimensional two particle one triplet fitting model (3D-2P-1T):

$$G(\tau) = \frac{1}{N} \left[\left\{ \frac{(1-F_2)(1+\tau/\tau_D)^{-1}}{\sqrt{1+(\tau/\tau_D)K^{-2}}} \right\} + \left\{ \frac{F_2 \times (1+\tau/\tau_{D_2})^{-1}}{\sqrt{1+(\tau/\tau_{D_2})K^{-2}}} \right\} \right] \left\{ 1 + \frac{F_{trip}}{(1-F_{trip})} \times e^{-(\tau/\tau_{trip})} \right\} + G_\infty$$

Where G_∞ is the convergence value for long times.

2.2.2 Advantages of fluorescence correlation spectroscopy

Fluorescence correlation spectroscopy (FCS) is a highly sensitive fluorescence microscopy technique that can be used to probe a wide range of biophysical processes including diffusion, ligand-receptor binding, molecular aggregation etc on artificial as well as on live cell membranes. This technique is able to measure at a very small volume (in the order of femtoliter) and at very low concentrations (~ 50 picomolar to few hundred nanomolar). Several biophysical parameters can be obtained by analyzing the experimentally FCS data,

among which diffusion coefficient is the most important and concentration is also a useful one to know. The comparative molecular brightness of different fluorophores can also be determined from the intensity per particle parameter.

2.2.2.1 Determination of diffusion coefficient from diffusion time

The diffusion coefficient of a freely moving particle in a solution is given by the Stokes-Einstein relationship

$$D = \frac{kT}{6\pi\eta R} \tag{2.9}$$

From the equation it is clear that the diffusion coefficient D is dependent on the viscosity of solution η and the hydrodynamic radius of the particles R. k is Boltzmann's constant and T is the absolute temperature in the expression.

If it is assumed that the molecules are spherical in shape, then the mass of a single molecule is given by

$$M = \rho V = \frac{4}{3}\pi R^3 \rho \tag{2.10}$$

Where ρ is the mass density of the molecule and V is the volume. Therefore the equations 2.6 and 2.7 state that the diffusion coefficient and the diffusion time of a particle is inversely proportional and proportional respectively to the cubic root of the mass.

$$D \propto M^{-1/3} \tag{2.11}$$

$$\tau_D \propto M^{1/3} \tag{2.12}$$

The parameter obtained directly by correlating the data from a typical FCS experiment, which measures the fluctuations in the fluorescence intensity from an open probe volume in a sample, is the diffusion time of the particle of interest. In order to get the diffusion coefficient of the particle of interest, first the setup need to be calibrated on the basis of some standard

dye molecules, having well established diffusion coefficient value. Then the diffusion coefficient of the particle of interest can be calculated using equation 2.11, where Rhodamine 6G has been used as standard to calibrate the system (Rho 6G, D=4.26x10^{-6}cm^{2}s^{-1}, Petrasek *et al*. *Biophys. J.* 2008).

$$D_x = \frac{\tau_{Rho}}{\tau_x} D_{Rho} \qquad (2.13)$$

D_{Rho} is the diffusion coefficient and τ_{Rho} is the diffusion time of Rhodamine 6G. D_x and τ_x are the diffusion coefficient and diffusion time of the particle of interest.

2.2.2.2 Determination of concentration from autocorrelation function

The mathematical expression for the autocorrelation function was given in equation 2.5

Now at $\tau = 0$, that equation can be simplified as

$$G(0) = \frac{\langle \delta F(t) \rangle^2}{\langle F(t) \rangle^2} + G(\infty) = \frac{1}{\mathrm{N}} + 1 \qquad (2.14)$$

Where G_∞ has been simplified as 1.

Equation 2.14 shows the reciprocal relationship between the number of particle and the amplitude of autocorrelation function, which means N with the increasing particle concentration, the amplitude of the ACF concomitantly decreased. Hence with the same fluorescence intensity fluctuation, the increase in particle number results in the increase in fluorescence intensity, leading to a decreased value of *G (0)*. Simultaneously, the concentration of the species which is related to the particle number through the equation:

$C = N / V_{\mathrm{eff}}$ (2.15)

is also reciprocal to *G (0)*. Thus from the amplitude of autocorrelation function, the concentration of the particle of interest can also be determined.

But V_{eff} cannot be determined by calibrating the system using a standard dye solution with a known concentration because, at very low, nanomolar, concentrations the number of particles in the focal volume N may be affected by several factors, such as precipitation of the dye molecules on the cover slips or photobleaching of the fluorophores. Therefore the determination of V_{eff} might not be accurate and the absolute concentration of the particle of interest would not be determined precisely. On the other hand, the diffusion coefficient of fluorescent particles should not depend upon the concentration. Hence, the diffusion coefficient of the particle of interest has to be determined first using equation 2.13. As K (= z/ω) is an experimentally obtained parameter in FCS, so after the determination of D and using equation 2.6 and 2.7, V_{eff} can be calibrated. Therefore the relative local concentration of the particle of interest can be determined using equation 2.15.

2.2.3 Instrumental set up for fluorescence correlation spectroscopy

The instrumental setup for the confocal FCS system used in this study, is an Olympus FV300 confocal microscope, with which hardware correlator (Flex-02-01D, correlator.com, Bridgewater, NJ, US) and Avalanche photo detectors (SPCM-AQR-14, Pacer Components, Berkshire, UK) are coupled in house. The instrument is equipped with 3 laser excitation sources; 488 nm Argon laser, 543 nm He-Ni laser and 633 nm He-Ni laser (all from Melles Griot, Singapore), which are directed to a water immersion objective (60×, NA1.2, Olympus, Singapore) through a long pass excitation dichroic mirror (488/543/633) and scanning mirror to excite the fluorescent samples.

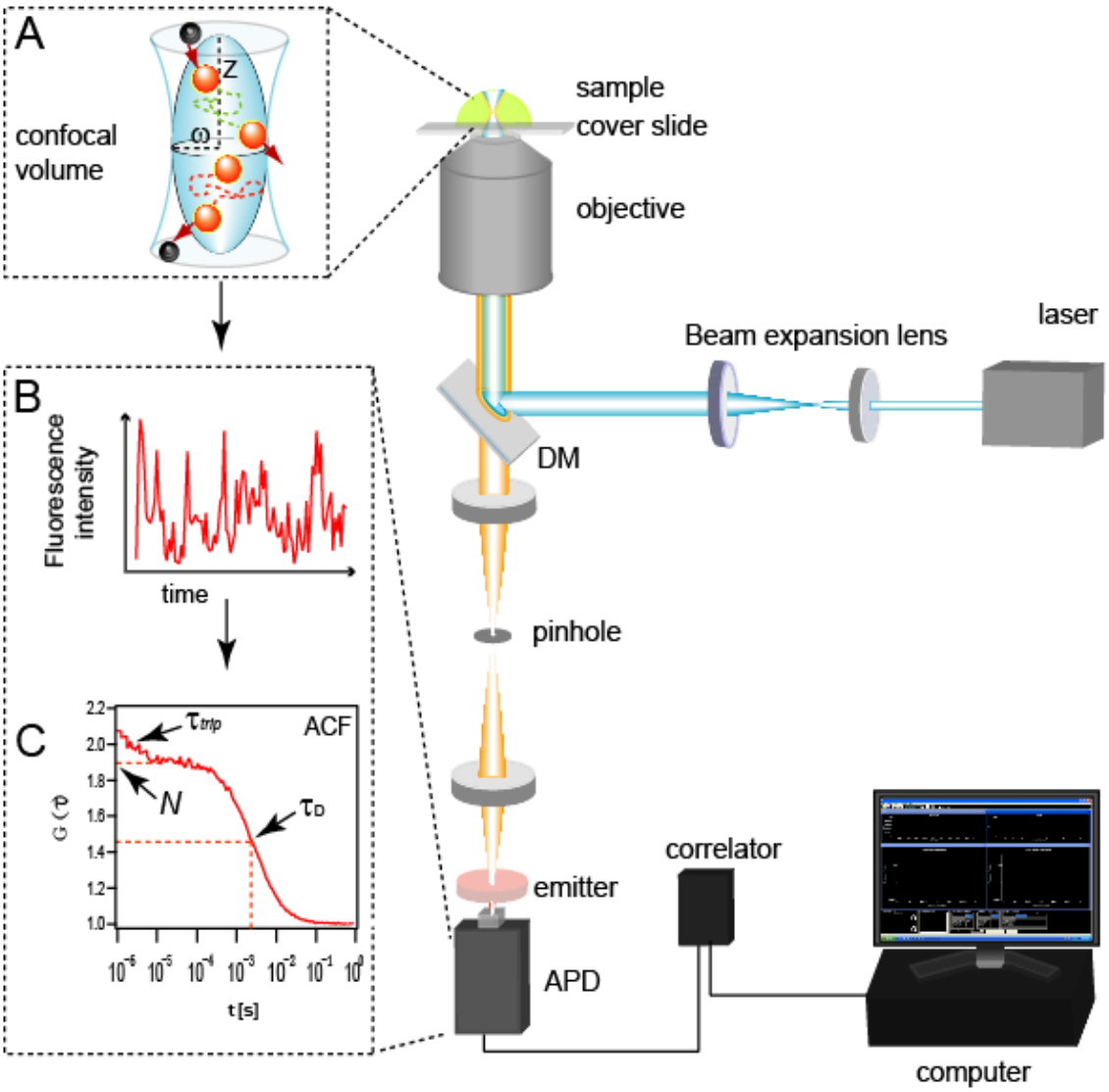

[Picture modified based on a drawing by Liu Ping]

Figure 2.4: *Schematic representation of the FCS instrumental setup. Figure in right illustrates the basic principle and instrumentation of FCS. NF is neutral density filter; AC, apochromat; DC, dichroic mirror and APD stands for avalanche photodiode. (A) Enlarged representation of the confocal volume shows the free Brownian motion of the fluorescent particles through the focal volume, which results fluctuations in the fluorescence intensity signal showed in (B). Correlating these fluctuations with time gives the ACF curve shown in (C). By fitting the ACF curve parameters like number of particles (N), τ_{trip} and diffusion time (τ_D) are obtained, which provide valuable information about concentrations and motility of the fluorescent particles.*

The emitted fluorescence signals from the samples are detected by the APD detectors after passing through the suitable emission filter, chosen from a range of available ones (Omega, USA), for the corresponding dye. For cell measurements, normally 50 - 100 mW laser power before the microscope objective is used. The samples are first imaged through XY plane scan of the Olympus Fluoview software followed by choosing a ROI by adjusting the proper Z plane and then performing the

FCS under fluorescence point scanning mode. The correlations are obtained from Flex12 software provided by the correlator company. The Avalanche photo detector creates intensity plots of the fluorescence signals from the sample, and the hardware correlator calculates the autocorrelation function thereafter. Finally the parameters like diffusion time, number of particles etc are obtained by fitting the ACFs with suitable home written fitting models using Igor pro software (Wavemetrics, Lake Oswego, OR, USA).

2.3 Imaging Total Internal Reflection Fluorescence Correlation Spectroscopy (ITIR-FCS)

Total internal reflection (TIR) is an optical phenomenon that occurs when a light ray from an optically denser medium strikes a boundary of an optically rarer medium at an angle larger than the critical angle (corresponding to those media) with respect to the normal of the surface. Critical angle (θ_c) is the smallest angle of incidence at which a light ray passing from one medium to another less refractive medium can be totally reflected from the boundary between the two; $\theta_c=\sin^{-1}(\eta_r/\eta_i)$, where η_i and η_r are refractive index of incident medium and refractive medium respectively. Once the incident angle is larger than the critical angle, no light can pass through the boundary and the whole light ray is reflected back to the optically denser medium generating only an evanescent wave at the interface. An evanescent wave is a nearfield standing wave with an intensity that exhibits an exponential decay with distance from the boundary where the wave was formed. TIR can only occur where light travels from a medium with a higher refractive index to one with a lower refractive index, for example, in case of TIR microscopy, it normally occurs when light passes from glass (η_g=1.52) to aqueous phase (η_w=1.33).

Total internal reflection fluorescence microscopy (TIRFM) is a powerful modality of fluorescence microscopy, which permits direct visualization of intracellular events including

endocytosis, which occur close to the membrane contacting the glass surface. It allows the study of cytoskeletal associations, molecular diffusions or membrane dynamics along with dynamic single molecule imaging **[163-165]**. The combination of TIRFM with FCS would greatly extend the possibilities of biophysical characterization of biological samples.

Fluorescence correlation spectroscopy (FCS) was originally conceived as a temporal correlation technique **[147]**. Later it was modified to perform correlation in the spatial domain under the name of Image Correlation Spectroscopy (ICS) **[166, 167]**. Though ICS is a useful technique, it has been used mainly to study the spatial distribution of receptors on the membrane, but it cannot determine the dynamics of a system since only spatial correlations are performed.

In order to solve this problem, several modifications have been introduced. Line-Scanning Fluorescence correlation spectroscopy is one of them, which can obtain ACFs directly from confocal images and can characterize the microscope **[168]**. The most promising extension of ISC to include temporal correlations was Image Cross-correlation Spectroscopy (ICCS) **[169]**, and thus allowed the measurement of dynamic behaviors of molecules on the cell surface **[170-172]**. In its later development as a technique, ICCS underwent some further modifications like, inclusion of vectorial information with the introduction of spatio-temporal ICS (STICS) **[173]**. STICS has been used to measure protein diffusion and protein flow in living cells, but the problem associated with this technique is its sensitivity towards the photophysics of the labeled molecules, such as bleaching **[173]**. Then k-space ICS (kICS) was introduced to overcome this problem, as it was not sensitive to bleaching and blinking artifacts **[174]**. Still the main obstacle for all these ICS methods is their time resolution, which is limited by the imaging rate of the microscope. As an alternative, Raster ICS (RICS) was developed to take advantage of the pixel/time structure within a raster scanning image, as obtained from confocal microscopy, to compute temporal correlations **[175]**. However, the

temporal resolution in RICS, although better than EMCCD based FCS at present, is not isotropic and is limited along a scanning line by the laser beam dwell time per pixel; i.e. it is limited between lines by the time it takes for the microscope to scan a whole line. In addition, the technique to be used for correlating the images depends on the diffusion coefficient or velocity being measured since each technique has its own characteristic time resolution.

Apart from these image-based methods like STICS, flow processes have been characterized using some other format of temporal FCS methods as well, for example, Two Beam Cross-correlation Spectroscopy **[176]** and Spatial Two Photon Cross-correlation Spectroscopy **[177]**. Flow velocity and flow directions have also been determined *in vivo* and have been demonstrated in zebra fish blood vessels **[178-180]**. Recently spatial cross-correlation spectroscopy has been carried out using a Spatial Light Modulator (SLM) as well **[181]**.

Most of the modern day conventional Fluorescence correlation spectroscopy (FCS) systems, generally use point detectors e.g. avalanche photodiodes (APD) or photomultiplier tubes (PMT) as detectors, and hence despite their good time resolution they are limited in multiplexing and could measure only up to 4 spots simultaneously. In order to perform multiplexed FCS experiments some group have also used 2 x 2 CMOS detector array **[182]** or an array of APDs **[183]** to detect up to four different spots. But in many cases, FCS experiments need to be performed on a large area to get an idea of membrane dynamics which can be obtained from EMCCD camera based FCS. The method was extended by Sisan *et al.* by using a spinning disk microscope to provide the first FCS images in which each pixel in the image was correlated **[184]**. However, that method requires the non-trivial synchronization of the spinning disk with the acquisition for FCS data if molecular processes are to be observed with high temporal resolution. Earlier the group of Wiseman has already shown that spatio-temporal image correlation can be achieved either in a confocal mode **[173]** or on in a TIR mode using an EMCCD **[174]**. However, the time resolution used in the TIR

mode was only 50 ms, not sufficient enough to obtain a temporal correlation function on each pixel.

In order to solve the above limitations and to perform FCS measurements simultaneously on a large number of spots, a new total internal reflection illumination based FCS method called imaging total internal reflection fluorescence correlation spectroscopy (ITIR FCS) has been introduced here **[142, 143]**. In this setup, an electron multiplying charge-coupled device (EMCCD) camera with 4 ms time resolution has been used as detector. The technique is efficient to measure the free diffusions, flow as well as directed movements on whole cell membranes. By the simultaneous determination of these parameters at the same time point, instead of a sequential acquisition, this technique reduces the overall measurement time. For the study of diffusion or 2 dimensional dynamics on cell membranes **[185]** or along planar lipid bilayers **[186]**, total internal reflection (TIR) illumination mode, with a penetration depth of up to a few hundred nanometers above the glass-aqueous interface provided by the evanescent wave field **[187]** is quite advantageous **[163]**. Detection of fluorescence signals in this mode has a good inherent axial resolution, and is suitable for surface/ membrane studies as the exponential decay and therefore limited penetration depth of the evanescent excitation field leads to strong reduction of the background signal from the bulk and consequently suppresses the cross-talk between the pixels. In this study, the image based approach of FCS enables multiplexing of measurements in TIR configuration with immediate applications in the field of live cell membrane dynamics.

2.3.1 Principles of ITIR-FCS

In case of the TIR illumination, the incident angle of the excitation laser source is controlled by a tilting mirror, placed in front of the illumination port of the microscope. Orientation of the mirror actually determines the angle at which the collimated beam enters into the

microscope and subsequently the angle at which the light beam exits from the microscope objective. If the beam enters at 0° to the optical axis of the microscope, it gives a parallel beam along the optical axis. By varying the angle of the laser beam with the optical axis, the angle of incidence at the glass-water interface can be adjusted greater than the critical angle (θc, 61° for the glass-water interface), to get the total internal reflection. The illumination region has a Gaussian profile in the plane of incidence and is larger than the detection area, but the intensity distribution remains uniform over the whole region of interest (ROI), where the image based FCS measurements are performed.

In the case of bilayers and cell membranes, diffusion occurs in the *xy* plane only, and the *z*-component of diffusion has no role to play in this case, hence ACF curves obtained from bilayer and cell membrane measurements are fitted to 2D diffusion model given by

$$G(\tau) = \frac{1}{4Na^2}[2a \times erf(\frac{a}{2\sqrt{D\tau + \sigma^2}}) + \frac{4\sqrt{D\tau + \sigma^2}}{\sqrt{\pi}}(e^{\frac{a^2}{4(D\tau+\sigma^2)}} - 1)]^2 \quad (2.17)$$

where $G(\tau)$ is the autocorrelation function, N is the number of particle per pixel, D is the Diffusion coefficient of the sample, a is the side length of the unit probe area in the object plane (i.e. if d is the side length of a single pixel in the object plane and n is the binning size, then a = n × d; hence for 1 × 1 binning a = d) and σ is basically a correction factor, which can be defined as the standard deviation of the approximated Gaussian Function (with center x_0) for the PSF of a microscope [**188**].

$$PSF(x, x_0) = \frac{1}{\sigma\sqrt{2\pi}} e^{-\frac{(x-x_0)^2}{2\sigma^2}} \quad (2.18)$$

Since the PSF of the microscope is finite in size, and on the order of the pixel size of the EMCCD, it has to be taken account of in the fitting of the ACFs. Hence the standard deviation of the Gaussian PSF is denoted by σ has considered as a fitting parameter. It should

be noted that both, the diffusion coefficient as well as the size of the PSF can be extracted directly from the fits and no separate calibration is needed.

2.3.2 Instrumental set up for imaging total internal reflection fluorescence correlation and cross-correlation spectroscopy

The Instrumental setup of the image based FCS system has been built around an inverted epifluorescence microscope (Axiovert 200M, Carl Zeiss, Singapore). Laser light (532 nm) from a dual color (491 and 532 nm) laser source (Dual Calypso, Cobolt, PhotoniTech Pte. Ltd., Singapore) has been beam-expanded three times with combination of apochromat lenses and focused at the conjugate image plane on the illumination port of the microscope. A dichroic mirror (560DRLP, Omega, Brattleboro, VT) reflected the incident laser light into a high numerical aperture (NA) objective (60×, NA 1.45, TIRF microscope, Olympus, Singapore). As the evanescent wave field is the excitation source for this technique, normally a high laser power (~6 mW) before the microscope is needed in this method. For light source of wavelength in the ranges of 500 to 650 nm, a maximum incident angle of 72.5º could be achieved with this system with an immersion oil having refractive index 1.52 **[142]**. (The refractive indices of glass and water are η_g = 1.52 and η_w = 1.33, respectively.) The fluorescence signals emitted from the fluorophores within the area under the selected ROI are collected by the same objective, then passed through the dichroic mirror and the emission filter (595AF60, Omega, Brattleboro, VT) before being collected by the EMCCD camera (Cascade II: 512, Photometrics, Tucson, AZ) mounted on the side port of the microscope. The camera and the microscope are being controlled by the Metamorph software (Universal Imaging Corp., Downingtown, PA). The back-illuminated EMCCD sensor has more than 90% quantum efficiency in the wavelength range from 500 to 650 nm and is a frame-transfer

device. The image section of the frame-transfer device has a physical dimension of 8.2 x 8.2 mm^2, which is divided into 512 x 512 pixels yielding 16 x 16 μm^2 / pixel **[182]**.

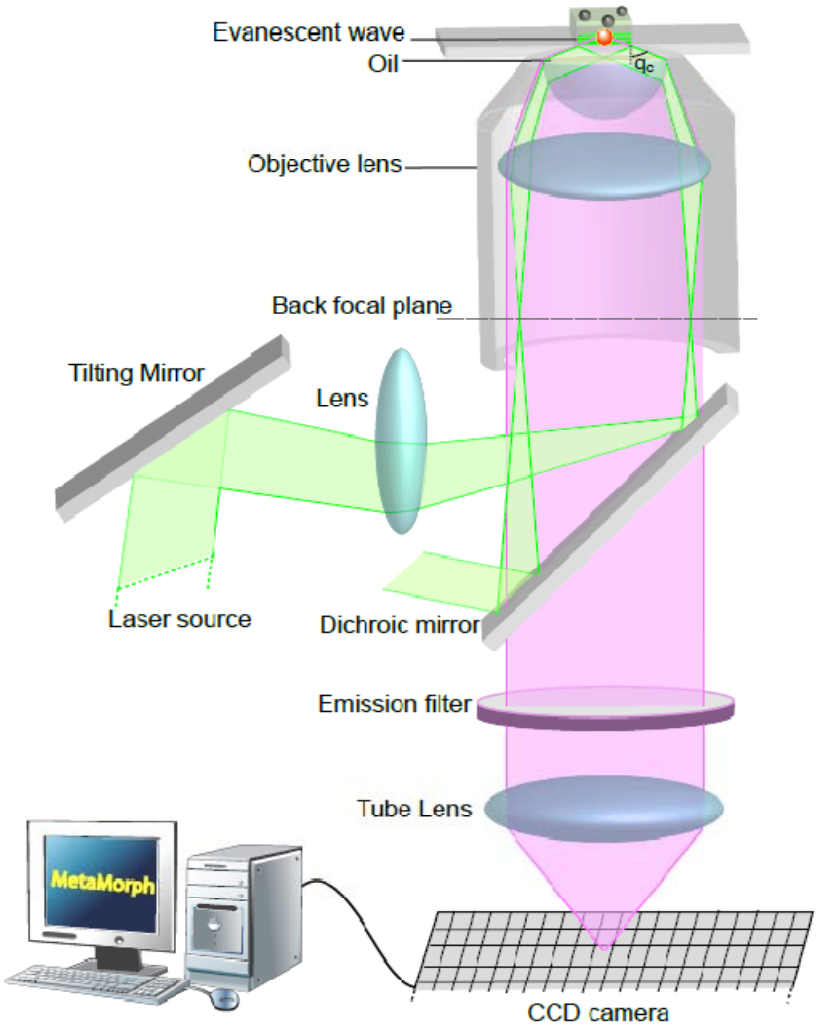

[Picture modified based on a drawing by Liu Ping]

Figure 2.5: *Schematic diagram of the instrumentation for imaging total internal reflection-fluorescence correlation and cross-correlation spectroscopy (ITIR- FCS and FCCS). The detailed description is given in the main text.*

Since different manufacturers use different tube length, the magnification factor for the instrument is 54.7 due to the usage of a 60× Olympus objective on a Zeiss microscope. For the camera, the overall time resolution is 33.9 ms for a 512 x 512; however, the best time resolution found is 4 ms for a ROI of 20 x 20 or smaller square array or a rectangular array having ≤ 20 rows and any number (1-512) of columns. 20,000 frames of the ROI at 4 ms time

resolution are normally acquired in stack format. Since the camera electronics need some time in each acquisition to stabilize before it can give a stable signal, the first 10,000 frames of the stacks were not considered in the analysis. The last 10,000 frames of the experimentally captured stacks are correlated using home written programs compiled in Microsoft VC++ .net 2003 to convert them into intensity stacks. These intensity stacks are then correlated using a logarithmic software to get the ACFs, which are then fitted with suitable home written fitting models, using Igor pro (version 6, Wavemetrics, Lake Oswego, OR). [*All the software, denoted "home written", were compiled by Jagadish Sankaran, a graduate student, from Wohland lab*.] A schematic representation of the system has been illustrated in *Fig. 2.5*.

2.3.2.1 Measurement technique for ITIRFCS and ITIRFCCS

The experimental measurement sequence starts with choosing a healthy cell under transmitted light (*Fig. 2.6 A*) followed by adjustment of the proper Z plane for TIRF image (*Fig. 2.6 B*). A rectangle shaped ROI of any dimension is then created that encompasses the area under the evanescence illumination field at the center. [Though ROI of any dimension can be measured using the technique, (50 x 70 pixels in *Fig 2.6*, with a 7 ms time resolution), most of the measurements have been performed on 20 x 20 pixel sized ROIs in order to achieve the best time resolution offered by the camera detector (4 ms).]

The stack of 20,000 frames of the ROI is then acquired with EM gain ~ 95% of the maximum and read using a 10-MHz digitizer. To find out the background counts, a similar stack of 20000 frames is recorded under identical experimental conditions without any excitation source. The minimum intensity detected from all the pixels within the ROI of this background stack is taken as the offset and the value is then subtracted from all the stacks acquired for the fluorescent samples. Autocorrelation functions $G(\tau)$, number of particles (N)

and diffusion time (τ_D) or diffusion coefficients (D) of the samples are then obtained from these stacks using software algorithm and suitable fitting model **[89]**.

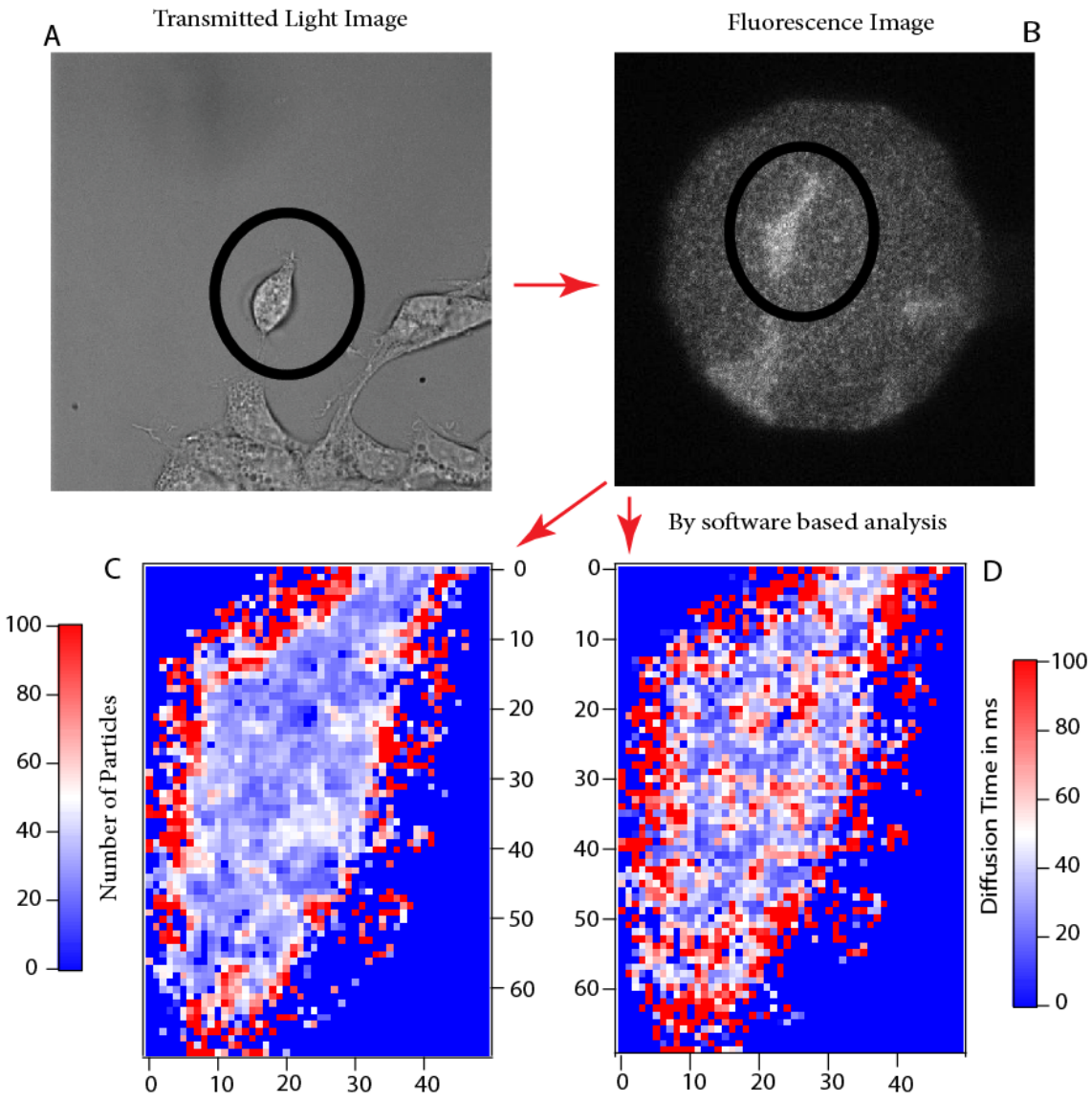

Figure 2.6: *Experimental steps for ITIRFCS and ITIRFCCS measurements. Picture A shows the transmitted light image of the chosen cell and B is its corresponding TIRF image. The quantitative images at pixel resolution of the same cell are shown in C and D, which represents the number of particles and diffusion times respectively, obtained after the software based analysis. The numbers on the x- and y-axes represent the pixel position.*

2.3.3 Comparison between ITIR-FCS and Confocal FCS

The widely used spectroscopic technique, Fluorescence Correlation Spectroscopy (FCS), is indeed a powerful tool to measure molecular dynamics, diffusion coefficients, molecular

interactions, membrane dynamics etc. But in spite of the required good time resolution it lacks the multiplexing and imaging capabilities, which also sometime are important criteria to study the membrane dynamics or cell membrane organization. Imaging Total Internal Reflection-Fluorescence Correlation Spectroscopy (ITIR-FCS) can be a promising solution is this context, which can probe diffusion phenomena on membranes with good temporal as well as spatial resolution. The overall advantage of confocal FCS is its very good time resolution, which is able to measure solution as well as at any part of cell or tissue, whereas, the main limitation of this method is its single point detection. Moreover, different points measured on same sample are not in same time frame. On the other hand, the major advantages of ITIR-FCS are the freedom from calibration as the detection area, i.e. the pixel size of the camera is always the same, reduced photobleaching/photodamage of biological samples and simultaneous multiplexed detection of a large spatial frame at the same time. This technique is limited by the time resolution of the camera and the penetration depth of the evanescence field.

Both of these techniques, confocal FCS and ITIR-FCS have their own advantages and disadvantages, and depending upon the users' need both of them can serve as very good biophysical tools. In order to determine the biophysical characteristics of fluorescently-tagged the sphingolipid associated peptide probe, SBD, on the plasma membrane of live human SHSY5Y neuroblastoma cells both of the above described techniques have been used in this study.

2.3.4 Imaging Total Internal Reflection-Fluorescence Cross Correlation Spectroscopy (ITIR- FCCS)

Several spectroscopic techniques have high temporal resolution but are limited to a single or at most a few spot measurements; alternatively, there are a variety of image based spatial

correlation techniques, having poor or anisotropic temporal resolution **[169, 174, 182, 184]**. Moreover, it has been suggested earlier that differences in the forward and backward correlations could be used to characterize non-equilibrium systems or anisotropic translocations **[176, 189, 190]**. Therefore, ITIR-FCS has further been extended to perform spatiotemporal cross correlation with the hope that the new method will bridge the above mentioned regimes by providing good isotropic spatial and temporal resolution simultaneously. The new method has been referred to as Imaging Total Internal Reflection-Fluorescence Cross Correlation Spectroscopy (ITIR-FCCS).

2.3.4.1 Principles of ΔCCF

Symmetric forward and backward spatial correlations (CCFs) on average are expected only for samples in which diffusion is isotropic (*Fig. 2.8*). For heterogeneous systems with non-isotopic diffusions forward and backward CCFs are not equivalent (*Fig. 2.8*).

Hence the difference in forward and backward CCFs for each pair of pixels, the ΔCCF, for homogeneous body should be close to zero, whereas that for heterogeneous systems should have some resultant value. Thus ITIR-FCCS can measure membrane dynamics with good spatial and temporal resolution giving access to anisotropic diffusion and potentially be a very powerful biophysical tool for membrane studies. Therefore heterogeneities in the diffusion coefficient on the cell membrane could be detected by analyzing distributions of ΔCCF values for neighboring pixels.

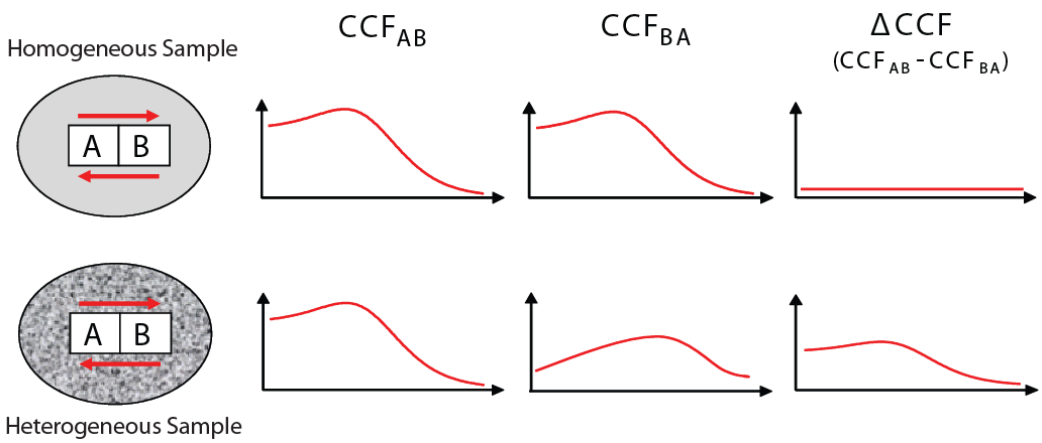

Figure 2.7: *Graphical representation explaining CCF and ΔCCF for homogenous and heterogeneous systems.*

2.3.4.2 Methodology of ΔCCF

The Spatial and temporal correlations in this method have been calculated using those stacks of 10000 image frames, which were captured for the ACF measurements on a suitable ROI with 4 ms acquisition time for each frame. The intensity values were obtained using a custom written program [again by Jagadish Sankaran], where background noise was subtracted. The spatiotemporal correlation was calculated using a suitable algorithm. In this study the CCFs between two areas, *A* and *B*, has been referred as the forward CCF or CCF_{AB} if the correlation has been calculated as $\langle F_A(t)\, FB(t+\tau)\rangle$ and as the backward CCF or CCF_{BA} if the correlation has been calculated as $\langle F_B(t)\, FA(t+\tau)\rangle$, where *B* is displaced with respect to *A* along the positive *x*- or *y*-direction. For diffusion in an isotropic phase, the forward and backward CCFs should be symmetric **[89]**.

Symmetric forward and backward CCFs are expected only for samples in which the translocation is isotropic. Therefore any anisotropy in the diffusion coefficients on a cell membrane could be detected by analyzing the differences between the forward and backward CCFs of neighboring pixels of the measured ROI. Forward and backward CCFs have been calculated on 1×1 binned areas between adjacent pixels in the horizontal direction. The backward CCFs (CCF_{BA}) have been subtracted from the forward CCFs (CCF_{AB}) for all the

400 pixels of the ROI and the results have been integrated to give a scalar value, which were then plotted as an image and referred to as ΔCCF images. From these analyses, values around zero for isotropic diffusions, whereas values with a wide distribution in case of heterogeneous samples presumably like the cell membrane would be expected.

The distribution of the ΔCCF values were plotted in the form of a histogram for each time point in the time series. The histograms were fitted with a Gaussian profile. The main parameter used in this study to observe the heterogeneity of a sample is kurtosis (k) of the ΔCCF histogram distributions. Kurtosis is a measure of the "peakedness" of any probability distribution, and in this study lower kurtosis value (flatter distribution profile) represents higher heterogeneity and lower heterogeneity reflected in higher kurtosis value (more peaked distribution profile). The parameter, kurtosis, has been calculated by the following formula:

$$k = \frac{1}{n}\sum_{i=0}^{i=n-1}\left(\frac{x_i - \mu_h}{\sigma_h}\right)^4 - 3 \qquad (2.19)$$

where n is the number of points (i.e. for 20×20 region, n = 400), μ_h and σ_h are the mean and the standard deviation of the histogram values respectively. In this technique the spatial resolution is diffraction limited as in other FCS techniques and the temporal resolution is limited by the frame rate of the imaging device.

Chapter 3:

Study of diffusion properties of SBD as a novel lipid raft marker

3.1 Introduction

Cholesterol- and sphingolipid-rich membrane microdomains known as lipid rafts are involved in a variety of cellular processes **[1, 193]**, and raft borne lipids and proteins have been implicated in several pathological conditions including neurodegeneration and inflammation **[40]**. Previously cholera toxin (CTxB) has been used to study the intracellular trafficking of raft borne lipids **[133, 137, 194-196]**. Studies on the uptake mechanisms, intracellular itineraries, and biophysical properties of raft associated proteins at the plasma membrane have revealed heterogeneity in their trafficking and dynamic behavior **[28, 197-199]**. How different ligands associate with raft domains and how they behave/move after attachment within the raft domains is a long asked question but has not been fully addressed. To begin to answer such questions, it is necessary to develop a diversity of markers to characterize the determinants of binding and trafficking behaviors.

Here the biophysical characterization has been done for a fluorescently tagged sphingolipid binding raft probe, Sphingolipid Binding Domain (SBD). This motif, identified by Fantini and colleagues in several glycolipid-associated proteins, was postulated to form a V3 loop structure that interacts with the sugar rings in glycosphingolipid headgroups **[200]**. It also has been known that SBD is targeted to endo-lysosomal compartments in a cholesterol-dependent manner, and it interacts with raft-like lipid mixtures **[123]**.

FCS analysis on live SHSY5Y cell membranes has been performed to describe the characteristics of SBD association with the plasma membrane. The fluidity of the membrane environment is reflected by the mobility of the fluorescent labels travel through the stationary confocal volume, and therefore in the diffusion time. Lipid-protein overlay experiments (fat blots) conducted by Hebbar *et al*. **[81]** suggest that SBD interacts with particular gangliosides and sphingomyelin, which are generally thought to reside in raft domains. Biochemical studies in that article also demonstrate that SBD interacts with detergent insoluble membrane fractions isolated from neuronal cells and the uptake of SBD occurs largely via cholesterol rich membrane microdomains **[81]**. In this FCS study diffusion behavior of SBD with 2 different fluorescent tags (Oregon Green and TMR) has been compared with the reference of CTxB as a raft associated marker (positive control) and DiI and Bodipy-Sphingomyelin as non-raft associated markers (negative controls), which specially demonstrates that SBD displays mobility characteristics consistent with raft association. Further, using pharmacological removal of cholesterol (using MβCD as a cholesterol depleting agent), it was confirmed that SBD association and uptake at the plasma membrane is cholesterol dependent. To check the sensitivity of these microdomains towards cholesterol, the study was then further extended to a series of measurements with gradual cholesterol removal by varying the MβCD concentration; and the results showed significant gradual change. In summary, SBD can serve as a useful tool for the study of cholesterol-dependent sphingolipid based membrane microdomains.

3.2 Materials and Methods

In order to compare between the dynamic behavior of the raft and the nonraft phases of live cell membranes, the following fluorescent probes were used in this study; $DiIC_{18}$ (Molecular Probes, catalog number D-282) and Bodipy FL Sphingomyelin (Molecular Probes, catalog

number D-7711) as non-raft markers (negative control), and cholera toxin subunit-B (Molecular Probes, catalog number V-34405) conjugated with Alexa Fluor-594 as an established raft marker (positive control) for this study. The single point mutated [K 16 E] 1-25 amino acid residue of amyloid beta peptide with an N-terminal Cysteine and an inert spacer (amino-ethoxy-ethoxy-acetyl) [sequence C-(amino-ethoxy-ethoxy-acetyl)$_2$-(DAEFRHDSGYEVHHQ**E**LVFFAEDVG)] was synthesized and conjugated with fluorescent dyes (TAMRA and Oregon Green) by BACHEM, Bubendorf, Switzerland.

3.2.1 Cell culture and plating for measurements

SH-SY5Y neuroblastoma (ATCC, USA) cells were grown at 37ºC in Dulbecco's Modified Eagle's Medium (DMEM / F12 (1:1); Gibco, USA) supplemented with 10% fetal bovine serum (FBS; Gibco, USA) and 1% antibiotic. For labeling, cells were plated on 8-well chambers with 0.17 mm coverslip bottoms (Nunc, Denmark); >24 hours prior to the drug treatments / measurements.

3.2.2 Incubation procedure of different markers

3.2.2.1 DiI

Stock solution of DiI was prepared by dissolving the powder form of the reagent in DMSO and kept at 4º C for long term storage. Concentration of this stock solution was determined using UV spectrophotometer. DiI working solution (~ 10 nM) was prepared by diluting the stock in complete growth medium. For staining, first cells in 8 well chamber were washed 3 times with HBSS (Gibco), supplemented with 10 mM HEPES (HBSS/HEPES) buffer followed by half an hour incubation with prepared DiI working solution at 37^o Celsius. The cells were then washed 3 times again with the same buffer and suspended in indicator free DMEM for measuring.

3.2.2.2 Bodipy FL Sphingomyelin

The concentration of the stock solution is 1 mg/ml in DMSO and stored at -20º C. The working solution was prepared by diluting the stock solution 100 fold in complete growth medium and cells in 8 well glass bottom chamber were incubated with this working solution for 30 mins at 37º C and followed the same washing technique and buffer and then put into indicator free DMEM for measuring.

3.2.2.3 Cholera toxin

1000 fold dilution of 1 mg/ml stock solution of the Alexa Fluor-594 conjugated cholera toxin subunit-B with chilled complete growth medium results the CTxB working solution. Cells in 8 well chambers were then washed 3 times with HBSS/HEPES buffer similarly as done before for the other markers and incubated for 30 min with the prepared CTxB working solution at 37^{o} C. The cells were then washed 3 times again with the same buffer and suspended in indicator free DMEM for measuring.

3.2.2.4 SBD-TMR and SBD-OG

To avoid aggregate formation, SBD was dissolved in 1,1,1,3,3,3-hexafluoro-2-propanol (HFIP; Merck), divided into aliquots, dried and stored at -20º C. For larger volumes of peptide, evaporation was done under a supply of inert nitrogen and lyophilized peptide was stored similarly at -20º C. The peptide was re-dissolved in DMSO immediately before use and diluted to a final working concentration of ~10 nM in HBSS/HEPES. The cells were then incubated for 30 min with this prepared SBD working solution at 37^{o} C, washed 3 times again with the same buffer and suspended in indicator-free DMEM for measurements.

3.2.3 Drug treatment

3.2.3.1 MβCD treatment

A 100 mM stock solution of the reagent was prepared by dissolving the powder MβCD (Sigma, USA) in de-ionized water and kept in room temperature for long term storage. For the drug treatment, the cells were first washed 3 times with HBSS/HEPES; followed by 30 minutes incubation at 37^{o} C with the working solution of MβCD, which was prepared by diluting the stock in serum free growth medium. The cells were then washed again 3 times with the same buffer followed by the as usual staining procedure for different dyes to measure their relative change in diffusion behavior.

3.2.4 Instrumentation

3.2.4.1 Confocal FCS

The confocal FCS instrumental setup used in this study has been described in section **2.2.3**. To excite Bodipy FL sphingomyelin and SBD-OG, the 488 nm Argon laser was used and the emitted fluorescence signal was detected by the APDs through a 510 AF23 emission filter (Omega, USA). The 543 nm He-Ni laser attached to the system was used as the excitation source for DiI, CTxB-Alexa-594, and SBD-TMR and the emitted fluorescence signals were detected through 595 AF60 emission filter (Omega, USA). For all the measurements 100 μW laser power before the microscope objective was used.

3.2.4.2 ITIR FCS

The image based FCS measurements carried out in this study was using the Zeiss inverted epifluorescence microscope setup as described in section **2.3.2**. The 532 nm laser was used to excite the only fluorescent probe TMR, attached with SBD used in this study. The laser power used for the excitation as measured before the objective was maintained at 6 mW for

all the measurements. The fluorescence signal from the sample was then collected by the cascade II EMCCD camera after passing through the 560 DRLP dichroic mirror and the 595 AF60 emission filter.

3.3 Results

3.3.1 Comparison between different raft and non-raft markers

The main goal of this study is to look at the diffusion of SBD, to characterize whether it displays raft-like behavior, i.e. diffusion behavior distinct from membrane-associated probes that do not interact specifically with sphingolipids. To compare the mobility of SBD on the plasma membrane with that of other raft- and nonraft-associated markers, FCS measurements on the plasma membrane of SH-SY5Y neuroblastoma cells were carried out. FCS records fluorescence autocorrelation functions $G(\tau)$, from a diffraction-limited confocal volume centered on the upper plasma membrane of the cell. Depending on the number of different fluorescent particle species passing through the confocal volume and their location with respect to the plasma membrane, different models need to be used to fit $G(\tau)$, incorporating one or more particles with different mobilities in two or three dimensions (i.e., one particle vs. two particles and two dimensions vs. three dimensions). The diffusion time, τ_D, is derived from the autocorrelation curve $G(\tau)$ and gives the time taken by the fluorescent probe to cross the stationary confocal volume. A multiple particle fit will result in a number of diffusion times, which are inversely proportional to the diffusion coefficients. The τ_D is characteristic of the viscosity in which the membrane probe resides. Faster movement of any probe through the stationary detection volume indicates that the corresponding fluid phase is less viscous while a longer diffusion time reflects a more viscous sample phase (cholesterol rich domains

in case of cell surface). Thus the diffusion time, τ_D, can be used to predict the membrane domain localization of the probe **[147]**.

In this study measurements were taken for 5 different markers; the nonraft markers DiI-C_{18} and Bodipy-FL-SM **[186, 201]**; the well established raft marker CTxB-Alexa-594 and the two forms of SBD; SBD-TMR and SBD-OG (*Fig. 3.1*).

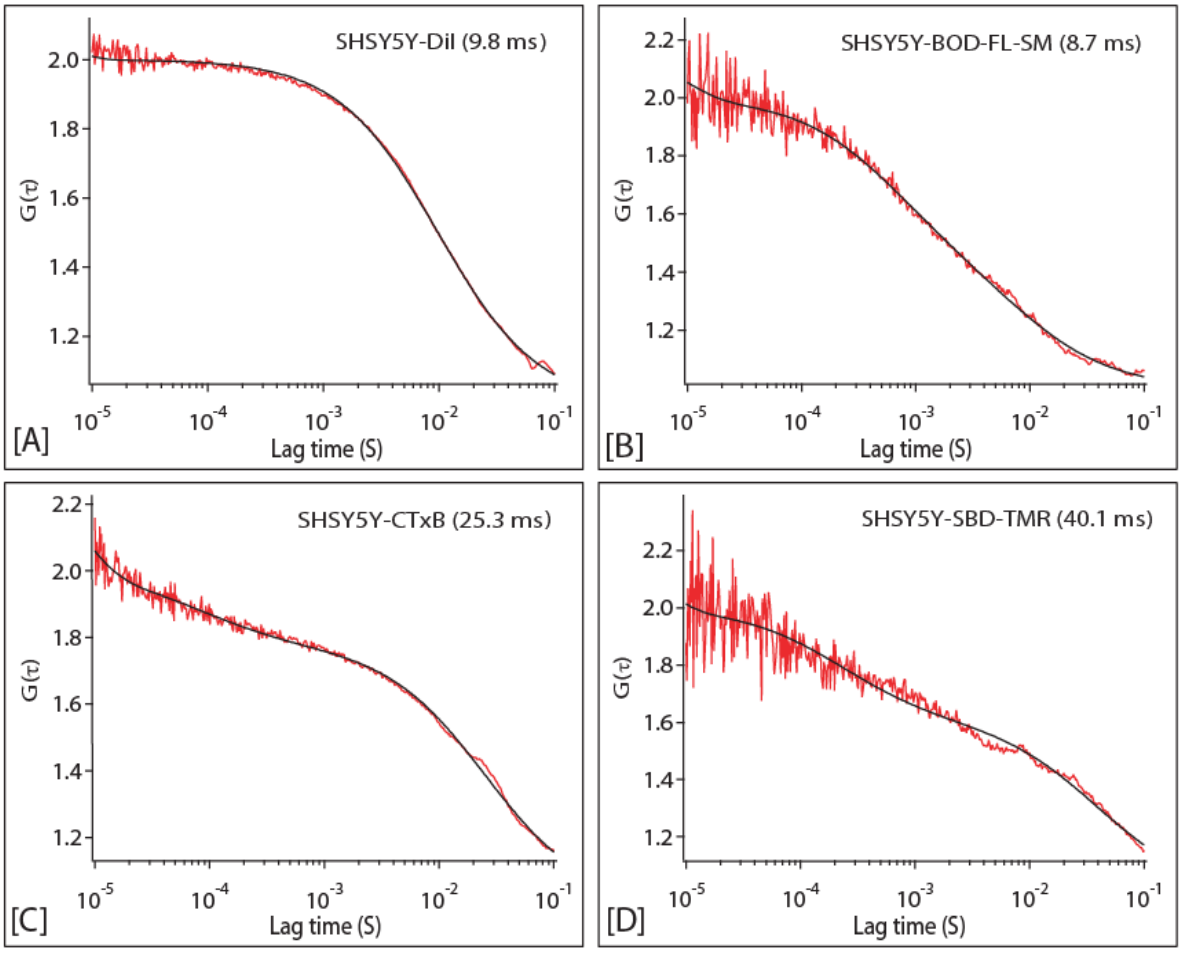

Figure 3.1: *Correlation curves of SBD (SBD-TMR; D) versus raft (CTxB; C) and nonraft markers (DiI-C18; A; and BODIPY-FL-SM; B) on SH-SY5Y cells are presented here. Normalized correlation curves G(τ) are shown over 100 ms time intervals obtained from different fluorescent labels on SH-SY5Y neuroblastoma cells. Experimentally obtained autocorrelation functions are given in red; black lines represent fits to the data. Functions gave the best fits to two-dimensional, two-particle models. SBD and CTxB contain a strong bleaching component, indicating the lower mobility of the structures in which they reside, whereas dialkyl-indocarbocyanine (DiI)-C_{18} and BODIPY-FL-SM were not influenced by bleaching.*

The $G(\tau)$ functions obtained from these measurements were fitted with different fitting models (mathematical expressions given in chapter 2) taking into account for the different sets of molecules moving in different dimensions with well separated diffusion speeds from

each other. As DiI does not give fluorescence signal in an unbound state resulting in a lack of a distinct 2nd set of particles, the $G(\tau)$ curves obtained from DiI experiments were fitted with a two-dimensional one-particle one-triplet (2D-1P-1T) model. For the rest of the markers a two-dimensional two-particle one-triplet (2D-2P-1T) model was used to fit the experimental curves. The 2 two-dimensional diffusing species were interpreted as a faster moving, nonraft-associated population of SBD/CTxB label in the plasma membrane in addition to a less mobile, raft-associated component. In agreement with the findings of Schwille and colleagues **[147]**, measurements of the raft marker CtxB-Alexa-594 were influenced by bleaching effects, presumably as a result of the low mobility of the protein in raft domains (*Fig. 3.1*).

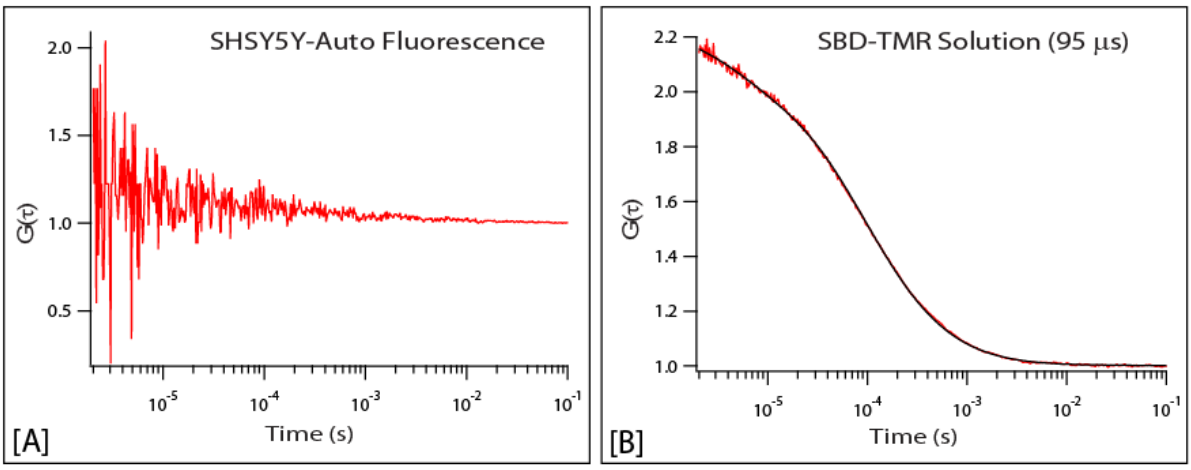

Figure 3.2: *The G(τ) graph of auto-fluorescence of SHSY5Y (A) shows that there is actually no correlation there and not possible to fit with any FCS fitting model.; Autocorrelation curve of SBD-TMR in solution (B) shown over 100 ms time interval (same as that of fig 3.1) producing a much shorter diffusion time clearly states the difference in diffusion with the membrane bound population. Experimentally obtained autocorrelation functions are in red; fits are given as black lines.*

In order to measure the contributions from free label in the medium (outside the cell) or internalized cytosolic marker (inside the cell) to $G(\tau)$, additional measurements were made outside and inside the cell with SBD-TMR. The diffusion times obtained for extracellular and intracellular SBD are 115 ± 5.8 µs and 499 ± 5.7 µs, respectively [**202**]. Values outside the cell were fitted to a three-dimensional, one-particle one triplet (3D-1P-1T) model, and values inside the cell were fitted to a three-dimensional, two-particle one triplet (3D-2P-1T) model.

Normally the diffusion times for the membrane-associated markers are expected to be not smaller than the millisecond range (τ_D for DiI, a typical nonraft membrane probe, is 10 ± 0.4 ms). Moreover, τ_D for free marker in solution is observed to be in the ~100 μs range. Therefore, readings dominated by those short time components were removed from the calculation of the average τ_D (*Fig. 3.2*).

It was found from the FCS measurements that SBD-TMR and SBD-OG measurements, similar to CTxB, were strongly influenced by bleaching. To separate these effects, which artificially bias the τ_D towards faster moving particles, and to get a broad overview about what fraction of the probes are really bound to the raft fraction and moving slowly on the membrane the τ_D frequencies was expressed as histograms. From this approach a large fraction (~40%) of τ_D of SBD-TMR and SBD-OG were found to be in the very slow moving (τ_D >30 ms) category (average τ_D of SBD-TMR and SBD-OG being ~50 ms), with a slightly greater contribution of slow-moving particles than CTxB (average τ_D ~25 ms) (*Fig. 3.3*). In contrast to the longer diffusion times (slower diffusion) of the raft markers, the τ_D values of DiI-C18 and Bodipy-FL-SM, were distributed to a large extent between 1 and 20 ms (*Fig. 3.3 A*), with the main contribution being in the 1–10 ms range; average τ_D values being 10 ± 0.4 ms for DiI-C18 and 10 ± 2 ms for Bodipy-FL-SM (*Fig. 3.3 E*). The histograms also reveal a bimodal distribution for the raft associated markers which is the same for SBD-TMR and SBD-OG, with a slow population diffusing at >30 ms and a slightly larger fast population diffusing mainly between 1 and 10 ms time range. The slower population indicates the raft associated fraction of the probe and not induced aggregation, as no changes in the counts per particle had been observed in this case, which one would find upon aggregation. The bimodal distribution is less pronounced but still well recognized in case of CTxB (*Fig 3.3 D*). [Note that, since there are almost no values in the >30 ms range for the non-raft associated markers

(*Fig. 3.3A*); all readings that have τ_D values >30 ms for the raft associated probes are pooled into one group in the histograms in *Fig. 3.3 B*.]

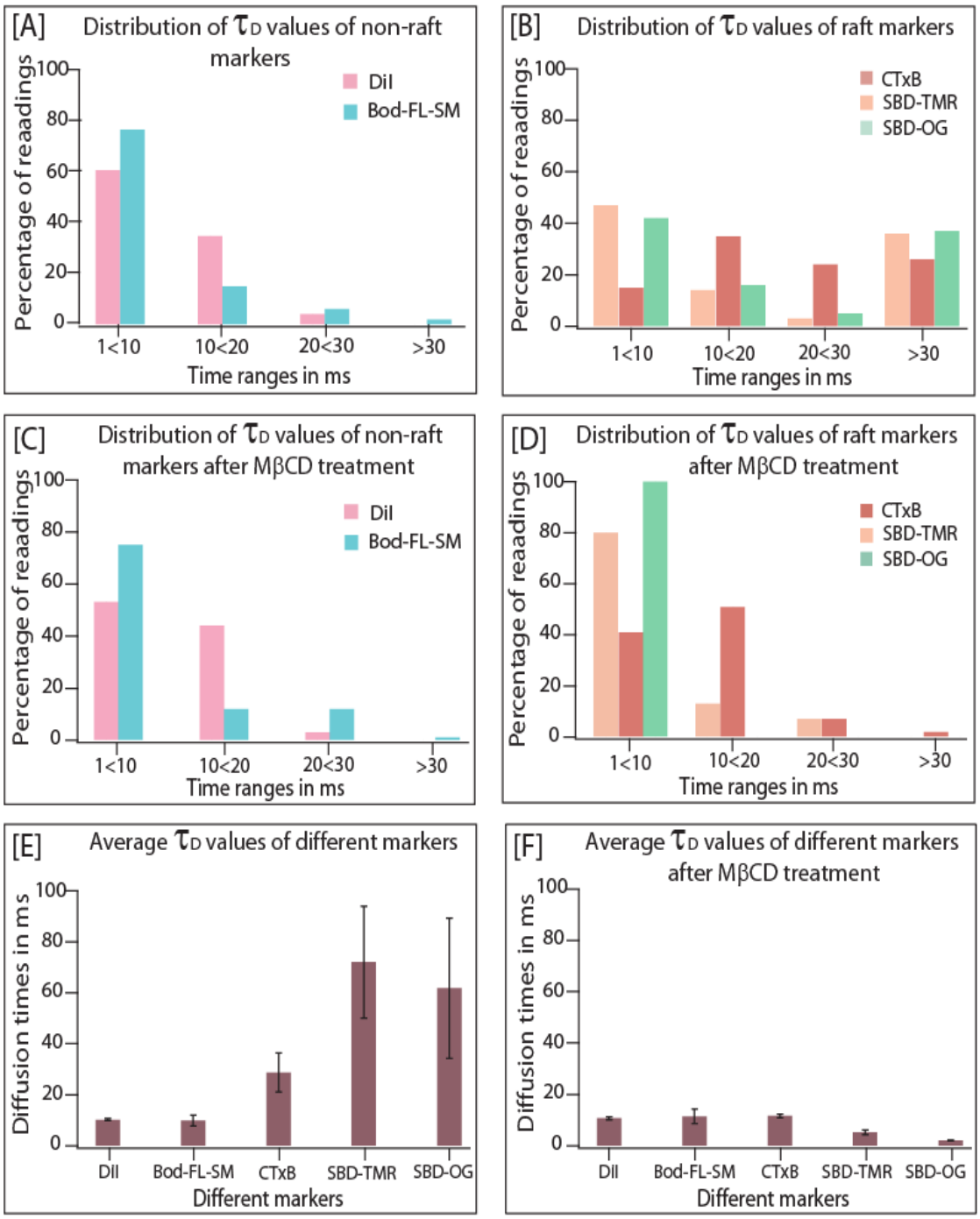

Figure 3.3: *The distribution of diffusion times for SBD along with raft- and nonraft markers. Histogram A shows the nonraft-localizing markers DiI and Bodipy-FL-SM, which shows most of the readings in the faster mobility ranges. In contrast, in B, CTxB-Alexa594, SBD-TMR, and SBD-OG give substantial fractions of readings in the low-mobility τ_D >30 ms range, typical for raft markers. The>30 ms cluster actually consist of values ranging from 30 ms to over 100 ms. C: Distribution of nonraft markers after cholesterol depletion is not altered significantly (compare with A). D: Distribution of raft markers after cholesterol depletion is shifted strongly toward faster diffusion times (1–10 ms range). E, F: Average diffusion times for all markers before and after cholesterol depletion. Error bars reflect SEM, for all the experiments, n is >50 measurements.*

3.3.2 Comparison between raft and nonraft markers after cholesterol depletion.

In order to look at the effects of raft disruption on the mobility of SBD, the diffusion times of SBD as well as all the control markers were measured on cells treated with 10 mM MβCD for 30 mins.

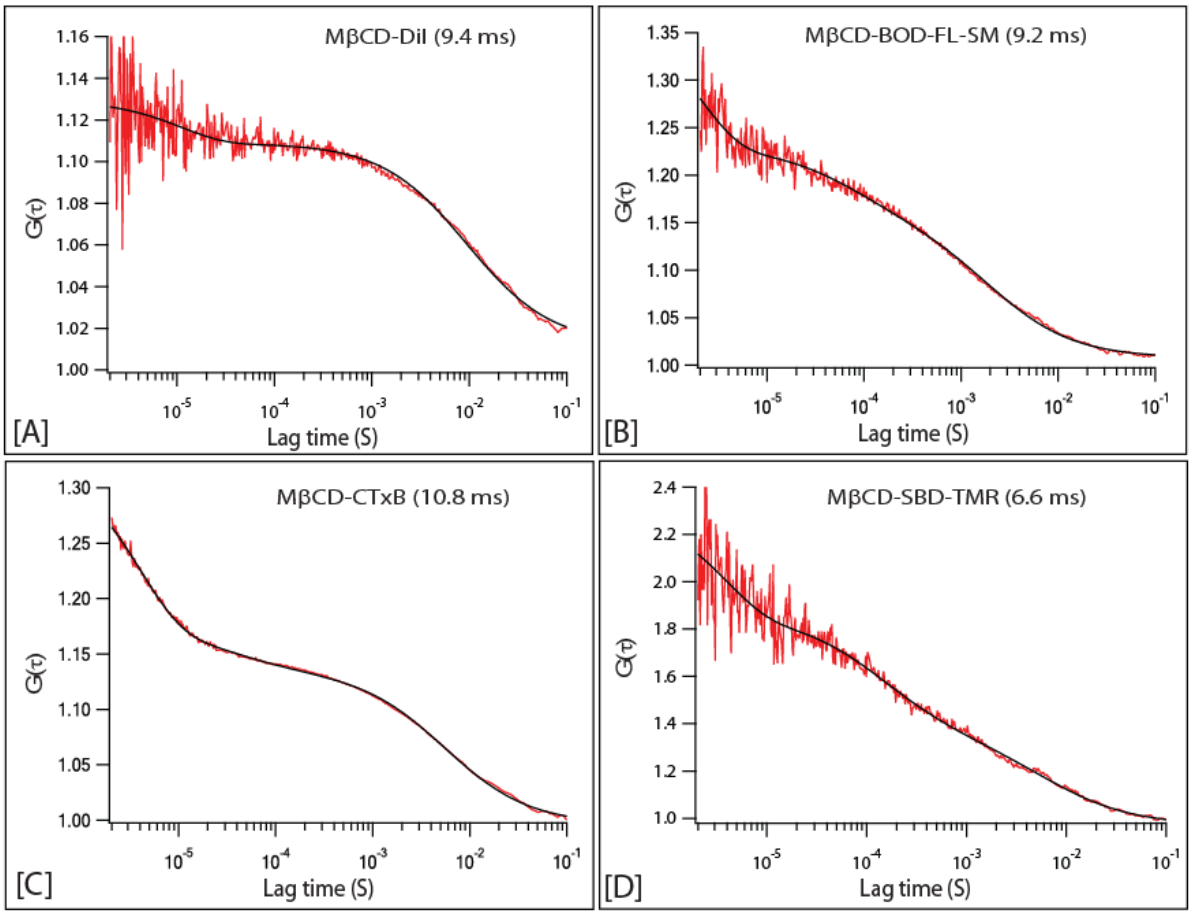

Figure 3.4: *Correlation curves of nonraft markers (DiI-C18; A; and Bodipy-FL-SM; B) versus raft markers (CTxB; C) and (SBD-TMR; D) in SH-SY5Y cells under cholesterol depleted condition (10 mM MβCD for 30 mins at 37° C). The curves G(τ) are shown over the same 100 ms time intervals. Functions gave the best fits to two-dimensional, two-particle models. Experimentally obtained autocorrelation functions are in red; fits are given in black. The bleaching components of SBD and CTxB, indication of the slower mobility has been gone completely and the curves merge with the time axis, similar to that of the non raft markers after the cholesterol removal from the membrane.*

It was found that the diffusion times of DiI and Bodipy-FL-SM under cholesterol depleted condition remained almost unchanged at 10.7 ± 0.6 and 11.5 ± 2.9 ms, respectively (*Fig. 3.3 E, F*), whereas τ_D values of SBD, indicating their raft association, were greatly reduced to 5.3 ± 0.9 and 4.1 ± 0.2 ms for SBD-TMR and SBD-OG, respectively (*Fig. 3.3 F*). The average

diffusion time of CTxB was also reduced to 11.6 ± 0.8 ms, consistent with its raft localization being dependent on cholesterol (*Fig. 3.3 F*). These changes are also reflected in the distributions of diffusion times represented as histograms (*Fig. 3.3 C, D*) , where all the slow moving components (>30 ms) were shifted towards the fast moving population diffusing mainly between 1 and 10 ms time range, and this is similar for all three raft associated markers; whereas the distributions of the nonraft markers (DiI and Bodipy-FL-SM) remained similar as before the drug treatment (mainly in 1-10 ms range) showing their non-dependency on cholesterol. The trend of shortening the diffusion time upon the MβCD treatment, obtained quantitatively from the histogram distributions can also be seen qualitatively in the ACFs of these markers (*Fig. 3.4*).

3.3.3 Effects of different laser powers on SBD and CTxB data due to varying extent of photobleaching

As it was found that the ACF curves of SBD-TMR and SBD-OG measurements, similar to CTxB, were strongly influenced by bleaching, which artificially biases the τ_D towards faster moving particles, measurements were carried out at different laser powers to check its influence on the diffusion times of the raft as well as non-raft markers. The non-raft marker DiI shows similar values (τ_D ~ 10 ms) at all laser powers indicating a limited influence of bleaching on the τ_D measurements (*Fig. 3.5*). For SBD and CTxB the diffusion time showed some increase at lower laser powers (25μW) indicating that photobleaching also plays a role in the measurements. However, the range of the average diffusion time for both raft markers and their significant difference from the non-raft marker (DiI) remained similar under all laser powers.

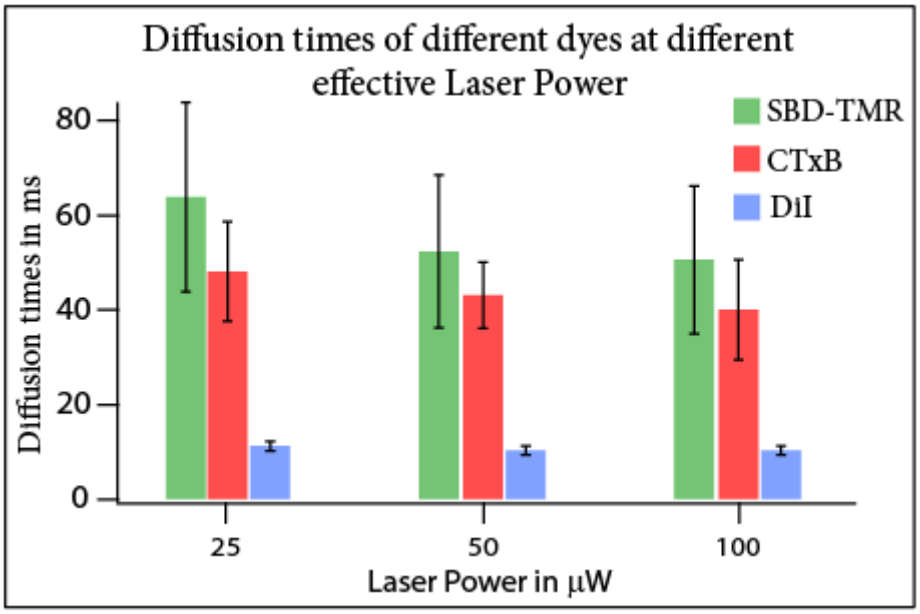

Figure 3.5: *Average diffusion times for SBD-TMR, CTxB and DiI different laser powers. Consisting with its bleaching free measurements DiI exerts similar diffusion times under all the 3 conditions, which reflects its non dependency on laser power. In case of SBD and CTxB, 50 mW and 100 mW laser powers result very close values where as 25 mW shows a little larger diffusion times when bleaching was significantly reduced, still the trend of raft markers and their difference with non-raft markers are similar under all the laser powers. Error bars reflect SEM. For all the experiments, n is >30 measurements.*

3.3.4 Effects of titrated cholesterol depletion by MβCD on the mobility of SBD

As an extension to prove SBD's raft association and the cholesterol dependency of its movement on the plasma membrane, cells were titrated with different concentrations of MβCD, a cholesterol depleting agent, and the results were compared for both, confocal FCS as well as ITIRFCS. Both of the formats showed the same expected trend. The diffusion time decreases with increase in concentration of MβCD, indicating increasing mobility and loss of raft association.

3.3.4.1 Confocal FCS results

For this study only SBD-TMR was used as a raft marker and the same histogram based distributions were done to analyze the data. It was found that, with increase in concentration of

MβCD (*Fig 3.6 A to F*), the slow moving component (τ_D > 30 ms) gradually reduced and vanished completely in cases of 5 and 10 mM (*Fig 3.6 E* and *F* respectively).

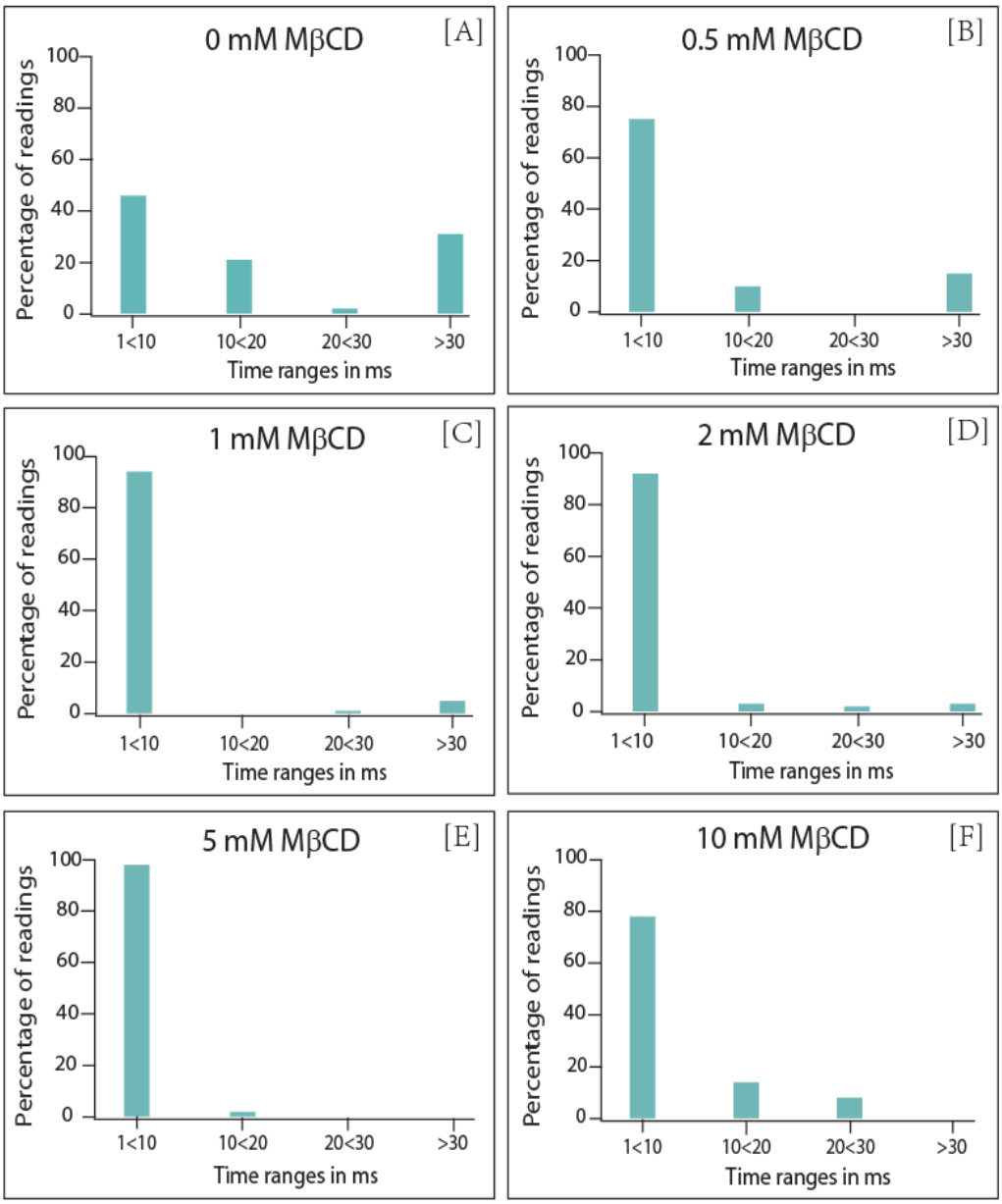

Figure 3.6: *The distribution of diffusion times for SBD-TMR under different extent of cholesterol depletion. Concentrations of the MβCD solution used are written on the top of every distribution panel. The distributions show with increase in concentration of MβCD (A to F), the slow moving component (τ_D > 30 ms) gradually reduced and vanished completely in cases of 5 and 10 mM (E and F respectively).*

Simultaneously, almost all the values concentrate in the 1-10 ms range, indicating comparatively faster and homogeneous distribution of the cell membrane. The average diffusion times also showed the same trend, i.e. the average τ_D values continued decreasing

with increasing MβCD concentration (*Fig 3.7 A*). At 0 mM MβCD the average τ_D value was ~70 ms which dropped to ~5 ms after treating with 5 mM MβCD and didn't show any further change in average diffusion time after treating with 10 mM MβCD (τ_D ~5 ms). This study indicates 5 mM of MβCD is sufficient for the complete disruption of SBD's raft association.

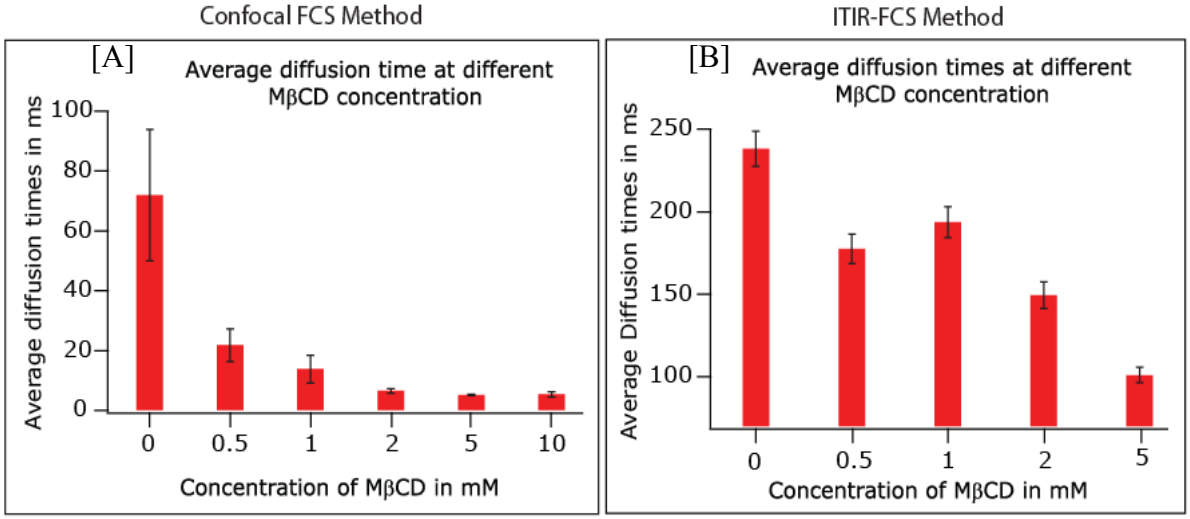

Figure 3.7: *Average diffusion times for SBD-TMR, measured on the upper membrane (A; with the confocal FCS instrument) and at the bottom membrane (B; with the ITIR-FCS instrument) of SHSY5Y neuroblastoma cells after different extent of cholesterol depletion with varying concentrations of MβCD. As the instrumentations were entirely different for these two methods, the diffusion times (which is not an instrument independent parameter) obtained from these two methods are in two different time scales. Though the confocal measurements show a greater change in average diffusion times still the trend of decrease in diffusion time with increase in MβCD concentration is similar for both the methods, reflecting the cholesterol dependency and raft association of the diffusion of SBD. Error bars reflect SEM, for all the experiments, n >50 measurements.*

3.3.4.2 ITIR-FCS results

Using ITIR-FCS, the new method to multiplex FCS measurements, mobilities of SBD-TMR were studied at the lower plasma membrane of SHSY5Y cells to get a global overview of change in diffusion times of the whole cell membrane after treating with different concentrations of MβCD. Diffusion time being an instrument dependent parameter and as the measurements are taken at the lower plasma membrane of the cell in case of ITIR-FCS, as a result, the values obtained using this method are of a different time scale compared to that of the confocal FCS method. However, this method also shows the same trend, as seen in the

case of confocal FCS, with increase in concentration of MβCD, the diffusion time decreases indicating increasing mobility and loss of raft association.

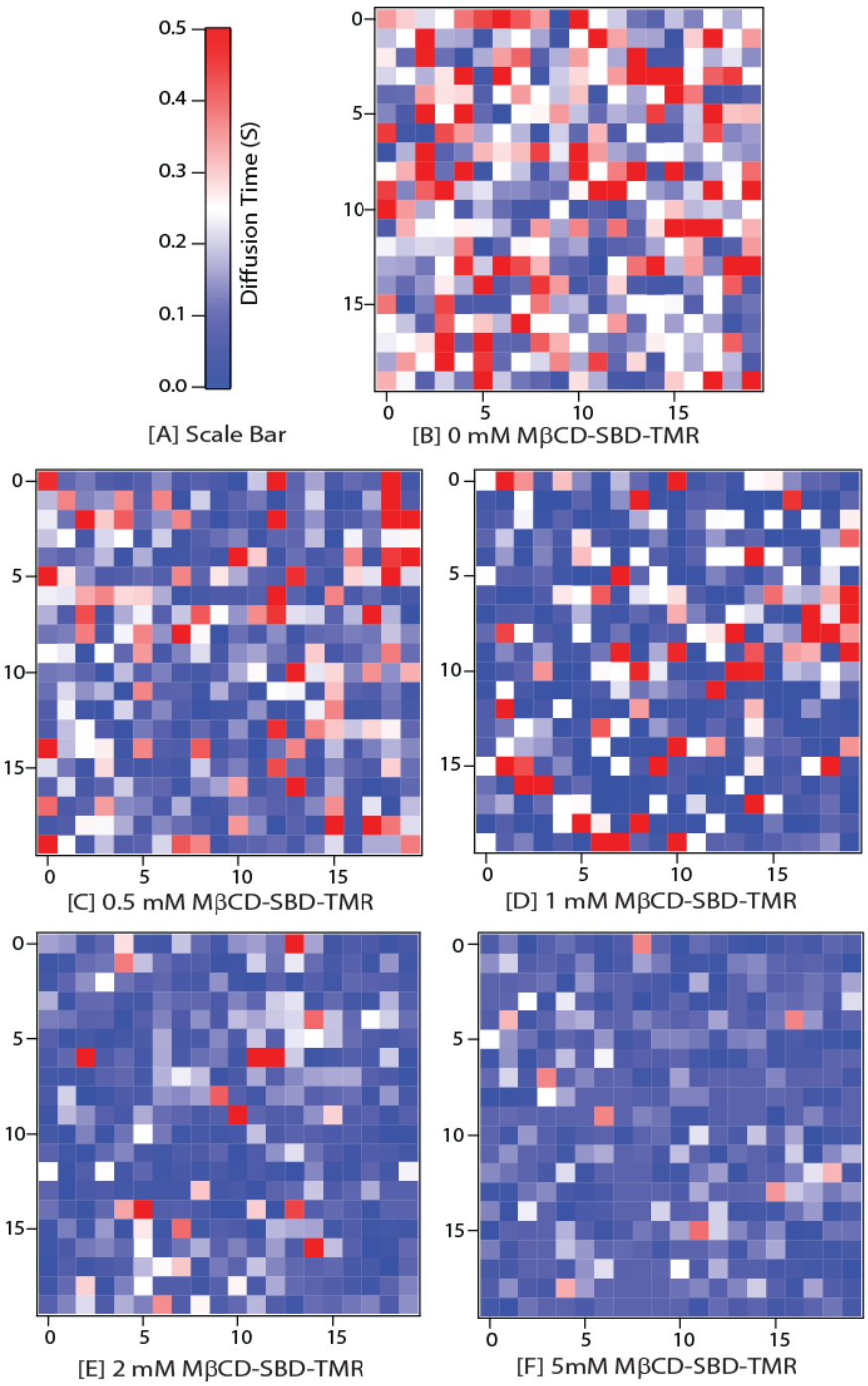

Figure 3.8: *Pictorial representation of diffusion times of SBD-TMR after treatment with varying concentrations of MβCD. The diffusion times are extracted by fitting ITIR-FCS data of a 20 x 20 pixels ROI on the lower cell membrane of SHSY5Y neuroblastoma cells. The x- and y-axis in the graphs are the pixel positions within the image. The color code is given in the scale bar and diffusion times increase from blue to white to red. The experiments show that the diffusion in the membrane increases with increasing concentrations of MβCD (B to F).*

The diffusion times of SBD-TMR at each point of the whole ROI (20 x 20 pixels) measured at the bottom plasma membrane of SHSY5Y cells treated with varying concentrations of MβCD are represented pictorially with different color codes to show the global dynamic view of the whole cell membrane. As the excitation source of this method is total internal reflection based, the laser doesn't go through the whole cell; the evanescent wave field penetrates maximum only up to ~200 nm. As a result the fluorescence signals obtained from the sample were purely from the lower membrane of the cell; hence the autocorrelation functions were fitted according to equation 2.17, as described in chapter 2, to get the diffusion times at each pixel of the measured ROI. The pictorial representations state the diffusion times of each and every pixel corresponding to the range of the representative color code shown in the scale bar (*Fig. 3.8 A*); which indicates the number of slow moving points gradually reduced and the fast moving points increases with increase in concentration of MβCD (*Fig. 3.8 B to F*), resulting in an overall speeding up of the diffusion in the whole membrane.

3.4 Discussion

These results show that SBD bound to the membrane of the mammalian neuroblastoma cells through a cholesterol dependent mechanism. The biophysical characterization of SBD's association with the plasma membrane has been done by examining its diffusion dynamics with FCS in human neuroblastoma cells. In this study, the τ_Ds of the nonraft markers (DiI and Bodipy-FL-SM) were distributed within a comparatively narrow range, unlike the raft markers, which were distributed in a very wide range of τ_D values. However, the clustering of the histogram of SBD τ_D values around >30 ms and ~1–10 ms is consistent with the estimates of Pinaud *et al*. **[53]** and Sharma *et al*. **[134]** that ~75% of a raft-associated glycosylphosphatidylinositol linked protein is actually present in the nonraft fraction. A

similar type of biphasic distribution of diffusion times for SBD and CTxB may reflect the existence of two distinct populations at the plasma membrane, one of which is associated with the liquid-ordered phase and the other might correspond to the SBD molecules perhaps more loosely associated with [**202**] the liquid-disordered phase. This mixed distribution is observed by other authors as well for a number of presumed raft-associated proteins **[36]**. It is interesting that, although the clustered histogram distribution of τ_D values of CTxB was very close to those of SBD, the τ_D value for this established raft marker on average was shorter than those of SBD (*Fig. 3.3 E*). This may indicate that CTxB and SBD are both at least partially raft-associated but that the dynamic nature of their resident domains is different.

Raft associated markers are expected to be bleached, because laterally they are less mobile than the surrounding nonraft membrane and thus are unable to leave the focus **[203, 204]**. Accordingly, some bleaching components have been seen in the measurements of SBD and CTxB, though the bleaching rate were less compared to the report by Bacia *et al.* for in vitro CTxB [**147**]. Therefore, the extremely slow mobile fraction observed in this study for SBD and CTxB compared with DiI, suggests their association to raft-like structures or cross-linked raft assemblies.

Drugs that remove cholesterol from the plasma membrane are known to inhibit the trafficking of lipid raft markers and have been used extensively as tools to differentiate between raft- and nonraft-mediated processes **[203, 205]**. Using FCS on neuroblastoma, under cholesterol depletion, the influence of bleaching on the autocorrelation function is in fact removed, and a large change in τ_D values for SBD was found. The shift is toward nonraft-like fast diffusion times. This is similar to the effect on the raft marker CTxB, whereas the nonraft markers did not show any significant change **[147]**. Moreover this change is gradual, and not abrupt, with respect to the concentration of the drug used as seen from the concentration variance experiments.

3.5 Summary

The FCS data shows that SBD's diffusion behavior at the plasma membrane is consistent with a substantial fraction being localized in raft domains of low mobility relative to that of the surrounding membrane. Looking at the confocal FCS and the ITIR-FCS results after the MβCD treatment, and considering the biochemical studies on SBD **[81]**, it can be said that, even in the absence of cholesterol, SBD is able to associate to some extent with the membrane and diffuse at the speed of nonraft markers. Overall this part of the study supports the notion that SBD can be used as a fluorescent tracer for the cholesterol-dependent, glycosphingolipid-containing slowly diffusing (raft like) microdomains in living cells.

Chapter 4:

SBD uptake pathway

4.1 Introduction

Endocytosis is the process by which cells absorb essential extracellular components (such as proteins and nutrients) by uptake through the cellular membrane. The process is required for a number of functions that are essential for proper cellular functions. Endocytosis is responsible for regulating many cellular processes including nutrient uptake, cell adhesion and migration, receptor signaling **[206]**, pathogen entry **[207]**, receptor down regulation, antigen presentation, neurotransmission, cell polarity, mitosis, growth and differentiation, and drug delivery **[208, 209]**. The endocytic pathways can be subdivided into four categories: namely, clathrin-mediated endocytosis, caveolae, macropinocytosis, and phagocytosis **[210]**. The major route for endocytosis in most cells, and the best-understood, is the clathrin-mediated pathway. This large protein forms a coated pit on the inner surface of the plasma membrane of the cell. It was also observed that, cells that lack clathrin or caveolae, internalize different essential molecules via alternative pathways. Some recent studies have shown that a highly prevalent clathrin-independent endocytic pathway known as the CLIC/GEEC is regulated by Rho GTPase activation protein **[211].** This CLIC/GEEC pathway relies upon cellular signaling and activation through small G proteins, but the mechanistic insight into the biogenesis of its tubular and tubulovesicular carriers are still not clear **[212]**. These findings of the clathrin-independent endocytic pathways had increased interest about the identification of the endocytic machinery and membrane-trafficking itineraries of these pathways. Among these non-clathrin pathways, some are based on

constitutive internalization mechanisms, whereas others are initiated by specific signals, e.g. cytokine signaling **[212, 213]**. It has been documented in some studies that some cargoes might be endocytosed through alternate or sequential pathways, depending on the structural properties of the cargo and the type of cell under investigation **[214-216]**. Several bacterial toxins, as well as the amyloid precursor protein (App), make their association with the plasma membrane and subsequent endocytosis via a raft-mediated mechanism, assisted by components common to clathrin- and/or dynamin-mediated uptake **[123, 217]**.

One well studied class of raft-borne endocytic cargos are the GPI-APs **[218]**, which are thought to internalize via cdc42, into a specialized 'GEEC' compartment **[133]**. Raft-associated adaptor proteins flotillin-1 and flotillin-2 constitute a separate internalization pathway from either caveolin or GPI-AP uptake **[137, 219]**. It is also widely accepted that the phenomena of clathrin-independent internalization are associated with plasma membrane nanoclusters or microdomains or lipid rafts, defined functionally by their requirement for sphingolipids and cholesterol **[220]**. Cholesterol serves an important role in clathrin-independent endocytosis, such as caveola formation **[221]**, and other raft-mediated uptake mechanisms. Caveolae are reported non-clathrin coated plasma membrane buds, which exist on the surface of most of the cell types. A certain level of cholesterol is required for the organization of raft-borne molecules into nanoclusters at the cell surface, estimated to be ~20-40% of the overall lipid at any given time **[52, 134, 222]**. The cholesterol content in membranes has been shown to influence the integrity and functions of lipid rafts in signal transduction **[223, 224]**. It is also known that overload of cholesterol and sphingolipids influences the membrane trafficking of raft adaptor proteins **[225]** and lipid raft constituents, as occurs in the lipid storage diseases **[15, 226]**.

It is obvious from the above discussion that cholesterol and sphingolipids are important for the uptake and trafficking of raft-associated molecules, but the rules that govern the endocytic

trafficking routes of these cargoes are not yet clear. Although distinct intracellular pathways are known for certain raft mediated uptake **[133, 134]**, it is still not clear how or whether the specific uptake mechanism also affects the subsequent intracellular targeting. Neither has there been any observation yet that would link the endocytic machinery (apart from cholesterol and sphingolipids) with a particular diffusion behavior on the cell surface **[52, 227]**.

In this chapter, the relationship between uptake mechanism, surface behavior and endocytic targeting of the recently characterized sphingolipid and raft-interacting probe, sphingolipid binding domain (SBD), has been investigated on mammalian neuroblastoma cells. SBD, consisting of the V3- loop domain of the amyloid beta peptide (Aβ) **[43]**, was shown to interact with a subset of glycosphingolipids, sphingomyelin and cholesterol in artificial membranes as well as with cholesterol- and sphingolipid-dependent microdomains in neurons **[123, 221]**. In this study, it is shown that SBD uptake is dependent on two different mechanisms – one is flotillin dependent uptake and the other is cdc42 dependent uptake. Generally these two pathways are independent and parallel to each other **[133, 137, 213]**. Blocking of either flotillin or cdc42 dependent pathways results only in partial suppression of the uptake of SBD into cells, whereas knocking out both pathways simultaneously nearly eliminates uptake. This suggests that there might be a synergic relationship between these two mechanisms. By contrast, drastic changes in the raft-like diffusion behavior of SBD are seen when either or both of these uptake pathways are perturbed.

4.2 Materials and Methods

Drugs used to knock down flotillin dependent and cdc42 dependent uptake pathways in this study are siRNA with the sequence 5′-UAACCUCCUCACUGAAGGdTdT-3′ was used against flotillin-2 (both from 1st BASE, Singapore) and Clostridium difficile toxin B

(Calbiochem), respectively. The transfection vector Lipofectamine-2000 and Opti-MEM I both were from Invitrogen.

4.2.1 Cell Culture

SH-SY5Y neuroblastoma cells were cultivated at 37° C in DMEM similarly as described in the previous chapter and plated in the 8 well chambers for measurements. In this study of SBD uptake mechanism; two markers have been used SBD-TMR and DiI; cells were treated with these markers similarly as described in chapter 3.

4.2.2 siRNA-Flotillin knockdown

Cells were grown in 8-well chambers with 0.17 mm coverslip bottoms one day before transfection. For the transfection, per well, 1 µl of Lipofectamine-2000 (Invitrogen) was diluted to 25 µl Opti-MEM I (Invitrogen) and the resultant solution was incubated for 5 min at room temperature. This mixture was then added to a second solution of 0.5 µl Si-RNA-Flotilin2 (20 µM) in 25 µl of Opti-MEM I and allowed to complex for 20 min at room temperature. After this incubation, 150 µl of full growth medium without antibiotics was added to the 50 µl Lipofectamine-2000 / siRNA-Flotillin2 mixture, and the resulting 200 µl was added to the cells after washed with buffer. In order to get better transfection efficiency, the same procedure as mentioned above was repeated one more time on the following day. The next day i.e. 48 h later the start point of the transfection, the cells were ready to proceed for further experiments.

4.2.3 Clostridium treatment

Cells in 8 well chambers were washed with buffer and incubated with 40 ng/ml Clostridium B toxins for 60 minutes at 37° C. The working solution was prepared by diluting the 10 µg/ml

aqueous stock solution in serum free growth medium. After the incubation cells were washed with buffer again and used for further staining with the markers.

4.2.4 Combined drug treatment

First the cells were transfected with siRNA-Flotillin2 according to the method described in 4.2.2, followed by incubation with Clostridium B according to 4.2.3 and finally with the markers (~ 50 nM SBD or DiI) and measure straight away.

4.3 Results

The uptake mechanism of the fluorescently tagged SBD peptide in neuroblastoma SH-SY5Y cells has been studied as it acts as a sphingolipid-interacting tracer with potential applications in the study of neurodegenerative disease **[116, 219]**.

4.3.1 Kinetics of SBD internalization in SH-SY5Y neuroblastoma

The study of the previous chapter suggests that, fluorescently tagged SBD can act as a sphingolipid-interacting tracer, which is the driving force to study the characteristics of uptake mechanism of the marker SBD in neuroblastoma SH-SY5Y cells. The kinetics of cellular internalization of SBD in SH-SY5Y cells (*Fig. 4.1*), without any drug treatment has been determined by normalizing the unit fluorescence intensity of internalized label at a given time point against the average unit fluorescence after complete internalization at 60 minutes. For this imaging based internalization study, a much higher concentration (10 μM) of the Tetramethylrhodamine (TMR)- or Oregon green (OG)- labeled SBD compared to that normally used in case of FCS studies (30 – 50 nM), was added to cells and the cellular fluorescence quantitatively assessed at different time points.

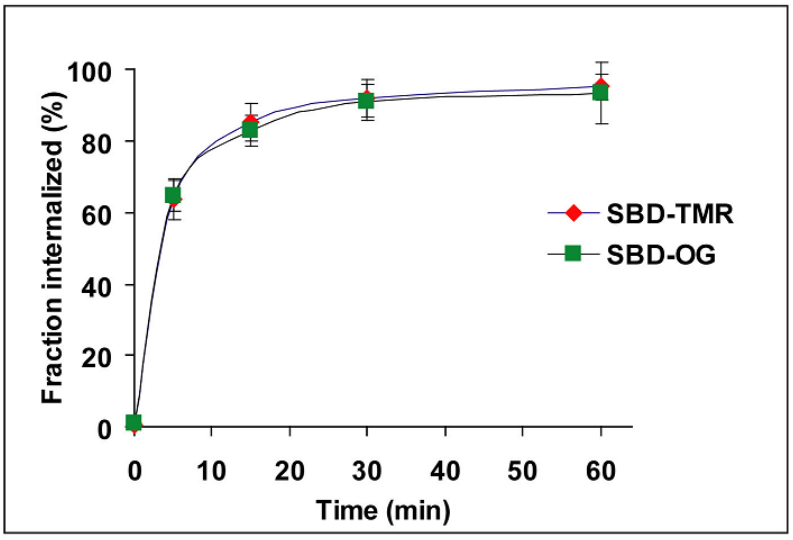

Figure 4.1: *Uptake rate of SBD into human neuroblastoma SH-SY5Y cells. SBD-TMR (red diamonds) and SBD-OG (green squares) into SH-SY5Y neuroblastoma over time, indicated by percent internalization, measured as average fluorescence intensity per pixel in cells being measured divided by maximum average fluorescence intensity per pixel reached after 60 minutes of chase in control cells. [Experiments and figure were done by Dawei Zhang].*

SBD was internalized rapidly, with >80% of maximum fluorescence obtained after 15 minutes of incubation. The internalization kinetics was nearly identical between TMR- and OG-tagged SBD (*Fig. 4.1*). The calculations have been carried out based on the fluorescence images taken by confocal microscopy. The average fluorescence intensity per pixel in cells had been measured and divided by maximum average fluorescence intensity per pixel reached after 60 minutes of chase in control cells.

4.3.2 Differentiation of intra- & extra- cellular SBD from the membrane bound fraction

In order to determine the uptake mechanism of SBD, FCS data has been used with a different approach in this study. Apart from diffusion time, the unbound versus membrane- bound fraction of the marker SBD has also been used here to interpret the uptake mechanism. As cell membranes (typically on the order of 5 nanometers) **[227]** are normally much thinner than the z-axis of the confocal volume (~ 1.2 µm) **[228]**, the fluorescent particles diffusing

through the confocal volume during the cell membrane measurements could easily be separable into two different components (referred as fraction 1 and fraction 2 in this study), giving rise to a close fit to the two dimensional two particle one triplet (2D-2P-1T) model. The two distinct diffusion times obtained from these fits are the slow component τ_{D1} (in the millisecond range) and the fast component τ_{D2} (in the microsecond range) respectively, and correspond to the membrane-bound 2D-diffusion (τ_{D1}), and the unbound 3D-diffusion (τ_{D2}). Hence for the confocal FCS measurements, the placement of the confocal laser spot played an important role here as the proportion of τ_{D1} and τ_{D2} would be affected if the confocal volume is not properly centered on the plasma membrane (*Fig. 4.2*).

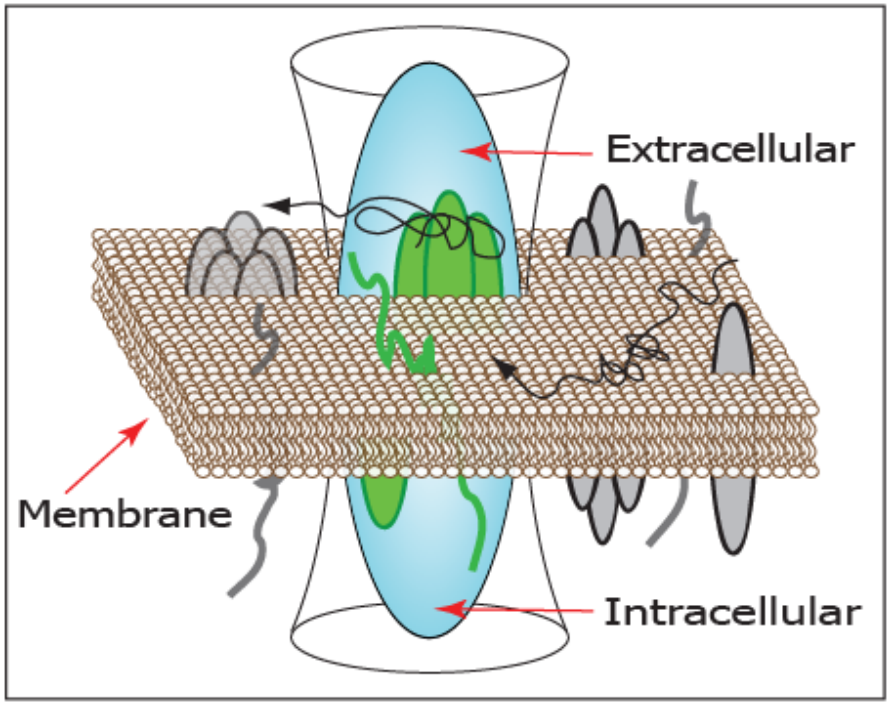

Figure 4.2: *Proper focusing condition for the membrane measurements. B shows the positioning of the cell membrane whereas A and C are the extracellular solution phase and intracellular cytosolic part respectively.*

$G(\tau)$ values obtained from measurements carried out completely outside or completely inside cells were best fitted to a 3 dimensional one particle one triplet (3D-1P-1T) model. By comparison with the τ_D values obtained from these control measurements for the unbound

label in solution (with an average τ_D in the microsecond range), it can be inferred that τ_{D2} is mostly attributable to this unbound population **[228]**. It should be noted that FCS measurements inside the cell also give a predominantly τ_{D2} (microsecond) component, possibly due to internalized SBD that might diffuse through endosomes.

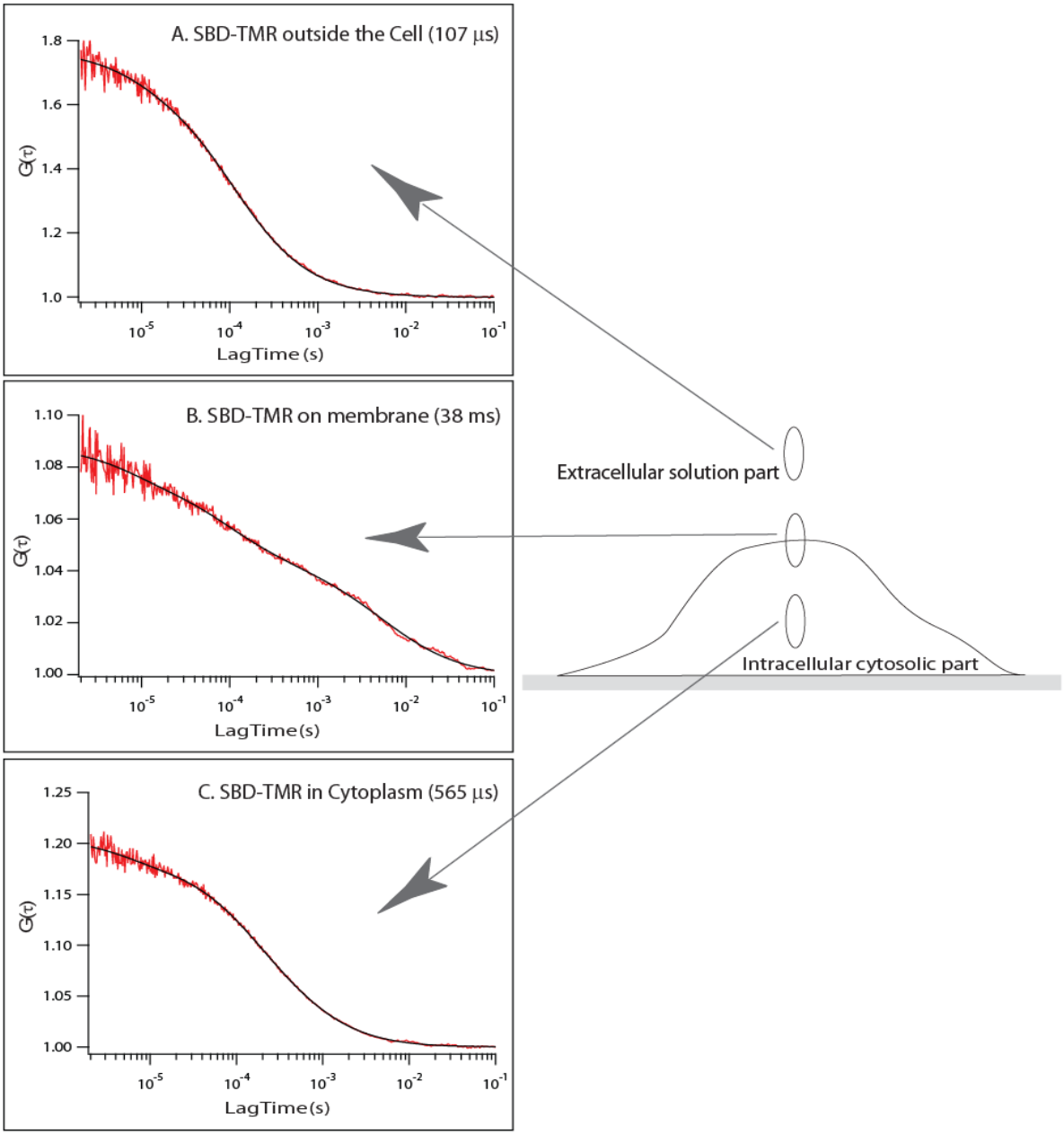

Figure 4.3: *Autocorrelation curves obtained at different positions when the confocal volume was placed completely outside the cell (extracellular), focused on the membrane and completely inside the cell (intracellular). The ACFs show completely different patterns at these 3 different positions with different diffusion rates. A shows typical extracellular diffusions of free dye (τ_D in the order of ~100 µs); B shows typical shape of membrane bound diffusion (τ_D in the order of ~50 ms) and C shows typical intracellular diffusions of cytoplasmic (τ_D in the order of ~500 µs). Both A and C are fitted with 3 dimensional one particle one triplet (3D-1P-1T) model where as B has been fitted with 2 dimensional two particle one triplet (2D-2P-1T) model.*

The ACFs obtained from the membrane measurements showed entirely different patterns as well as different diffusion rates (*Fig. 4.3*) from the control measurements, which were measured by placing the focal spot at different positions (completely outside and inside the cell) in z direction.

The extracellular free dye (*Fig. 4.3 A*) moves with a much faster rate (τ_D in the order of ~100 µs) compare to the intracellular fraction (τ_D in the order of ~500 µs) of SBD (*Fig. 4.3 C*). Whereas the shape of the ACF as well as the diffusion time range of the membrane bound fraction (τ_D in the order of ~50 ms) are totally different from the rest of the two (*Fig. 4.3 B*). The average number of particles (N) counted in these experimental conditions for these 3 different focal spot positioning were also significantly different from each other, the typical values being: intracellular: 16.8 ± 3.9, on the plasma membrane: 59.6 ± 3.5, extracellular 0.9 ± 0.0.

The proportion of τ_{D1} and τ_{D2} (which are very important parameters for this study) would be affected if the confocal volume is not centered properly on the plasma membrane, so special care was taken to ensure that the confocal volume was always properly positioned at the plasma membrane. First the cells were imaged followed by intensity scan through z-axis. FCS measurements were carried out at the z-place producing highest fluorescent intensity. Each experimentally obtained ACF and the τ_D values also compared with the control measurements to ensure that the corresponding measurement has really been carried out on the membrane.

4.3.3 Differentiation between intracellular and extracellular SBD

As mentioned in the previous section that cell membranes are typically on the order or 5 nanometers) **[227]** whereas the z-axis of the confocal volume is ~ 1.2 µm **[228]**, so it is quite obvious that, if the upper membrane of the cell is focused properly, the overall fluorescent

signal will consist of 3 different sets of particles: the topmost part will be populated by the unbound extracellular dye particles diffusing freely in the solution phase, the middle part will show signal due to the membrane bound fraction and the bottom most part will be consisted of cytosolic SBD. Since the experimentally obtained data from membrane measurements have been fitted according to the best suited two particle model, and both the extracellular as well as the cytosolic SBD diffuse in the micro second time range, it is difficult to know the contribution of each population towards the faster moving τ_{D2}. Hence, in order to explain the characteristic behavior of τ_{D2} (which is a combination of these two), it is necessary to understand the difference between these two populations from experiments carried out separately at those positions.

The average intracellular τ_D had a value of 499.3 ± 35.7 µs, whereas extracellular τ_D was only 115 ± 5.8 µs. For a better understanding of their ranges, the distributions of τ_Ds of both of these populations were plotted in the same frame (*Fig. 4.4*) which shows the clear separation between the extracellular and intracellular SBD.

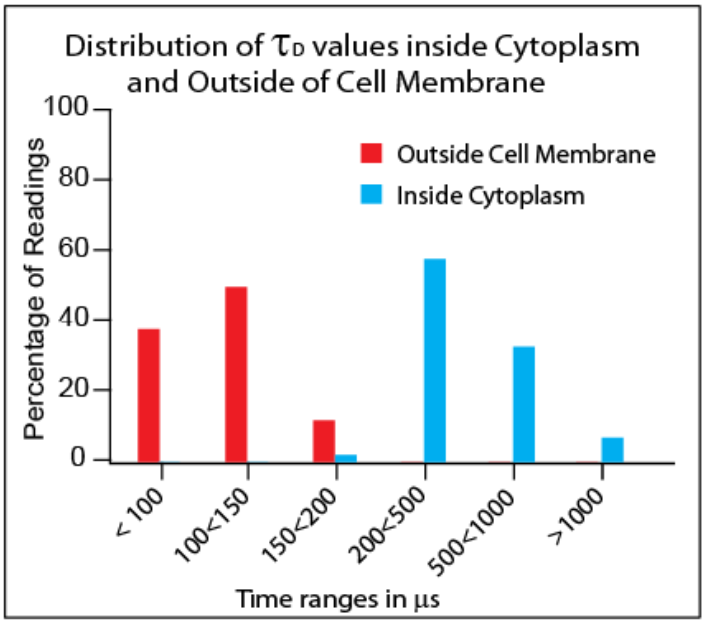

***Figure 4.4**: Extracellular vs. cytosolic τ_D values for SBD. The histogram distribution of τ_D values obtained when the confocal volume was placed completely outside the cell (extracellular), vs. completely inside the cell (intracellular) show different diffusion rates, with intracellular SBD being slower. Average intracellular τ_D was 499.3 ± 35.7 µs, whereas extracellular τ_D was only 115 ± 5.8 µs.*

There was a clear difference in the average number of particles (*N*) as well. The intracellular and extracellular number of particles before any drug treatment was: 16.8 ± 3.9 and 0.9 ± 0.0 respectively; whereas after the combined drug treatments they change to: 7.6 ± 0.7 and 0.9 ± 0.0 respectively. Upon completion of the incubations with the markers, the excess dyes were washed off and the measurements carried out in fluorescently inactive medium. Hence, the number of particles in the extracellular part (background being 0.4 ± 0.0) does not change significantly, whereas the intracellular population (background signal due to autofluorescence of cell being 1.9 ± 1.6) dropped by a factor of ~2 due to reduced uptake.

4.3.4 Inhibition Rho GTPase or flotillin affects interaction of SBD with the cell surface

FCS was used to study the effects of blocking different mechanisms of SBD uptake using specific drugs, on its diffusion behavior at the plasma membrane surface of SH-SY5Y neuroblastoma cells. The diffusion time generally reflects the membrane fluidity, which is normally larger for the less mobile raft domains compared to that of the non-raft phase **[52, 229-232]**; as was shown in the previous chapter, SBD displays a slow diffusion component at the plasma membrane, similarly to CTxB, but unlike non-raft markers DiI and Bodipy-FL-SM, which remain uniformly distributed on the plasma membrane **[81]**. Thus diffusion times (τ_D) from a confocal spot centered at the plasma membrane can be used to deduce the membrane microdomain association for any fluorescently tagged probe.

As described in the section 4.3.2; data from membrane measurements were best fitted to the two dimensional two particle one triplet (2D-2P-1T) model. By comparing the proportion of particles that fall into the τ_{D1} or τ_{D2} categories (Fraction τ_{D1} or Fraction τ_{D2}) it is possible to determine whether the binding of SBD to the plasma membrane is affected under different treatments; as care was taken (described in section 4.3.2) to ensure that the confocal volume

was always properly focused at the plasma membrane. Fraction τ_{D1} and Fraction τ_{D2} were plotted for the untreated control cells versus the cells treated with either flotillin-2 siRNA or clostridium toxin, or both (*Fig. 4.5 A*).

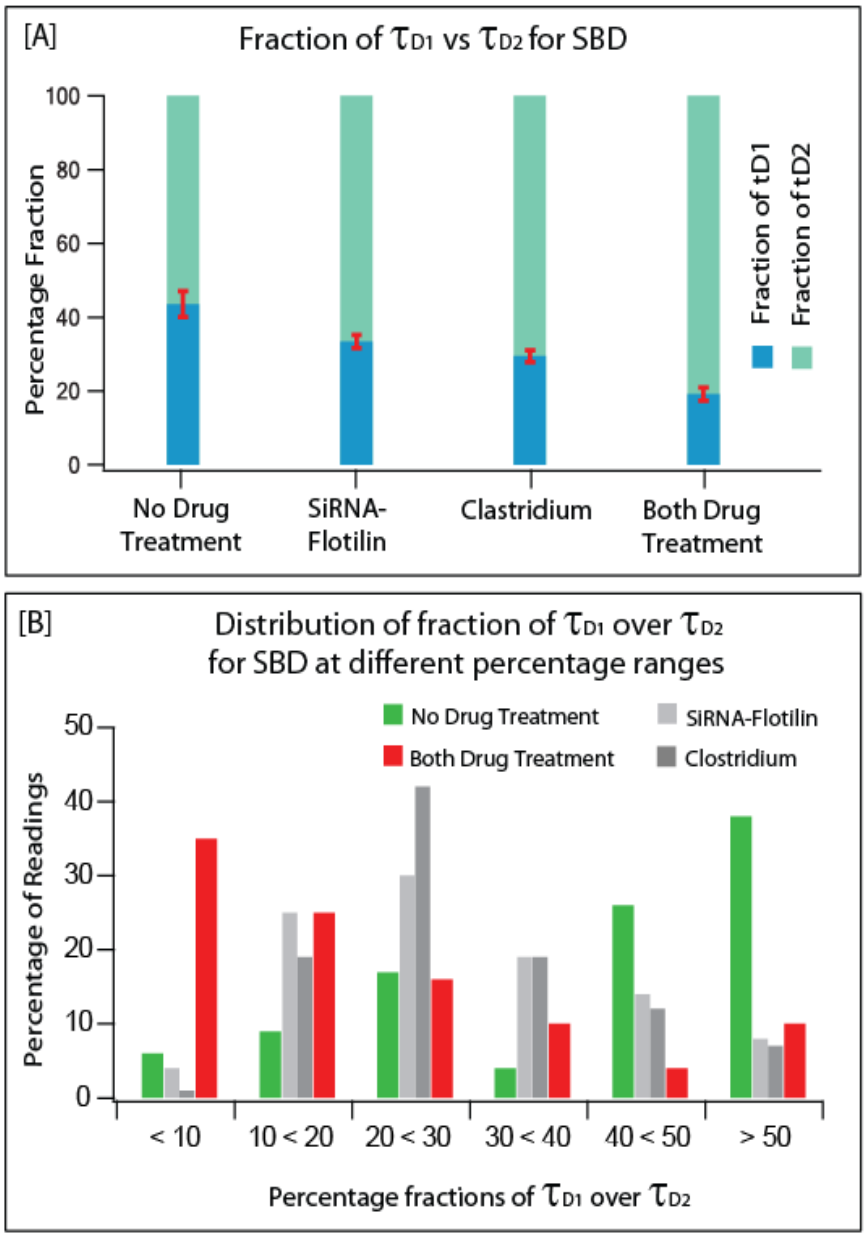

Figure 4.5: *Flotillin-2 and a Rho family GTPase act synergistically on SBD uptake, and both affect the proportion of SBD exhibiting slow diffusion (τ_{D1}). (A) Average proportions of FCS measurements fitting to τ_{D1} or τ_{D2} after interference with flotillin, Rho family GTPases, or both, show that the fraction of the faster diffusing component, τ_{D2} (light green), increased. (B) Histogram showing the distribution of FCS readings where the given proportion of τ_{D1} to τ_{D2} (given as percentage τ_{D1} on the x-axis) occurred. In control cells (green bars), most readings gave >40% τ_{D1}, whereas treatment with both flotillin-2 siRNA and clostridium (red bars) shifted the proportion of τ_{D1} in most measurements to <10%. Either treatment alone (gray bars) gave intermediate proportions of τ_{D1}.*

The fraction of τ_{D1} (the presumptive membrane-bound, millisecond range) fell from 44% in controls to 33% with flotillin-2 siRNA, 29% with clostridium treatment, and 19% in case of both treatments. Thus, the magnitude of the effect of knocking out either of the uptake mechanisms alone was similar, and removing both of them gave an almost perfectly additive effect on the binding of SBD. This implies that the effects of flotillin and cdc42 on the binding of SBD are additive, if it is assumed that a decreased proportion of Frn1 reflects the loss of binding.

By plotting the percentage fraction of τ_{D1} in the different readings as a histogram instead of an average (*Fig. 4.5 B*), it can be seen that the distribution of readings shifts from predominantly τ_{D1} (>50% putative membrane-bound particles) to smaller fractions of τ_{D1} (20-30%) under either siRNA or clostridium toxin treatment, and even smaller fractions (<10%) under both treatments simultaneously; which also states that the decreased proportion of Fraction1 reflects the loss of binding under drug treated conditions.

From the previous chapter it is known that the raft markers SBD as well as CTxB possess larger average diffusion time values compare to that of the non-raft markers, and a bimodal distribution of τ_D values, which shrinks to a narrow distribution lacking the slower (τ_D >30 ms components) upon disrupting rafts. This suggested that the long diffusion time might correspond to the proportion of molecules that is associated (transiently) with the rafts or nanoclusters on the plasma membrane.

An interesting question is now whether the bimodal diffusion distribution was related to the different uptake mechanisms that affect SBD internalization into cells. Indeed, when treated with either clostridium toxin or siRNA flotillin-2, or both, the slow component of τ_{D1} disappeared, being reflected in the much faster average τ_D (*Fig. 4.6 A*) as well as in the shift of the histogram distribution to between 1-10 millisecond (*Fig. 4.6 B*) under each of the three treatments.

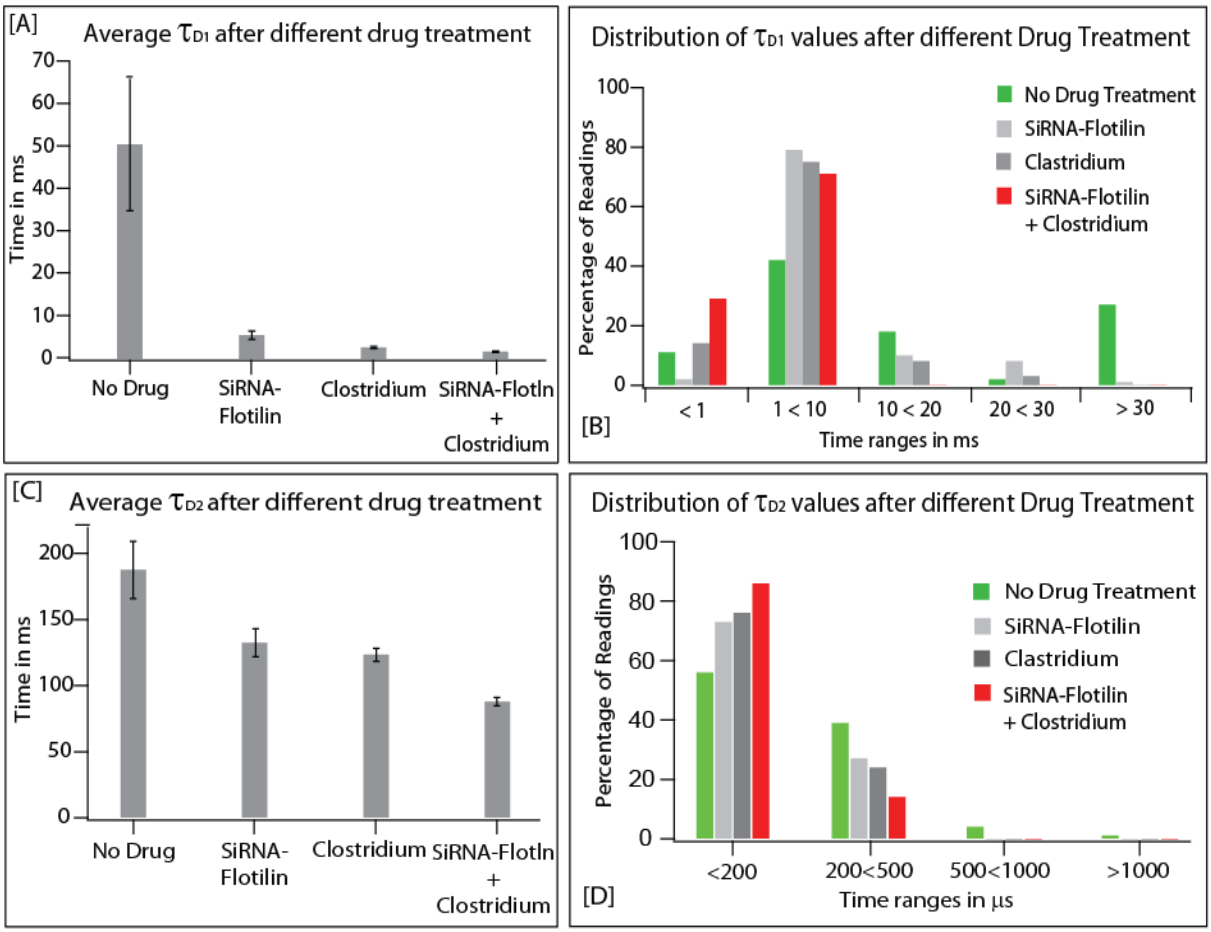

Figure 4.6: *Both flotillin and Rho family GTPase are required for the slow raft-like diffusion component of SBD. (A)Average τ_{D1} values (in milliseconds; y-axis) after interference with flotillin-2 or Rho family GTPases by clostridium toxin, or both. τ_{D1} values were as follows: control, 50.6±15.6 milliseconds; SiRNA flotillin, 5.6 ± 0.88 milliseconds; clostridium, 2.7 ± 0.21 milliseconds; siRNA-flotillin + clostridium, 2.0 ± 0.27 milliseconds. (B) Histogram distribution of τ_{D1} values after the above treatments, showing disappearance of the slow (>30 milliseconds) component after either treatment alone (gray shades), or both together (red). (C) Average τ_{D2} values (in microseconds; y-axis) after above treatments. τ_{D2} is lower overall. τ_{D2} values were as follows: control, 187.5 ± 21.2 microseconds; SiRNA-flotillin, 132.4 ± 8.7 microseconds; clostridium, 123.3 ± 4.9 microseconds; SiRNA-flotillin + clostridium, 93.7 ± 4.5 microseconds. Histogram distribution of τ_{D2} values after above treatments. After both treatments together, a higher percentage of readings gave τ_{D2} values of <100 microseconds (red). Error bars in A and C represent means ± s.e.m.*

In contrast to the τ_{D1} values, τ_{D2} values were not as strongly affected, although the average τ_{D2} sped up by about 50% (*Fig. 4.6 C*), and the histogram of τ_{D2} did show a shift of τ_{D2} towards faster values under the combined flotillin-2-RNAi + clostridium treatment (but not either treatment alone) (*Fig. 4.6 D*). This shift in τ_{D2} could be explained as in section 4.3.3. The fraction τ_{D2} derives from freely diffusing SBD both outside the cell as well as inside the cell, and extracellular SBD has an average τ_D of 115 ± 5.8 microseconds (exclusively <200

microseconds; n=24 readings) whereas cytosolic τ_D averages 499.3 ± 35.7 microseconds (exclusively >200 microseconds; n=45 readings) (*Fig. 4.3*).

Now less efficient binding due to effect of the drug treatments also results in less SBD entering the cell, [the average number of particles (N) counted in the no drug treated conditions were: intracellular 16.8 ± 3.9, extracellular 0.9 ± 0.0 whereas after the combined drug treatment they were: intracellular: 7.6 ± 0.7 and extracellular 0.9 ± 0.0] as a result τ_{D2} values in case of the drug treated cells consist of comparatively more contribution from the faster extracellular free dyes which reflects in the faster average τ_{D2} values.

4.3.5 Comparison of the effects of drug treatments on SBD with effects on non-raft marker DiI

In order to determine whether the decrease in τ_D values was a result of a general increase in membrane fluidity induced by the siRNA and clostridium treatments, the τ_D values of the DiI, which should be uniformly distributed on the plasma membrane SH-SY5Y neuroblastoma cells were measured before and after these drug treatments. The average diffusion time values as well as the histogram distributions of τ_D remained unaffected after each individual and combined drug treatments (*Fig. 4.7*). As DiI does neither give any significant fluorescence in solution phase nor internalizes inside the cell, the ACFs obtained from all the DiI measurements are best fitted to two dimensional one particle one triplet (2D-1P-1T) model only.

The results above suggest that the combined effects of flotillin and Rho family GTPase on binding of SBD are stronger than either one alone and are additive; however, removing either flotillin or Rho GTPases completely abolishes the slow diffusion component of SBD, both of these mechanisms must be absolutely required for this raft-like diffusion behavior.

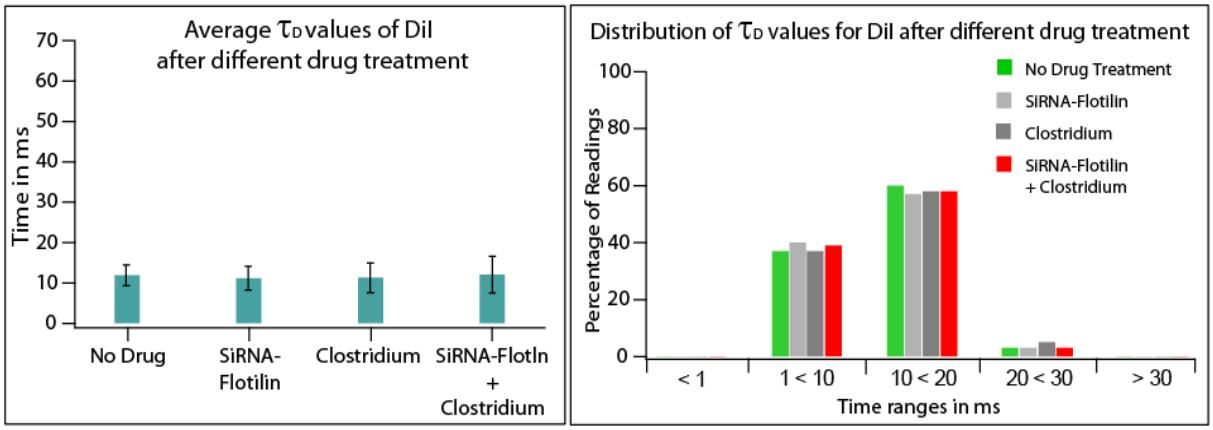

Figure 4.7: *Diffusion of the non-raft localized lipophilic dye, DiI C18, was unaffected by SiRNA flotillin-2 and clostridium treatment. (A) Average τ_D values of DiI are shown after different treatments: control 11.9 ± 2.6 ms; siRNA flotillin-2 11.2 ± 2.9 ms; clostridium 11.3 ± 3.7 ms; siRNA flotillin-2 + clostridium 12.1 ± 4.6 ms. (B) Histogram distribution of τ_D values of DiI are shown after different treatments, given as percentage of readings falling into the different time range bins, in milliseconds.*

4.4 Discussion

The uptake mechanisms of SBD, a fluorescently tagged sphingolipid interacting peptide probe, were examined based on the diffusion behavior and percentage of association with the plasma membrane in a human neuroblastoma cell line, SHSY5Y. Unlike other so far characterized microdomain-associated cargoes, SBD endocytosis is affected approximately equally by two different pathways, one cdc42-mediated, and the other lipid-raft-associated adaptor protein, flotillin mediated **[213, 231]**. This work shows that these two pathways probably not separate, but that they are additive i.e. operate together. The main role of cdc42 is regulating the GEEC pathway, specific for the uptake of GPI linked proteins **[133]**, which in some cases can also be endocytosed by flotillin-mediated mechanisms **[137, 217]**.

The study about SBD uptake mechanism based on colocalozation of fluorescent probes by Zhang *et al*. **[202]** shows that SBD uptake is strongly affected by dynamin interference. The studies of Mayor and colleagues **[133, 229]** with GPI-APs, suggests that the cdc42 pathway is non-overlapping with dynamin mechanisms. On the other hand it has been documented several times that an uptake mechanism has been jointly mediated by dynamin and flotillin.

For example, Aβ (the parent molecule of SBD) and amyloid precursor protein (App) both requires dynamin as well as flotillin for their uptake into the cells **[230, 231]**. It is also reported that uptake mechanism of polyethylenimine (PEI) and Lipofectamine are also both dynamin- as well as flotillin-mediated **[137]**; but this was unaffected by cholesterol depletion, indicating these might not be lipid raft associated mechanisms. According to literature and moreover according to this study as knockout of both cdc42 and flotillin together virtually eliminates the SBD uptake, it can be postulated that dynamin takes part in flotillin mediated uptake mechanism and does not constitute a third independent mechanism.

FACS quantification done by Zhang *et al*. **[202]** indicates that removing either the flotillin pathway or the cdc42 pathway by treatment with SiRNA-flotillin and clostridium toxin, respectively, exerted moderate effects on SBD uptake, whereas knockout of both mechanisms together nearly eliminates the uptake. This reduced uptake was associated with reduced cell-surface-bound (i.e. washable) SBD after either treatment, and with stronger loss of cell-surface binding after both treatments.

Accordingly, the FCS experiments also showed that blocking of any one pathway exerted moderate effects on SBD association with the plasma membrane, whereas knockout of both mechanisms together nearly eliminates the association. In case of either pathway blocking, the fraction of SBD diffused at the fastest rate, (indicating less binding), was almost similar, and blocking both pathway showed almost an additive effect. The opinion of a single, highly efficient uptake process dependent on both flotillin and cdc42 simultaneously is also supported by the observation that knockout of either mechanism alone completely abolishes the slowest diffusion component (*Fig 4.8*). The uptake of CTxB (another established lipid raft associated probe) also shows similar kind of mechanism, where flotillin-siRNA alone had no significant effect, DynK44A DN alone showed much less severe effect but the simultaneous

treatment of DynK44A DN and flotillin-siRNA knocked out ~80% uptake **[137]**. Similarly this study predicts that there might be a direct interaction between flotillin and cdc42.

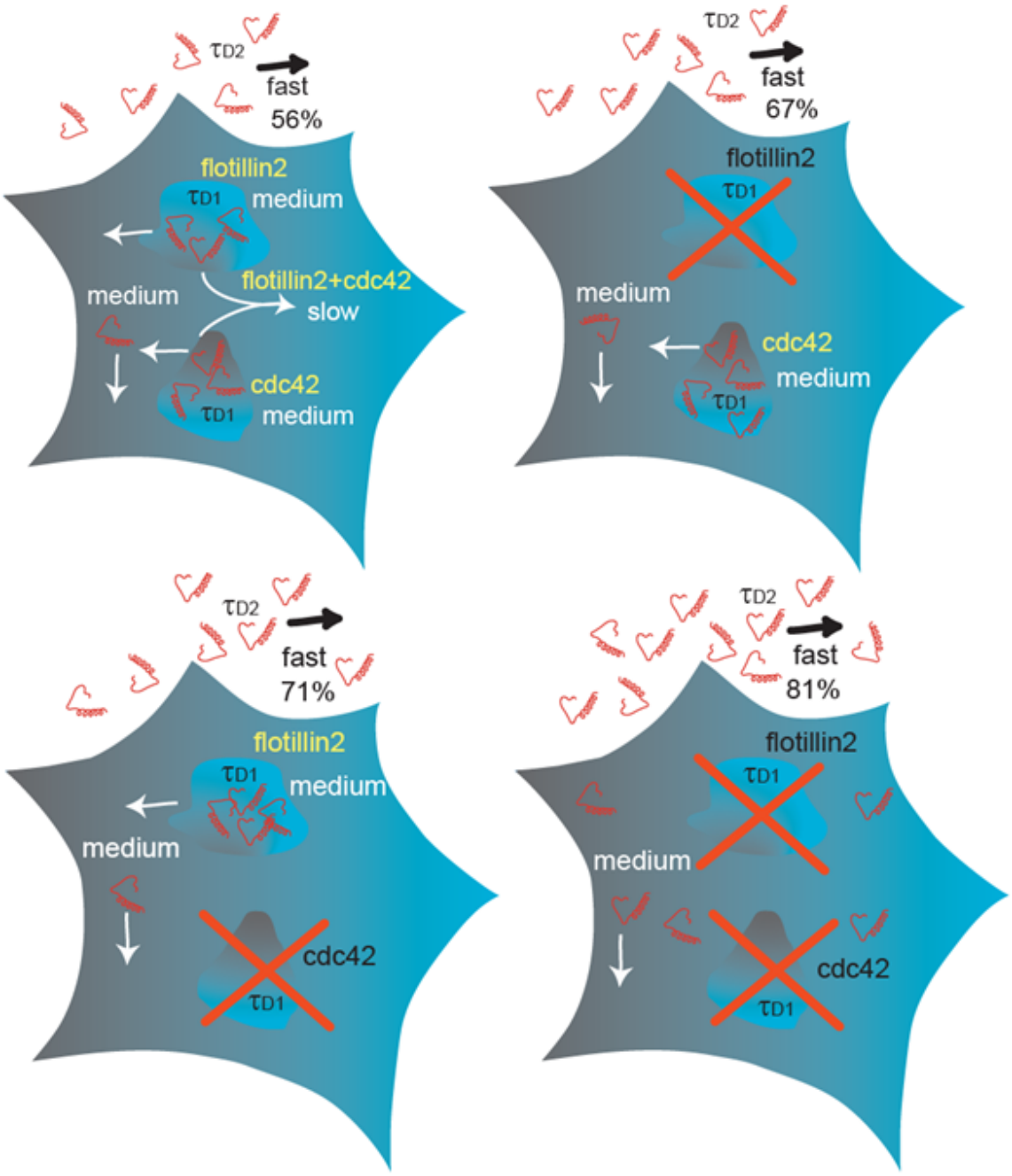

[Picture modified based on a drawing by Rachel S. Kraut]

Figure 4.8: *Model showing proposed origin of the slow-, medium- and fast-diffusing SBD components. In the model, τ_{D2} represents the fast (microsecond range), unbound population of SBD that is presumably outside the cell (56%), but still registered by FCS measurement. Both flotillin and cdc42 associated mechanisms alone can mediate suboptimal uptake and medium-speed diffusion (1–10 milliseconds). Flotillin and cdc42 together synergistically mediate slow (>50 milliseconds) diffusion and efficient uptake. When either or both flotillin- or cdc42-mediated uptake mechanisms are knocked out, the fast unbound population of SBD increases to 67%, 71% or 81%, respectively, and the very slow (50 milliseconds) diffusion component is removed. A small proportion of SBD associated with neither mechanism remains at the surface and diffuses at a medium speed (1–10 milliseconds).*

In the previous chapter it was shown that, the diffusion of SBD at the plasma membrane distributed into two categories: some with medium mobilities (τ_D values ~1-10 milliseconds) and some with slow mobilities (τ_D values ~50 milliseconds), whereas the non-raft-associated lipid analogs DiI and Bodipy-FL-SM diffused only in the medium mobility (τ_D ~1-10 milliseconds) range. Interestingly, CTxB also showed a very similar bimodal distribution.

The longer diffusion times could be abolished by cholesterol and sphingolipid depletion indicating that the slowly diffusing fraction might correspond to the proportion of molecules that are associated (transiently) with rafts or nanoclusters **[134]**. This kind of SBD like bimodal diffusion behavior has been reported earlier by Lommerse and colleagues **[232]**, and in one recent study by Pinaud *et al*. **[53]**. Some other groups also have derived the diffusion constants from anisotropy recovery after photobleaching and fluorescence recovery after photobleaching (ARAP and FRAP) experiments **[52]** and by high-speed single-particle tracking techniques **[225]** on raft and non-raft molecules; however, these either showed complete immobility associated with nanoclusters, or uniformly distributed hop-diffusion behaviors, irrespective of raft or non-raft localization.

The question arises whether these apparently raft associated long diffusion times are corresponding to uptake by cdc42- and/or flotillin-mediated mechanisms. Surprisingly, neither of these mechanisms was absolutely required to achieve uptake, but the slow diffusing component was completely abolished when either mechanism was knocked out. This suggests that the slow diffusion might in fact correspond to a highly efficient, synergistic uptake mode of cdc42 + flotillin. A model proposing this link between diffusion behavior and uptake mode is shown in *Fig. 4.8*. Some alternative approaches like colocalization by super-resolution fluorescence imaging, or fluorescence cross-correlation spectroscopy also could be used to test the validity this model, in parallel with the studies of uptake kinetics.

4.5 Summary

This study suggests that cdc42- and flotillin-associated uptake sites both correspond to domains of intermediate mobility, but they can cooperate to form low-mobility, efficiently internalized domains. It also can be said that the surface behavior of a cargo is determined by a combination of endocytic accessory proteins of the membrane compartments. This study can be concluded with the proposal that the uptake of SBD might behave similarly to its parent molecule Aβ, even though the physiological consequences of Aβ administration is not clear. Finally, accumulation of SBD in the raft components is traced by the endocytic accessory proteins such as cdc42 and flotillin.

Chapter 5:

Investigation of dynamic cell membrane organization

5.1 Introduction

Until the 1990s, the fluid mosaic model was the widely accepted description of a biological membrane **[46]**. Published in 1972, it put an end to the other previously existing and competing models assuming triple layers, with a lipid core layer and two protein layers, one on each side. The fluid mosaic model, based on thermodynamic and functional considerations, postulated instead that proteins as the active components of signal transduction and transport can span the entire thickness of a lipid bilayer. Protein-lipid interaction was thought to be stabilized through hydrophobic (fat soluble) contact points on the surface of the proteins **[45]**.

Over the last decades, it has become clear that the plasma membrane of cells, far from being uniform, is highly dynamic yet organized, consisting of a multitude of interacting micron and nano sized subdomains within the lipid membrane. These domains play important roles in signal transduction and trafficking and sometimes serve as platforms for the production of neurotoxic proteins such as amyloid beta in Alzheimer's disease and prion protein in transmissible encephalopathies. The wide membrane domains are mainly, nanometer sized cholesterol and sphingolipid enriched lipid rafts to large, micron sized ceramide rich platforms **[42, 90, 233]**. These highly heterogeneous structures and the presence of "lipid rafts", which are regions of lower mobility, embedded in a fluid phase of higher mobility **[42]**, the cell membrane exhibits a range of different diffusion coefficients mainly in the

millisecond time scale **[234]**. Hence, in order to understand these dynamic organizations of cell membrane, suitable techniques that can incorporate spatial as well as temporal measurements of diffusion are needed, which allow to get a picture of how the membrane works as a system on a larger scale.

Imaging Total Internal Reflection-Fluorescence Correlation Spectroscopy (ITIR-FCS, as described in chapter 2) has been shown here as a possible means to study 2D surfaces with a time resolution of 4 ms allowing the resolution of lipid and protein dynamics at each pixel of an EMCCD camera **[142, 143]**. Moreover, it also has been shown that ITIR-FCCS reflects the anisotropic movement on cell membranes, and thus the dynamic membrane organization of living cells. The technique has been applied here to study diffusion and transport processes to resolve the dynamic heterogeneity in membranes that cannot be addressed easily by other spectroscopic methods. A generalized expression for cross-correlations between any two areas of any size and shape on a CCD chip **[89]** has been used to extract the diffusion coefficient and velocity parameters. By using the ΔCCF values for neighboring pixels, the anisotropic transport in cell membranes has been investigated and these differences have been related to the membrane organization of living human SHSY5Y neuroblastoma cells. In particular, the organization of the liquid ordered phase, tracked by SBD, and the liquid disordered phase, represented by DiI, has been described here in this part of the study. Further the cells were perturbed by the removal of cholesterol by methyl-β-cyclodextrin (MβCD), and by the disruption of the cytoskeleton by latrunculin A to observe the relative difference in the dynamic organizations of these two phases.

5.2 Materials and Methods

In this part of the study, the so far well characterized sphingolipid rich domain associated probe, TMR-conjugated SBD has been used as a marker for the raft regions and the

previously mentioned lipophilic lipid analog $DiIC_{18}$ has been used as a marker for the non-raft regions of the cell membrane. For the depletion of cholesterol from the cell surface, MβCD has been used in a similar way as mentioned in chapter 3. Latrunculin-A (Sigma-Aldrich, catalog number: L5163), which is known to de-polymerize the actin has been used in this study to perturb the actin cytoskeleton of the SH-SY5Y human neuroblastoma cells.

5.2.1 Cell culture and staining with markers

SH-SY5Y neuroblastoma cells were cultured and plated on 8-well chambers >24 hours prior to the drug treatments/measurements; and the staining with DiI and SBD also has been done as has been described in the previous chapters.

5.2.2 MβCD treatment

5.2.2.1 End point measurements

To see only the complete effect of MβCD of cholesterol depletion, cells were treated with 5 mM of MβCD as described in chapter 3, followed by staining with SBD or DiI, also as described in the previous chapters and measured at room temperature.

5.2.2.2 Time chase measurements

The incubation sequence of time chase studies is just reverse to that of the end point measurements with respect to the drug and the marker. In this case, the cells in 8 well chambers were first incubated with the markers (SBD-TMR / DiI) for 30 minutes at 37º C, washed with the buffer and suspended in indicator and serum free DMEM for measurement. 5 mM MβCD was then added to the cells on stage and were chased for 30 minutes, taking readings at 10 minutes intervals.

5.2.3 Latrunculin-A treatment

Cells in 8 well chambers were washed with buffer and incubated with the markers (SBD-TMR / DiI) first, for 30 minutes at 37º C, then they washed with the buffer and suspended in indicator free DMEM for measurement. The 200 μM stock solution of Latrunculin-A in DMSO was diluted in serum free growth medium in order to prepare the 5 μM working solution. This working solution was then added to the cells on microscope stage and was incubated for 30 min, taking readings at 10 min intervals.

5.2.4 Instrumentation

The instrument used in this part of the study is the total internal reflection based FCS setup, described in chapter 2. Both of the fluorescent probes, DiI and TMR conjugated SBD were excited using the 532 nm laser coupled with the system. The power of the excitation laser source was maintained at 6 mW as measured before the microscope objective for all the measurements, and the fluorescence signal from the sample was collected by the EMCCD after passing through a 560 DRLP dichroic mirror and 595 AF60 emission filter.

5.3 Results

5.3.1 System compatibility

The distribution of the different lipid classes that make up the cell membranes, including sphingolipids, cholesterol and glycerophospholipids, are highly heterogeneous. For better identification of this heterogeneity through ITIR-FCS results, different possible shapes of the ACF curves obtained from single pixels for various samples including autofluorescence of the SHSY5Y cells, SBD before and after MβCD treatment were analyzed first. These results were compared with the background signal as well, which arises due to the electronics of the

detector (*Fig. 5.1*). From the figures it is clear that the background signal (*Fig. 5.1 A*) is noisy and distinct from any fluorescent signal. The autofluorescence of the SHSY5Y cell exhibits a very flat profile with almost vanishing amplitude, entirely different from the ACFs of any fluorescent dye containing probe like TMR-conjugated SBD. The ACFs using SBD-TMR as the lipid raft associated marker, shows a shortening of the diffusion time upon the MβCD treatment (*Fig. 5.1 B*), consistent with the results obtained through conventional point FCS method.

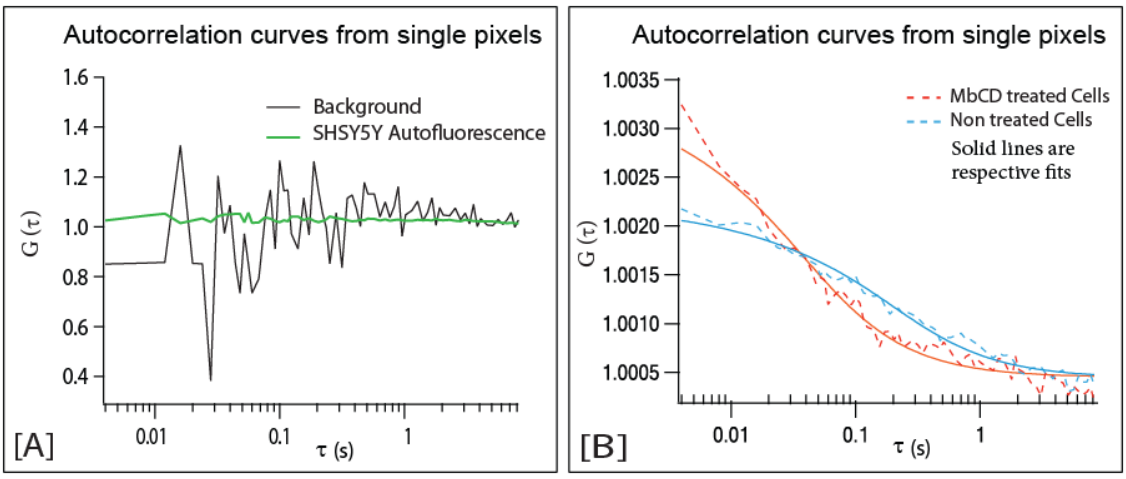

Figure 5.1: *Representative correlation functions from single pixels for Different conditions. In A, the black line represents ACFs obtained from background measurements and the green line represents the autofluorescence of human Neuroblastoma (SHSY5Y) cells, whereas B shows ACFs obtained from SBD-TMR labeled cells. Dashed lines in B represent the experimentally obtained raw curve and the solid lines are the respective fits. Blue one correspond to only SBD-TMR labeled cells, without any drug treatment, and the red one corresponds to MβCD treatment on the SBD-TMR labeled cells. The D for non treated cells is 0.38 μm²/s while that for MβCD treated cells is 1.97 μm²/s.*

5.3.2 Autofluorescence of SHSY5Y Neuroblastoma cells.

Unlike conventional FCS, the signals from the entire ROI (20 x 20 pixels) are analyzed in case of ITIR-FCS without being biased to any particular point. Therefore, it is important to make sure that the analyzed value is due to the movement of the desired fluorescent probe, and not influenced by the autofluorescence of the cell. As the total autofluorescence intensity consists of a large number of dim molecules, a high value for the number of particles is

expected in case of autofluorescence of any cell, and this was obtained through ITIR-FCS experiments as well (*Fig. 5.2 A*). In case of autofluorescence measurements, the absence of any bright marker leads to very poor fluorescence signal to noise ratio **[142]**. Therefore this absence of mobility of any bright particle resulted in lack of proper ACFs and the pictorial representation of that condition (*Fig. 5.2 B*) reflects an almost immobile state. The flat curves from most of the pixels produces individual diffusion times larger than a second, resulting in an average diffusion coefficient on the order of 0.01 $\mu m^2/s$. This value is most likely bleaching dominated and is more than 50 times and 200 times slower compare to the movement of SBD and DiI on the cell surface, respectively. Therefore, during the analysis of diffusion coefficients of SBD or DiI, any pixels producing values in that range were excluded from the analysis of average value.

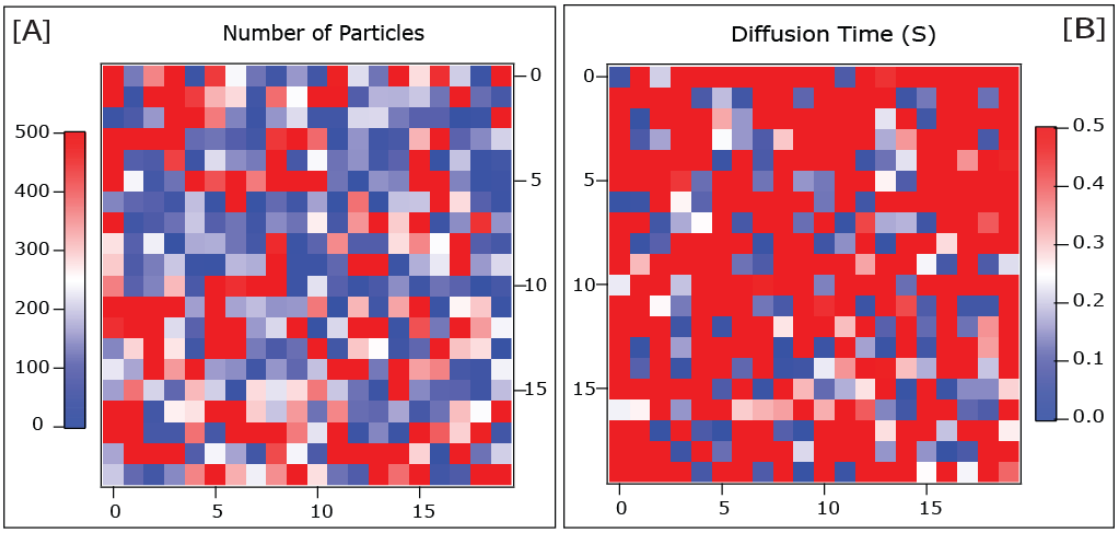

Figure 5.2: *Number of particle (A) and diffusion time (B) images over the entire ROI (20 x 20 pixels) without binning for the autofluorescence of SHSY5Y cells. The numbers on the x- and y-axes represent the pixel position.*

5.3.3 Independency of diffusion parameter with concentration.

The time chase measurements involve repeated measurements on the same ROI of a particular cell, which results in loss of some local fluorophores due to photobleaching. In

order to check whether this loss of intensity has any effects on the diffusion parameters of the probes, comparisons between number of particles and diffusion times of the same experimentally obtained stacks were carried out for SBD-TMR labeled cells under both MβCD treated and non-treated conditions (*Fig. 5.3* and *Fig. 5.4*). In case of no drug treated control cells irrespective of the gradual decrease in the number of fluorescent particles (simultaneous decrease in overall fluorescence intensity) due to repeated measurements taken on the same spot (*Fig. 5.3 A, B*), the overall diffusion times through the entire ROI remained unchanged (*Fig. 5.3 D, E*). On making a move to a new cell in the same sample dish, diffusion time didn't show any significant change (*Fig. 5.3 F*) despite an expected increase in intensity (*Fig. 5.3 C*).

Similar time chase analysis was carried out for cells measured in the presence of 5 mM MβCD, to monitor the gradual loss of cholesterol from cell surface and simultaneous loss of raft association of SBD. The existence of MβCD in the medium during experiment, results in a gradual decrease in average diffusion time (*Fig. 5.4 E-G*) with progress in time, indicating the gradual loss of raft-association of SBD. Simultaneously, a decrease in number of particles (*Fig. 5.4 A-C*) due to photobleaching upon repeated measurements taken on the same ROI of a single cell was also observed. However this decrease in intensity has no significant influence on the diffusion time. Moving on to a new cell in the same sample dish did not show any sign of recovery of the diffusion time (*Fig. 5.4 H*) although an increase in number of particles (i.e. overall fluorescence intensity) was observed (*Fig. 5.4 D*). This observation clearly indicates that the decrease in the diffusion time is purely due to the effect of the drug (MβCD), and intensity or any other external parameter has no significant role to play in this context.

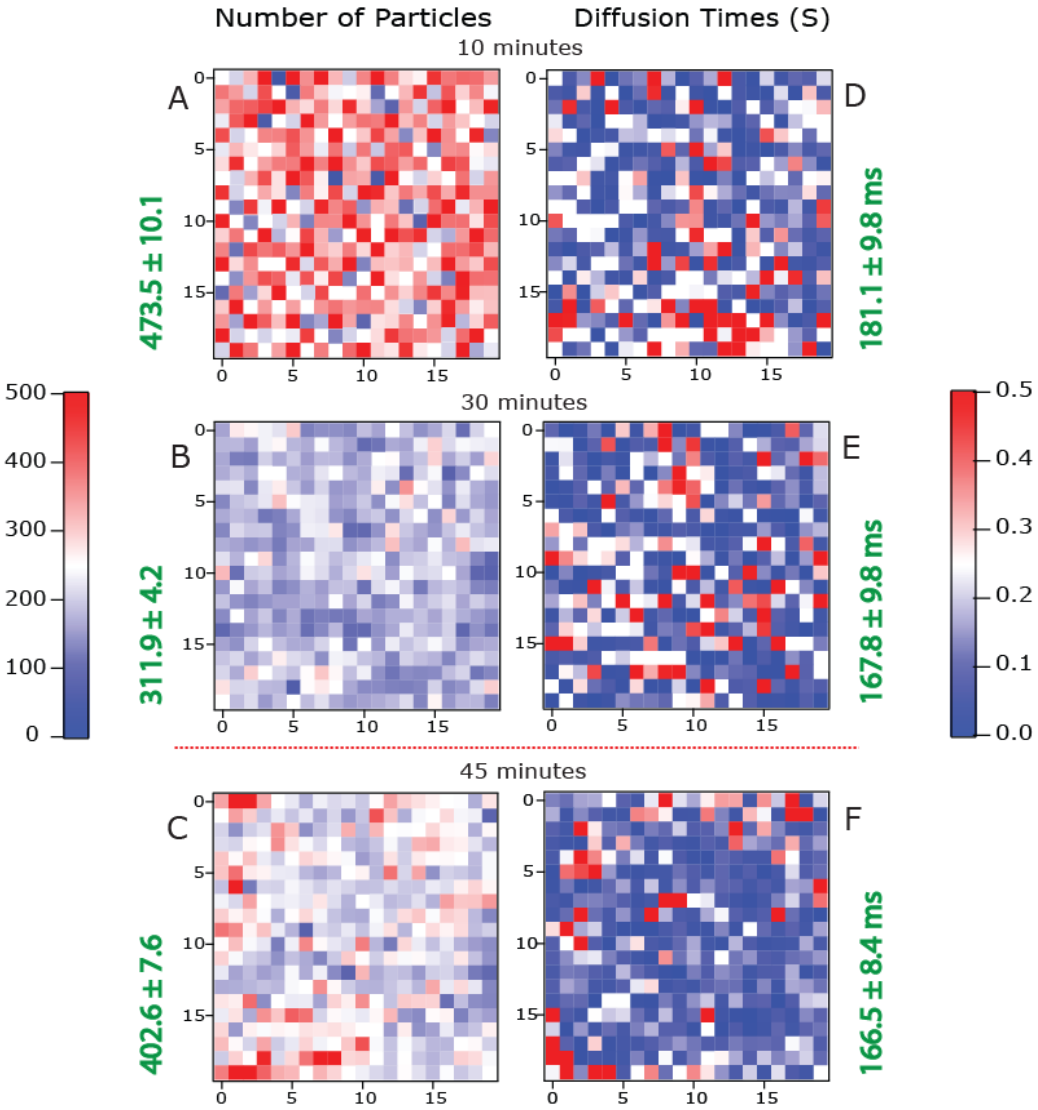

Figure 5.3: *Quantitative pictorial representations of number of particles and diffusion times over the measured ROI on the no drug treated control cell membranes during the time chase experiments. A, B and C represents number of particles whereas D, E and F represents diffusion times according to the respective color scales. A, B, D and E are images of the same position of a single cell at various time point whereas C and F represents another cell at extended measurement time. The numbers on the x- and y-axes represent the pixel position. Average values for each picture are indicated in green.*

All these results together suggest that the newly established technique, ITIR-FCS is sensitive enough to measure the complex heterogeneous cell membrane organization and is able to point out any small alteration in that organization due to external perturbations. With the essential supporting information, the technique was ready to study the heterogeneous dynamic cell membrane organization, in the light of mobility of "lipid rafts", cholesterol and

proteins that can be stabilized to coalesce, forming platforms that function in membrane signaling and trafficking **[35]**.

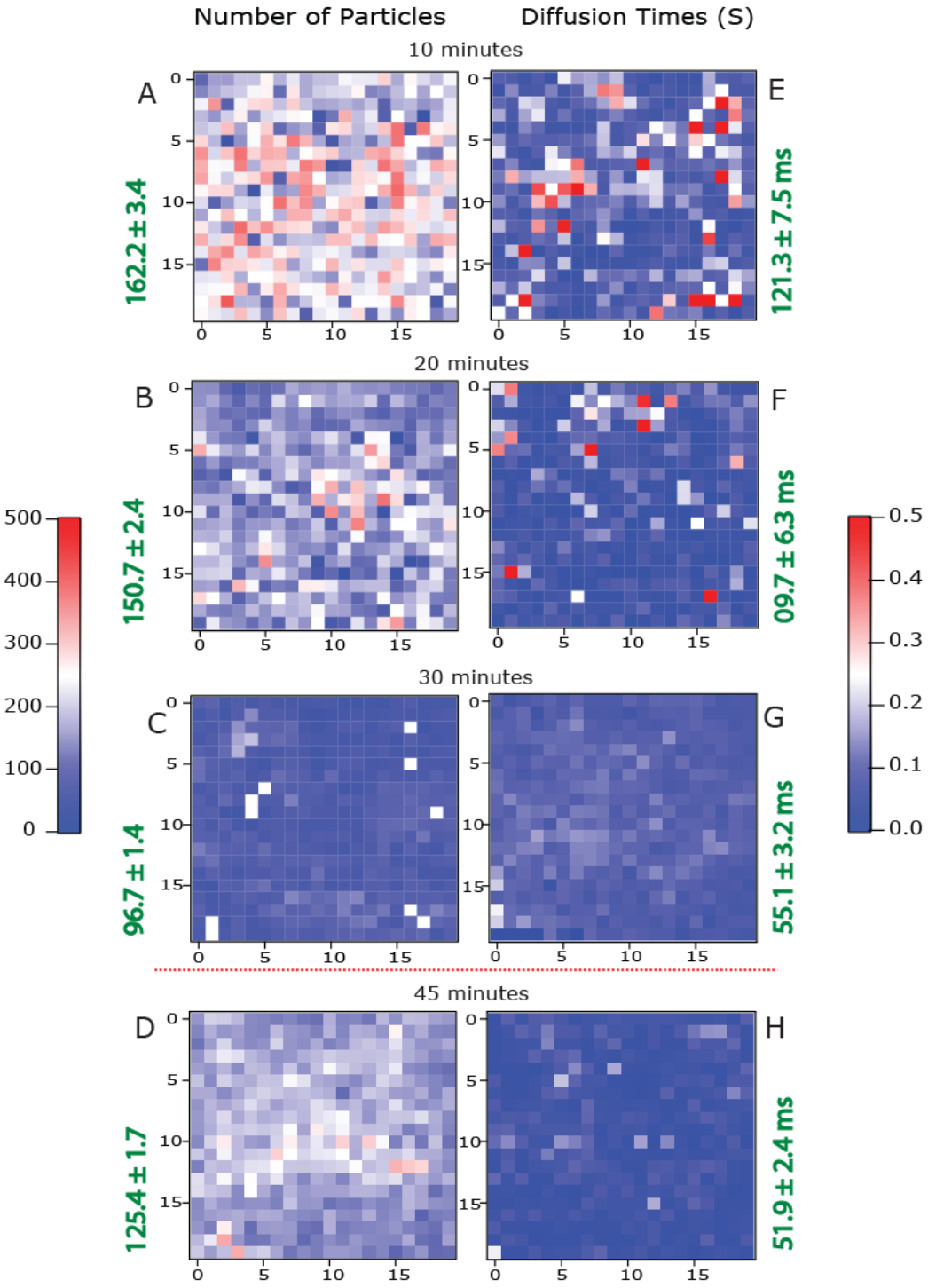

Figure 5.4: *ACF images of 20x20 pixel ROIs of cells labeled with SBD-TMR. A,B,C and D represents number of particles whereas E,F,G and H represents diffusion times according to the respective color scales. A–C and E--G images are of same position of a single cell after various times of incubation with MβCD. D and H represents the picture of the ROI of another cell at extended incubation with MβCD. The numbers on the x- and y-axes represent the pixel position. Average values for each picture are indicated in green.*

5.3.4 Autocorrelation based small scale organizational analysis

In order to investigate the cell membrane organization, SBD and DiI have been used in this study as the markers for the lipid raft and non-raft phase of the same SHSY5Y neuroblastoma cells, respectively. This investigation has been performed in the light of diffusion under normal versus perturbed conditions (disruption of the rafts) of the cell surface, which mainly have been done through two different ways, depleting cholesterol and disrupting actin cytoskeleton. MβCD is a common drug that is used to disrupt the lipid rafts as it extracts cholesterol from membranes. Reduced cholesterol content in cell membranes leads to a delocalization of raft associated proteins, and the loss of raft-like diffusion behavior **[81, 223, 235]**. There is some evidence which states that the raft related components are linked to the cytoskeleton **[147, 238, 239]**. Latrunculin A is an agent, which has been shown to change the diffusive behavior of rafts and raft associated proteins like CTxB by disrupting the actin cytoskeleton **[52, 147]**.

The diffusion coefficient has been used in this study as a measure of the fluidity of the membrane. For the analysis of diffusion coefficient only, a 3×3 binning of pixels (software based binning) have been used throughout, since the size of a 3×3 binned area (852×852 nm^2) corresponds to the typical pinhole size used in confocal FCS. These autocorrelation of 3×3 binned regions have been fitted with Eq. 2.17 and the obtained values of *D* were expressed as a histogram for each time point.

The average diffusion coefficient of membrane bound SBD-TMR (0.7 ± 1.1 $\mu m^2/s$) gradually increases over a time interval of 30 minutes by about a factor of 2-3 (1.7 ± 1.1 $\mu m^2/s$) upon addition of MβCD (*Table 5.1*). Accordingly, the diffusion coefficient histograms show a progressive shift towards higher diffusion coefficients (*Fig. 5.5 B*).

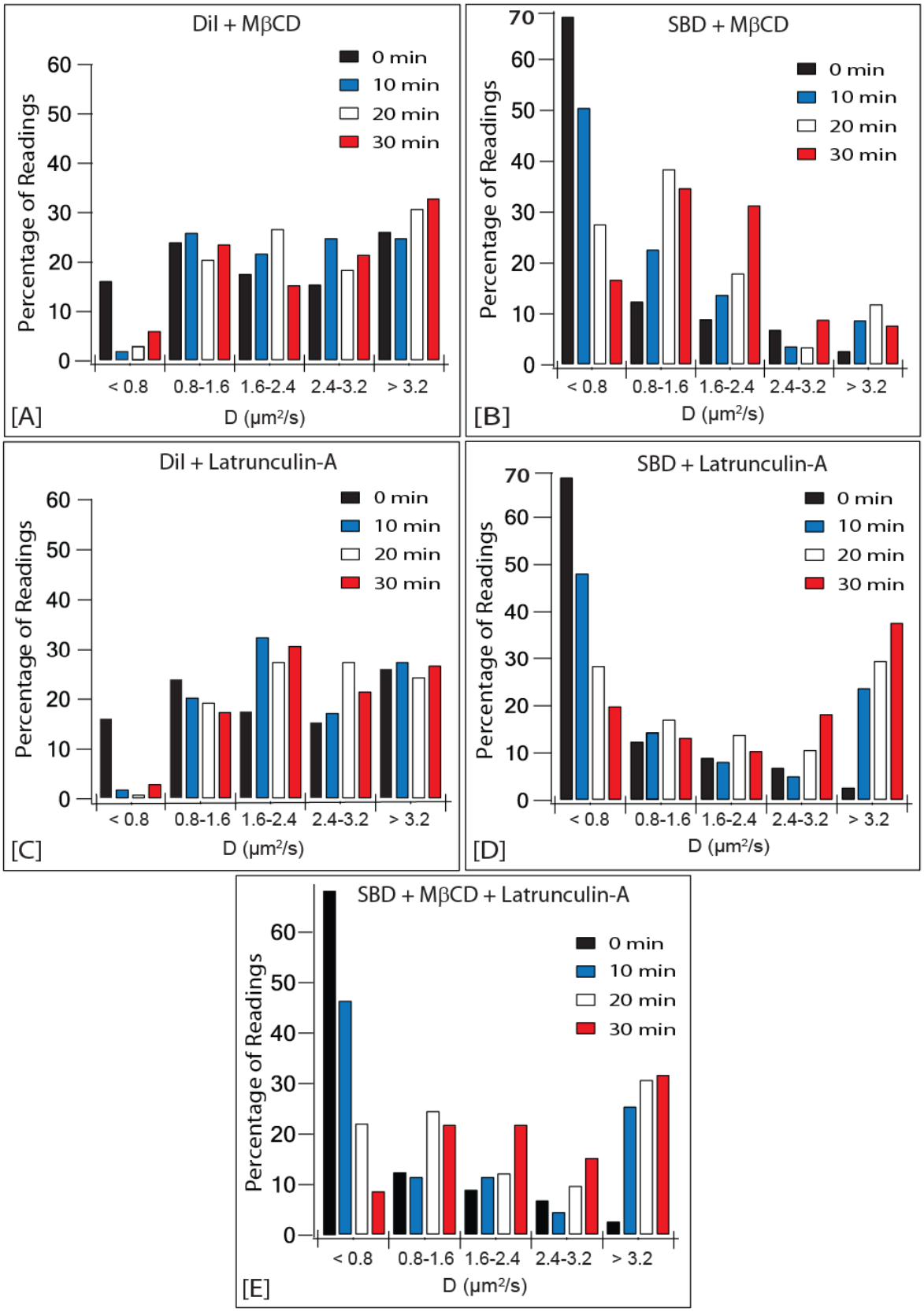

Figure 5.5: *Effects of MβCD and latrunculin-A treatments on the diffusion coefficients (D) of SBD- and DiI-labeled cells. (A–E) Histogram based distributions of diffusion coefficients (D) at various times of incubation with MβCD (A, B), latrunculin-A (C, D) and both drug (E) for SBD-TMR- and DiI-labeled cells.*

This change is consistent with the expectation that there is an increase in lateral mobility of raft related lipids and proteins on the cell membrane after cholesterol removal. An even stronger effect was seen after latrunculin-A treatment. The diffusion coefficient of membrane bound SBD-TMR changes by about a factor of 4 (2.9 ± 2.2 $\mu m^2/s$) in this case (*Table 5.1*). A similar effect was observed when the cells were incubated with both MβCD and latrunculin-A simultaneously and the diffusion coefficient increases to 2.8 ± 2.0 $\mu m^2/s$ (*Table 5.1*). In contrast, the diffusion coefficient of DiI, which mimics the diffusion of the liquid disordered phase of the cell membrane, increased by only a small fraction (less than 20%) under both circumstances. As shown by the histograms (*Fig. 5.5 A* and *Fig. 5.5 C*) it is mainly the abolishment of the very slow diffusive fraction of DiI with $D < 0.8\ \mu m^2/s$ which results in a change of the average diffusion coefficient from 2.5 ± 2.0 $\mu m^2/s$ to 3.0 ± 2.0 $\mu m^2/s$ and 2.8 ± 1.8 $\mu m^2/s$ for MβCD and latrunculin-A treatments respectively. In all of these cases, the large standard deviation of the diffusion coefficients indicates strong variations in the diffusion coefficients on the cell membrane, in agreement with the partitioning of SBD into different lipid regions **[81]**. This interpretation is consistent with the dynamic partitioning of raft proposed earlier **[53, 240, 241]**. These experiments show that both cholesterol content as well as the integrity of the cytoskeleton is important for the raft-like behavior of SBD but have a much lower influence on DiI, a marker for the liquid disordered, non-raft related membrane fraction.

	Untreated	**MβCD**	**Lat-A**	**Lat-A + MβCD**
DiI	**2.54 ± 2.04**	**2.98 ± 1.98**	**2.84 ± 1.84**	**-**
SBD	**0.7 ± 1.05**	**1.68 ± 1.06**	**2.89 ± 2.24**	**2.81 ± 1.97**

Table 5.1: *Average diffusion coefficients of raft (SBD) and non-raft (DiI) markers on SHSY5Y neuroblastoma cells after treatment with MβCD and latrunculin A (Lat) for 30 minutes. All data are given as* ***D*** *(Mean ± SD)* $\mu m^2/s$.

5.3.5 Cross-correlation based large scale organizational analysis

The possible changes associated with the larger scale organization of the cell membrane have been investigated by the means of ΔCCF frequency histograms (*Fig. 5.6* and *Fig. 5.7*) before and after cholesterol removal and cytoskeleton disruption. No fits are involved in the cross-correlation based approach, the ΔCCF values were calculated directly from experimental data and therefore no fitting model is involved in this method [**89**]. In order to differentiate between the histograms representing different perturbed condition, the fourth central moment of the histogram values, also called as kurtosis, has been calculated for each of them. The kurtosis is mainly a measure of the difference of a particular distribution from a standard Gaussian distribution. A larger kurtosis value indicates a distribution with a higher peak around the mean but more values at the extremes compared to a Gaussian distribution. A lower kurtosis value characterizes a distribution with a flatter peak around the mean having fewer values at the extremes.

Without MβCD addition, the ΔCCF images of SBD-TMR labeled cells are characterized by low kurtosis values close to 0 (*Fig. 5.7 B*). A sudden increase in kurtosis values to about 10 was observed for the ΔCCF distributions of the cells after 10 minutes of incubation with MβCD. The kurtosis then gradually decreases with time until after 30 min of incubation still with drug present, when it reaches a similar range to that of non-treated cells (*Fig. 5.7 B*). Therefore, during the incubation with MβCD (30 min) the fluidity of the membrane, as characterized by the diffusion coefficient, increases due to cholesterol removal. At the same time the membrane organization, in contrast to the fluidity, reaches a new state, which is similar to that of its initial condition (before the addition of the drug), as shown by the ΔCCF distribution (*Fig. 5.6 B*). No further changes in ΔCCF distribution took place for cells incubated longer than 30 minutes with MβCD (*Fig. 5.10*).

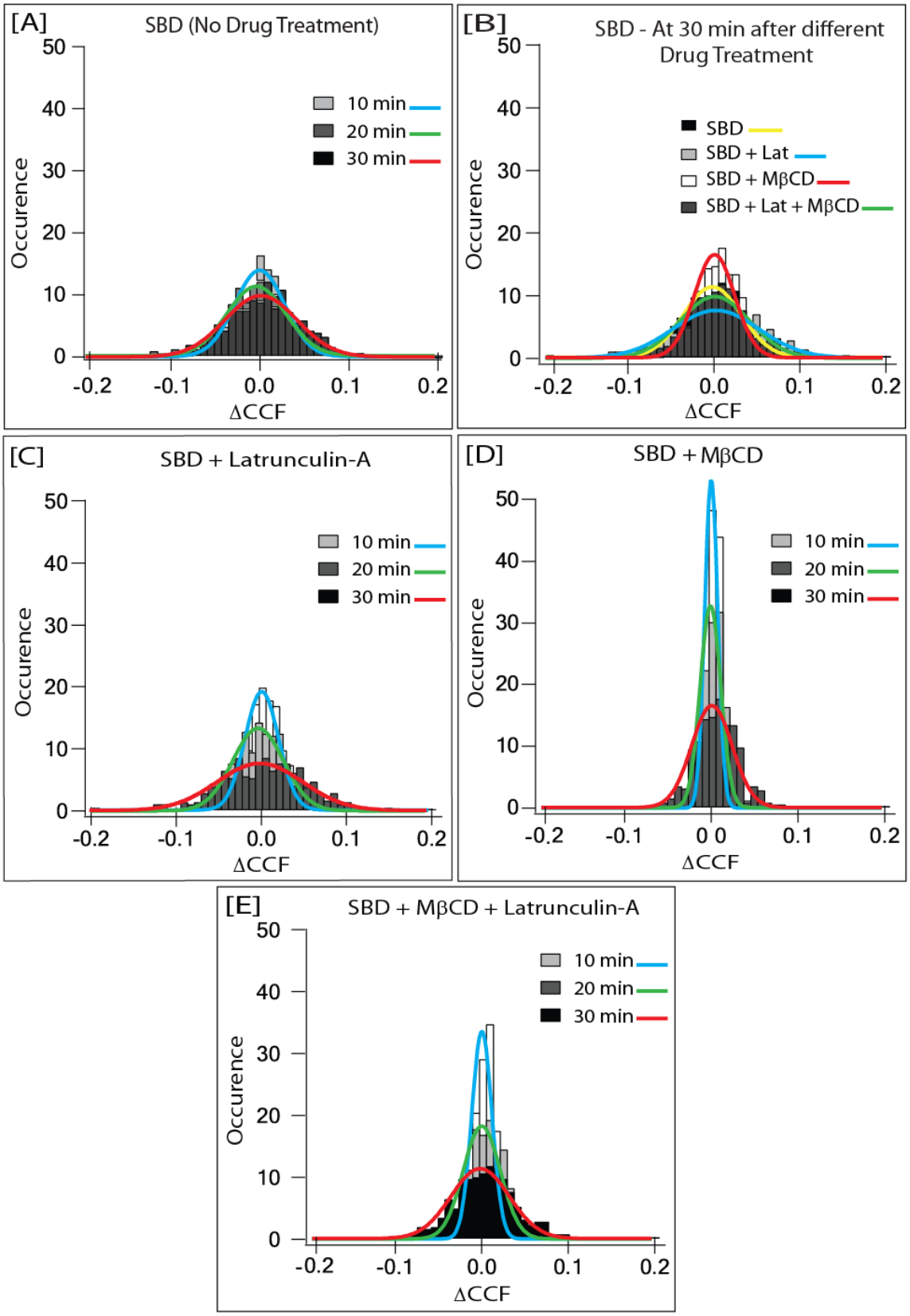

Figure 5.6: *ΔCCF histograms at different incubation times for cells labeled with SBD after different drug treatments (C for Latrunculin-A, D for MβCD, and E for both drugs) and no drug treatment (A) as control experiment. B represents ΔCCF histograms after 30 minutes of incubation for cells labeled with SBD and treatment without and with MβCD, latrunculin A or both. Gaussian fits to the distribution are indicated by dotted lines.*

These results are consistent with earlier findings that MβCD treatment leads to an overall loss of cholesterol dependent membrane lipid domains, and to a re-organization of the remaining non-extracted lipids **[242]**. It should also be noted that some other reports **[243]** found an indirect increase of glycerophospholipids as a result of the disorganization in the membrane upon cholesterol removal **[243]**; and it has been hypothesized that some compensatory changes in membrane lipid composition could take place after depletion of cholesterol **[244]** which could be an explanation for these findings.

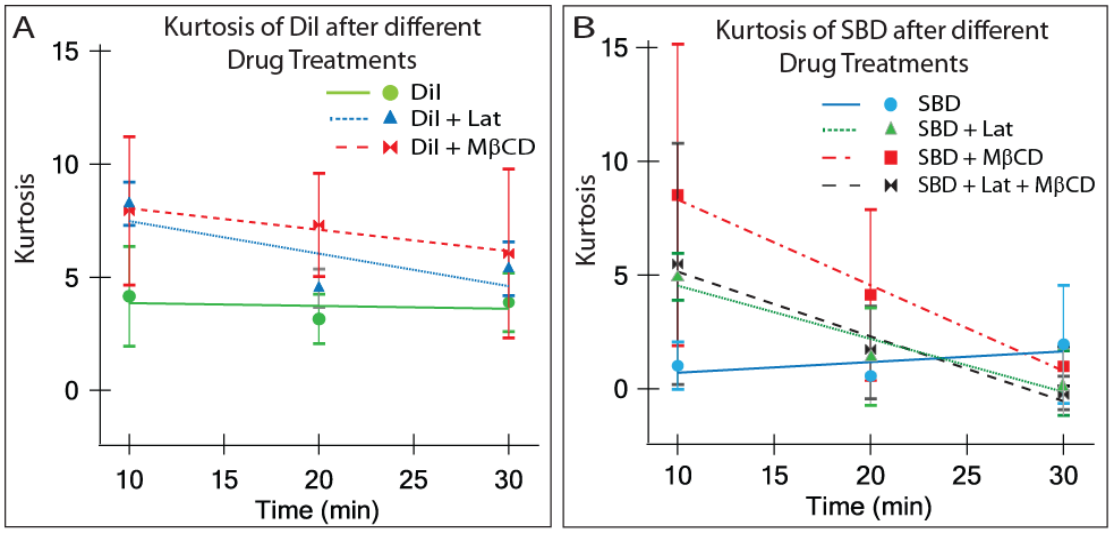

Figure 5.7: *Development of the kurtosis of the ΔCCF distributions showed in figure 5.8 and 5.9. A represents kurtosis values for cells labeled with DiI with different drug treatments and no drug treatment, while B represents the same for SBD. High kurtosis value for DiI indicates towards a very narrow distribution of ΔCCF values i.e. great extent of homogeneity of the liquid disordered phase. Small kurtosis value of SBD indicates the wider distribution of ΔCCF values representing the high degree of heterogeneity of ordered domains.*

Treatment of SBD-TMR labeled cells with latrunculin-A also initially leads to an increased value of kurtosis but at somewhat lower (around 4, with a less pronounced central peak; *Fig. 5.6 C*) than that of MβCD treatment (*Fig. 5.6 D*). Similar with MβCD treatment, within the 30 minutes the incubation time, kurtosis reaches to the values somewhat near to zero (*Fig. 5.7 B*) and the distribution of ΔCCF values achieves a slightly broader distribution than the untreated cells (*Fig. 5.6 C*). Treatment of the SBD-TMR labeled cells with both drugs MβCD

and latrunculin-A, lead to a similar behavior of the ΔCCF histograms (*Fig. 5.6E*) as treatment with only latrunculin A.

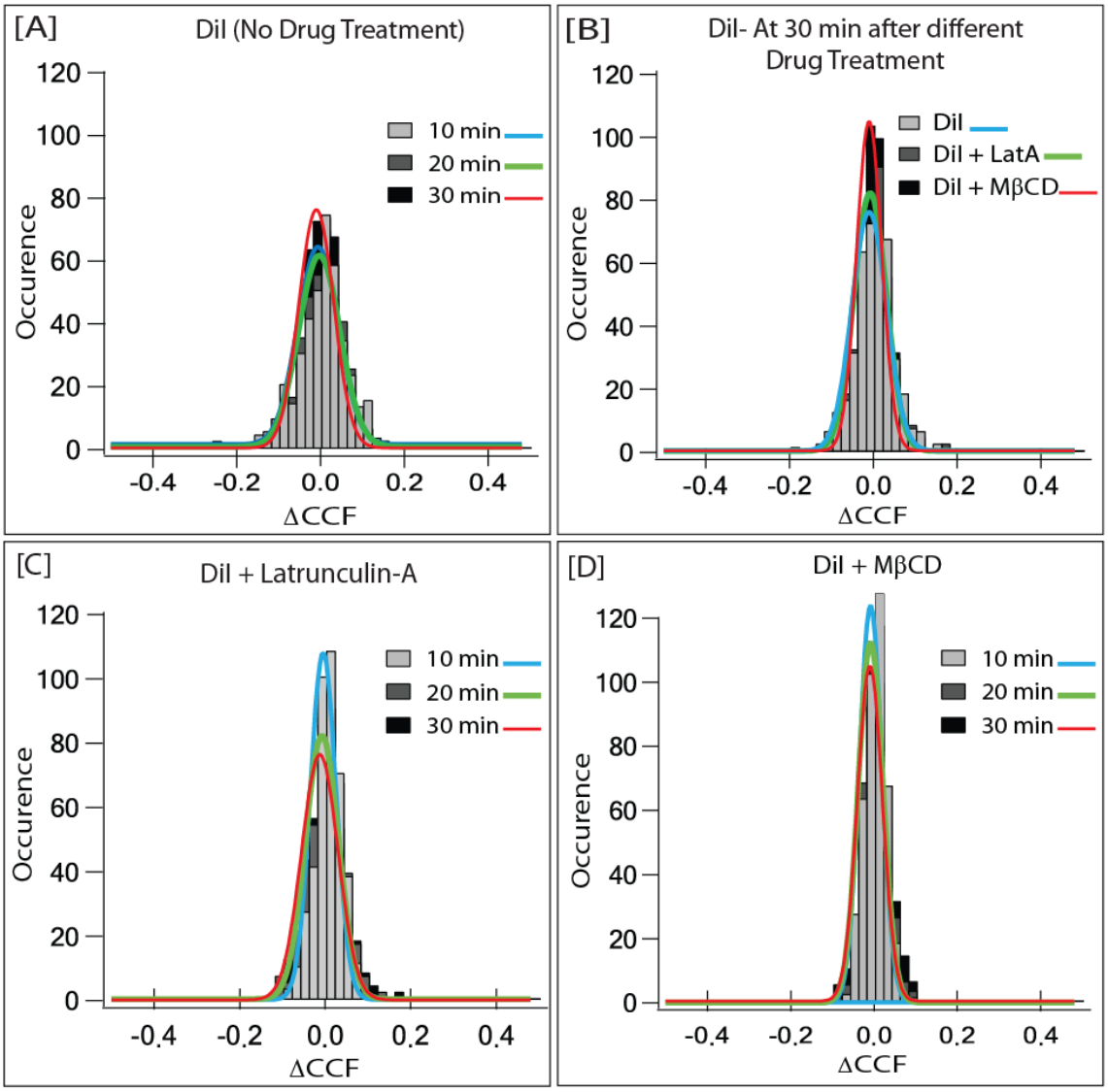

Figure 5.8: *ΔCCF histograms at different incubation times for cells labeled with DiI after different drug treatments (C for Latrunculin-A and D for MβCD) and no drug treatment (A) as control experiment. B represents ΔCCF histograms after 30 minutes of incubation for cells labeled with DiI and treatment without and with MβCD or latrunculin A. Gaussian fits to the distribution are indicated by dotted lines.*

Treatments of MβCD and latrunculin-A on the cells labeled with DiI, should reflect the organizational change of the liquid disordered phase of the cell membrane due to the depletion of cholesterol and disruption of the cytoskeleton. But only very small changes in the kurtosis values have been observed in either cases of MβCD or latrunculin-A treatments (*Fig. 5.7 A*).

The ΔCCF histograms exhibited narrow distributions, and didn't show any significant changes throughout the 30 minutes of incubation with the drugs (*Fig. 5.8 C* for Latrunculin-A and D for MβCD), similar to its untreated condition (*Fig. 5.8 A*). This implies that cholesterol or cytoskeleton does not have any direct influence on the organizational distribution of the liquid disordered phase of cell membrane.

The changes take place in membrane equilibrium during the incubation with the drug could be a possible explanation for the changes in ΔCCF distributions upon drug treatment. The normally wide ΔCCF distribution may arise due to the restriction of SBD diffusion due to cytoskeletal confinements **[245]**. Alternatively, internalization of SBD, may also lead to wider, non isotropic values of ΔCCF on the cell membrane. It has been shown that, MβCD treatment disturbs the internalization of SBD into SHSY5Y cells **[81]**. Hence, inhibition of internalization, as seen in MβCD-treated cells, may result in a disruption of this flux which results in the narrower distributions of ΔCCF histograms. This phenomenon has been illustrated in *Fig. 5.9*, which shows the ΔCCF images of cells labeled with SBD-TMR and treated with MβCD, latrunculin-A, and both the drugs, after various time points of incubation. The scale bar indicates that the whitish dim appearance corresponds to a more homogeneous narrower distribution of ΔCCF, having most of the values close to zero, while the dark more granular appearance represents more heterogeneous organization. Images in the 1st row (A–C), representing untreated cells are very heterogeneous. Upon addition of drugs, the images become less granular and the heterogeneity is restored to various degrees after completion of the action of the drug, as shown in *Fig. 5.9 F, I,* and *L*. The heterogeneity in these completed stages is comparable to that of those in initial stages before the treatments.

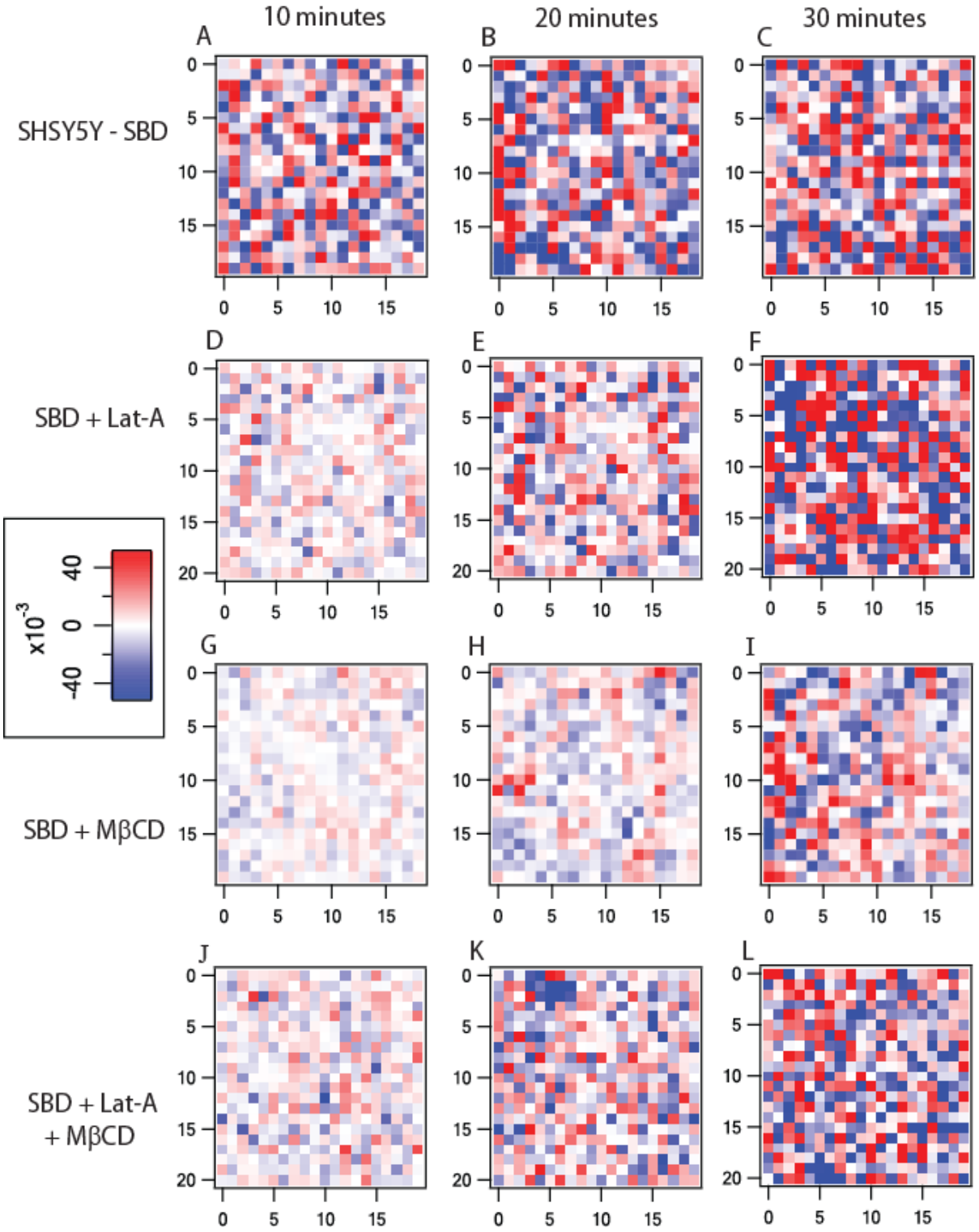

Figure 5.9: *ΔCCF images of cells labeled with SBD-TMR. A–C Images of no drug treated control cells. Panels D–F, G–I, and J–L show the ΔCCF images for cells treated with latrunculin-A, MβCD and both the drugs, respectively, after various times of incubation. Images in A–C are very heterogeneous. Upon addition of drugs, the images become less granular and the heterogeneity is restored to various degrees after increased incubation of the drug, as shown in F, I, and L. The heterogeneity in these images is comparable to that seen in images A–C. The numbers on the x- and y-axes represent the pixel position.*

However, in both normal and all drug treated conditions, the mean position of the ΔCCF distribution is around zero (*Fig. 5.6*), because there is no macroscopic flux present in the system **[248]**. Therefore, the disturbance in internalization would result in an altered membrane organization and transport patterns during the action of the drug, until a new membrane equilibrium is reached.

5.3.6 Confirmation of saturation of drug effect

In order to check whether the impact of MβCD on the cells has been completed within the 30 min incubation time, two extra set of measurements have been conducted on cells which have been treated with MβCD for times longer than 30 minutes, and on untreated cells, i.e. a negative control. For both cases no changes in the distribution of ΔCCF values were observed, confirming that the MβCD action was completed within 30 minutes incubation time and the cells which have been treated with MβCD for more than 30 minutes re-establish a similar membrane organization as untreated cells on scales above the optical resolution limit (*Fig. 5.10*).

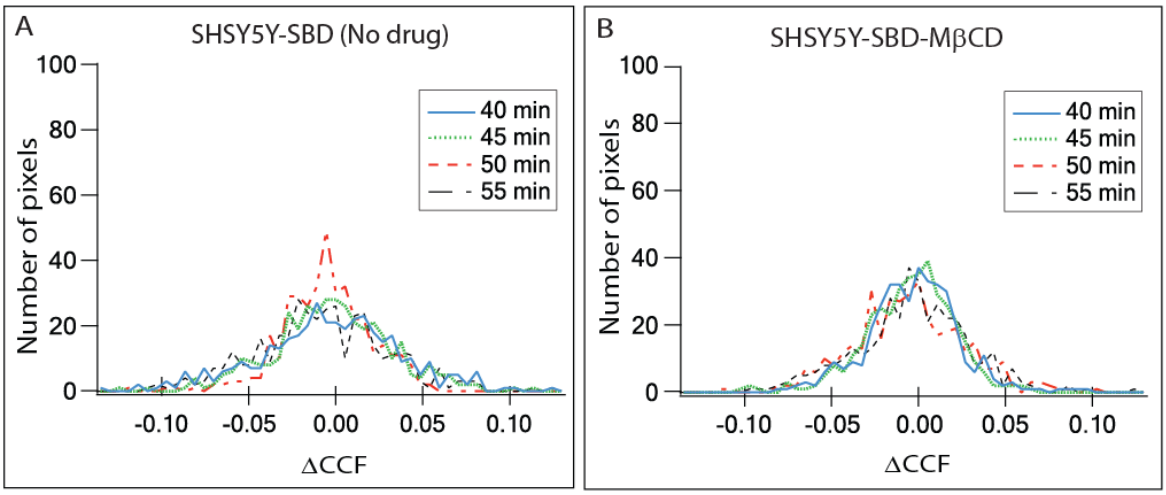

Figure 5.10: *ΔCCF distributions of SBD-TMR on SHSY5Y cell membranes, for untreated (A) and MβCD treated (B) cells after incubation time longer than 30 minutes. In each case the distributions have been measured on one single cell.*

5.4 Discussion

Overall, the findings of this study indicate that DiI, the marker for the liquid disordered lipid phase on cell membranes, has limited dependency on cholesterol and the cytoskeleton, which is reflected in the limited change in the diffusion coefficient or ΔCCF distribution during treatment with MβCD or latrunculin A, respectively. However SBD, the marker associated with the ordered lipid domains or rafts of the cell surface, is influenced by both cholesterol and the cytoskeleton **[147]**. Disruption of the cytoskeleton results in lifting the diffusion coefficients of SBD to the similar range of DiI **[240]**, while removal of cholesterol also increases the diffusion coefficient of SBD, but to a lesser extent. Therefore, it seems that the cytoskeleton is the main barrier to the far-diffusion of SBD and the coupling of SBD to the cytoskeleton is mediated by cholesterol. Moreover, the outcome of this study are consistent with the proposal that the cell membrane is organized on at least two different length scales **[52]**, one below the resolution limit in nanodomains **[134, 248]** by the cholesterol content and another at larger scales, organized by the cytoskeleton. This study also supports the outcomes of chapter 3, that SBD partitions partly into cholesterol dependent microdomains **[81]**, which are connected to the cytoskeleton **[147]**. Furthermore, this study to conduct the comparison between different lipid markers and the effects of removal of different lipids from the cell surface to further elucidate the dynamic organization of cell membranes and the nature of the linkage between SBD, cholesterol and the cytoskeleton, which is addressed in the next chapter.

5.5 Summary

In this chapter, ITIR-FCCS has been introduced as an extension of ITIR-FCS for the investigation of transport and diffusion processes in cell membranes. The diffusion

coefficients extracted from the experiments are in good agreement with the findings of progressive research groups. The anisotropic translocation studied to demonstrate the membrane organization can in principle be studied by determining the difference of the forward and backward correlations as so-called ΔCCF images. The approach has been successfully used to demonstrate the cell membrane organization and heterogeneity by using different markers for the liquid disordered phase and for lipid microdomains and their observation under the different conditions of cholesterol removal or cytoskeleton de-polymerization. Finally, ITIR-FCCS gives adequate spatial and temporal resolution to be able to measure membrane dynamics, and thus presents a powerful biophysical tool to provide novel insights into membrane organization.

Chapter 6:

Importance of sphingolipids and glycosphingolipids for microdomain organization

6.1 Introduction

Lipids are the basic structural units of the cell membrane, a partially permeable barrier that controls the directed flux of molecules in and out of the cytoplasm **[248]**. At recent time, the understanding about the complicated membrane structure, consists of membrane lipids including sterols and ceramide, and the relevant proteins, is being refined constantly **[249]**. According to the present understanding, different lipid species concentrate different parts and compartments of the membrane to form various membrane phases and domains **[250-252]**. The amount of different lipid classes present in the cell membrane depends upon the type of cell, but for the majority of cases phospholipids are the most abundant lipid species. Phospholipids and cholesterol content help to maintain the membrane fluidity at physiological conditions **[253]**. One more major constitutional lipid class of the cell membrane is the sphingolipid family. Some lipids of this family help to protect the cell surface from harmful external environmental factors, by forming a mechanically stable and chemically resistant outer leaflet of the plasma membrane **[254, 255]**. Glycolipids are minor components of cell membranes containing a carbohydrate moiety **[256, 257]**. Lipids of this class are members of the large and heterogeneous family of sphingolipids and form complex patterns on eukaryotic cell membranes **[258]**. Sialic acid containing glycolipids concentrate mainly on the plasma membrane of neuronal cells. These components are found mostly in

clustered conditions in membrane domains [**259**], though there are some *in vitro* evidence as well that says they are fairly evenly distributed, e.g. by EM.

For maintaining the usual cellular processes including normal cell growth and respond to surrounding environmental changes, the cell membrane must possess a dynamic structure **[259]**. Alteration in the total content of any single lipid class leads to a change in the fluidity and dynamic organization of the cell membrane **[260-263]**. In order to have a complete biophysical characterization of the newly established lipid raft associated peptide probe SBD, and for better understanding of the dynamic organization of the lipid rich membrane domains, compositions of the raft associated lipids have been altered and the change in mobility of the cell membrane has been checked using ITIR-FCS and ITIR-FCCS as the instrumental techniques in this part of the study. As described in the previous chapter also, the time chase experiments with ITIR-FCCS provides a new way to understand any dynamic changes associated with a larger length scale on the cell surface due to the effect of any external perturbation, which cannot be obtained from only diffusion coefficients or imaging experiments. Diffusion behaviours and active transportations of SBD-TMR along with 2 other fluorescently tagged raft associated probes CTxB and J116S and DiI as a non-raft associated liquid disordered phase marker have been characterized here to mimic the overall dynamic membrane organizations under normal versus different lipid depleted conditions [J116S is a raftophilic membrane domain targeting steroid probe (determined by JADO's liposome partitioning assays) from JADO Technologies, Germany, whose structure is not published by the company.]

The fluorophore containing probes, whose dynamic properties have been studied here under normal and perturbed conditions, are associated mainly with raft lipids including sphingolipids, glycosphingolipids and sphingomyelin. Overall, the dynamic properties of

these probes have been looked under different classes of lipids disrupted conditions to describe the importance of these lipids in the dynamic cell membrane organization.

6.2 Materials and Methods

In order to check the role of membrane lipids such as sphingolipids, glycosphingolipids, sphingomyelin, for the dynamic cell membrane organization, the drugs that have been used to perturb the lipid composition of the cell membrane are: Fumonisin B1 [FB1, (A.G. Scientific Inc., catalog number F-1022)], N-Butyldeoxynojirimycin [NB-DNJ, (Sigma-Aldrich, catalog number B8299)] and sphingomyelinase (Smase) from *Bacillus cereus* (Sigma-Aldrich, catalog number S7651). FB1 is known for the disruption of sphingolipid metabolism by inhibiting the enzyme ceramide synthase. NB-DNJ is a potential inhibitor of different enzymes including α-glucosidase I and II. It also inhibits the biosynthesis of glycosphingolipids by inhibiting the ceramide-specific glucosyltransferase. Smase breaks down the sphingomyelin into phosphocholine and ceramide. For the recovery of the cells from these perturbed conditions, GM1 (Avanti Polar Lipids, Inc. 860065P) and sphingomyelin (Sigma-Aldrich, catalog number S7004) were added to the medium after the NB-DNJ and Smase treatments respectively. The organizational and dynamic changes took place on the cell membrane due to these drug treatments and the respective recoveries have been traced with different lipid associated fluorescent probes, namely, $DiIC_{18}$ for the liquid disordered phase, where as the recently established sphingolipid associated probe SBD (conjugated with TMR), cholera toxin subunit-B (conjugated with Alexa Fluor-594) and J116S (JADO Technologies GmbH, Dresden, Germany) for the liquid ordered raft phase.

6.2.1 Cell culture and staining with the markers

SH-SY5Y neuroblastoma cells were grown similarly as described in the earlier chapters at 37º C in Dulbecco's Modified Eagle's Medium supplemented with 10% fetal bovine serum and 1% antibiotic. For labeling, cells were plated on 8-well chambers with 0.17 mm coverslip bottoms (Nunc, Denmark); >24 hours prior to the drug treatments / measurements.

Incubations with SBD, CTxB and DiI have performed in the similar way that already been described in the earlier chapters. The other marker used in this chapter, J116S is a cell membrane microdomain targeting probe from JADO Technologies GmbH. A 10 mM stock solution of J116S in DMSO is normally kept in -20º C for long term storage. Working solution was prepared by diluting it up to ~100nM in serum free DMEM and the cells in 8 well chamber were incubated with this working solution at 37º C for 30 minutes. Cells were then washed with HBSS/HEPES buffer as usual and put in indicator free DMEM for measurements.

6.2.2 Alteration of sphingolipids content of the cell surface

6.2.2.1 Fumonisin B1 treatment

Using the ITIR-FCS, time chase measurements with respect to the drug were carried out. Cells in 8 well chambers were first washed 3 times with HBSS/HEPES buffer and incubated with the markers (SBD-TMR / DiI / J116S) for 30 minutes at37º C followed by 3 times washing, again with the buffer and suspended in indicator and serum free DMEM for measurement. After taking the 1st measurement at 0 min, FB1 (prepared in imaging medium) was added to the medium in such a manner so that the resultant concentration of the medium became 10 μM with respect to FB1. The cells were then measured for 120 minutes, taking readings at every 30 minutes.

6.2.2.2 Recovery from Fumonisin B1 treatment

In a separate 8 well chamber, cells were treated with FB1 for two hours, followed by 3 times wash with HBSS/HEPES buffer and then put back into usual full growth medium. Cells were kept in 37º C incubator >24 hours to recover from the effect of FB1. They were then treated with the markers (SBD-TMR / DiI / J116S) according to the previously described manner and measured after suspended in indicator free DMEM.

6.2.3 Alteration of glycosphingolipids content of the cell surface

6.2.3.1 NB-DNJ treatment

N-Butyldeoxynojirimycin inhibits the biosynthesis of cellular glycosphingolipids, and this drug needs much longer incubation time than the other two. Hence, only end point measurements and no time chase experiments were performed in case of NB-DNJ treatment. Cells in 8 well chamber were incubated with 10 μm NB-DNJ (which was prepared in full growth medium from the 5mM aqueous NB-DNJ stock solution) for >48 hours at 37º C, followed by incubation with the markers (SBD-TMR / CTxB / DiI / J116S) for 30 minutes at37º C sandwiched between three times washing before and after with the same buffer HBSS/HEPES and finally suspended in indicator free DMEM for measurement.

6.2.3.2 Adding back GM1 to the NB-DNJ treated cells

In separate 8 well chambers, cells were treated with NB-DNJ for >48 hours, washed 3 times with HBSS/HEPES and then put back into usual full growth medium. Cells were kept in 37º C incubator to recover from the effect of NB-DNJ. Chambers were taken out from the incubator ~24 hours and ~48 hours later and treated with the markers (SBD-TMR / CTxB / DiI / J116S) as mentioned before and measured after suspended in indicator free DMEM.

As NB-DNJ substantially knocks out glycosphingolipids and hence ganglioside GM1 from the cell surface **[31]**, a set of experiments were performed after add back GM1 externally to the cells. 10 mM GM1 stock solution was prepared by dissolving the white powder in a mixture of chloroform, methanol and water with a ratio of 65:25:4 as suggested by the manufacturer company. In order to prepare a 50 μM GM1 working solution, the stock solution was dried and the resultant solid mass was dissolved in 2μl of EtOH followed by made up the volume up to 1 ml with complete growth media. NB-DNJ treated cells were then incubated 12 hours with this GM1 working solution at 37º C and treated further with the markers (SBD-TMR / CTxB / DiI / J116S) as mentioned earlier and measured after suspended in indicator free DMEM.

6.2.4 Alteration of sphingomyelin content of the cell surface

6.2.4.1 Sphingomyelinase treatment

Similar to the FB1, sphingomyelinase treatments are also time chase studies with respect to the drug (enzyme) and the incubation sequence of drug and marker is reverse to that of the NB-DNJ treatment. Cells in 8 well chambers were first incubated with the markers (SBD-TMR / DiI / J116S) for 30 minutes at 37º C, washed with the buffer and suspended in indicator free DMEM for measurement. After taking the 1st measurement at 0 min Smase (prepared in imaging medium) was added to the imaging chambers in such a manner so that the resultant concentration of the medium became 50 mUnit/ml with respect to Smase. The cells were chased for 60 minutes, taking readings at 20 minute intervals.

6.2.4.2 Adding back Sphingomyelin to the Smase treated cells

In separate 8 well chambers, cells were treated with Smase for one hour, washed 3 times with HBSS/HEPES and then incubated with sphingomyelin at 37º C for >4 hours to get back to

the normal level of cellular sphingomyelin. To prepare SM working solution, first the SM stock (in 1:1 $CHCl_3$+MeOH) was dried followed by dissolving that dried mass in 2µl EtOH and then made up the volume up to 1 ml with full growth medium. Sphingomyelin concentration of this resultant solution was 5µg/ml. After the 4 hour incubation with SM, cells were washed 3 times again with buffer and treated with the markers (SBD-TMR / DiI / J116S) as mentioned earlier and measured after suspended in indicator free DMEM.

6.3 Results

The main focus of this part of the work is to investigate the role of sphingolipids, (ceramide, glycosphingolipids, sphingomyelin), in the dynamic cell membrane organization. Here, the mobility of SBD along with other raft- and nonraft-associated markers have been compared under normal conditions versus conditions in which those lipids were depleted on the plasma membrane of SH-SY5Y neuroblastoma cells. Since the distributions of these lipids are highly heterogeneous, the membrane exhibits a range of diffusion coefficients due to the presence of rigid regions enriched with these lipids. Depletion or reduction of these lipids on cell membranes leads to disruption of those rigid clusters or so called “rafts”, and loose the raft-like diffusion behavior. The diffusion coefficients of these markers have been used as the measure of the fluidity of the membrane where as the possible changes in the larger scale organization of the membrane have been investigated by the means of ΔCCF images and their distribution histograms.

In this context it should be mentioned that all the ΔCCF distributions shown in this study exclude the values (outliers) that didn’t fall in the specified distribution range. About 12 % of the measurements didn’t have any outliers, the rest about 88% of the measurements had outliers, but not in significant (< 2%) proportion with respect to the number of readings. Each measurement/data set consist of 420 ΔCCFs, and the number of outliers in each set of data

ranges from 0 to 8 with 2 exceptions where number of outliers were 12 and 21 respectively (still less than 5%). [The chosen distribution range is from -0.5 to +0.5 and the absolute values for the outliers are typically between 0.5 and 1; with few rare exceptions where the value is >1.]

6.3.1 Identification of the raft like diffusion behavior of J116S

In order to get an overview whether the diffusion behavior of the new probe, J116S (average τ_D being ~30 ms), is really associated with the raft fraction, the τ_D distribution histogram of this marker has been compared with other established raft markers, CTxB and SBD. From this approach a large fraction (~40%) of τ_D of J116S were found to be in the very slow moving (τ_D >30 ms) category, similar to CTxB, SBD-TMR and SBD-OG and even a greater similarity with CTxB towards the contribution for the faster-moving particles (1-10 and 10-20 ms ranges) (*Fig. 6.1*). This similarity with CTxB reflects in the average diffusion times as well, the τ_D values being 28 ± 0.4 ms and 28 ± 2 ms for J116S and CTxB respectively.

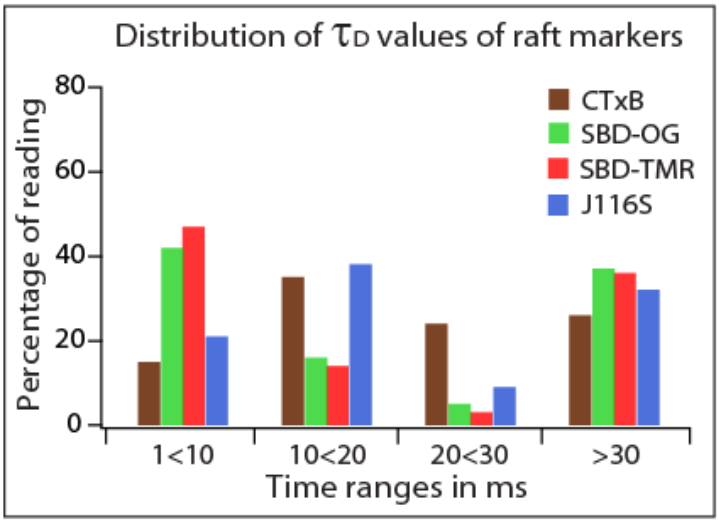

Figure 6.1: *The comparison of distribution of diffusion times for J116S with other raft associated markers SBD and CTxB. Histograms show percentages of readings that gave τ_D in the indicated millisecond time ranges. The overall distribution of J116S is quite similar to CTxB-Alexa594 and the substantial fraction of readings in the low-mobility τ_D >30 ms range, typical for raft markers, is similar with SBD-TMR and SBD-OG as well. For all of these experiments, n is >50 measurements.*

6.3.2 Effect of disruption of sphingolipid metabolism and recovery

It was found from the diffusion coefficient analysis that, for unperturbed cells, all the raft associated probes, SBD-TMR, CTxB and J116S exhibits diffusion coefficients in the similar range which is much smaller than that of the non-raft associated marker DiI. Fumonisin B1 is a drug that disrupts the sphingolipid metabolism by inhibiting the enzyme ceramide synthase **[264, 266, 267]**, and thereby disrupts the de novo biosynthesis of sphingolipid. Hence incubation with this drug results in the disruption of rafts from cell membranes and the raft associated proteins loss their raft-like diffusion behavior.

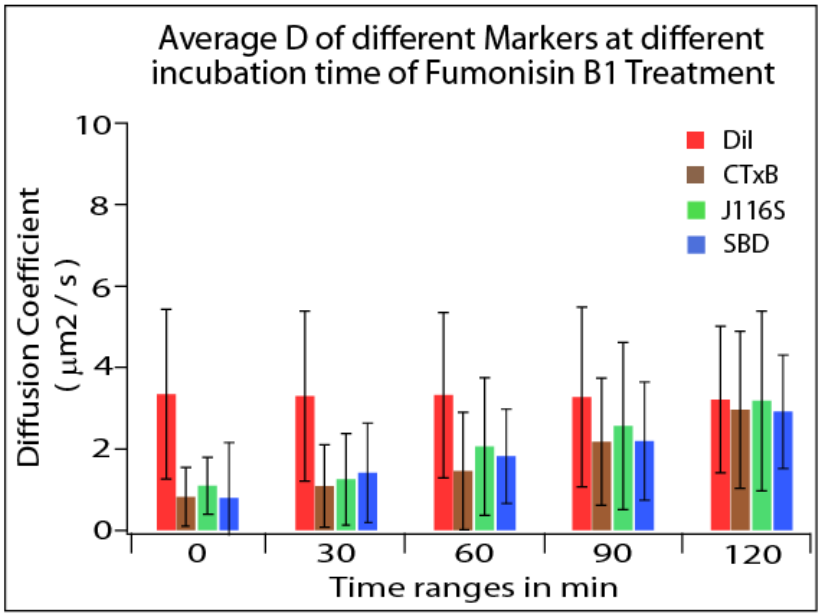

Figure 6.2: *Gradual effects of Fumonisin B1 treatment at different time points of the incubation. Average diffusion coefficients for different markers over the entire incubation period with the drug have been plotted here. Standard deviations denoted by those large error bars reflect the heterogeneity of the related cell membrane.*

The average diffusion coefficient of membrane bound SBD-TMR (0.8 ± 1.3 $\mu m^2/s$), CTxB (0.8 ± 0.7 $\mu m^2/s$) and J116S (1.1 ± 0.7 $\mu m^2/s$) gradually increases over a time interval of 120 minutes by about a factor of 3-4 (2.9 ± 1.4 $\mu m^2/s$), (2.9 ± 1.9 $\mu m^2/s$) and (3.2 ± 2.1 $\mu m^2/s$), respectively, whereas no such change was observed in case of DiI under similar circumstances (*Fig. 6.2*). These changes are consistent with the expectation that there is an

increase in lateral mobility of raft related lipids and proteins on the cell membrane after reduction of sphingolipids. No further changes in the diffusion coefficients of the raft associated markers took place for cells incubated up to 180 minutes with FB1 [(3.0 ± 1.6 $\mu m^2/s$), (2.9 ± 1.5 $\mu m^2/s$) and (3.1 ± 1.7 $\mu m^2/s$) for the markers, respectively].

Upon removing the drug to let the cells recover from its effect, the raft associated markers returned closer to their native state, which was reflected in the regained comparative slower diffusion coefficient values (1.5 ± 1.1 $\mu m^2/s$), (1.3 ± 0.9 $\mu m^2/s$) and (1.3 ± 1.5 $\mu m^2/s$) for SBD-TMR CTxB and J116S respectively. The large standard deviations for all the values with or without the drug treatments indicate strong variations of diffusion coefficients on the cell membrane, due to the partitioning of the markers into different lipid regions **[81]** and in agreement with the previously proposed dynamic partitioning of raft models **[53, 240, 241]**. All these diffusion coefficient values indicate the importance of sphingolipids towards the raft-like dynamic behaviors of the corresponding markers, simultaneously the lack of any significant influence on the dynamics of non-raft or liquid disordered fraction of the cell membrane. The recovery studies reflects that the existence of microdomains depends upon chemical equilibrium of the cell membrane, removal of any external perturbation reestablishes the chemical balance of different lipids leading to the reformation of the raft like less mobile membrane clusters.

The possible changes associated with the larger scale organization on the cell membrane due to the disruption and recovery of the sphingolipid metabolism have been investigated by the ΔCCF frequency histogram based approach, described elaborately in the previous chapter. The heterogeneities of cell membrane should be reflected on analyzing the ΔCCF values. Before the FB1 addition, the ΔCCF histograms of SBD and J116S labeled cells are characterized by comparatively flat and widely distributed profiles (*Fig. 6.2 B*). A comparatively sharp and narrowly distributed profile was obtained for CTxB where as DiI

show much narrow distribution of the histograms, indicating pretty even mobility of the lipid species for the corresponding membrane phase. Aggregate formations of CTxB on the cell surface **[268]** might be the reason for narrower distribution of the probe compared to the other raft associated markers SBD and J116S.

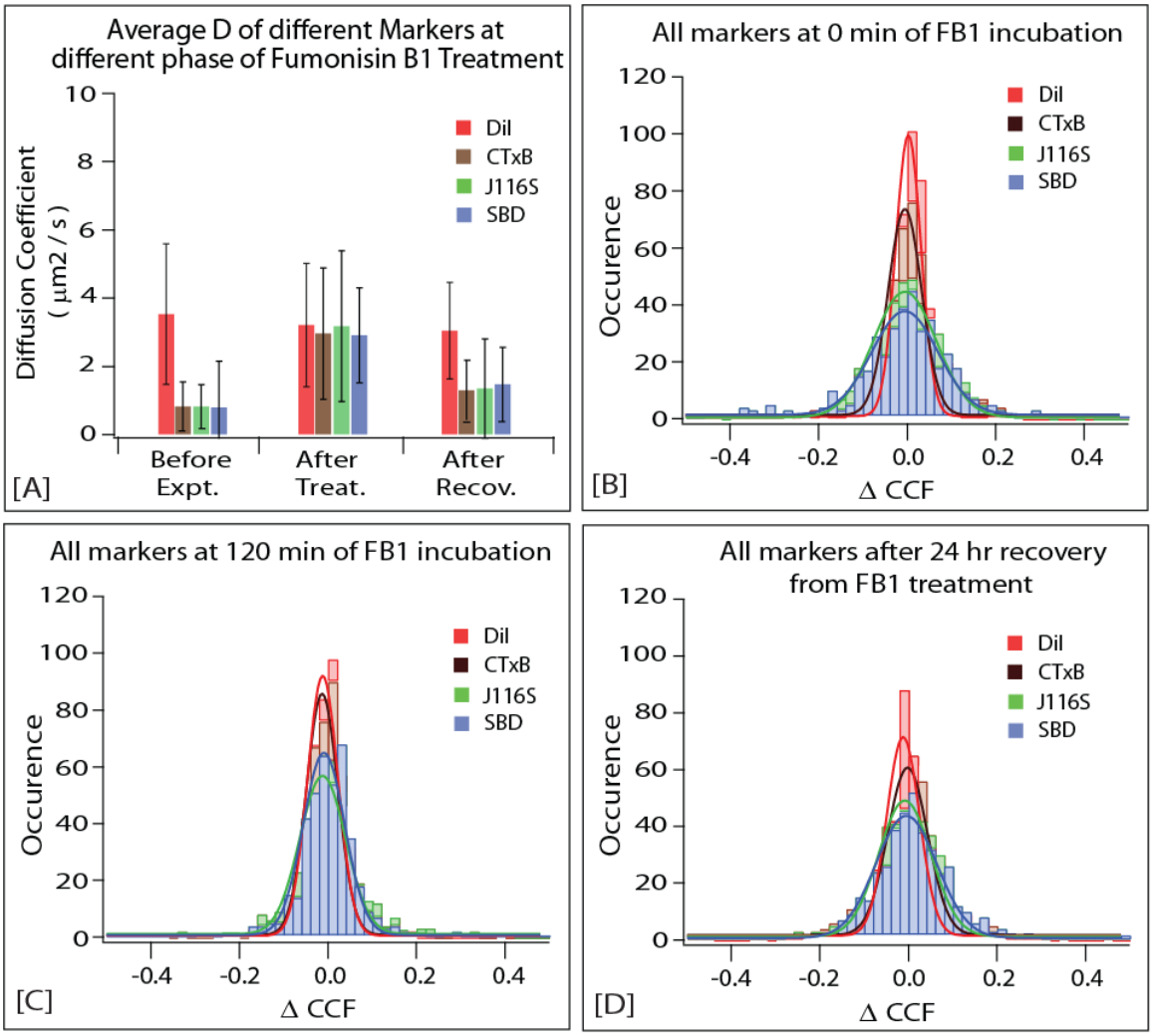

Figure 6.3: *Effects of disruption of the sphingolipid metabolism [by Fumonisin B1 treatment] on different markers at different phases of the experiments. Picture A shows the average diffusion coefficients for different markers before the treatment, after the treatment and after the recovery from the drug treatment. Error bars reflect standard deviations. B, C and D represent ΔCCF distributions for all the markers before the treatments, after the treatments and after the recoveries from the drug treatments respectively. Gaussian fits to the distributions are indicated by solid lines with respective colors.*

Narrowing in the distributions of all raft associated markers were observed for the ΔCCF histograms after 30 min of incubation with FB1 indicating a decrease in anisotropic movements. The distributions maintain their narrow profile over the entire incubation period

of 120 min (*Fig. 6.4*) and didn't come back to any state similar to the non-treated cells, which was obtained in case of cytoskeleton disruption (*Fig. 5.7*).

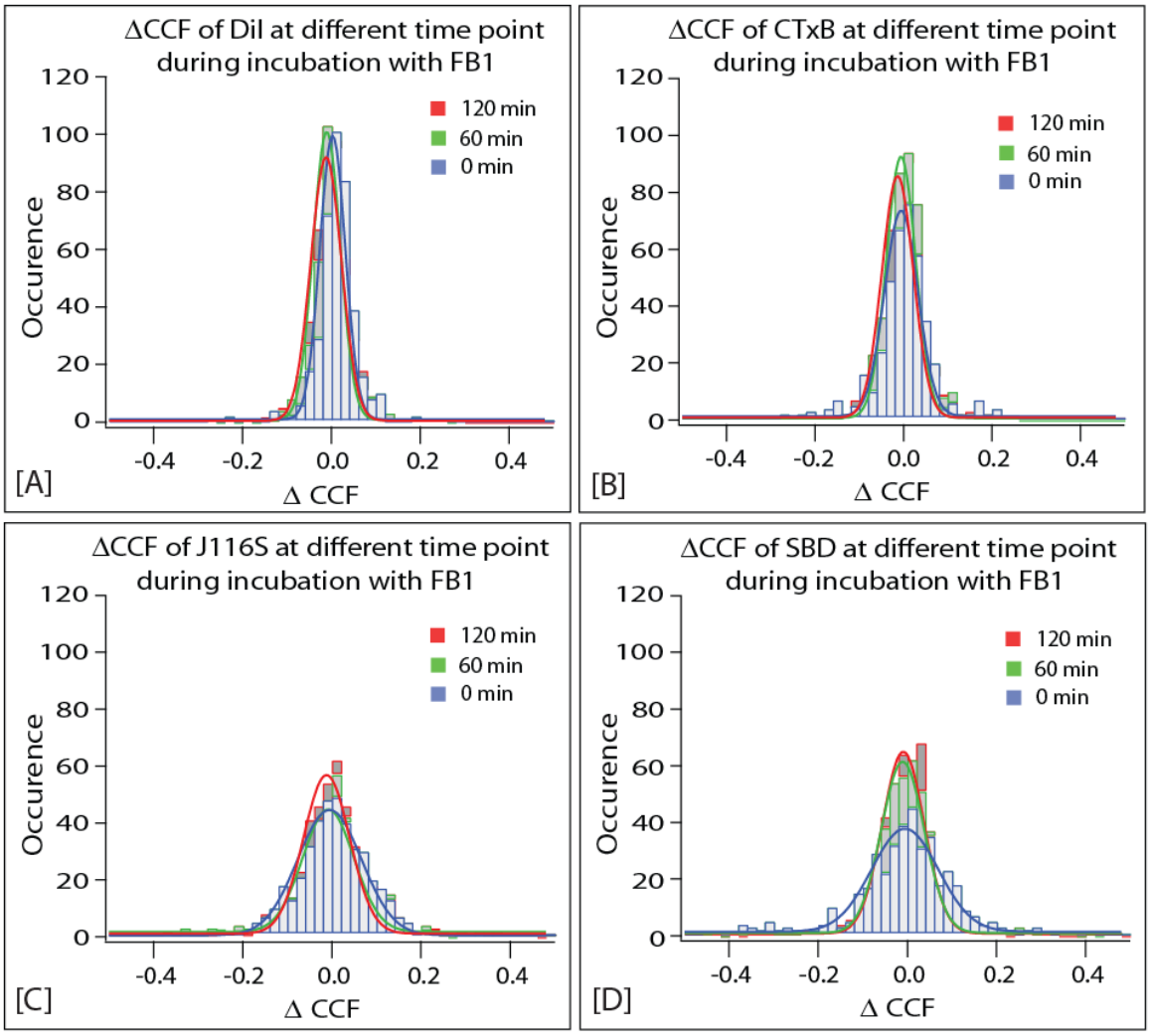

Figure 6.4: *Gradual effects of Fumonisin B1 treatment over the entire incubation period on the distributions of the ΔCCF histograms of different markers. A, B, C and D represent ΔCCF distributions for DiI, CTxB, J116S and SBD respectively at different time points with the drug. Gaussian fits to the distributions are indicated by solid lines with respective colors.*

Therefore, by reducing the sphingolipid content of the membrane, FB1 makes a permanent impact on the fluidity (characterized by the diffusion coefficient), whereas the membrane organization shown by the ΔCCF distribution does not show significant changes in case of CTxB and J116S (*Fig. 6.3 B* and *C*). No further changes in ΔCCF distribution took place for cells incubated longer than 120 minutes with FB1. These results are consistent with earlier findings that FB1 treatment leads to an overall loss of sphingolipid associated membrane

domains **[265]**. On the other hand DiI maintained its narrow distribution profile throughout the entire experiment

In order to check whether the lipid extraction leads to any permanent damage of the cell, recovery of the cells from the drug effects were also monitored. Measurements were performed after 24 hours since the drug was withdrawn from the medium. All the markers tend to come back closer to the condition before the drug treatment (Fig 6.3 D). Over the recovery period cells would have been able to synthesize sufficient amount of new sphingolipids to go back to the original distribution. Overall these findings show that the external perturbations to alter the lipid contents of the cell membrane can lead to a different equilibrium state for the membrane with altered dynamic condition, but that does not change the overall original properties of the membrane. Removal of the external perturbation effect can bring back the cells to their native state.

6.3.3 Effect of inhibition of glycosphingolipid biosynthesis and recovery

N-Butyldeoxynojirimycin (NB-DNJ) is a drug that inhibits the catalytic function of ceramide-specific enzyme glucosyltransferase at the first step of the biosynthesis of glycosphingolipid [**259**]. Hence treatment with this drug also results in the disruption of rafts from cell membrane and the raft associated proteins loss their raft-like diffusion behavior. The drug treatment results in a 3 to 4 fold increase of the average diffusion coefficient of membrane bound SBD-TMR and J116 (0.8 ± 1.3 $\mu m^2/s$ to 2.9 ± 2.1 $\mu m^2/s$) and (1.1 ± 0.7 $\mu m^2/s$ to 3.2 ± 1.9 $\mu m^2/s$) respectively, whereas DiI shows a very small decrease in the diffusion coefficient value (3.3 ± 2.1 $\mu m^2/s$ to 2.7 ± 1.7 $\mu m^2/s$) under similar circumstances (*Table 6.1*). These changes are also consistent with the expectation that there should be an increase in lateral mobility of raft related lipids and proteins on the cell membrane after reduction of glycosphingolipids. As gangliosides are sialylated glycosphingolipids, NB-DNJ treatment

probably reduces the amount of GM1 on the cell surface. This was reflected in an insufficient binding of CTxB to the cell membrane after this drug treatment, preventing the measurement from producing good ACFs. Dim fluorescence signals were obtained from the CTxB measurements, which resulted in very flat ACFs. Individual ACFs are similar to those recorded for the autofluorescence on SHSY5Y cells (*Fig 5.2 A*).

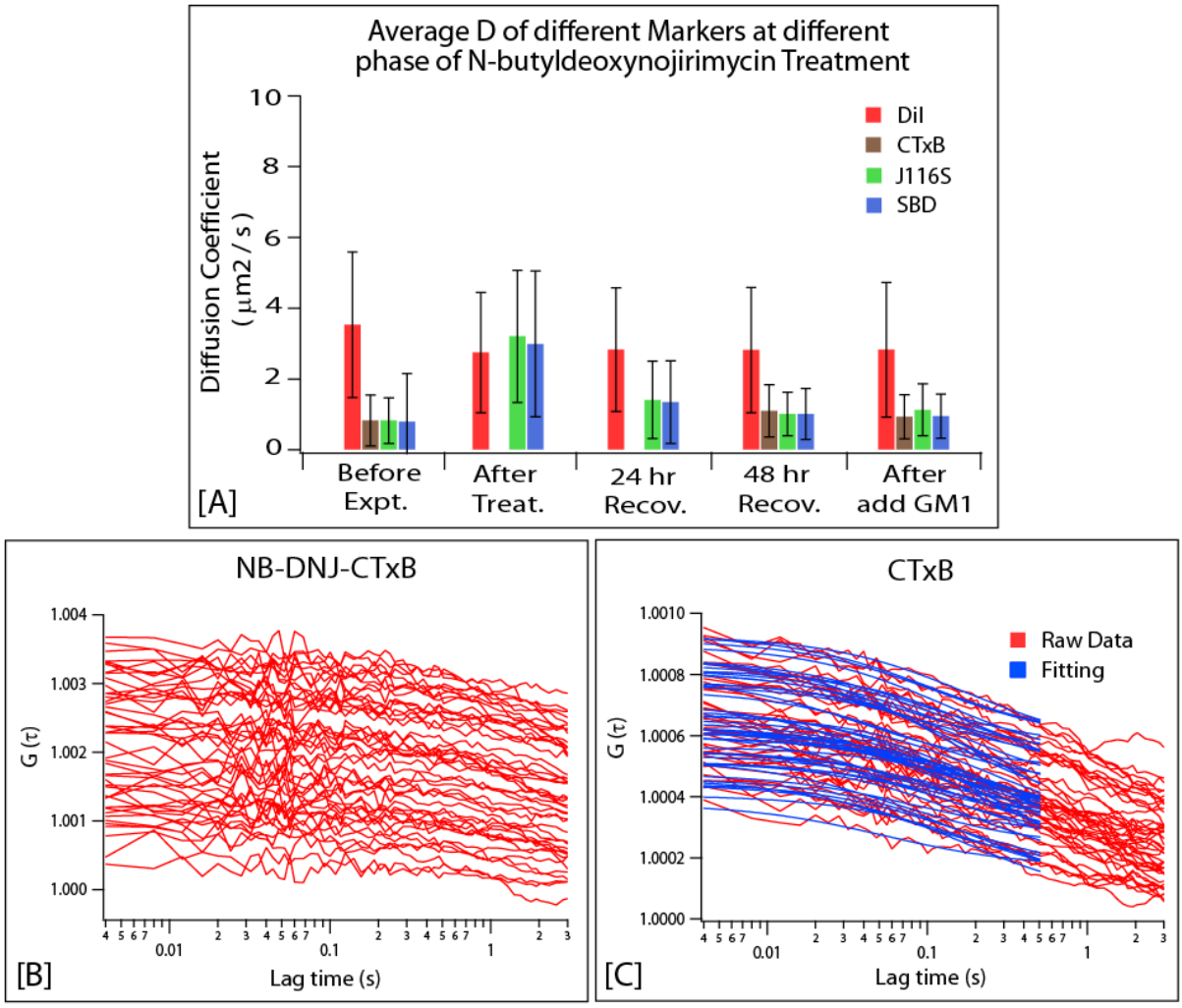

Figure 6.5: *Effects of inhibition of glycosphingolipid biosynthesis [by N-Butyldeoxynojirimycin treatment] at different phases of the experiments. Graph A shows the average diffusion coefficients for different markers before the treatment, after the treatment and after different stages of recovery. Error bars reflect standard deviations. Graph B represents the ACFs obtained for CTxB after the NB-DNJ treatment. Individual ACFs looks more similar to the autofluorescence ACFs obtained for SHSY5Y cells. Graph C shows the typical ACFs obtained for good ITIRFCS measurements with CTxB.*

Cells were then recovered over a period of 48 hours to let them synthesize new glycosphingolipids. Even after drug removal for24 hours the recovery was not complete, and

as at this point the diffusion coefficients of SBD-TMR and J116 were (1.4 ± 1.1 $\mu m^2/s$) and (1.3 ± 1.2 $\mu m^2/s$) respectively. After 48 hours of recovery all the markers seemed to revert to their original state, displaying D values of 1.0 ± 0.7 $\mu m^2/s$ for SBD, 1.0 ± 0.6 $\mu m^2/s$ for J116S and 1.1 ± 0.7 $\mu m^2/s$ for CTxB. replenishing cells with GM1 lead to a complete recovery of the cells from the effects of NB-DNJ, giving rise to D values of 0.9 ± 0.6 $\mu m^2/s$ for SBD, 1.1 ± 0.7 $\mu m^2/s$ for J116S and 0.9 ± 0.6 $\mu m^2/s$ for CTxB. The consistent diffusion coefficient values after the recoveries suggest that the inhibition of biosynthesis of glycosphingolipids doesn't damage the cell membrane composition permanently. Upon acquiring new glycosphingolipids either by synthesis by the cells themselves or by replenishment from an outside source, the cell membrane regains its original dynamic heterogeneity.

Loss and regaining of the heterogeneity in terms or larger organizations on the cell surface is also reflected in the corresponding ΔCCF distributions. After treatment, consistent with the ACFs, CTxB didn't produce any kind of well defined distribution. All the ΔCCF values were scattered over the entire distribution range of *Fig. 6.6 A*. SBD and J116S tend to squeeze towards a narrower distribution, with a higher central peak value. But surprisingly after drug treatment, DiI produced a comparatively flat Gaussian profile (*Fig. 6.6 A*). This might be due to increase in the ceramide level on the cell surface upon drug treatment.

After 24 hours of recovery, all the markers still show profiles that represent perturbed conditions. After 48 hour recovery, all the raft associated markers tend to return much closer but not completely to their original, native state. SBD and J116S produce much wider distributions compared to their values before drug treatment while the distribution of CTxB is a bit narrower. DiI didn't show any tendency to revert back to its original state even after 48 hours of recovery. That indicates the increased amount of ceramide in the cell membrane might still be dispersed over the whole cell membrane even after 48 hours of recovery, and not neutralized due to normal cellular processes. Upon replenishment of GM1, all the

markers except SBD came back very closely to their ΔCCF distributions of the native state. DiI reverts to its usual narrower and J116S to its normal wider distributions, leaving CTxB in between. But SBD went even closer to a DiI-like distribution rather than flattening out.

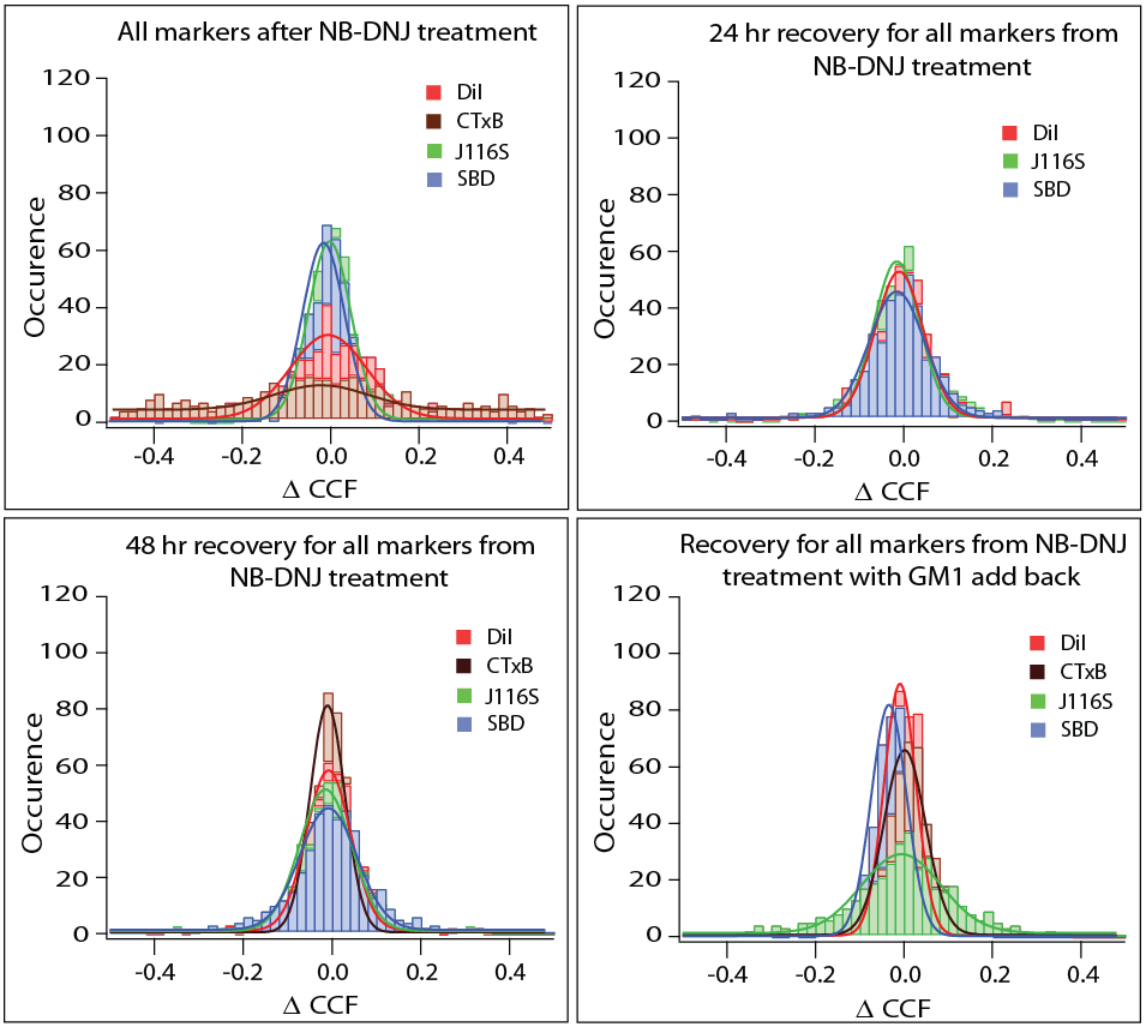

Figure 6.6: *Effects of inhibition of glycosphingolipid biosynthesis [by N-Butyldeoxynojirimycin treatment] on different markers at different phases of the experiments. Picture A represents the ΔCCF distributions for all the markers after the NB-DNJ treatments. B, C and D represent the same at different stages of recoveries, 24 hour, 48 hour and GM1 add back respectively. Gaussian fits to the distributions are indicated by solid lines with respective colors.*

This is consistent with the biochemical studies that GM1 is not the preferred target of SBD, at physiological pH **[123]**. And thus SBD might concentrate in less number of larger pools instead if it's usual distribution of large number of smaller clusters. Altogether these findings demonstrate the importance of glycosphingolipids for heterogeneous cell membrane.

6.3.4 Effect of sphingomyelin disintegration and recovery

Sphingomyelinase from *Bacillus cereus* was used to disintegrate the cell membrane sphingomyelin into phosphocholine and ceramide **[269]**. It has already been mentioned that, for unperturbed cells, all the raft associated probes, SBD-TMR, CTxB and J116S display similar diffusion coefficients that are much smaller than the non-raft associated marker DiI.

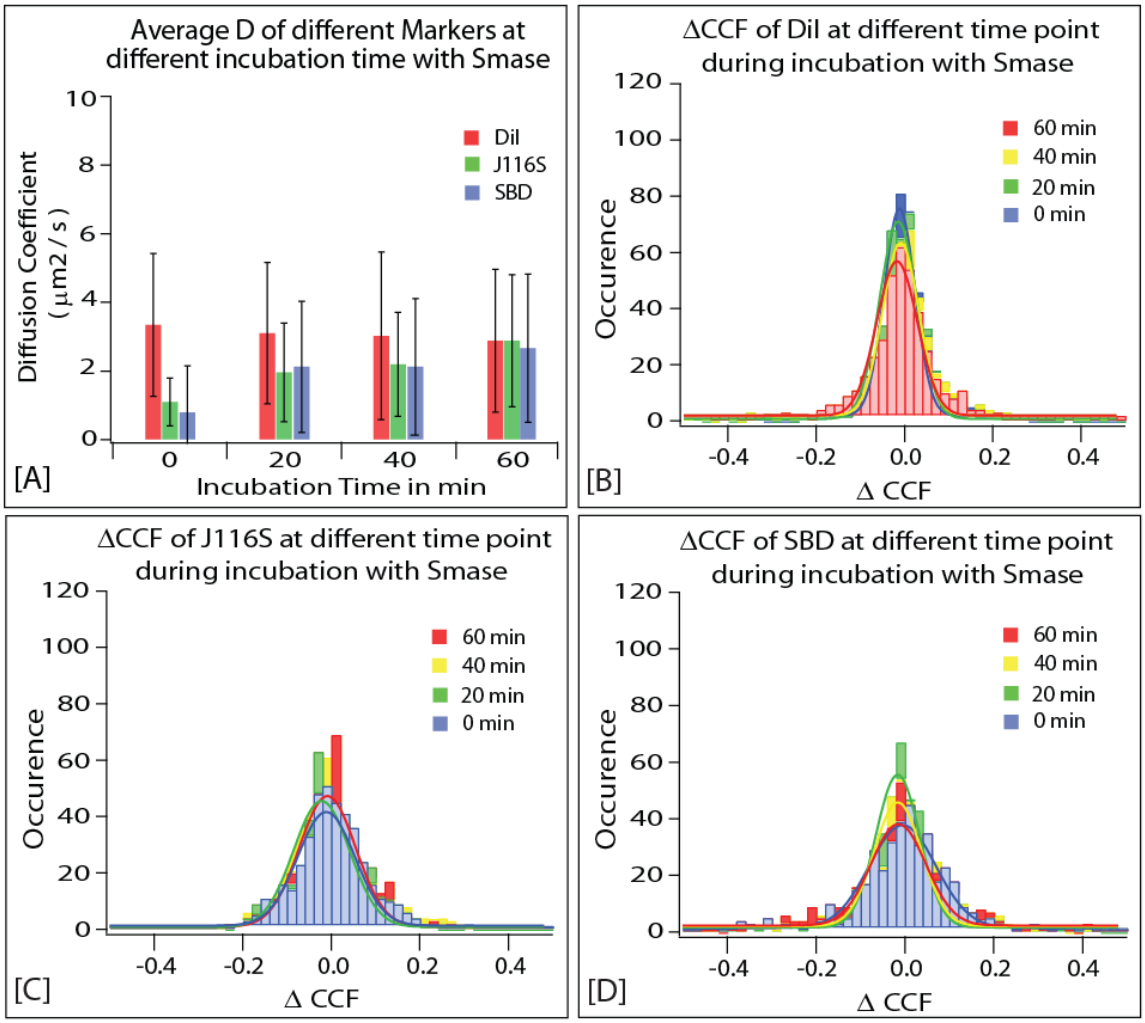

Figure 6.7: *Gradual effects of disintegration of sphingomyelin into ceramide and phosphocholine [by Sphingomyelinase treatment] on different markers at different time points of the incubation period. Picture A represents the average diffusion coefficients for different markers at different time points of the incubation with the enzyme. Standard deviations denoted by those large error bars reflect the heterogeneity of the related membrane phase. B, C and D show the ΔCCF distributions for DiI, J116S and SBD respectively over the entire incubation period with the drug. Gaussian fits to the distributions are indicated by solid lines with respective colors.*

Therefore incubation with this drug results in the disruption of rafts from cell membranes and the raft associated proteins lose their raft-like diffusion behavior. The average diffusion

coefficients of membrane bound SBD-TMR (0.8 ± 1.3 $\mu m^2/s$) and J116S (1.1 ± 0.7 $\mu m^2/s$) gradually increase over a time interval of 60 minutes by a factor of about 3-4 (2.7 ± 2.2 $\mu m^2/s$) and (2.9 ± 1.9 $\mu m^2/s$) respectively, whereas no such change was observed in case of DiI under the same circumstances (Table 6.1). These changes are consistent with the expectation that there is an increase in lateral mobility of raft related lipids and proteins on the cell membrane after reduction of sphingomyelin **[271]**.

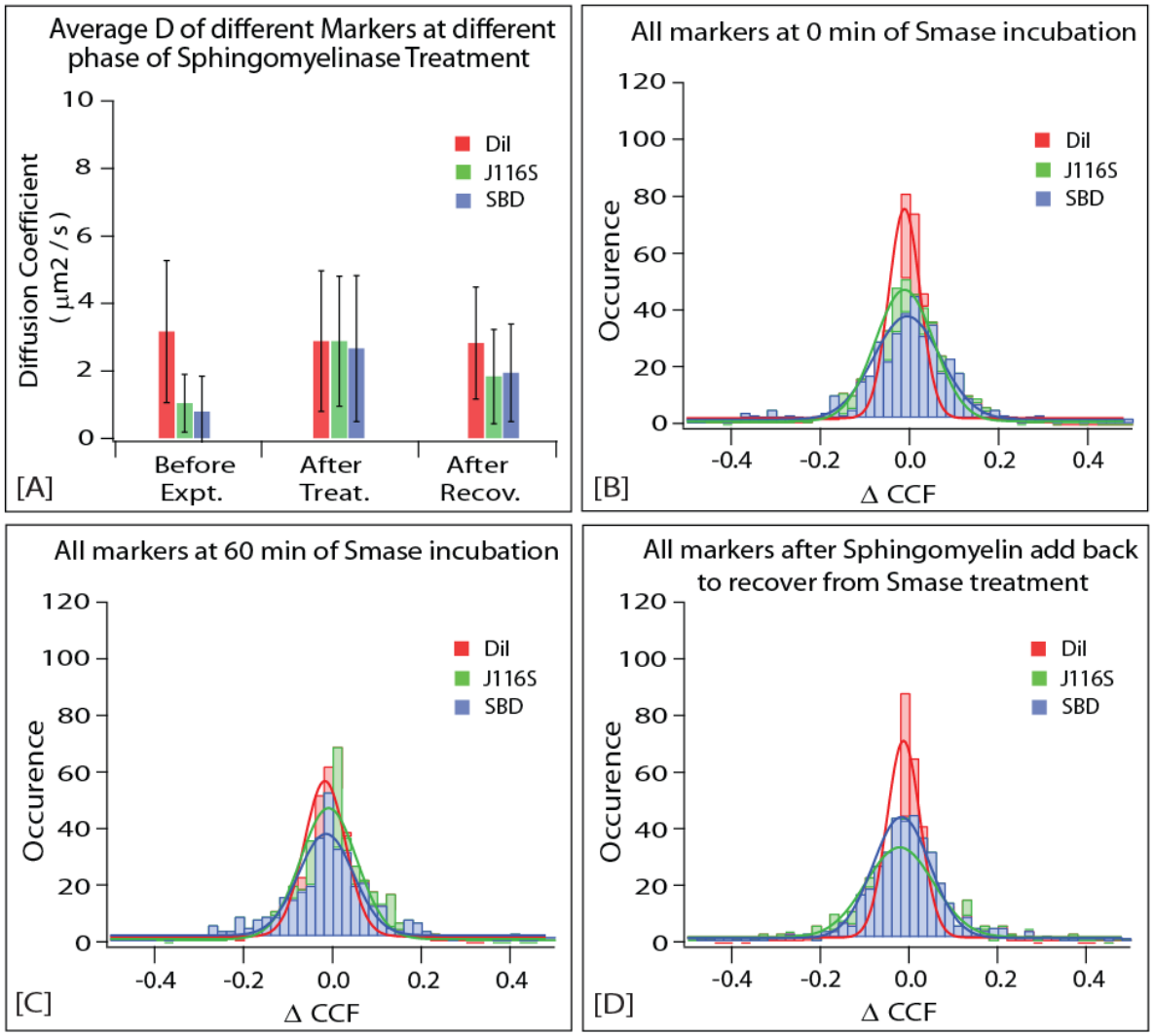

Figure 6.8: *Effects of disintegration of sphingomyelin [by Sphingomyelinase treatment] on different markers at different phases of the experiments. Picture A shows the average diffusion coefficients for different markers before the treatment, after the treatment and after the add back of sphingomyelin. Error bars reflect standard deviations. B, C and D represent ΔCCF distributions for all the markers before the treatments, after the treatments and after the sphingomyelin add back respectively. Gaussian fits to the distributions are indicated by solid lines with respective colors.*

Similar to earlier occasions, changes in the membrane heterogeneity due to drug effects were analyzed based by ΔCCF distributions. It was already mentioned that the distributions of ΔCCF histograms for SBD and J116S on untreated cells are comparatively flat and wide (*Fig. 6.7 B*) whereas DiI displays a comparatively sharp and narrowly distributed profile. Upon adding the enzyme Smase, no significant change was observed in the distributions of ΔCCF histograms for J116S. The histograms maintain their wider distribution profile over the entire incubation period of 60 min (*Fig. 6.7 C*). SBD showed some narrowing and a small increase in the central peak height after 20 min of incubation with the enzyme and then gradually decreased with time until it reached a similar range of that of non-treated cells after 60 min of incubation (*Fig. 6.7 D*).

Surprisingly, DiI showed a gradual decrease in the central peak height of the distribution over the entire 60 minutes of incubation, indicating an increase in anisotropic or restricted movements in the liquid disordered phase of the cell membrane. This might be due the increased level of ceramide on the cell surface that had been produced due to the disintegration of sphingomyelin and lifts up the heterogeneity of the membrane fluid phase.

After adding back sphingomyelin (SM) from an external source, the cells regained their slow mobility to some extent indicating the reformation of rigid membrane domains (*Fig. 6.3 D*). But the elevated amount of ceramide on the membrane surface might restrict the formation of these domains to a certain limit, and that is why a complete recovery (similar to the recoveries from the other two drug treatments) was not obtained [**272**].

The ΔCCF distribution of SBD and J116S didn't show any significant changes at the end of the incubation with the enzyme Smase, and the measurements after SM replenishment also didn't that scenario (*Fig. 6.8 D*). But the elevated amount of ceramide in the fluid phase of the membrane was not neutralized by the external addition of SM. As a result the ΔCCF

histogram of DiI couldn't reach back to its original state of a narrow distribution which is an indication of an isotropic and homogeneous fluid phase.

Therefore, the increase in ceramide content of the membrane, due to the Smase function alters the membrane fluidity (reflected by the diffusion coefficient), and leaves a permanent impact on the membrane organization shown by the ΔCCF distribution (*Fig. 6.7 A* and *Fig. 6.7 C*). This is in agreement with other findings which show that Smase treatment leads to an overall loss of sphingomyelin and an increase in ceramide associated membrane domains **[273]**. These findings show that the effect exerted by Smase alters the lipid contents of the cell membrane and can lead to a deep impact on the dynamic organization of the cell membrane.

Marker	Diffusion Coefficient (D) in μm^2/sec						
	Before treatment	FB1 treatment		NB-DNJ treatment		Smase treatment	
		After treatment	After recovery	After treatment	After recovery	After treatment	After recovery
DiI	**3.3 ± 2.1**	**3.2 ± 1.8**	**3.1 ± 1.4**	**2.7 ± 1.7**	**2.8 ± 1.8**	**2.9 ± 2.1**	**2.8 ± 1.7**
CTxB	**0.8 ± 0.7**	**2.9 ± 1.9**	**1.3 ± 0.9**	**--**	**0.9 ± 0.6**	**--**	**--**
J116S	**1.1 ± 0.7**	**3.2 ± 2.1**	**1.3 ± 1.5**	**3.2 ± 1.9**	**1.1 ± 0.7**	**2.9 ± 1.9**	**1.8 ± 1.4**
SBD	**0.8 ± 1.3**	**2.9 ± 1.4**	**1.5 ± 1.1**	**2.9 ± 2.1**	**0.9 ± 0.6**	**2.7 ± 2.2**	**1.9 ± 1.4**

Table 6.1: *Average diffusion coefficients of raft (SBD, CTxB and J116S) and non-raft (DiI) markers without any drug treatment, after treatment with FB1, NB-DNJ and Smase and after the recoveries respectively.*

6.4 Discussion

Since the effects on ΔCCF are different from the effects on diffusion after various treatments, the findings of this study strongly indicate that the type of information about overall dynamic organization of the live cell surface obtained from ITIR-FCCS is unique and cannot be obtained by conventional measurements of diffusion coefficients alone. Considering the results obtained from DiI experiments for example, no significant changes took place in the

diffusion coefficient values upon the described drug treatments; hence it was impossible to infer from this parameter itself any changes in the liquid disordered phases due the effects of drug treatment. ΔCCF distributions quite clearly indicate that the liquid disordered phase of the cell membrane became more heterogeneous upon NB-DNJ and Smase treatments.

This heterogeneity in the liquid disordered phase might arise due to the increase in ceramide level upon NB-DNJ and Smase treatments **[270, 271]**. FB1 treatment doesn't lead to production of any ceramide and consequently this treatment doesn't show any significant change in the ΔCCF distributions of DiI. The formation of ceramide gel domain due to the Smase treatment is well supported by the findings of Silva & Prieto, Alonso & Goni and others **[273-275]**. Once produced, the ceramide possibly doesn't leave the cell membrane even after SM replenishment, which was reflected in the incomplete recovery of the ΔCCF distribution profile for DiI. A similar phenomenon happens in case of NB-DNJ treatment and recovery. The production of ceramide on the membrane surface, leading to the formation of ceramide domains, was documented before **[276-278].**

However SBD and the other markers associated with the ordered lipid domains or rafts of the cell surface have been influenced by the alteration of all lipid levels. For all of these cases diffusion coefficients increased by factors of 3-4 to become similar to that of DiI (non-raft phase) and went back closer to their unperturbed state upon recovering the respective lipid levels. These findings indicate the essentiality of each of those lipids towards a raft like diffusion behavior. All three raft associated markers show changes in their ΔCCF distributions upon drug treatments. Sphingolipid reduction resulted in decrease in heterogeneity or raft association for all the liquid ordered phase markers. Glycosphingolipid reduction leads to decrease in heterogeneity for SBD and J116S and almost blocked the uptake of CTxB. Gangliosides are composed of glycosphingolipids and sialic acids; hence NB-DNJ treatment significantly reduces the binding site for CTxB, the ganglioside GM1 on

the cell surface **[279, 280]**. However, the sphingomyelin reduction didn't lead to a significant change in the ΔCCF distributions of the raft associated markers SBD and J116S. The increased cholesterol level upon Smase treatment **[281-283]** might retain the heterogeneity and rigidity of the raft phase and didn't allow homogenizing too much with the surrounding liquid disordered phase.

Overall, it seems that the cell itself cannot reestablish the chemical equilibrium quickly enough in the presence of the drugs which cause the alteration of the sphingolipid and glycosphingolipid levels on the cell surface. Once the external perturbation sources are removed and cells are allowed to settle down for a long time period, then only cells can revert to their native states. Therefore, it can also be inferred that alterations of these lipid levels do not lead to any permanent irreversible damage of the cell surface.

6.5 Summary

The ΔCCF histogram distribution is a good tool to measure the anisotropic translocation and demonstrate the heterogeneity in membrane organization. Successful application of the method has been shown by observing various liquid ordered- and disordered- phase associated markers under different lipid altered conditions. The findings of this part have indicated the possibility of formation of gel phase due to increased ceramide levels on the cell membrane **[273, 274]**. This will add interest towards the study of the dynamic properties of gel domains on live cell surface in future. Finally, the importance of sphingolipids, glycosphingolipids and sphingomyelin towards the dynamic rigidity and heterogeneity of the liquid ordered phase of the cell membrane have been addressed.

Chapter 7:
Conclusion and Outlook

7.1 Conclusion

In the fields of membrane heterogeneity and lipid trafficking, one of the most interesting and challenging projects is the tracing of the sub-cellular movement and localization of different lipid species, such as the various sphingolipids and glycolipids. The major limitation associated with this field was the lack of well known reliable markers that can be used to trace the lipid microdomains or sphingolipids in living neurons or other cells. Hence, the characterization of a potential marker as a tool to distinguish the different pathways of various types of sphingolipids and their behavior in perturbed conditions (e.g. cholesterol depletion, sphingolipid modification) became an important task. Molecular fluorophore conjugated, first 25 amino acid sequence of Amyloid beta, containing the V3 loop structure and termed as sphingolipid-binding domain (SBD), has been characterized for the sphingolipid rich domains found in the plasma membrane that constitute rafts.

The biochemical studies done on synthetic membranes for SBD binding produce evidence that SBD interacts with raft lipids including sphingomyelin, cholesterol, and glycosphingolipids, but not much specific interaction to any particular ganglioside [**123**]. Lipid-protein interaction assays with DRM fractions and fat blots also have been done to determine SBD's affinity for raft-type lipids. Additionally, results from pharmacological inhibitor studies provide evidence for the glycosphingolipid dependence of SBD uptake at the membrane [**81**]. Thus from those studies it was clear that, SBD can potentially be used to trace the intracellular pathways of sphingolipid- containing domains. Moreover, the fact that

SBD behaves similarly in drosophila and mammalian neurons validates its potential use as a tool in the field of lipid trafficking [**123**]. All those information obtained for SBD from the biochemical studies are the basis for the biophysical studies performed in this study.

Along with the biochemical and bio-imaging based approach by other group members, the FCS based biophysical studies done in this project help to characterize SBD as an efficient lipid raft marker that can trace the trafficking and dynamic behavior of sphingolipids. Further, the dependency of SBD's raft association and lateral movement on the cholesterol content of the cell surface has also been shown in this study. Upon depletion of cholesterol, the diffusion rate of SBD increases to a rate that is characteristic for non-raft associated probes like DiI or BODIPY-SM.

The fact that SBD doesn't get taken up via a clathrin-dependent pathway and the findings, that the highly prevalent clathrin-independent CLIC/GEEC endocytic pathway is regulated by Rho GTPase activation has increased the interest about the identification of the endocytic machinery and membrane-trafficking itineraries of these pathways. In this study, it has been shown that SBD uptake is dependent on two different mechanisms – one is flotillin dependent uptake and the other is cdc42 dependent uptake. Generally these two pathways are independent and parallel to each other. Blocking of either flotillin or cdc42 dependent pathways results only in partial suppression of the uptake of SBD into cells, whereas knocking out both pathways simultaneously nearly eliminates the SBD uptake. This suggests that there might be an additive relationship between these two mechanisms. By contrast, drastic changes in the raft-like diffusion behavior of SBD has been seen when either or both of these uptake pathways were perturbed. In summary, accumulation of SBD in the raft components is monitored by the endocytic accessory proteins such as cdc42 and flotillin.

After establishing SBD as a lipid ordered phase associated marker, it was used for further understanding of the dynamic cell membrane organization between liquid ordered and

disordered phase and the importance of some membrane components towards this organization. This goal has also been successfully achieved by using different markers for the liquid ordered and disordered phase under different perturbed conditions including cholesterol removal, cytoskeleton de-polymerization, alteration of sphingolipid and glycosphingolipid content of cell surface. It has been found that the mobility of SBD is influenced greatly by cholesterol and the cytoskeleton. Disruption of the cytoskeleton results in lifting the diffusion coefficients of SBD to the similar range of DiI, the liquid disordered phase marker, while removal of cholesterol also increases the diffusion coefficient of SBD, but to a lesser extent. In case of reduced sphingolipid, glycosphingolipid and sphingomyelin on the cell surface, the lateral movement of SBD (and the other raft associated markers as well) increased to become similar to that of the non-raft phase and went back closer to its unperturbed state upon reverting to their respective lipid levels. Therefore, the alterations of these lipid levels do not lead to any permanent irreversible damage of the cell surface. Once the external perturbation sources are removed and cells are allowed to settle down for sufficient time period, cells can go back to their native states and regain raft association. This has been reflected by the diffusion of SBD and other raft associated markers. Moreover, the outcome of this study are consistent with the proposal that the cell membrane is organized on different length scales, namely below the resolution limit in nanodomains and above the resolution limit of raft-phases.

To address this different length scale based heterogeneity of the membrane, recently developed imaging FCS methods, ITIR-FCS and ITIR-FCCS, were successfully applied in this study. The diffusion coefficients extracted from ITIR-FCS experiments are in good agreement with the findings of other research groups [**52, 53**], with the advantage of multiplexing readings in single measurement time. The exponential decay and therefore limited penetration depth of the evanescent excitation field provides the TIR illumination

mode a good inherent axial resolution. This method leads to strong reduction of the background signal from the bulk and consequently suppresses the cross-talk between the neighboring pixels. Therefore techniques based on this illumination mode are very much suitable for surface studies. The instrumental setup of ITIRFCS is equipped with an EMCCD camera as the detector to make the technique efficient for measuring the free diffusions, flow as well as directed movements on whole cell membranes. In this study, the image based FCS has been introduced with its immediate applications in the field of live cell membrane dynamics.

The newly established ITIR-FCCS method based on ΔCCF approach has been successfully applied to study the diffusion and transport processes to resolve the dynamic heterogeneity in cell membranes. The membrane heterogeneity has not been addressed so easily still convincingly, by any other spectroscopic methods yet. This makes ITIR-FCCS more unique and important technique. Overall, ITIR-FCCS with its adequate spatial and temporal resolution has come up as a powerful biophysical tool to provide novel insights into membrane organization.

Finally, this research has introduced a novel peptide probe and a new technique to resolve the membrane heterogeneities which will help to identify the processes that lead to different neurodegenerative and other diseases associated with these.

7.2 Outlook

SBD has come up as a novel fluorescent tracer for the cholesterol-dependent, glycosphingolipid-containing microdomains in living cells. Its diffusion parameters along with biochemical and bio-imaging studies already establish it as a good lipid raft associated probe. The probable mechanism of its uptake by live cells has been described in this study. However, a number of quarries are yet to address related to this probe.

SBD gets taken up by a Flotillin and Rho GTPase dependent pathway in a cholesterol and sphingolipid dependent manner. However, it is still unclear what is the exact binding site or receptor for SBD on cell surface. In case of CTxB, the probe used as a positive control in this work, ganglioside GM1 is the sole binding target. Hence, it's easier to select the cell types for which this probe can be used as membrane tracer; cells not having GM1 can easily be eliminated. Similarly, with the knowledge of proper binding sites, it will also be easier to choose suitable cell types having the appropriate glycolipids for SBD binding.

Some studies including Kusumi *et al*., Pinaud *et al*., suggest that the restricted movements of the raft associated markers are due to their confined movements inside a raft cluster and once that cluster dissociates the marker hop to anther cluster and keep on doing so. This behavior of raft associated marker sometimes describes their bimodal diffusion behavior as well. Single particle tracking with SBD can help to better understand this hopping behavior of the raft associated proteins / receptors and it can also focus some light on the existence time of any individual raft cluster.

For further studies about SBD and its behavior, fluorescence anisotropic measurements can be done to get an overview about the shape and orientation of the molecule at bound state and any possible aggregation.

Although it has been indicated in literature including our study that raft clusters are of at least two organizational length scales, there is still no direct evidence saying whether a single cluster consist of only one type of receptor or can contain different binding receptors. Dual color spatial cross-correlation of SBD with other raft markers like CTxB or J116S can address this question, to understand the receptor composition of rafts / nanoclusters on live cell surface.

Finally, broadening of the applications of the image based FCS and FCCS techniques can be carried out. With total internal reflection illumination mode the technique is limited to the

lower membrane of a single cell layer type sample only due the exponential decay of the evanescent wave field. But with single plane illumination mode the imaged based correlation and cross-correlation methods can be used deep inside the tissue as well, and then these imaging based FCS and FCCS will have much broader applicability and acceptability.

References:

1. K. Simons, and E. Ikonen. “Functional rafts in cell membranes.” 1997, *Nature*, 387, 569-572.
2. G. van Meer. “Cellular Lipidomics”. 2005, *EMBO J.*, 24, 3159-3164.
3. J. Fantini, N. Garmy, R. Mahfoud and N. Yahi “Lipid rafts: structure, function and role in HIV, Alzheimer’s and prion diseases.” 2002, *Exp. Rev. Mol. Med.*, 4, 27, 1-22.
4. J.M. Cordy, N.M. Hooper, A.J. Turner. “The involvement of lipid rafts in Alzheimer's disease.” 2006, *Mol. Membrane Biol.*, 23, 111-122.
5. S. Vainio, I. Bykov, M. Hermansson, E. Jokitalo, P. Somerharju, and E. Ikonen. “Defective insulin receptor activation and altered lipid rafts in Niemann-Pick type C disease hepatocytes.” 2005, *Biochem J.*, 391, 465-472.
6. D.L. Fortin, M.D. Troyer, K. Nakamura, S.I. Kubo, M.D. Anthony, and R.H. Edwards. “Lipid Rafts Mediate the Synaptic Localization of **α**-Synuclein.” 2004, *J. Neuroscience*, 24, 6715-6723.
7. E.E. Benarroch. “Lipid rafts, protein scaffolds, and neurologic disease.” 2007, *Neurology*, 69, 1635-1639.
8. T. Hatano, S.I. Kubo, S. Imai, M. Maeda, K. Ishikawa, Y. Mizuno and N. Hattori. **“**Leucine-rich repeat kinase 2 associates with lipid raft**s**.” 2007, *Human Mol. Gene.*, 2007, 16, 678-690.
9. N.M. White, D. Jiang, J.D. Burgess, I.R. Bederman, S.F. Previs, T.J. Kelley. “Altered cholesterol homeostasis in cultured and in vivo models of cystic fibrosis.” 2007, *Am. J. of physiology*, Lung cellular and molecular physiology 292(2), L 476-486.
10. E. Ikonen. “Cellular cholesterol trafficking and compartmentalization.” 2008, *Nat. rev. Mol. cell boil.*, 9(2), 125-138.
11. K. Kitatani, J. Idkowiak-Baldys and Y.A. Hannun. “The sphingolipid salvage pathway in ceramide metabolism and signaling.” 2007, *Cell. Signal.*, 20, 1010-1018.
12. K. Fiedler, R.G. Parton, R. Kellner, T. Etzold, K. Simons. “VIP36, a novel component of glycolipid rafts and exocytic carrier vesicles in epithelial cells.” 1994, *EMBO J.*, 13(7):1729-1740.
13. S. Heino, S. Lusa, P. Somerharju, C. Ehnholm, V.M. Olkkonen, E. Ikonen. “Dissecting the role of the golgi complex and lipid rafts in biosynthetic transport of cholesterol to the cell surface.” 2000, *Proc. Natl. Acad. Sci. U S A.*, 97, 8375-8380.
14. L. Cubells, S. Vila de Muga, F. Tebar, P. Wood, R. Evans, M. Ingelmo-Torres, M. Calvo, K. Gaus, A. Pol, T. Grewal, C. Enrich. “C Annexin A6-Induced Alterations in

Cholesterol Transport and Caveolin Export from the Golgi Complex." 2007, *Traffic*, 8, 1568-1589.

15. R.E. Pagano, V. Puri, M. Dominguez, D.L. Marks. "Membrane Traffic in Sphingolipid Storage Diseases." 2000, *Traffic*, 1, 807-815.
16. D.J. Sillence, F.M. Platt. "Storage diseases: new insights into sphingolipid functions." 2003, *Trends Cell Biol.*, 13, 195-203.
17. Yang-Yi Fan, David N. McMurray, Lan H. Ly and Robert S. Chapkin. "Dietary (n-3) Polyunsaturated Fatty Acids Remodel Mouse T-Cell Lipid Rafts". 2003, Nutritional Immun., 133, 1913-1920.
18. S.L. Sturley, M.C. Patterson, and P. Pentchev. "Unraveling the sterol-trafficking defect in Niemann-Pick C disease." 2009, *Proc. Natl. Acad. Sci. U S A*., 106(7), 2093-2094.
19. J. Fullekrug, K. Simons. "Lipid rafts and apical membrane traffic." 2004, *Annal. New York Acad. Sci.*, 1014, 164-169.
20. M.D. Ledesma, J.S. Da Silva, K. Crassaerts, A. Delacourte, B. De Strooper, and C.G. Dotti. "Brain plasmin enhances APP α-cleavage and Aβ degradation and is reduced in Alzheimer's disease brains." 2000, *EMBO Rep.,* 1, 530–535.
21. K.S. Vetrivel, and G. Thinakaran. "Amyloidogenic processing of β-amyloid precursor protein in intracellular compartments." 2006, *Neurology,* 66, S69-S73.
22. A. Choudhury, M. Dominguez, V. Puri, Deepak K. Sharma, Keishi Narita, Christine L. Wheatley, David L. Marks and Richard E. Pagano "Rab proteins mediate Golgi transport of caveola-internalized glycosphingolipids and correct lipid trafficking in Niemann-Pick C cells." 2002, *J. Clin. Invest.,* 109,1541-1550.
23. D.J. Sillence and F. M. Platt. "Glycosphingolipids in endocytic membrane transport." 2004, *Seminars in Cell & Dev. Biol., 15,* 409-416.
24. Y. Sagiv, K. Hudspeth, J. Mattner, N. Schrantz, R.K. Stern, D. Zhou, P.B. Savage, L. Teyton and A. Bendelac. "Cutting Edge: Impaired Glycosphingolipid Trafficking and NKT Cell Development in Mice Lacking Niemann-Pick Type C1 Protein." 2006, *J. Immunology*, 177, 26-30.
25. T.Y. Wang, J.R. Silvius. "Different sphingolipids show differential partitioning into sphingolipid/cholesterol-rich domains in lipid bilayers." 2000, *Biophys. J*, 79, 1478-1489.
26. J.R. Silvius and T. Wang. "Partitioning of sphingolipids into liquid-ordered (raft-like) lipid domains: Ceramide exhibits a uniquely high affinity for lipid rafts." 2002, *Mol Biol. Cell*, 13, 358A.

27. R.D. Singh, V. Puri, J.T. Valiyaveettil, D.L. Marks, R. Bittman, and R.E. Pagano. “Selective Caveolin-1–dependent Endocytosis of Glycosphingolipids.” 2004, *Mol. Biol. Cell*., 14, 3254–3265.
28. R. Ishitsuka, T. Kobayashi. “Lysenin: A new tool for investigating membrane lipid organization.” 2004, *Anatom. Sci. Internatl*., 79, 184-190.
29. V.R. Gupta, H.K. Patel, S.S. Kostolansky, R.A. Ballivian, J. Eichberg. “Steven R. Blanke Sphingomyelin Functions as a Novel Receptor for Helicobacter pylori VacA”. 2008, *PLoS Pathogens*, 4(5), e1000073.
30. Y.O. Iwashita, Y. Shimada, A.A. Waheed, M. Hayashi, M. Inomata, M. Nakamura, M. Maruya, S. Iwashita. “Perfringolysin O, a cholesterol-binding cytolysin, as a probe for lipid rafts”. 2004, *Anaerobe*, 10(2), 125-134.
31. D.L. Marks, R.E. Pagano. “Endocytosis and sorting of glycosphingolipids in sphingolipid storage disease.” 2002, *Trends in Cell Biol*., 12(12), 605-613.
32. J. Walter, R. Fluhrer, B. Hartung, M. Willem, C. Kaether, A. Capell, S. Lammich, G. Multhaup, C. Haass. “Phosphorylation regulates intracellular trafficking of beta-secretase.” 2001, *J. Biol. Chem*., 276, 14634-14641.
33. N. Sawamura, M. Ko, W. Yu, K. Zou, K. Hanada, T. Suzuki, J.S. Gong, K. Yanagisawa and M. Michikawa. “Modulation of Amyloid Precursor Protein Cleavage by Cellular Sphingolipids.” 2004, *J. Biol. chem.*, 279, 11984-11991.
34. P. Haberkant, O. Schmitt, F.X. Contreras, C. Thiele, K. Hanada, H. Sprong, C. Reinhard, F.T. Wieland and B. Brügger. “Protein-sphingolipid interactions within cellular membranes.” 2008, *J. Lipid Res*., 49, 251-262.
35. D. Lingwood, K. Simons. “Lipid rafts as a membrane-organizing principle.” 2010, Science, 327, 5961, 46-50.
36. B.F. Lillemeier, J.R. Pfeiffer, Z. Surviladze, B.S. Wilson, M.M. Davis. “Plasma membrane-associated proteins are clustered into islands attached to the cytoskeleton”. 2006, *Proc Natl Acad Sci U S A*., 113, 18992-18997.
37. L.H. Chamberlain, R.D. Burgoyne, and G.W. Gould. “SNARE proteins are highly enriched in lipid rafts in PC12 cells: Implications for the spatial control of exocytosis”. 2001, *Proc Natl Acad Sci U S A*., 98, 5619-5624.
38. A.K. Kenworthy. “Have we become overly reliant on lipid rafts?” 2008, EMBO *reports,* 9(6), 531-535.
39. A. Kusumi, K. Suzuki. “Toward understanding the dynamics of membrane-raft-based molecular interactions.” 2005, *Biochim. Biophys. Acta.*, 1746, 234-251.
40. K. Simons, and R. Ehehalt. “Cholesterol, lipid rafts, and disease.” 2002, *J Clin Invest*., 110, 597-603.

41. Z. Korade, A.K. Kenworthy. "Lipid rafts, cholesterol, and the brain." 2008, *Neuropharmacology*, 55, 1265-273.
42. L.J. Pike. “The challenge of lipid rafts.” 2009, *J. Lipid Res*., 50, S323-328.
43. R. Mahfoud, N. Garmy, M. Maresca, N. Yahi, A. Puigserver, and J. Fantini. “Identification of a Common Sphingolipid-binding Domain in Alzheimer, Prion, and HIV-1 Proteins.” 2002, *J. Biol. chem.*, 279, 11292-11296.
44. A. Stier, E. Sackmann. "Spin labels as enzyme substrates. Heterogeneous lipid distribution in liver microsomal membranes." 1973, *Biochim. Biophys. Acta,* 311, 400-408.
45. M.J. Karnovsky, A.M. Kleinfeld, R.L. Hoover, R.D. Klausner. "The concept of lipid domains in membranes." 1982, *J. Cell Biol.,* 94, 1-6.
46. S.J. Singer, G.L. Nicolson. "The fluid mosaic model of the structure of cell membranes." 1972, *Science,* 175, 720-731
47. J.N. Israelachvili, S. Marcelja, R.G. Horn. "Physical principles of membrane organization." 1980, *Q. Rev. Biophys.* 13, 121-200.
48. R.B. Gennis, and A. Jonas. **“**Protein-Lipid Interactions.” 1977, Annual Rev. Biophys. and Bioeng., 6, 195-238.
49. T.N. Estep, D.B. Mountcastle, Y. Barenholz, R.L. Biltonen, T.E. Thompson. "Thermal behavior of synthetic sphingomyelin-cholesterol dispersions." 1979, *Biochemistry,* 18, 2112–2117.
50. F. Goodsaid-Zalduondo, D.A. Rintoul, J.C. Carlson, W. Hansel. "Luteolysis-induced changes in phase composition and fluidity of bovine luteal cell membranes." 1982, *Proc. Natl. Acad. Sci. U.S.A.,* 79, 4332-4336.
51. K. Simons, G. van Meer. "Lipid sorting in epithelial cells." 1988, *Biochemistry,* 27, 6197-6202.
52. D. Goswami, K. Gowrishankar, S. Bilgrami, S. Ghosh, R. Raghupathy, R. Chadda, R. Vishwakarma, M. Rao, and S. Mayor. “Nanoclusters of GPI-Anchored Proteins Are Formed by Cortical Actin-Driven Activity.” 2008, *Cell*, 135, 1085-1097.
53. F. Pinaud, F., X. Michalet, G. Iyer, E. Margeat, H. P. Moore. “Dynamic partitioning of a glycosyl-phosphatidylinositol-anchored protein in glycosphingolipid-rich microdomains imaged by singlequantum dot tracking.” 2009, *Traffic*, 10, 691-712.
54. T. Baumgart, A.T. Hammond, P. Sengupta, S.T. Hess, D.A. Holowka, B.A. Baird, W.W. Webb. “Large-scale fluid/fluid phase separation of proteins and lipids in giant plasma membrane vesicles.” 2007, *Proc Natl Acad Sci U S A*., 104, 3165-3170.

55. S.L. Veatch, P. Cicuta, P. Sengupta, A. Honerkamp-Smith, D. Holowka and B. Baird. "Critical Fluctuations in Plasma Membrane Vesicles". 2008, ACS Chem. Biol., 3(5), 287-293.
56. N.A. Baumann, D.P. Sullivan, H. Ohvo-Rekila, C. Simonot, A. Pottekat, Z. Klaassen, C.T. Beh, A.K. Menon. "Transport of newly synthesized sterol to the sterol-enriched plasma membrane occurs via nonvesicular equilibration." 2005, *Biochemistry*, 44, 5816-5826.
57. A. Uittenbogaard, Y. Ying, E.J. Smart. "Characterization of a cytosolic heat-shock protein-caveolin chaperone complex. Involvement in cholesterol trafficking." 1998, *J. Biol. chem.,* 273, 6525-6532.
58. A. Tagawa, A. Mezzacasa, A. Hayer, A. Longatti, L. Pelkmans, A. Helenius. "Assembly and trafficking of caveolar domains in the cell: caveolae as stable, cargo-triggered, vesicular transporters." 2005, *J. Biol. chem.,* 170, 769-779.
59. J. Liu, C.C. Chang, E.J. Westover, D.F. Covey, T.Y. Chang. "Investigating the allosterism of acyl-CoA:cholesterol acyltransferase (ACAT) by using various sterols: in vitro and intact cell studies." 2005, *Biochem. J.*,391, 389-397.
60. M. Holtta-Vuori, E. Ikonen. "Endosomal cholesterol traffic: vesicular and non-vesicular mechanisms meet." 2006, *Biochem. Soc. Trans.*, 34, 392-394.
61. L. Izem, R.E. Morton. "Possible role for intracellular cholesteryl ester transfer protein in adipocyte lipid metabolism and storage." 2007, The *J. Biol. chem.,* 282, 21856-21865.
62. D. Peretti, N. Dahan, E. Shimoni, K. Hirschberg, S. Lev. "Coordinated lipid transfer between the endoplasmic reticulum and the Golgi complex requires the VAP proteins and is essential for Golgi-mediated transport." 2008, *Mol. Biol. Cell.*, 19, 3871-3884.
63. S. Chandran, C.E. Machamer. "Acute Perturbations in Golgi Organization Impact De Novo Sphingomyelin Synthesis" 2008, *Traffic*, 9, 1894-1904.
64. N. Khelef, T.T. Soe, O. Quehenberger, N. Beatini, I. Tabas, F.R. Maxfield. "Enrichment of acyl coenzyme A:cholesterol O-acyltransferase near trans-golgi network and endocytic recycling compartment." 2000, *Arteriosclerosis, thrombosis, and vascular biology*, 20, 1769-1776.
65. K. Fiedler, R.G. Parton, R. Kellner, T. Etzold, K. Simons. "VIP36, a novel component of glycolipid rafts and exocytic carrier vesicles in epithelial cells." 1994, *EMBO J.*, 13, 1729-1740.
66. S. Heino, S. Lusa, P. Somerharju, C. Ehnholm, V.M. Olkkonen, E. Ikonen. "Dissecting the role of the golgi complex and lipid rafts in biosynthetic transport of cholesterol to the cell surface." 2000, *Proc. Natl. Acad. Sci. U.S.A.,* 97, 8375-8380.

67. L. Cubells, S.V. de Muga, F. Tebar, P. Wood, R. Evans, M. Ingelmo-Torres, M. Calvo, K. Gaus, A. Pol, T. Grewal, C. Enrich. “Annexin A6-Induced Alterations in Cholesterol Transport and Caveolin Export from the Golgi Complex.” 2007, *Traffic*, 15, 1568-1589.
68. A. Godi, A. Di Campli, A. Konstantakopoulos, G. Di Tullio, D.R. Alessi, G.S. Kular, T. Daniele, P. Marra, J.M. Lucocq, M.A. De Matteis. “FAPPs control Golgi-to-cell-surface membrane traffic by binding to ARF and PtdIns(4)P.” 2004, *Nat. cell boil*., 6, 393-404.
69. S. Boehm. “Selective inhibition of M-type potassium channels in rat sympathetic neurons by uridine nucleotide preferring receptors.” 1998, *British pharmacol. J.*, 124, 1261-1269.
70. D.A. Brown, and Rose, J.K. “Sorting of GPIanchored proteins to glycolipid-enriched membrane subdomains during transport to the apical cell surface.” 1992, *Cell*, 68, 533-544.
71. E. London, and D.A. Brown, “Insolubility of lipids in triton X-100: physical origin and relationship to sphingolipid/cholesterol membrane domains (rafts).” 2000, *Biochim. Biophys. Acta*, 1508, 182-195.
72. E.K. Fridriksson, P.A. Shipkova, E.D. Sheets, D. Holowka, B. Baird, and F.W. McLafferty. “Quantitative analysis of phospholipids in functionally important membrane domains from RBL-2H3 mast cells using tandem high-resolution mass spectrometry.” 1999, *Biochemistry*, 38, 8056-8063.
73. H. Heerklotz. "Triton promotes domain formation in lipid raft mixtures." 2002, *Biophys. J.* 83, 2693-2701.
74. P. Drevot, C. Langlet, X.J. Guo, A.M. Bernard, O. Colard, J.P. Chauvin, R. Lasserre and H.T. He. “TCR signal initiation machinery is pre-assembled and activated in a subset of membrane rafts.”2002, *Embo J*., 21, 1899-1908.
75. J. Matko, and J. Szollosi, “Landing of immune receptors and signal proteins on lipid rafts: a safe way to be spatio-temporally coordinated?” 2002, *Immunol. Lett*., 82, 3-15.
76. H.A. Rinia, and B. de Kruijff. “Imaging domains in model membranes with atomic force microscopy.” 2001, *FEBS Lett.,* 504, 194-199.
77. R. Varma, and S. Mayor. “GPI-anchored proteins are organized in submicron domains at the cell surface.” 1998, *Nature*, 394, 798-801.
78. A. Pralle, P. Keller, E.L. Florin, K. Simons, and J.K.H. Hörber. “Sphingolipid-cholesterolrafts diffuse as small entities in the plasma membrane of mammalian cells.” 2000, *J Cell Biol.,* 148, 997-1008.
79. D.A. Zacharias, J.D. Violin, A.C. Newton, R.Y. Tsien. “Partitioning of lipidmodified monomeric GFPs into membrane microdomains of live cells.” 2002, *Science*, 296, 913-916.

80. T. Friedrichson, and T.V. “Kurzchalia. Microdomains of GPI-anchored proteins in living cells revealed by crosslinking.” 1998, *Nature*, 394, 802-805.
81. S. Hebbar, E. Lee, M. Manna, S. Steinert, G. SravanKumar, M. Wenk, T. Wohland, and R. Kraut. “A fluorescent sphingolipid binding domain peptide probe interacts with sphingolipids and cholesterol-dependent raft domains.” 2008, *J. Lipid Res.*, 49, 1077-1089.
82. A. Rietveld A, K. Simons. “The differential miscibility of lipids as the basis for the formation of functional membrane rafts.” 1998, *Biochim. biophys. Acta*, 1376(3), 467-479.
83. S. Chiantia, N. Kahya, J. Ries, and P. Schwille. “Effects of ceramide on liquid-ordered domains investigated by simultaneous AFM and FCS.” 2006, *Biophys. J.*, 90, 4500-4508.
84. S.L. Veatch and S.L. Keller. “Separation of Liquid Phases in Giant Vesicles of Ternary Mixtures of Phospholipids and Cholesterol”. 2003, *Biophys. J.*, 85, 3074-3083.
85. S. Chiantia, N. Kahya, and P. Schwille. “Raft domain reorganization driven by short- and long-chain ceramide: A combined AFM and FCS study.” 2007, *Langmuir*, 23, 7659-7665.
86. C. Yuan, J. Furlong, P. Burgos, and L.J. Johnston. “The Size of Lipid Rafts: An Atomic Force Microscopy Study of Ganglioside GM1 Domains in Sphingomyelin/DOPC/Cholesterol Membranes.” 2002, *Biophys. J.*, 82, 2526-2535.
87. K. Simons and R. Ehehalt. “Cholesterol, lipid rafts, and disease.” 2002, *J. Clin. Invest.,* 110, 5, 597-603.
88. S.R. Shaikh, B.D. Rockett, M. Salameh and K. Carraway. “Docosahexaenoic Acid Modifies the Clustering and Size of Lipid Rafts and the Lateral Organization and Surface Expression of MHC Class I of EL4 Cells.” 2009, *J. Nutr.,* 139, 9, 1632-1639.
89. J. Sankaran, M. Manna, L. Guo, R. Kraut, T. Wohland. “Diffusion, transport, and cell membrane organization investigated by imaging fluorescence cross-correlation spectroscopy.” 2009, *Biophys. J.*, 97, 2630-2639.
90. L.J. Pike, “Rafts defined: a report on the Keystone Symposium on Lipid Rafts and Cell Function.” 2006, *J. Lipid Res*., 47, 1597-1598.
91. U. Wrackmeyer, G.H. Hansen, T. Seya and E.M. Danielsen. “Intelectin: A Novel Lipid Raft-Associated Protein in the Enterocyte Brush Border”. 2006, 45, *Biochem*, 9188-9197.
92. J. Füllekrug, K. Simons. “Lipid rafts and apical membrane traffic.” 2004, *Annals New York Acad. Sci.*, 1014, 164-169.

93. K. Simons, and D. Toomre. “Lipid rafts and signal transduction.” 2000, *Nat. Rev. Mol. Cell. Biol.*, 1, 31-39.
94. T. Fujiwara, K. Ritchie, H. Murakoshi, K. Jacobson, A. Kusumi. “Phospholipids undergo hop diffusion in compartmentalized cell membrane”, 2002, J Cell Biol. 157(6),1071-1781.
95. A. Kusumi, Y.M. Shirai, I.K. Honda, K.G.N. Suzuki, T.K. Fujiwara. “Hierarchical organization of the plasma membrane: Investigations by single-molecule tracking vs. fluorescence correlation spectroscopy.”, 2010, *FEBS Letters*, *584, 1814-1823.*
96. P.H.M. Lommerse, B.E.S. Jagalska, H.P. Spaink and T. Schmidt. “Single-molecule diffusion measurements of H-Ras at the plasma membrane of live cells reveal microdomain localization upon activation.” 2005, *J Cell Sci*. 118, 1799-1809.
97. R. Lasserre, X.J. Guo, F. Conchonaud, Y. Hamon, O. Hawchar, A.M. Bernard, S. M. Soudja, P.F. Lenne, H. Rigneault, D. Olive, G. Bismuth, J. A Nunès, B. Payrastre, D. Marguet and H.T. He. “Raft nanodomains contribute to Akt/PKB plasma membrane recruitment and activation.” Nat. Chem. Biol. 4(9), 538-547.
98. G.R. Chichili, W. Rodgers. “Cytoskeleton-membrane interactions in membrane raft structure.” 2009, *Cell. Mol. Life Sci*., 66, 2319-2328.
99. H.T. Wright, J.D. Robertus. "The intersubunit disulfide bridge of ricin is essential for cytotoxicity". 1997, *Arch Biochem Biophys,* 256, 280-284.
100. E. Ikonen. “Roles of lipid rafts in membrane transport.” 2001, *Curr. Opin. Cell. Biol.*, 13, 470-477.
101. F.G. van der Goot, and T. Harder. “Raft membrane domains: from a liquid-ordered membrane phase to a site of pathogen attack.” 2001, *Semin. Immunol.,* 13, 89-97.
102. G.S. Baron, K. Wehrly, D.W. Dorward, B. Chesebro and B. Caughey. “Conversion of raft associated prion protein to the protease-resistant state requires insertion of PrP-res (PrP(Sc)) into contiguous membranes.” 2002, *Embo J.*, 21, 1031-1040.
103. A. Kakio, S. Nishimoto, K. Yanagisawa, Y. Kozutsumi, K. Matsuzaki. “Interactions of amyloid beta-protein with various gangliosides in raftlike membranes: importance of GM1 ganglioside-bound form as an endogenous seed for Alzheimer amyloid.” 2002, *Biochemistry*, 41, 7385-7390.
104. E.E. Prieschl, and T. Baumruker, “Sphingolipids: second messengers, mediators and raft constituents in signaling.” 2000, *Immunol. Today*. 21, 555-560.
105. E.J. Smart, *et al*. (1999) Caveolins, liquid-ordered domains, and signal transduction. *Mol. Cell Biol*., 19, 7289-7304.

106. G.S. Baron and B. Caughey. Effect of Glycosylphosphatidylinositol Anchor-dependent and -independent Prion Protein Association with Model Raft Membranes on Conversion to the Protease-resistant Isoform", 2003, *J Biol. Chem*., 278, 14883-14892.
107. Y. Maeda, Y. Tashima, T. Houjou, M. Fujita, T. Yoko-o, Y. Jigami, R. Taguchi and Taroh Kinoshita. "Fatty Acid Remodeling of GPI-anchored Proteins Is Required for Their Raft Association.", 2007, *Mol. Biol. Cell*, 18, 1497-1506.
108. J. Benting, A. Rietveld, I. Ansorge, K. Simons. "Acyl and alkyl chain length of GPI-anchors is critical for raft association in vitro." 1999, *FEBS Lett.,* 462, 47-50.
109. S.I. Hakomori. "Cell adhesion/recognition and signal transduction through glycosphingolipid microdomain." 2000, *Glycoconj. J*., 17, 143-151.
110. R.S. Boyd, R. Jukes-Jones, R. Walewska, D. Brown, M.J.S. Dyer, and K. Cain. "Protein Profiling of Plasma Membranes and Lipid Rafts Defines Aberrant Signaling Pathways in Mantle Cell Lymphoma." 2008, B*lood*, 112 (11), 145.
111. M.R. Bryant, C.B. Marta, F.S. Kim, and R. Bansal. "Phosphorylation and Lipid Raft Association of Fibroblast Growth Factor Receptor-2 In Oligodendrocytes." 2009, *GLIA*, 57, 935–946.
112. K. Badizadegan, A.A. Wolf, C. Rodighiero, M. Jobling, T.R.Hirst, R.K. Holmes, W.I. Lencer. "Floating cholera toxin into epithelial cells: functional association with caveolae-like detergent-insoluble membrane microdomains." 2000, *Int J Med. Microbiol.,* 290, 403-408.
113. T. Nishiki, Y. Tokuyama, Y. Kamata, Y. Nemoto, A. Yoshida, K. Sato, M. Sekiguchi, M. Takahashi, S. Kozaki. "The high-affinity binding of Clostridium botulinum type B neurotoxin to synaptotagmin II associated with gangliosides GT1b/GD1a." 1996, *FEBS Lett*., 378, 253-257.
114. L. Rajendran and K. Simons. "Lipid rafts and membrane dynamics". 2005, J. Cell Sci., 118, 1099-1102.
115. J. Fantini, D. Hammache, G. Piéroni, N. Yahi. "Role of glycosphingolipids microdomains in CD4-dependent HIV-1 fusion." 2000, *Glycoconj. J*., 17, 199-204.
116. L. Abrami, M. Fivaz, and F.G. van der Goot. "Adventures of a pore-forming toxin at the target cell surface." 2000, *Trends Microbiol.*, 8, 168-172.
117. C.A. Lingwood. "Glycolipid receptors for verotoxin and Helicobacter pylori: role in pathology." 1999, *Biochim. Biophys. Acta*, 1455, 375-386.
118. T. Falguières, F. Mallard, C. Baron, D. Hanau, C. Lingwood, B. Goud, J. Salamero, and L. Johannes. "Targeting of Shiga toxin B-subunit to retrograde transport route in association with detergent-resistant membranes." 2001, *Mol. Biol. Cell*, 12, 2453-2468.

119. A. Nusrat, C. von Eichel-Streiber, J.R. Turner, P. Verkade, J.L. Madara, and C.A. Parkos. “Clostridium difficile toxins disrupt epithelial barrier function by altering membrane microdomain localization of tight junction proteins.” 2001, *Infect. Immun.,* 69, 1329-1336.
120. T.J. Pucadyil, P. Tewary, R. Madhubala, A. Chattopadhyay. “Cholesterol is required for *Leishmania donovani* infection: implications in leishmaniasis.” 2004, *Mol. Biochem. Parasitol.*, 133, 145-152.
121. S. Dreschers, P. Franz, C.A. Dumitru, B.Wilker, K. Jahnke, E. Gulbins. “Infections with human rhinovirus induce the formation of distinct functional membrane domains.” 2007, *Cell. Physiol. Biochem*., 20, 241-254.
122. E. Gassert, E. Avota, H. Harms, G. Krohne, E. Gulbins, S.S. Schaulies. “Induction of Membrane Ceramides: A Novel Strategy to Interfere with T Lymphocyte Cytoskeletal Reorganisation in Viral Immunosuppression.” 2009, *PLoS Pathogens*, 5, 10, e1000623.
123. S. Steinert, E. Lee, G. Tresset, R. Hortsch, S. Hebbar, J. Sundram, S. Kesavapany, and R. Kraut, “A fluorescent glycolipid-binding peptide probe traces cholesterol dependent microdomain-derived trafficking pathways.” 2008, *PLoS one*, 3, e2933.
124. S.A. Poulsen, A.A. Watson, D.P. Fairlie, D.J. Craik. “Solution structures in aqueous SDS micelles of two amyloid beta peptides of A beta(1-28) mutated at the alpha-secretase cleavage site (K16E, K16F).” 2000, *J Str. Biol*. 130, 142-152.
125. G.M. Kuziemko, M. Stroh, R.C. Stevens. “Cholera Toxin Binding Affinity and Specificity for Gangliosides Determined by Surface Plasmon Resonance.” 1996, *Biochemistry*, 35, 6375–6384.
126. B.C. Lagerholm, G.E. Weinreb, K. Jacobson, N.L. Thompson. “Detecting microdomains in intact cell membranes.” 2005, *Annu. Rev. Phys. Chem*., 56, 309-336.
127. P.W. Janes, S.C. Ley, A.I. Magee. “Aggregation of Lipid Rafts Accompanies Signaling Via the T Cell Antigen Receptor.” 1999, *J. Cell Biol.*, 147, 447-461.
128. P. Antes, G. Schwarzmann. K. Sandhoff. “Detection of protein mediated glycosphingolipid clustering by the use of resonance energy transfer between fluorescent labelled lipids. A method established by applying the system ganglioside GM1 and cholera toxin B subunit.” 1992, *Chem. Phys. Lipids*, 62, 269-280.
129. R.H. Massol, J.E. Larsen, Y. Fujinaga, W.I. Lencer, T. Kirchhausen. “Cholera toxin toxicity does not require functional Arf6- and dynamin-dependent endocytic pathways.” 2004, *Mol. Biol. Cell*, 15, 3631-3641.
130. H. Shogomori, and A.H. Futerman. “Cholesterol depletion by methyl-betacyclodextrin blocks cholera toxin transport from endosomes to the Golgi apparatus in hippocampal neurons.” 2001, *J. Neurochem*., 78, 991-999.

131. M.L. Torgersen, G. Skretting, B. van Deurs, and K. Sandvig. “Internalization of cholera toxin by different endocytic mechanisms.” 2001, *J. Cell Sci*., 114, 3737-3747.
132. B.J. Nichols, A.K. Kenworthy, R.S. Polishchuk, R. Lodge, T.H. Roberts, K. Hirschberg, R.D. Phair, and J. Lippincott-Schwartz. “Rapid Cycling of Lipid Raft Markers between the Cell Surface and Golgi Complex.” 2001, *J. Cell Biol.*, 153, 529-542.
133. S. Sabharanjak, P. Sharma, R.G. Parton, and S. Mayor. “GPI-anchored proteins are delivered to recycling endosomes via a distinct cdc42-regulated, clathrinindependent pinocytic pathway.” 2002, *Dev Cell*., 2, 411-423.
134. P. Sharma, R. Varma, R.C. Sarasij, Ira, K. Gousset, G. Krishnamoorthy, M. Rao, and S. Mayor. “Nanoscale organization of multiple GPI-anchored proteins in living cell membranes.” 2004, *Cell,* 116, 577-589.
135. A.K. Kenworthy, N. Petranova, M. Edidin. “High-resolution FRET microscopy of cholera toxin B-subunit and GPI-anchored proteins in cell plasma membranes.” 2000, *Mol. Biol. Cell*, 11, 1645-1655.
136. C. Neumann-Giesen, B. Falkenbach, P. Beicht, S. Claasen, G. Lüers, C.A.O. Stuermer, V. Herzog and R. Tikkanen. “Membrane and raft association of reggie-1/flotillin-2: role of myristoylation, palmitoylation and oligomerization and induction of filopodia by overexpression.” 2004, *Biochem. J.,* 378, 509-518.
137. O.O. Glebov, N.A. Bright, and B.J. Nichols. “Flotillin-1 defines a clathrinindependent endocytic pathway in mammalian cells.” 2006, *Nat Cell Biol*., 8, 46-54.
138. L. Pelkmans, J. Kartenbeck, A. Helenius. “Caveolar endocytosis of simian virus 40 reveals a new two-step vesicular-transport pathway to the ER.” 2001, *Nat. Cell Biol*., 3, 473-483.
139. S. Mayor, R.E. Pagano. “Pathways of clathrin-independent endocytosis.” 2007, *Nat. Rev. Mol. Cell Biol.,* 8, 603-612.
140. X. Shi, L.S. Teo, X. Pan, S.W. Chong, R. Kraut, V. Korzh, T. Wohland. “Probing events with single molecule sensitivity in zebrafish and *Drosophila* embryos by fluorescence correlation spectroscopy.” 2009, *Dev. Dynamics*, 238, 3156-3167.
141. T. Ariga, K. Kobayashi, A. Hasegawa, M. Kiso, H. Ishida, T. Miyatake. “Characterization of high-affinity binding between gangliosides and amyloid beta-protein.” 2001, *Arch. Biochem. Biophys*., 388, 225-230.
142. B. Kannan, L. Guo, T. Sudhaharan, S. Ahmed, I. Maruyama, and T. Wohland. “Spatially resolved Total Internal Reflection Fluorescence Correlation Microscopy using an Electron Multiplying Charge-Coupled Device Camera.” 2007, *Anal. Chem.*, 79, 4463-4470.

143. L. Guo, J.Y. Har, J. Sankaran, Y. Hong, B. Kannan, and T. Wohland. “Molecular diffusion measurements in lipid bilayers over wide concentration ranges: A comparative study.” 2008, *ChemPhysChem*, 9, 721-728.
144. D. Mudge, E. Elson and W. W. Webb’; “Thermodynamic fluctuations in a reacting system; measurement by Fluorescence Correlation Spectroscopy.” 1972, *Phys. Rev. Letter*, 29, 705.
145. K. Bacia and P. Schwille; “A dynamic view of cellular processes by in vivo fluorescence auto- and cross-correlation spectroscopy.” 2003, *Methods,* 29, 74-85.
146. M.A. Hink, J.W. Borst and A. Visser. “Fluorescence correlation spectroscopy of GFP fusion proteins in living plant cells.” 2003, *Biophotonics*, *Pt B*, 93-112.
147. K. Bacia, D. Scherfeld, N. Kahya and P. Schwille. “Fluorescence correlation spectroscopy relates rafts in model and native membranes.” 2004, *Biophys. J.* 87, 1034-1043.
148. E.P. Petrov and P. Schwille. “Fluorescence correlation spectroscopy on undulating membranes.” 2005, *Biophys. J.* 88, 524A-525A.
149. U. Kumar, A. Baragli, and R.C. Patel. “Probing molecular interactions in single and live cells with fluorescence spectroscopy.” 2003, *Trac-Trends in Analytical Chemistry* 22, 537-543.
150. P. Schwille and W.W. Webb. “Ultrasensitive determination of molecular dynamics in cells by one- and two-photon fluorescence correlation spectroscopy.” 2000, *Biophys. J.* 78, 280A-280A.
151. Q. Ruan, Y. Chen, E. Gratton, M. Glaser, and W.W. Mantulin. “Cellular Characterization of Adenylate Kinase and Its Isoform: Two-Photon Excitation Fluorescence Imaging and Fluorescence Correlation Spectroscopy.” 2002, *Biophys. J.* 83, 3177-3187.
152. G. Bose, P. Schwille, and T. Lamparter. “The Mobility of Phytochrome within Protonemal Tip Cells of the Moss Ceratodon purpureus, Monitored by Fluorescence Correlation Spectroscopy.” 2004, *Biophys. J.* 87, 2013-2021.
153. M. Weiss, H. Hashimoto, and T. Nilsson. “Anomalous Protein Diffusion in Living Cells as Seen by Fluorescence Correlation Spectroscopy.” 2003, *Biophys. J.* 84, 4043-4052.
154. G. Meacci, J. Ries, E. Fischer-Friedrich, N. Kahya, P. Schwille, and K. Kruse. “Mobility of Min-proteins in Escherichia coli measured by fluorescence correlation spectroscopy.” 2006, *Physical Biology,* 3, 255-263.
155. Y. Ohsugi, K. Saito, M. Tamura, and M. Kinjo. “Lateral mobility of membrane-binding proteins in living cells measured by total internal reflection fluorescence correlation spectroscopy.” 2006, *Biophys. J.* 91, 3456-3464.

156. T. Rosales, V. Georget, D. Malide, A. Smirnov, J. H. Xu, C. Combs, J. R. Knutson, J. C. Nicolas, and C. A. Royer. "Quantitative detection of the ligand-dependent interaction between the androgen receptor and the co-activator, Tif2, in live cells using two color two photon fluorescence cross-correlation spectroscopy." 2007, *European Biophysics Journal with Biophysics Letters,* 36, 153-161.
157. R. Rigler, Ü. Meseth, J. Widengren, and P. Kask. "Fluorescence correlation spectroscopy with high count rate and low background: analysis of translational diffusion." 1993, *Eur. Biophys. J.* 22, 169-175.
158. S.R. Aragon, R. P. "Fluorescence correlation spectroscopy and Brownian rotational diffusion." 1975, *Biopolymers,* 14, 119-137.
159. E.L. Elson, D. Mudge. "Fluorescence correlation spectroscopy. I. Conceptual basis and theory." 1974, *Biopolymers,* 13, 1-27.
160. D. Magde, W.W. Webb, E.L. Elson. "Fluorescence correlation spectroscopy. III. Uniform translation and laminar flow." 1978, *Biopolymers,* 17, 361-376.
161. U. Meseth, T. Wohland, R. Rigler, and H. Vogel. "Resolution of Fluorescence Correlation Measurements." 1999, *Biophys. J.* 76:1619-1631.
162. K. Perronet, G. Schull, P. Raimond and F. Charra. "Single-molecule fluctuations in a tunnel junction: A study by scanning-tunnelling-microscopy–induced luminescence". 2006, *Europhys. Lett.,* 74, 313.
163. D. Axelrod. "Total Internal Reflection Fluorescence Microscopy in Cell Biology" 2001, *Traffic*, 2, 764-774.
164. O. Gliko, G.D. Reddy, B. Anvari, W.E. Brownell, P. Saggau. "Standing wave total internal reflection fluorescence microscopy to measure the size of nanostructures in living cells" 2006, *J Biomed Opt.*, 11, 064013.
165. D.K. Hoover, E.J. Lee and Md. N. Yousaf. "Total Internal Reflection Fluorescence Microscopy of Cell Adhesion on Patterned Self-Assembled Monolayers on Gold." 2009, *Langmuir*, *25*, 2563-2566.
166. N.O. Petersen, Pia L. Höddelius, P.W. Wiseman, O. Seger, and K.E. Magnusson. "Quantitation of Membrane Receptor Distributions by Image Correlation Spectroscopy: Concept and Application." 1993, *Biophys. J.,* 65, 1135-1146.
167. D.L. Kolin, and P. W. Wiseman. "Advances in image correlation spectroscopy: Measuring number densities, aggregation states, and dynamics of fluorescently labeled macromolecules in cells." 2007, *Cell Biochem. Biophys*., 49, 141-164.
168. J. Balaji, J.; Maiti S. "Quantitative measurement of the resolution and sensitivity of confocal microscopes using line-scanning fluorescence correlation spectroscopy". 2005, *Microscopy Res. Tech*., 66 (4), 198-202.

169. M. Srivastava, and N. O. Petersen. “Image cross-correlation spectroscopy: A new experimental biophysical approach to measurement of slow diffusion of fluorescent molecules.” 1996, *Methods in Cell Science,* 18, 47-54.
170. A. Nohe, E. Keating, M. Fivaz, F. G. van der Goot, and N.O. Petersen. “Dynamics of GPI-anchored proteins on the surface of living cells.” 2006, *Nanomedicine : the official journal of the American Academy of Nanomedicine*, 2, 1-7.
171. A. Nohe, E. Keating, C. Loh, M. T. Underhill, and N. O. Petersen. “Caveolin-1 isoform reorganization studied by image correlation spectroscopy.” 2004, *Faraday Discuss,* 126, 185-195.
172. M. Srivastava, and N. O. Petersen. “Diffusion of transferrin receptor clusters.” 1998, *Biophys. Chem.,* 75, 201-211.
173. B. Hebert, S. Costantino, and P. W. Wiseman. “Spatiotemporal image correlation Spectroscopy (STICS) theory, verification, and application to protein velocity mapping in living CHO cells.” 2005, *Biophys. J.*, 88, 3601-3614.
174. D.L. Kolin, D. Ronis, and P. W. Wiseman. “k-Space Image Correlation Spectroscopy: A Method for Accurate Transport Measurements Independent of Fluorophore Photophysics.” 2006*, Biophys. J.*, 91, 3061-3075.
175. M.A. Digman, P. Sengupta, P. W. Wiseman, C. M. Brown, A. R. Horwitz, and E. Gratton. “Fluctuation Correlation Spectroscopy with a Laser-Scanning Microscope: Exploiting the Hidden Time Structure.” 2005, *01*, 88, L33-36.
176. M. Brinkmeier, K. Dorre, J. Stephan, and M. Eigen. “ Two beam cross correlation: A method to characterize transport phenomena in micrometer-sized structures.” 1999, *Anal. Chem.*, 71, 609-616.
177. P.S. Dittrich, and P. Schwille. “Spatial two-photon fluorescence cross-correlation Spectroscopy for controlling molecular transport in microfluidic structures.” 2002, *Anal. Chem*., 74, 4472-4479.
178. X. Pan, H. Yu, X. Shi, V. Korzh, and T. Wohland. “Characterization of flow direction in microchannels and zebrafish blood vessels by scanning fluorescence correlation spectroscopy.” 2007, *J. Biomed. Opt.*, 12, 014034.
179. S. Korzh, X. F. Pan, M. Garcia-Lecea, C. L. Winata, X. T. Pan, T. Wohland, V. Korzh, and Z. Y. Gong. “Requirement of vasculogenesis and blood circulation in late stages of liver growth in zebrafish.” 2008, *BMC Dev. Biol*., 8, 15.
180. X. Pan, X. Shi, V. Korzh, H. Yu, and T. Wohland. “Line scan fluorescence correlation spectroscopy for three-dimensional microfluidic flow velocity measurements.” 2009, *J. Biomed. Opt.* , 14, 024049.

181. Y. Blancquaert, J. Gao, J. Derouard, and A. Delon. “Spatial fluorescence cross-correlation spectroscopy by means of a spatial light modulator.” 2008, *J. Biophotonics*, 1, 408-418.
182. M. Go¨sch, A. Serov, T. Anhut, T. Lasser, A. Rochas, P.A. Besse, R.S. Popovic, H. Blom, R. Rigler. “Parallel single molecule detection with a fully integrated single-photon 2×2 CMOS detector array.” 2004, *J. Biomed. Opt.*, 9, 913-921.
183. M. Go¨sch, H. Blom, S. Anderegg, K. Korn, P. Thyberg, M. Wells, T. Lasser, R. Rigler, A.M.S. Hard. “Parallel dual-color fluorescence cross-correlation spectroscopy using diffractive optical elements.” 2005, *J. Biomed. Opt.*, 10, 054008.
184. D.R. Sisan, R. Arevalo, C. Graves, R. McAllister, and J. S. Urbach. “Spatially resolved fluorescence correlation spectroscopy using a spinning disk confocal microscope.” 2006, *Biophys. J.*, 91, 4241-4252.
185. H. Pick, A.K. Preuss, M. Mayer, T. Wohland, R. Hovius, and H. Vogel. “Monitoring Expression and Clustering of the Ionotropic $5HT_3$ Receptor in Plasma Membranes of Live Biological Cells”, 2003, *Biochemistry*, 42, 877-884.
186. A.R. Burns, D.J. Frankel, T. Buranda “Local Mobility in Lipid Domains of Supported Bilayers Characterized by Atomic Force Microscopy and Fluorescence Correlation Spectroscopy.” 2005, *Biophys. J.*, 89, 1081-1093.
187. N.L. Thompson, T.P. Burghardt, D. Axelrod. “Measuring surface dynamics of biomolecules by total internal reflection fluorescence with photobleaching recovery or correlation spectroscopy.” 1981, *Biophys. J.*, 33, 435-454.
188. B. Zhang, J. Zerubia, and J.C. Olivo-Marin. “Gaussian approximations of fluorescence microscope point-spread function models.” 2007, *Applied Optics*, 46(10), 1819-1829.
189. M.F. Tompsett, G.F. Amelio, W.J. Bertram, Jr. R.R. Buckley, W.J. McNamara, J.C. Mikkelsen, Jr. D.A. Sealer, "Charge-coupled imaging devices: Experimental results". 1971, *IEEE Transactions on Electron Devices,* 18, 992-996.
190. B. Kannan, J.Y. Har, P. Liu, I. Maruyama, J.L. Ding, and T. Wohland “Electron Multiplying Charge-Coupled Device Camera Based Fluorescence Correlation Spectroscopy.” 2006, *Anal. Chem.*, 78, 3444-3451.
191. D.A. Brown, and E. London. “Functions of lipid rafts in biological membranes.” 1998, *Annu Rev Cell Dev Biol*., 14, 111-136.
192. W.I. Lencer, and D. Saslowsky. “Raft trafficking of AB5 subunit bacterial toxins.” 2005, *Biochim Biophys Acta*., 1746, 314-321.
193. H. Shogomori, and A.H. Futerman. “Cholesterol depletion by methyl-betacyclodextrin blocks cholera toxin transport from endosomes to the Golgi apparatus in hippocampal neurons.” 2001, *J. Neurochem*., 78, 991-999.

194. M.L. Torgersen, G. Skretting, B. van Deurs, and K. Sandvig. “Internalization of cholera toxin by different endocytic mechanisms.” 2001, *J. Cell Sci*., 114, 3737-3747.
195. W. Drobnik, H. Borsukova, A. Bottcher, A. Pfeiffer, G. Liebisch, G.J. Schutz, H. Schindler, and G. Schmitz. “Apo AI/ABCA1-dependent and HDL3-mediated lipid efflux from compositionally distinct cholesterol-based microdomains.” 2002, *Traffic,* 3, 268-278.
196. C. Gomez-Mouton, J.L. Abad, E. Mira, R.A. Lacalle, E. Gallardo, S. Jimenez-Baranda, I. Illa, A. Bernad, S. Manes, and A.C. Martinez. “Segregation of leading-edge and uropod components into specific lipid rafts during T cell polarization.” 2001, *Proc Natl Acad Sci U S A*., 98, 9642-9647.
197. A.E. Schade and A.D. Levine. “Lipid raft heterogeneity in human peripheral blood T lymphoblasts: a mechanism for regulating the initiation of TCR signal transduction.” 2002, *J Immunol*., 168, 2233-2239.
198. N. Kahya, D. Scherfeld, K. Bacia, B. Poolman, and P. Schwille. “Probing lipid mobility of raft-exhibiting model membranes by fluorescence correlation spectroscopy.” 2003, *J Biol Chem*., 278, 28109-28115.
199. P.A. Orlandi and P.H. Fishman. “Filipin-dependent inhibition of cholera toxin: evidence for toxin internalization and activation through caveolae-like domains.” 1998, *J Cell Biol*. 141, 905-915.
200. J. Fantini, “How sphingolipids bind and shape proteins: molecular basis of lipidprotein interactions in lipid shells, rafts and related biomembrane domains.” 2003, *Cell Mol Life Sci*., 60, 1027-1032.
201. J. Widengren and P. Thyberg. “FCS cell surface measurements—photophysical limitations and consequences on molecular ensembles with heterogenic mobilities.” 2005, *Cytometry A*. 68, 101-112.
202. D. Zhang, M. Manna, T. Wohland and R. Kraut. “Alternate raft pathways cooperate to mediate slow diffusion and efficient uptake of a sphingolipid tracer to degradative and recycling compartments.” 2009, *J. Cell Sci*., 3715-3728.
203. M. Simons, P. Keller, B. De Strooper, K. Beyreuther, C.G. Dotti, and K. Simons. “Cholesterol depletion inhibits the generation of beta-amyloid in hippocampal neurons.” 1998, *Proc Natl Acad Sci U S A*., 95, 6460-6464.
204. M. Miaczynska, L. Pelkmans and M. Zerial “Not just a sink: endosomes in control of signal transduction.” 2004, *Current Opinion in Cell Biology*, 16, 400-406.
205. L.K. Medina-Kauwe. “Alternative endocytic mechanisms exploited by pathogens: New avenues for therapeutic delivery?” 2007, *Advanced Drug Delivery Reviews*, 59, 798-809.

206. M. Miaczynska and H. Stenmark. “Mechanisms and functions of endocytosis.” 2008, *J. Cell Biol.*, 180, 7-11.
207. M. Marsh and H. T. McMahon. “The Structural Era of Endocytosis.” 1999, *Science*, 285, 215-220.
208. M. Marsh, “Endocytosis.” *Oxford University Press*, p. vii. ISBN 978-0-19-963851-2.
209. R. Lundmark, G.J. Doherty, M.T. Howes, K. Cortese, Y. Vallis, R.G. Parton, and H.T. McMahon. “The GTPase-Activating Protein GRAF1 Regulates the CLIC/GEEC Endocytic Pathway.” 2008, *Current Biology*, 18, 1802-1808.
210. C. Lamaze, A. Dujeancourt, T. Baba, C.G. Lo, A. Benmerah, and A. Dautry-Varsat. “Interleukin 2 receptors and detergent-resistant membrane domains define a clathrin-independent endocytic pathway.” 2001, *Mol. Cell* 7, 661-671.
211. S.Mayor, and R.E. Pagano, “Pathways of clathrin-independent endocytosis.” 2007, *Nat. Rev. Mol. Cell Biol.* 8, 603-612.
212. K. Deinhardt, O. Berninghausen, H.J. Willison, C.R. Hopkins, and G. Schiavo. “Tetanus toxin is internalized by a sequential clathrin-dependent mechanism initiated within lipid microdomains and independent of epsin1.” 2006, *J. Cell Biol.* 174, 459-471.
213. R.H. Massol, J.E. Larsen, Y. Fujinaga, W.I. Lencer, and T. Kirchhausen. “Cholera toxin toxicity does not require functional Arf6- and dynamin-dependent endocytic pathways.” 2004, *Mol. Biol. Cell,* 15, 3631-3641.
214. K. Sandvig, B. Spilsberg, S.U. Lauvrak, M.L. Torgersen, T.G. Iversen, and B. van Deurs. “Pathways followed by protein toxins into cells.” 2004, *Int. J. Med. Microbiol.* 293, 483-490.
215. L. Abrami, S. Liu, P. Cosson, S.H. Leppla, and F.G. van der Goot. “Anthrax toxin triggers endocytosis of its receptor via a lipid raft-mediated clathrin-dependent process.” 2003, *J. Cell Biol.* 160, 321-328.
216. S. Mayor and H. Riezman. “Sorting GPI-anchored proteins.” 2004, *Nat. Rev. Mol. Cell Biol.* 5, 110-120.
217. M.F. Langhorst, A. Reuter, F.A. Jaeger, F.M. Wippich, G. Luxenhofer, H. Plattner, and C.A. Stuermer. “Trafficking of the microdomain scaffolding protein reggie-1/flotillin-2.” 2008, *Eur. J. Cell Biol.* 87, 211-226.
218. J.F. Hancock. “Lipid rafts: contentious only from simplistic standpoints.” 2006, *Nat. Rev. Mol. Cell Biol.* 7, 456-462.
219. N.M. Hooper. “Detergent-insoluble glycosphingolipid/cholesterol-rich membrane domains, lipid rafts and caveolae.” 1999, *Mol. Membr. Biol.* 16, 145-156.
220. R. Lasserre, X. J. Guo, F. Conchonaud, Y. Hamon, O. Hawchar, A. M. Bernard, S. M. Soudja, P. F. Lenne, H. Rigneault, D. Olive, G. Bismuth, J. A. Nunes, B. Payrastre, D.

Marguet, and H. T. He. “Raft nanodomains contribute to Akt/PKB plasma membrane recruitment and activation.” 2008, *Nat. Chem. Biol.*, 4, 538-547.

221. C. Gomez-Mouton, R.A. Lacalle, E. Mira, S. Jimenez-Baranda, D.F. Barber, A.C. Carrera, A.C. Martinez and S. Manes. “Dynamic redistribution of raft domains as an organizing platform for signaling during cell chemotaxis.” 2004, *J. Cell Biol.,* 164, 759-768.
222. E.C. Jury, F. Flores-Borja, and P.S. Kabouridis. “Lipid rafts in T cell signaling and disease.” 2007, *Sem in. Cell Dev. Biol.* 18, 608-615.
223. A. Pol, S. Martin, M.A. Fernandez, M. Ingelmo-Torres, C. Ferguson, C. Enrich, and R.G. Parton. “Cholesterol and fatty acids regulate dynamic caveolin trafficking through the Golgi complex and between the cell surface and lipid bodies.” 2005, *Mol. Biol. Cell,* 16, 2091-2105.
224. K. Simons and J. Gruenberg. “Jamming the endosomal system: lipid rafts and lysosomal storage diseases.” 2000, *Trends Cell Biol.*, 10, 459-462.
225. C. Eggeling, C. Ringemann, R. Medda, G. Schwarzmann, K. Sandhoff, S. Polyakova,V.N. Belov, B. Hein, C. von Middendorff, A. Schonle. “Direct observation of the nanoscale dynamics of membrane lipids in a living cell.” 2008, *Nature,* 457, 1159-1162.
226. M.F. Langhorst, A. Reuter, and C.A. Stuermer. “Scaffolding microdomains and beyond: the function of reggie/flotillin proteins.” 2005, *Cell Mol. Life Sci.,* 62, 2228-2240.

227. V. Heinrich, K. Ritchie, N. Mohandas, E. Evans. “Elastic thickness compressibilty of the cell membrane.” 2001, *Biophys. J.*, 81, 3, 1452-1463.
228. P. Schwille and E. Haustein “Fluorescence Correlation Spectroscopy An Introduction to its Concepts and Applications” 2001, *Biophysics Textbook Online*, 1-33.
229. R. Chadda, M.T. Howes, S.J. Plowman, J.F. Hancock, R.G. Parton, and S. Mayor. “Cholesterol-sensitive Cdc42 activation regulates actin polymerization for endocytosis via the GEEC pathway.” 2007, *Traffic,* 8, 702-717.
230. L. Saavedra, A. Mohamed, V. Ma, S. Kar, and E.P. de Chaves. “Internalization of beta-amyloid peptide by primary neurons in the absence of apolipoprotein E.” 2007, *J. Biol.Chem.,* 282, 35722-35732.
231. Schneider, L. Rajendran, M. Honsho, M. Gralle, G. Donnert, F. Wouters, S.W. Hell, and M. Simons. “Flotillin-dependent clustering of the amyloid precursor protein regulates its endocytosis and amyloidogenic processing in neurons.” 2008, *J. Neurosci.,* 28, 2874-2882.

232. P.H. Lommerse, K. Vastenhoud, N.J. Pirinen, A.I. Magee, H.P. Spaink, and T. Schmidt. "Single-molecule diffusion reveals similar mobility for the Lck, Hras, and K-ras membrane anchors." 2006, *Biophys. J.,* 91, 1090-1097.
233. Y. Zhang, X. Li, K. A. Becker, and E. Gulbins. "Ceramide-enriched membrane domains-Structure and function." 2009, *Biochim. Biophys. Acta-Biomembr*., 1788, 178-183.
234. A.J. Garcia-Saez, and P. Schwille. "Fluorescence correlation spectroscopy for the study of membrane dynamics and protein/lipid interactions." 2008, *Methods,* 46, 116-122.
235. H. Qian, S. Saffarian, and E. L. Elson. "Concentration fluctuations in a mesoscopic oscillating chemical reaction system." 2002, *Proc. Natl. Acad. Sci. U. S. A*., 99, 10376-10381.
236. H. Qian, and E. L. Elson. "Fluorescence correlation spectroscopy with high-order and dual-color correlation to probe nonequilibrium steady states." 2004, *Proc. Natl. Acad. Sci. U. S. A.*, 101, 2828-2833.
237. S. Mukherjee, and F. R. Maxfield. "Membrane domains." 2004, *Annu. Rev. Cell Dev. Biol*., 20, 839-866.
238. P. Caroni, "Actin cytoskeleton regulation through modulation of PI(4,5)P-2 rafts." 2001, *Embo J*., 20, 4332-4336.
239. S. Seveau, R. J. Eddy, F. R. Maxfield, and L. M. Pierini. "Cytoskeleton-dependent Membrane Domain Segregation during Neutrophil Polarization." 2001, *Mol. Biol. Cell*, 12, 3550-3562.
240. A.K. Kenworthy, B. J. Nichols, C. L. Remmert, G. M. Hendrix, M. Kumar, J. Zimmerberg, and J. Lippincott-Schwartz. "Dynamics of putative raft-associated proteins at the cell surface." 2004, *J. Cell Biol*., 165, 735-746.
241. E.D. Sheets, G. M. Lee, R. Simson, and K. Jacobson. "Transient confinement of a glycosylphosphatidylinositol-anchored protein in the plasma membrane." 1997, *Biochemistry*, 36, 12449-12458.
242. E. Ottico, A. Prinetti, S. Prioni, C. Giannotta, L. Basso, V. Chigorno, and S. Sonnino. "Dynamics of membrane lipid domains in neuronal cells differentiated in culture." 2003, *J. Lipid Res.*, 44, 2142-2151.
243. S. Ilangumaran, and D. C. Hoessli. "Effects of cholesterol depletion by cyclodextrin on the sphingolipid microdomains of the plasma membrane." 1998, *Biochem. J.*, 335, 433-440.
244. J.S. Goodwin, K. R. Drake, C. L. Remmert, and A. K. Kenworthy. "Ras diffusion is sensitive to plasma membrane viscosity." 2005, *Biophys. J*., 89, 1398-1410.

245. A. Kusumi, C. Nakada, K. Ritchie, K. Murase, K. Suzuki. “Paradigm shift of the plasma membrane concept from the two-dimensional continuum fluid to the partitioned fluid: high-speed single molecule tracking of membrane molecules.” 2005, *Annu. Rev. Biophys. Biomol. Struct.*, 34, 351-378.
246. J.F. Joanny. “Active Behavior of the Cell Cytoskeleton.” 2001, *Progress of Theoretical Physics*, 165, 100-102.
247. K. Jacobson, O. G. Mouritsen, and R. G. W. Anderson. “Lipid rafts: at a crossroad between cell biology and physics.” 2007, *Nat. Cell Biol*., 9, 7-14.
248. R. Phillips, T. Ursell, P. Wiggins & P. Sens. “Emerging roles for lipids in shaping membrane-protein function.” 2009, 459, 379-385.
249. D.M. Engelman, “Membranes are more mosaic than fluid.” 2005, *Nature,* 438, 578-580.
250. T. Harder. “Formation of Functional Cell *Membrane Domains*: The Interplay of lipid- and protein- mediated interactions.” 2003, *Phil. Trans. R. Soc. Lond. B.,* 358, 863-868.
251. O.G. Mouritsen and K. Jørgensen. “A New Look at Lipid-Membrane Structure in Relation to Drug Research.” *Pharmac. Res.,* 1998, 15, 10, 1507-1519.
252. G. van Meer, J. Wolthoorn and S. Degroote. “The fate and function of glycosphingolipid glucosylceramide.” 2003, *Phil. Trans. R. Soc. Lond. B.,* 358, 1433, 869-873.
253. G. Weeks and F. *G.* Herring. “The lipid composition and membrane fluidity of Dictyostelium iscoideum plasma membranes at various stages during differentiation.” 1980, *J. Lipid Res.*, 21, 681-686.
254. Y.A. Hannun and R.M. Bell. “Functions of sphingolipids and sphingolipid breakdown products in cellular regulation.” 1989, *Science*, 243, 4890, 500-507.
255. S. Lahiri and A.H. Futerman. “The metabolism and function of sphingolipids and glycosphingolipids.” 2007, *Cell. Mol. Life Sci.,* 64, 2270- 2284.
256. P. Mastromarino , L. Cioè, S. Rieti and N. Orsi. “Role of membrane phospholipids and glycolipids in the Vero cell surface receptor for rubella virus.” 1990, *Med. Microbio. Immun.,* 179 (2), 105-114.
257. T. taki, Y. Hirabayashi, Y. Suzuki, M. Matsumoto and K. Kojima. “Comparative Study of Glycolipid Compositions of Plasma Membranes among Two Types of Rat Ascites Hepatoma and Normal Rat Liver.” 1978, *J. Biochem.*, 83 (5), 1517-1520.
258. G. van Meer and Q. Lisman. “Sphingolipid Transport: Rafts and Translocators.” 2002, *J. Biol.Chem.,* 277(29), 25855-25858.
259. S. Hakomori. “Structure, organization, and function of glycosphingolipids in membrane.” 2003, *Curr. Opin. Hematol.* 10, 16-24.

260. J.D. Hood & D.A. Cheresh. “Role of integrins in cell invasion and migration.” 2002, *Nat. Rev. Cancer,* 2, 91-100.
261. A.A. Spector and M.A. Yorek. “Membrane lipid composition and cellular function.” *1985, J. Lipid Res.,* 26, 1015-1035.
262. A. Prinetti, V. Chigorno, S. Prioni, N. Loberto, N. Marano, G. Tettamanti and S. Sonnino. “Changes in the Lipid Turnover, Composition, and Organization, as Sphingolipid-enriched Membrane Domains, in Rat Cerebellar Granule Cells Developing *in Vitro.”* 2001, *J. Biol.Chem.,* 276(24), 21136-21145.
263. E.E. Williams. “Membrane Lipids: What Membrane Physical Properties are Conserved during Physiochemically-Induced Membrane Restructuring?” 1998, *Int. Compar. Biol. [Amer. Zool.]*, 38, 280-290.
264. E. Wang, W.P. Norred C.W. Bacon. “Inhibition of sphingolipid biosynthesis by fumonisins.” 1991, *J. Biol. Chem.* 266, 14486-144490.
265. H.S. Yoo W.P. Norred, J. Showker. “Elevated sphingoid bases and complex sphingolipid depletion as contributing factors in fumonisin-induced cytotoxicity.” 1996, *Toxicol. Appl. Pharmacol*. 138, 211-218.
266. R.T. Riley, E.N. Enongene, K.A. Voss. “Sphingolipid perturbations as mechanisms for fumonisin carcinogenesis.” 2001, *Environ Health Persp*. 109, (Suppl 2), 301-308.
267. V.L. Stevens and J. Tang. “Fumonisin B_1-induced Sphingolipid Depletion Inhibits Vitamin Uptake via the Glycosylphosphatidylinositol-anchored Folate Receptor.” 1997, *J. Biol. Chem.*, 272(29), 18020-18025.
268. R. Wang, J. Shi, A.N. Parikh, A.P. Shreve, L. Chen, B.I. Swanson. “Evidence for cholera aggregation on GM1-decorated lipid bilayers.” 2004, *Colloids Sruface B, Biointerface*, 33, 45-51.
269. S. Chatterjee. “Neutral Sphingomyelinase: past, present and future.” 1999, *Chem. Phys. Lipids*, 102, 79-96.
270. P.M. Loadman, R.M. Phillips, L.E. Lim, M.C. Bibby. “Pharmacological properties of a new aziridinylbenzoquinone, RH1 (2,5-diaziridinyl-3-(hydroxymethyl)-6-methyl-1,4-benzoquinone), in mice - cytochrome b_5 reductase in human tumour cells.” 2000, 59, 7, 831-837.
271. R.A. Zager, K.M. Burkhart and A. Johnson. “Sphingomyelinase and Membrane Sphingomyelin Content.” 2000, *J. Am. Soc. Nephrol.,* 11, 894-902.
272. Md.R. Ali, K.H. Cheng, and J. Huang.“Ceramide Drives Cholesterol Out of the Ordered Lipid Bilayer Phase into the Crystal Phase in 1-Palmitoyl-2-oleoyl-*sn*-glycero-3-phosphocholine/Cholesterol/Ceramide Ternary Mixtures”. 2006, *Biochem*., 45(41), 12629-12638.

273. L.C. Silva, A.H. Futerman and M.Prieto. “Lipid Raft Composition Modulates Sphingomyelinase Activity and Ceramide-Induced Membrane Physical Alterations.” 2009, *Biophys. J.*, 96, 8, 3210-3222.
274. L.C. Silva, R.F.M. de Almeida, B.M. Castro, A. Fedorov and M. Prieto. “Ceramide-Domain Formation and Collapse in Lipid Rafts: Membrane Reorganization by an Apoptotic Lipid” 2007, *Biophys. J.*, 92, 2, 502-516.
275. M.P. Veiga, J.L. Arrondo, F.M. Goñi, and A. Alonso. “Ceramides in phospholipid membranes: effects on bilayer stability and transition to nonlamellar phases.” 1999, *Biophys J.* 76, 342-350.
276. S.N. Pinto, L.C. Silva, R.F.M. de Almeida, M. Prieto. “Ceramide Gel Domain Formation in a Phospholipid Bilayer: The Impact of Ceramide Acyl Chain.” 2010, *Biophys. J.*, 98(3), 664a-664a.
277. P. Liu and R.G.W. Anderson. “Compartmentalized Production of Ceramide at the Cell Surface.” 1995, *J. Biol.Chem.,* 270(10), 27179-27185.
278. C.R. Bollinger, V. Teichgräber and E. Gulbins. **“**Ceramide-enriched membrane domains.” 2005, *BBA – Mol. Cell Res.,* 1746(3), 284-294.
279. A. Puri, S.S. Rawat, H.M.J Lin, C.M. Finnegan, J. Mikovits, F.W. Ruscetti, R. Blumenthal. *“*An inhibitor of glycosphingolipid metabolism blocks HIV-1 infection of primary T-cells.” 2004, *AIDS*, 18(6), 849-858.
280. C. Porto, M. Cardone, F. Fontana, B. Rossi, M.R. Tuzzi, A. Tarallo, M.V. Barone, G. Andria and G. Parenti. “The Pharmacological Chaperone N-butyldeoxynojirimycin Enhances Enzyme Replacement Therapy in Pompe Disease Fibroblasts.” 2009, *Mol. Therapy,* 17(6), 964-971.
281. Md. Jafurulla, Thomas J. Pucadyil and Amitabha Chattopadhyay. **“**Effect of sphingomyelinase treatment on ligand binding activity of human serotonin$_{1A}$ receptors.” 2008, *BBA-Biomembrane*, 1778(10), 2022-2025.
282. M.I. Pörn and J.P. Slotte. “Localization of cholesterol in sphingomyelinase-treated fibroblasts.” 1995, *Biochem. J.,* 308, 269–274.
283. S. Chatterjee. “Neutral sphingomyelinase action stimulates signal transduction of tumor necrosis factor-alpha in the synthesis of cholesteryl esters in human fibroblasts.” 1994, *J. Biol.Chem.,* 269, 879-882.